Investigating the Role of Lipopolysaccharide-Stimulated Monocytes in the Development of Immune Tolerance in Community-Acquired Pneumonia Patients

Ioana-Beatrice Neamtu

Dr. Brendon Scicluna, Primary Supervisor

Prof. Jean Paul Ebejer, Co-Supervisor

Centre for Molecular Medicine and Biobanking

University of Malta

June, 2025

A dissertation submitted in partial fulfilment of the

requirements for the degree of M.Sc. in Bioinformatics

L-Università ta' Malta
Centre for Molecular
Medicine & Biobanking

Declaration of Authenticity

L-Università ta' Malta

FACULTY/INSTITUTE/CENTRE/SCHOOL *Centre for Molecular Medicine and Biobanking*

DECLARATIONS BY POSTGRADUATE STUDENTS

Student's Code *2210377*

Student's Name & Surname *Ioana-Beatrice Neamtu*

Course *Master of Science in Bioinformatics*

Title of Dissertation

Investigating the Role of Lipopolysaccharide-Stimulated Monocytes in the Development of Immune Tolerance in Community Acquired Pneumonia Patients

(a) Authenticity of Dissertation

I hereby declare that I am the legitimate author of this Dissertation and that it is my original work.

No portion of this work has been submitted in support of an application for another degree or qualification of this or any other university or institution of higher education.

I hold the University of Malta harmless against any third party claims with regard to copyright violation, breach of confidentiality, defamation and any other third party right infringement.

(b) Research Code of Practice and Ethics Review Procedures

I declare that I have abided by the University's Research Ethics Review Procedures.

Research Ethics & Data Protection form code CMMB-2024-00011

As a Master's student, as per Regulation 77 of the General Regulations for University Postgraduate Awards 2021, I accept that should my dissertation be awarded a Grade A, it will be made publicly available on the University of Malta Institutional Repository.

Signature of Student

IOANA-BEATRICE NEAMTU

Name of Student

09.06.2025

Date

Dedications

*To my parents, **Florin** and **Sorela Neamțu**, thank you for believing in me without hesitation, for sacrificing endlessly, and for working tirelessly to keep me in school overseas, even when it broke your hearts to be apart and strained every resource you had. Your love carried me through every storm. This achievement is as much yours as it is mine.*

*To my grandmother, **Mia**, and to my aunt, **Dani**, thank you for welcoming me back home with open arms, year after year, as if I had never left, reminding me that no matter the distance, family is where I will always belong.*

*To **Oița** and **Bunelu**, you would have been so proud of me. I feel your love still, and I carry it forward. And to **Maruka**, my little bunny and quiet guardian, thank you for watching over me.*

You are all with me, always.

And, lastly, as a reminder to future me, no matter how long it takes or how heavy the weight, I am capable of enduring, rising, and finishing what I start.

Acknowledgements

This work would not have been possible without the unwavering support of those around me. I would like to acknowledge the help, guidance, and encouragement received throughout this journey.

To my supervisors, **Doctor Brendon Scicluna** (Primary Supervisor), **Professor Jean Paul Ebejer** (Co-Supervisor), and to **Professor Richard Muscat**, Director of the Centre for Molecular Medicine and Biobanking, thank you for your mentorship, patience, and for providing the space necessary to develop both scientifically and personally. Your guidance was instrumental in navigating the complexities of this project and in fostering independent and critical thinking.

To the **ELDER-BIOME** clinical study team, whose foundational work enabled this dissertation, I express my sincere gratitude. Particular thanks are extended to **Doctor Brendon Scicluna**, principal investigator of the study and primary supervisor, for generously providing access to the transcriptomic dataset and for guiding the project with scientific integrity and sustained commitment.

To **Miss Stephanie Meli** and **Doctor Analisse Cassar**, thank you for encouraging the pursuit of a Master of Bioinformatics at the University of Malta. Your belief in my potential was a decisive influence in undertaking this academic path.

To **the lecturing staff of the MSc in Bioinformatics program**, thank you for the clarity, dedication, and enthusiasm that defined your teaching. Your lectures and willingness to engage in open discussion created a learning environment that fostered critical inquiry and interdisciplinary understanding.

Finally, sincere appreciation is extended to **the administrative and technical staff at the Centre for Molecular Medicine and Biobanking, University of Malta**. Your support with the operational and logistical aspects of this dissertation was essential and greatly valued.

Abstract

Introduction: Pneumonia remains a leading cause of morbidity and mortality worldwide. Beyond antibiotic treatment, disease severity hinges on how monocytes balance immune defence and tolerance, a process which may paradoxically worsen outcomes.

Background: Emerging evidence links monocyte "tolerance" in CAP to DNA methylation and metabolic shifts, yet why patients differ in cytokine output remains unclear. We hypothesized that transcriptional changes in monocytes underlie this heterogeneity.

Methodology: The study included samples from a previously executed prospective observational investigation of CAP patients and control subjects (ELDERBIOME; NCT02928367). Specifically, RNA-seq data of monocytes purified from 75 patients, stimulated with LPS- or not. In addition, TNF-α levels in supernatants were used to stratify samples as LPS responders or non-responders. Read libraries were prepared using the KAPA RNA HyperPrep Kit with RiboErase. Sequencing was performed on the Illumina HiSeq 4000 platform. Bioinformatics included standard quality control metrics, graph-based read alignment, and subsequent *DESeq2* modelling, and pathway/network enrichment.

Results and Discussion: At *padj* ≤ 0.01, LPS reshaped expression of 7,033 genes (3,878 upregulated; 3,155 downregulated). Enrichment pinpointed heightened cytokine and interferon pathways, with type I interferons (*IFNB1*) strongly induced. TNF-α stratification revealed two distinct monocyte states: high responders amplified interferon signalling and HLA class II expression; low responders favoured antioxidant, ECM, and solute transport programmes.

Conclusion: These findings uncover transcriptional blueprints explaining patient-specific monocyte behaviour in CAP. Understanding this immune polarity could guide strategies to rebalance hyperinflammation without compromising pathogen clearance.

Table of Contents

List of Figures and Tables

List of Abbreviations

A	Adenine
ACSL	Acyl-CoA Synthetase Long Chain Family Member
ADAMTS	A Disintegrin and Metalloproteinase with Thrombospondin Motif
ADM	Adrenomedullin
AKT	Protein Kinase B
ANKRD	Ankyrin Repeat Domain
Apeglm	Adaptive Prior Estimation for Generalised Linear Models
APL	Adjusted Profile Likelihood
APOL	Apolipoprotein L
ARDS	Acute Respiratory Distress Syndrome
ASC	Apoptosis-Associated Speck-like Protein Containing a C-terminal caspase-recruitment domain
Ashr	Adaptive Shrinkage in R
ATAC	Assay for Transposase-Accessible Chromatin
ATP	Adenosine Triphosphate
BACH	Transcription Factor Broad-Complex, Tramtrack and Bric a brac (BTB) Domain and Cap'N'Collar (CNC) Homology
B	Bursa
B2M	Beta-2-Microglobulin
BAM	Binary Alignment Map
BATF	Basic Leucine Zipper Activating Transcription Factor-Like
BCAT	Branched Chain Amino Acid Transaminase
BCL	B-cell Lymphoma
BMP	Bone Morphogenetic Protein
bp/BP	Base Pairs/Biological Process
C	Cytosine
CALHM	Calcium Homeostasis Modulator Family Member

CAP	Community-Acquired Pneumonia
CC	Cellular Component
CCL	C Motif Chemokine Ligand
CCR	C-C Chemokine Receptor
ccRCC	Clear Cell Renal Cell Carcinoma
CD	Cluster of Differentiation
cDNA	Complementary DNA
CEBP	CCAAT/Enhancer-Binding Protein
ChaC	Glutathione Specific Gamma-Glutamylcyclotransferase
ChIP	Chromatin Immunoprecipitation Platform
CLR	C-type Lectin Receptor
CMMB	Centre for Molecular Medicine and Biobanking
COPD	Chronic Obstructive Pulmonary Disease
CPT	Carnitine Palmitoyltransferase
CREB	Cyclic Adenosine Monophosphate Response Element-binding Protein
csv	Comma-Separated Values
CtBP	C-terminal Binding Protein
CTGF	Connective Tissue Growth Factor
CTL	Cytotoxic T Lymphocyte
CXCL	C-X-C Motif Chemokine Ligand
CXCR	C-X-C Chemokine Receptor
DC	Dendritic Cell
DDIT	DNA Damage Inducible Transcript
DDX3Y	Aspartate-Glutamate-Alanine-Aspartate (DEAD)-box Helicase 3, Y-linked
DEG	Differentially Expressed Gene
DESeq2	Differential Expression Sequencing Version 2
DHCR	Dehydrocholesterol Reductase
DNA	Deoxyribonucleic Acid

DNase-HS-Chr	Deoxyribonuclease Hypersensitive Sites on Chromosome
ECM	Extracellular Matrix
E. coli	*Escherichia coli*
EGF	Early Growth Response
EHMT	Euchromatic Histone-Lysine N-Methyltransferase
EIF1AY	Eukaryotic Translation Initiation Factor 1A, Y-linked
ELDER-BIOME	Effect of Leukocyte DNA Methylation and Microbiome Diversity on Host Defense Mechanisms During Community-Acquired Pneumonia
ELN	Elastin
EP300	Adenovirus Early Region 1A-associated Protein p300
EPHA	Ephrin Type-A Receptor
ETV	Erythroblast Transformation Specific Variant Transcription
F	Coagulation Factor
FASTA	Fast Alignment Search ToolAll
FASTQ	FASTQuality
FCRL	Fc Receptor Like
FDR	False Discovery Rate
FN	Fibronectin
F/REC	Faculty Research Ethics Committee
FTP	File Transfer Protocol
G	Guanine
GBP	Guanylate Binding Protein
GDF	Growth/Differentiation Factor
GLM	Generalised Linear Model
GO	Gene Ontology
GSEA	Gene Set Enrichment Analysis
GSK	Glycogen Synthase Kinase
GTF	Gene Transfer Format
GTPase	Guanosine Triphosphatase

GRCh38.p14	Genome Reference Consortium Human Build 38 Assembly and Patch Version 14
HKme	Histone Lysine Methylation
HBC	Harvard Chan Bioinformatics Core
HERC	Homologous to the E6-AP Carboxyl Terminus and Regulator of chromosome condensation 1-Like Domain Containing E3 Ubiquitin Protein Ligase
HIC	Hypermethylated in Cancer
HIF	Hypoxia-Inducible Factor
HISAT	Hierarchical Indexing for Spliced Alignment of Transcripts
HIV	Human Immunodeficiency Virus
HLA	Human Leukocyte Antigen
HMOX	Haem Oxygenase
HTS	High-Throughput Sequencing
HTSlib	HTS C Library
ICU	Intensive Care Units
ID	Inhibitor of DNA Binding/ Identifier
IFI	Interferon-Induced Protein
IFIH	Interferon Induced with Helicase C Domain
IFIT	IFI With Tetratricopeptide Repeats
IFN	Interferon
IL/ Il	Interleukin
iNOS	Inducible Nitric Oxide Synthase
IQR	Interquartile Range
IRAK	IL Receptor-Associated Kinase
IRF	IFN Regulatory Factor
IRS	Insulin Receptor Substrate
ISG	IFN-Stimulated Gene
ISGF	ISG Factor
Jak-STAT	Janus Kinase-Signal Transducer and Activator of Transcription

KDM	Lysine Demethylase
KEGG	Kyoto Encyclopedia of Genes and Genomes
KLF	Krüppel-Like Factor
LDLR	Low-Density Lipoprotein Receptor
LIF	Leukaemia Inhibitory Factor
LINC00278	Long Intergenic Non-Protein Coding RNA 278
Log FC	Logarithm of the Fold Change
LPS	Lipopolysaccharide
LTS	Long Term Support
Ly6C	Lymphocyte Antigen 6 Complex
MA	Mean Average
MAFF	Maf Basic Leucine Zipper Transcription Factor F
MAPK	Mitogen Activated Protein Kinase
MARE	MAF Recognition Element
MAVS	Mitochondrial Antiviral-Signalling Protein
MCP	Monocyte Chemoattractant Protein
ME	Malic Enzyme
MF	Molecular Function
MHC	Major Histocompatibility Complex
MLL	Mixed-Lineage Leukaemia
MMP	Matrix Metallopeptidase
mRNA	Messenger RNA
MRP	human Multidrug Resistance Proteins
MRSA	Methicillin-Resistant *Streptococcus aureus*
MyD88	Myeloid Differentiation Primary Response 88
N	Ambiguous Nucleotide
NADPH`	Nicotinamide Adenine Dinucleotide Phosphate
ncRNA	Non-Coding RNA
NES	Normalised Enrichment Score

NF-κB	Nuclear Factor Kappa-Light-Chain-Enhancer of Activated B-Cells
NFIL	Nuclear Factor IL-Regulated Protein
NGS	Next-Generation Sequencing
NK	Natural Killer
NLRP	Nucleotide-Binding Domain, Leucine-Rich-Containing Family, Pyrin Domain-Containing
NO	Nitric Oxide
NSCLC	Non-Small Cell Lung Cancer
ORA	Over-Representation Analysis
OTOF	Otoferlin
padj	Adjusted *p*-Value
PARP	Poly Adenosine Diphosphate-Ribose Polymerase
PBMC	Peripheral Blood Mononuclear Cell
PCA	Principal Component Analysis
PD	Programmed Cell Death Protein
PDGFRL	Platelet-Derived Growth Factor Receptor Like
PEL	Protein Enhancer of Liver
PHACTR	Phosphatase and Actin Regulator
PIK	Phosphatidylinositol Kinase
PLAUR	Plasminogen Activator, Urokinase Receptor
PLC	Phospholipase C
PPAR	Peroxisome Proliferator-Activated Receptor
PPI	Protein-Protein Interaction
PRC	Polycomb Repressive Complex
PRKY	Protein Kinase Y-Linked
PSM	Proteasome
PSME	Proteasome Activator Subunit
PTGS	Prostaglandin-Endoperoxide Synthase
QC	Quality Control

RA	Receptor Antagonist
RANBP	Rat Sarcoma Virus-Related Nuclear Protein Binding Protein
RIG	Retinoic Acid-Inducible Gene
RIPK	Receptor-Interacting Serine/Threonine-Protein Kinase
rlog	Regularized log Transformation
RLR	RIG-I-like Receptor
RNA	Ribonucleic Acid
RNA-seq	RNA Sequencing
RPMI	Roswell Park Memorial Institute
RPS4Y	Ribosomal Protein S4 Y-Linked
RSV	Respiratory Syncytial Virus
RUNX	Runt-Related Transcription Factor
RXRG	Retinoid X Receptor Gamma
SAM	Sequence Alignment Map
SARS-CoV	Severe Acute Respiratory Syndrome Coronavirus
SE	Single-End
SERPING	Serpin Family G Member
SIRS	Systemic Inflammatory Response Syndrome
SLC	Solute Carrier
SMAD	Small Mothers Against Decapentaplegic
SPIA	Signalling Pathway Impact Analysis
SQLE	Squalene Epoxidase
STING	Stimulator of IFN Genes
STRING	Search Tool for the Retrieval of Interacting Genes/Proteins
STS	Suppressor of Thymocyte-cell Receptor Signalling
T	Thymine/Thymocyte
Tfh	T Follicular Helper
TGF	Transforming Growth Factor
TGFBR	TGF-β Receptor

TH/Th	Inflammatory T-Helper Cells
THBS	Thrombospondin
Tim	T-Cell Immunoglobulin and Mucin-Domain Containing
TLR	Toll-Like Receptor
TMEM	Transmembrane Protein
TNF/ Tnf	Tumour Necrosis Factor
TNFAIP	TNF-α-Induced Protein
TNFRSF	TNF Receptor Superfamily Member
TNFSF	TNF Ligand Superfamily Member
TP	Tumour Protein
TREM	Triggering Receptor Expressed on Myeloid Cells
Treg	Regulatory T-Cell
TRIF	Toll/IL-1 Receptor-Domain-Containing Adaptor-Inducing β IFN
TSIX	X-Inactive Specific Transcript Regulatory Antisense RNA
TTTY	Testis-Specific Transcript, Y-Linked
TXNRD	Thioredoxin Reductase
UBE	Ubiquitin-Conjugating Enzyme
UBL	Ubiquitin Like Modifier Activating Enzyme
UTY	Ubiquitously Transcribed Tetratricopeptide Repeat Containing, Y-Linked
USP9Y	Ubiquitin Specific Peptidase 9 Y-Linked
VEGF	Vascular Endothelial Growth Factor
vs	Versus
VST	Variance-Stabilising Transformation
WISP	Wingless-Related Integration Site 1 Inducible Signalling Pathway Protein
XIST	X-Inactive Specific Transcript
XL	Extra Large
ZFY	Zinc Finger Protein, Y-linked

1. INTRODUCTION

Pneumonia continues to be one of the most significant infectious diseases worldwide, causing widespread illness and mortality while straining healthcare systems (Musher and Thorner, 2014; Cilloniz *et al.*, 2016). Among its various forms, Community-Acquired Pneumonia (CAP) remains a particularly severe concern, frequently leading to hospitalisation and even death, despite notable progress in antimicrobial treatments and medical care (Torres *et al.*, 2014). Its incidence follows a distinct "U"-shaped pattern, disproportionately affecting two vulnerable populations: neonates, whose underdeveloped immune systems struggle to mount an effective defence (Cilloniz *et al.*, 2016; Musher and Thorner, 2014), and the elderly, who face age-related immune decline, chronic illnesses, and diminished vaccine efficacy (Torres *et al.*, 2014). Beyond these groups, individuals with pre-existing conditions, including diabetes, chronic respiratory diseases or immunosuppressive therapy, are also at a heightened risk of severe CAP and its complications, making the disease a persistent global health challenge (Torres *et al.*, 2014).

CAP is often classified as an acute respiratory infection and its effects do not always end with clinical recovery. For some patients, immune function remains impaired long after the initial infection has resolved, leaving them highly susceptible to secondary infections, prolonged hospital stays, and, in severe cases, sepsis (Hotchkiss *et al.*, 2013b, 2013a). This long-term immune dysfunction is not unique to CAP; similar post-infectious immune suppression has been documented following severe influenza (DeWolf *et al.*, 2022), bacterial sepsis (Hotchkiss *et al.*, 2013b; Shalova *et al.*, 2015), and even Coronavirus Disease 2019 (COVID-19) (Gupta *et al.*, 2025; Skevaki *et al.*, 2025). Understanding why some individuals recover fully while others remain immunologically compromised is a critical, yet unresolved question in infectious disease research.

While the mechanisms of immune suppression in sepsis are well studied, the molecular basis of CAP-induced immune dysfunction remains largely unexplored, particularly in patients who do not develop sepsis (Hotchkiss *et al.*, 2013b, 2013a). Some research suggests that CAP-related immune suppression may mirror sepsis-induced immunosuppression, where monocytes remain dysfunctional long after the acute infection has resolved, leading to the heightened risk of secondary infections, such as nosocomial infections and worse clinical outcomes (Hotchkiss *et al.*, 2013b; Shalova *et al.*, 2015). However, whether CAP and sepsis share the same underlying immunological mechanisms, or represent distinct forms of immune dysregulation, is still unknown (Allam *et al.*, 2023; Brands *et al.*, 2021; Otto *et al.*, 2022), highlighting the need for further investigation. Despite increasing awareness of these long-term immunological consequences, the specific molecular events driving CAP-related immune suppression remain poorly characterised, particularly regarding how monocytes, as key innate immune cells, are transcriptionally altered during recovery (Brands *et al.*, 2021; Reijnders *et al.*, 2023).

Monocytes are crucial regulators of innate immunity, serving as first responders during infection and playing a key role in maintaining immune balance (Ginhoux and Jung, 2014; Jakubzick *et al.*, 2017). Their plasticity allows them to rapidly adapt in response to pathogens and inflammatory signals, ensuring an effective and proportionate immune reaction (Ginhoux and Jung, 2014). However, in CAP, this adaptability can take an unexpected turn, where monocytes may become functionally reprogrammed, entering a state of immune tolerance in which cytokine production is significantly reduced (Biswas and Lopez-Collazo, 2009; Brands *et al.*, 2021). While this shift may serve as a protective mechanism to prevent excessive inflammation, it can also weaken host defence to secondary infections (Brands *et al.*, 2021). Understanding what drives this monocyte reprogramming is crucial for unravelling the mechanisms of CAP-related immune suppression (Wiersinga and van der Poll, 2022).

Ex vivo studies provide compelling evidence that monocytes from CAP patients display widespread immune suppression when exposed to *Escherichia* (*E.*) *coli* Lipopolysaccharide (LPS) stimulation, leading to reduced production of both pro-inflammatory cytokines (Tumour Necrosis Factor (TNF), Interleukin (IL)-1β) and regulatory cytokines (IL-10) (Biswas and Lopez-Collazo, 2009; Brands *et al.*, 2021). This suggests that CAP-induced immune tolerance is not merely a selective suppression of inflammatory pathways, but it appears to involve a broader functional impairment of monocytes (Brands *et al.*, 2021). However, this effect is not universal as, while some CAP patients appear to recover normal monocyte function relatively quickly, others remain in a state of prolonged immune dysfunction, highlighting inter-individual variability in immune reprogramming (Otto *et al.*, 2022; Palma Medina *et al.*, 2023; Ritchie and Singanayagam, 2020). Growing transcriptomic evidence suggests that persistent metabolic reprogramming, especially in cholesterol biosynthesis, may drive long-term monocyte dysfunction and immune vulnerability in CAP survivors (Brands *et al.*, 2021). Research now indicates that transcriptional reprogramming outmatches epigenetic modifications as the primary cause of monocyte dysfunction (Brands *et al.*, 2021; Lorente-Sorolla *et al.*, 2019). A complete restructuring of immune gene expression has been shown through the identification of approximately 3,000 Ribonucleic Acid (RNA) transcripts during acute CAP (Brands *et al.*, 2021). The epigenetic modifications found in Deoxyribonucleic Acid (DNA) show limited distribution across specific regulatory sites like Deoxyribonuclease Hypersensitive Sites on Chromosome 22 (DNase-HS-Chr22), while showing minimal evidence of global methylation patterns (Brands *et al.*, 2021; Lorente-Sorolla *et al.*, 2019).

Pathways that involve cholesterol metabolism emerge as key contributors to immune tolerance among the transcriptional changes identified in Brands *et al.* (2021). Metabolic programmes function as regulators of cytokine systems while maintaining a suppressed state of monocytes (Brands *et al.*, 2021). The emerging data reveal several gene-level and regulatory changes in CAP patients but the

complete network of pathways that regulate this immune tolerance needs more comprehensive mapping (Koelwyn *et al.*, 2018; Otto *et al.*, 2022). A comprehensive molecular study is essential for two purposes: understanding both the initiation and maintenance of this reprogramming process and creating specific immunotherapies for vulnerable CAP patients (Spann *et al.*, 2012).

The clinical field recognises post-infectious immune suppression in CAP but lacks an approved biomarker to detect patients experiencing prolonged immune dysfunction (Hotchkiss *et al.*, 2013b). Standardised indicators are absent which prevents monitoring of immune recovery and patient stratification for early clinical interventions (Hotchkiss *et al.*, 2013a). The link between sepsis and monocyte dysfunction persists through reduced cytokine production and widespread transcriptional alterations (Hotchkiss *et al.*, 2013b; Lorente-Sorolla *et al.*, 2019) but similar immunological patterns have not been fully studied in non-septic CAP cases (Brands *et al.*, 2021). Recent research found hair zinc content to potentially correlate with CAP severity, but this correlation is exploratory and lacks validation as an immune biomarker (Nasution *et al.*, 2024). Personalised management strategies remain difficult to execute because current assessment tools for immune status following CAP are not reliable.

The essential unresolved issue in CAP-related immune suppression becomes even more complex when considering personalised treatment approaches, because immune tolerance shows substantial differences between patients (Urbán *et al.*, 2022). The unrevealed variables which affect immune recovery variability stem from individual metabolic characteristics and sex-related immune system variations between patients (Brands *et al.*, 2021; Klein and Flanagan, 2016; Takahashi *et al.*, 2020). The analysis of these factors would assist scientists in discovering molecular markers which reveal immune tolerance patterns (Brands *et al.*, 2021). The identification of biomarkers for patient stratification along with the creation of targeted therapeutic approaches for CAP-associated immune suppression would be supported by such findings (Urbán *et al.*, 2022).

The main obstacle in understanding this process lies in determining the exact genes and pathways responsible for immune suppression. The research method of Differential Expression of Genes (DEG) analysis serves as a valuable solution to identify the transcriptional changes which define immune dysfunction (Schuurman *et al.*, 2021; Severino *et al.*, 2014). This method enables researchers to differentiate immune-tolerant monocytes from active pro-inflammatory monocytes, thus revealing crucial molecular networks that maintain suppression and therapeutic targets (Brands *et al.*, 2021; Schuurman *et al.*, 2021).

Using a computational method, this research builds upon Brands *et al.* (2021) to investigate the differences in LPS-induced immune tolerance among monocytes from CAP patients. The mechanisms behind CAP monocyte suppression have been documented (Brands *et al.*, 2021), yet the cause of extended tolerance periods in some patients, while others recover quickly, remains unknown (Hopp *et al.*, 2018; Kullberg *et al.*, 2022). The research investigates how distinct cytokine responses relate to transcriptional differences while focusing on their impact on post-CAP immune suppression susceptibility (Hopp *et al.*, 2018). Through RNA sequencing (RNA-seq) data analysis, this research plans to discover molecular patterns which explain immune suppression continuation in specific individuals and the effects of monocyte reprogramming on patient outcomes (Brands *et al.*, 2021). The main goal of this research is to determine TNF-α production, a classic pro-inflammatory cytokine, after *ex vivo* LPS stimulation (Brands *et al.*, 2021). By comparing controlled monocytes treated with Roswell Park Memorial Institute (RPMI) medium (serving as a baseline control) and monocytes stimulated with LPS, this study will identify DEGs related to both immune suppression and recovery mechanisms by performing bulk RNA-seq (Brands *et al.*, 2021; Love *et al.*, 2014). Through this approach, this research aims to describe molecular pathways that govern monocyte dysfunction, identifying which genetic programmes sustain immune tolerance (Brands *et al.*, 2021; Subramanian *et al.*, 2005; G. Yu *et al.*, 2012). These changes in gene expression may provide new targets for therapeutic interventions to enhance monocyte function in

CAP patients (Otto *et al.*, 2022). Furthermore, this study will also address another critical aspect of this research that involves the analysis of sex differences in monocyte immune tolerance. Males and females show different immune responses in various infectious diseases (Klein and Flanagan, 2016; Scully *et al.*, 2020; Takahashi *et al.*, 2020). However, does this difference exist in the context of CAP-induced immune suppression? This study will perform sex-stratified transcriptomic analyses to reveal whether biological sex affects monocyte programming and if it contributes to the observed variability in immune tolerance outcomes (Brands *et al.*, 2021; Maher *et al.*, 2022). These findings can inform the development of personalised immunomodulatory approaches, considering sex-specific factors in future therapeutic strategies for CAP-related immune suppression (Maher *et al.*, 2022).

Cytokine responses are important for understanding immune function, yet they account for only a limited aspect of the overall immune response. This study will extend cytokine profiling by analysing DEGs, biological pathways, and protein interaction networks related to LPS-induced immune tolerance to gain a comprehensive understanding of CAP-induced immune suppression (Brands *et al.*, 2021; Love *et al.*, 2014; Szklarczyk *et al.*, 2023). This research aims to identify molecular signatures that can be used as biomarkers for risk stratification and precision medicine approaches through bulk RNA-seq data and in-depth computational analyses (Subramanian *et al.*, 2005; T. Wu *et al.*, 2021; G. Yu *et al.*, 2012). Christaki and Giamarellos-Bourboulis (2014) emphasise that the identification of precise immune phenotypes is the first step toward developing biomarkers and personalised interventions in infectious diseases (Christaki and Giamarellos-Bourboulis, 2014).

Understanding the molecular mechanisms behind immune tolerance in CAP is not only important for improving the outcome of pneumonia patients but also may apply to other post-infectious immune syndromes (Hotchkiss *et al.*, 2013b; Shalova *et al.*, 2015). Long-term monocyte reprogramming could have implications in post-viral

conditions, bacterial sepsis and chronic inflammation-associated diseases (Brands *et al.*, 2021). By revealing specific immune suppression pathways in non-septic CAP, this research offers valuable information for sepsis-induced immune dysfunction (Hotchkiss *et al.*, 2013a; Lorente-Sorolla *et al.*, 2019), which will improve patient risk assessments and treatment plans for long-term immune recovery (Savvateeva *et al.*, 2019).

1.1 Research Question

To what extent does transcriptional reprogramming drive prolonged immune tolerance in monocytes from CAP patients, and how do sex-specific immune adaptations influence the development of this tolerance, potentially affecting an individual's susceptibility to secondary infections?

The purpose of this research is to determine whether immune suppression in CAP is driven by transcriptional shifts and if biological sex differences affect immune tolerance outcomes, which may impact post-infectious immune recovery and the reinfection likelihood.

1.2 Hypothesis

Against this backdrop, the study hypothesis posits that changes in the transcriptional activity of monocytes during pneumonia contributes to inter-individual variation in *ex vivo* cytokine responses.

1.3 Study Aims and Objectives

Monocytes, the principal cells of innate immunity, often acquire immunological tolerance post infection, thus compromising their ability to fight off further infections (Biswas and Lopez-Collazo, 2009; Brands *et al.*, 2021; Ginhoux and Jung,

2014). Nonetheless, the extent to which this sustained immune suppression in CAP is caused by apoptosis-induced immune cell depletion versus (vs) transcriptional reprogramming of gene expression beyond the acute phase of infection is not well understood (Brands *et al.*, 2021; Hotchkiss *et al.*, 2013a; Lorente-Sorolla *et al.*, 2019; Torres *et al.*, 2014). Furthermore, literature identifies biological sex as a known factor affecting immune responses, but its contribution to the immune tolerance in CAP patients has not been well examined (Klein and Flanagan, 2016; Takahashi *et al.*, 2020).

This study is aimed at understanding the role of transcriptional reprogramming in the development and maintenance of immune tolerance in monocytes from CAP patients. A particular focus is on the suppression of cytokines and the consequences on the immune system (Biswas and Lopez-Collazo, 2009; Brands *et al.*, 2021). In addition, this research will also examine the sex differences in immune tolerance and how biological sex may influence immune trajectories (Klein and Flanagan, 2016; Takahashi *et al.*, 2020). The findings may also assist in identifying potential biomarkers and new therapeutic targets for CAP-related immune dysfunction (Brands *et al.*, 2021).

1.3.1 Aims

The main objective of this research is to elucidate the molecular basis of immune tolerance in monocytes from CAP patients. It is aimed at investigating whether transcriptional reprogramming could be the cause of the suppression of cytokine production and the increased vulnerability to secondary infections.

Through the identification of DEGs and regulatory pathways of immune suppression, this study aims to determine why some patients recover their immune function, while others remain immunologically affected. Furthermore, it examines whether there are any differences between males and females in the reprogramming of

monocytes, as well as associated sex-specific immune adaptations that may influence recovery and disease progression.

Finally, this study aims to enhance the knowledge on post-infectious immunosuppression in CAP survivors, with regards to biomarker identification, precision immunotherapy, and development of new therapeutic strategies for managing immune dysfunction in these patients.

1.3.2 Objectives

To address these research aims, the study will:

1. Conduct RNA-seq bioinformatic analysis on monocytes from CAP patients and healthy controls, following *ex vivo* stimulation with LPS or RPMI medium, to allow for the identification of DEGs linked to immune tolerance and transcriptional reprogramming.
2. Stratify monocytes based on TNF-α production, using it as a prototypical pro-inflammatory cytokine marker, to help assess transcriptional variations associated with cytokine suppression and immune activation.
3. Map key immune regulatory pathways that sustain immune tolerance, focusing on cytokine signalling networks, metabolic reprogramming, and protein-protein interactions (PPIs) involved in monocyte dysfunction.
4. Analyse sex-based differences in monocyte transcriptional profiles to determine whether immune tolerance is influenced by biological sex, revealing potential sex-specific immune adaptations.

By addressing these objectives, this study aims to provide a comprehensive molecular framework for understanding transcriptional reprogramming in CAP-related immune suppression. The findings will, hopefully, contribute to biomarker discovery, personalised medicine, and targeted therapeutic strategies for patients at risk of prolonged immune dysfunction.

1.4 Approach

This research uses computational and transcriptomic approaches to investigate immune tolerance in CAP monocytes through bulk RNA-seq data analysis from a cohort study by Brands *et al.* (2021). The dataset includes blood-derived monocyte transcriptomes from 172 individuals, spanning different CAP disease stages, and healthy controls. The analysis will focus on 92 samples to understand transcriptional reactions in CAP patients and healthy individuals during *ex vivo* stimulation using LPS or RPMI as a control medium. The study also utilises a secondary dataset of 37 samples that includes TNF-α response level stratification to investigate both cytokine response variability and potential sex-based immune differences (Klein and Flanagan, 2016; Takahashi *et al.*, 2020).

The study of immune dysfunction through cytokine profiling and surface marker analysis gives restricted information about immune responses. This study employs high-resolution molecular profiling for immune suppression analysis because suppression emerges from complex regulatory mechanisms (Love *et al.*, 2014; Subramanian *et al.*, 2005). Key molecular pathways and biomarkers of immune tolerance will be identified through bioinformatics and network-based analyses (Szklarczyk *et al.*, 2023; T. Wu *et al.*, 2021; G. Yu *et al.*, 2012).

This systems-level investigation is an essential strategy to understanding monocyte reprogramming mechanisms, helping explain CAP immune tolerance mechanisms and their clinical importance for risk assessment and stratification, and therapeutic approaches (Brands *et al.*, 2021).

1.5 Document Structure

The Introduction section develops the research hypothesis which suggests immune tolerance in CAP monocytes functions mainly through transcriptional and molecular

processes rather than apoptosis mechanisms alone. This section explains the research targets and main objectives by using bioinformatics approaches to study immune tolerance pathways and cytokine suppression and metabolic adaptations. The research contributes to the scientific literature by establishing its connection to Brands *et al.* (2021). The study focuses on immune suppression in non-septic conditions and its clinical implications for treatment.

The Background and Literature Review presents a thorough examination of monocyte immune tolerance along with its relation to CAP and LPS-induced immune suppression. The section examines monocyte biology while studying immune responses to inflammatory stimuli and the extensive effects of immune tolerance on disease severity and susceptibility to secondary infections. This study presents the bioinformatics methodologies that it employs including RNA-seq processing and DEG analysis and functional enrichment methods. A systematic literature review of relevant studies contextualises these findings, identifying key regulatory pathways and knowledge gaps in LPS-induced immune tolerance.

The Methodology section explains the computational approach for analysing bulk RNA-seq data obtained from 92 participants across acute-phase and recovery-stage CAP patients together with healthy controls. This section describes the data preprocessing methods as well as DEG analysis and pathway enrichment techniques which ensure high methodological quality and reproducibility. The analysis of monocyte transcriptomes uses methods to discover DEGs linked to immune suppression which connects transcriptional patterns to cytokine response variability and immune adaptation.

The Results and Discussion chapter shows the results of DEG analysis and functional enrichment studies on the changes in the transcription of monocytes after LPS stimulation. The results are displayed using Principal Component Analysis (PCA) plots, heatmaps and volcano plots to represent the transcriptional changes. The Gene Ontology (GO) enrichment, Gene Set Enrichment Analysis (GSEA) and Search Tool for the Retrieval of Interacting Genes/Proteins (STRING) PPI networks provide

further insights into monocyte activation pathways, immune tolerance and CAP transcriptional reprogramming. Results from RNA-seq data indicate a broad transcriptional response to LPS, including pro-inflammatory pathways, notably Interferon *(IFN)-β1* signalling and cytokines and chemokines activation. On the other hand, Small Mothers Against Decapentaplegic (*SMAD*)*-6*, Hypermethylated in Cancer (*HIC*)-1, and *CD180* are downregulated which indicates their role in immune regulation and tolerance. A second data set which stratifies the data by TNF-α response levels reveals different transcriptional signatures between high and low cytokine responders and biological sex as a key covariate influencing immune responses.

The Conclusion is a summary of the findings of the study in relation to its hypothesis and objectives and a reflection of the study's scientific contribution and methodological limitations. It stresses the need for experimental validation and gives suggestions for future research, including septic patients and experimental approaches to further investigate immune tolerance mechanisms in CAP. Since monocyte driven immune suppression is not fully understood, the study points out critical areas for further research into post-infectious immune regulation.

Finally, the Appendix presents supplementary materials including datasets, computational scripts and bioinformatics methodologies used in this study.

2. BACKGROUND AND LITERATURE REVIEW

The function of monocytes in the immune response is complex and requires understanding of immune tolerance and its implications in sepsis and inflammation. This chapter outlines the origins, types, and roles of monocytes in the immune system, and the effects of LPS in inducing immune suppression. It discusses historical views on immune tolerance in sepsis and expands this to non-septic diseases such as CAP, where similar immunological features are emerging. It also examines major molecular pathways and regulatory mechanisms that lead to monocyte reprogramming and shows both commonalities and differences in LPS-induced tolerance among the conditions. Furthermore, it details the approaches that are employed in the investigation of these phenomena at the transcriptomic level which include DEG analysis, pathway enrichment and PPI network modelling. In addition, these sections provide the basis to appreciate the immunological heterogeneity and the molecular structure of monocyte responses in infection-related immune modulation.

2.1 Monocyte Biology and Immune Tolerance in CAP

Monocytes are among the key cells of the innate immune system, involved in activation as well as regulation of the immune response (Brands *et al.*, 2021; Mihori *et al.*, 2024). Upon encountering microbial products such as LPS, monocytes can exhibit immune tolerance (del Fresno *et al.*, 2009; Kumar, 2022), which is a state of decreased cytokine secretion, modified transcriptional patterns, and diminished secondary stimulation (Brands *et al.*, 2020; Kullberg *et al.*, 2022; W.-T. Ma *et al.*, 2019). This phenomenon, often termed immune suppression in clinical conditions, is important in the regulation of the host defence and tissue damage during prolonged or repeated inflammatory challenges (Hopp *et al.*, 2018; Méndez-Enríquez and Hallgren, 2019). In CAP, recent findings indicate that monocyte-induced immune tolerance may persist into the resolution phase, with consequences for the course

of disease, susceptibility to recurrent infections, and immune system functioning (Brands *et al.*, 2020; Otto *et al.*, 2022)

The following subsection examines the Biological Processes (BPs) of this tolerance through the perspective of monocyte lineage development, classification, flexibility, and LPS effects on immune responses in CAP.

2.1.1 Origins and Classification of Monocytes

Monocytes make up approximately five percent of circulating nucleated cells in the peripheral blood of normal adults and form part of the myeloid lineage (Pang and Koh, 2023). These cells emerge from haematopoietic stem cells (HSCs) in the tightly controlled process of myelopoiesis that begins in the foetal liver during foetal development and shifts to the bone marrow as the main production site after birth (Geissmann and Mass, 2015; McGrath *et al.*, 2015; Yáñez *et al.*, 2017). Released into circulation, monocytes execute essential immunological roles including pathogen detection, inflammatory cytokine release, and the direction of both innate and adaptive immune responses (Prinyakupt and Pluempitiwiriyawej, 2015). In addition to their systemic immune surveillance role, monocytes differentiate into tissue-resident macrophages and Dendritic Cells (DCs), thus integrating circulatory and tissue-based branches of the innate immune system (Hettinger *et al.*, 2013; Schneider *et al.*, 2014).

HSCs produce monocytes in a homeostatic manner under normal conditions. Nevertheless, in the case of microbial infections or tissue damage, inflammatory cytokines and growth factors may induce rapid myelopoiesis, which in turn leads to an elevated number of monocytes to fulfil greater immune requirements (Arora *et al.*, 2018; DeWolf *et al.*, 2022; Ugel *et al.*, 2015). These cells are not a homogenous group but rather consist of phenotypically and functionally heterogeneous subgroups. In humans, monocytes are subdivided into three major subsets according to their surface expression of Cluster of Differentiation (CD) 14 and CD16: classical

($CD14^{++}CD16^{-}$), intermediate ($CD14^{++}CD16^{+}$), and non-classical ($CD14^{dim}CD16^{+}$) monocytes (Passlick *et al.*, 1989; Zawada *et al.*, 2011; Ziegler-Heitbrock *et al.*, 2010). The subsets separate based on lineage-specific transcription factors. Non-classical monocytes differentiate through nuclear receptor 4A1 (Y. P. Zhu *et al.*, 2016) whereas classical monocytes use purine-rich box1 transcription factor, IFN Regulatory Factor (*IRF*) *8*, and Krüppel-Like Factor (*KLF*) *4* for their differentiation. These transcriptional regulators determine cell identity along with controlling the cells' functional responses to inflammatory signals (Guilliams *et al.*, 2018).

Each monocyte subset demonstrates unique functions. The circulating pool contains mostly classical monocytes because these cells demonstrate exceptional phagocytic capabilities along with fast recruitment to sites of infection or tissue damage (Kapellos *et al.*, 2019). Classical monocytes can migrate into inflamed tissues by using C-C Chemokine Receptors (CCRs) CCR1, CCR2, CCR5 and C-X-C Chemokine Receptors (CXCRs) CXCR1, and CXCR2 (Shi and Pamer, 2011) When they activate, they release IL-6, IL-8, C-C Motif Chemokine Ligands (CCLs) CCL2, CCL3 and CCL5 along with other cytokines and chemokines which increase local immune responses and bring more leukocytes to the area (Jakubzick *et al.*, 2017; Weber *et al.*, 2000; K. L. Wong *et al.*, 2011). Intermediate monocytes demonstrate both excellent antigen-presenting abilities along with powerful cytokine responses when activated by Toll-like Receptors (TLRs). The cells produce TNF-α, IL-1β, IL-6, and CCL3 and display strong responses to microbial ligands (J. Lee *et al.*, 2017; K. L. Wong *et al.*, 2011). These cells show elevated CCR5 expression which research connects to higher Human Immunodeficiency Virus (HIV)-1 infection rates (Ellery *et al.*, 2007; Kapellos *et al.*, 2019; Zawada *et al.*, 2011). These monocytes primarily function as inflammatory cells, yet they display regulatory adaptability through certain cytokine-dependent processes that lead to IL-10 secretion and tumour-targeting responses (Kapellos *et al.*, 2019; Skrzeczyńska-Moncznik *et al.*, 2008; Szaflarska *et al.*, 2004). Non-classical monocytes do not migrate to inflamed tissues, as they perform debris clearance and patrol the vascular endothelium while performing phagocytosis

through complement and FcγR pathways (Kapellos *et al.*, 2019). The vascular homeostasis and immune surveillance, along with inflammation resolution, depend on non-classical monocytes to interact with endothelial cells while promoting neutrophil adhesion through TNF-α and by participating in tissue repair mechanisms (Chimen *et al.*, 2017; Kapellos *et al.*, 2019).

Monocyte subsets show extensive transcriptional variation according to single-cell transcriptomics and mass cytometry analyses, which demonstrate additional functional characteristics beyond traditional surface marker identification (Günther *et al.*, 2019; Kapellos *et al.*, 2019). The three monocyte subsets show high adaptability in their functions when they encounter environmental signals such as LPS (Canè *et al.*, 2019; Shalova *et al.*, 2015). When monocytes are LPS stimulated, they experience transcriptional modifications which lead to an immune tolerant state characterised by reduced cytokine release and reduced responsiveness to subsequent stimuli (Brands *et al.*, 2021; del Fresno *et al.*, 2009). LPS-induced tolerogenic reprogramming stands as a critical mechanism during CAP, since recent studies demonstrate that LPS-tolerant monocytes survive past the acute infection period to cause long-term immunosuppression and elevated secondary infection risks (Brands *et al.*, 2020, 2021).

Monocyte diversity and adaptability play an essential role in maintaining immune homeostasis and preventing disease due to their ability to modify their functional profiles to fight pathogens while protecting against immunopathology within the recurring inflammatory conditions of CAP (Arora *et al.*, 2018; Quinton and Mizgerd, 2015).

2.1.2 Functional Diversity of Monocytes in Respiratory Infections

In the context of respiratory infections, upon tissue infiltration, monocytes differentiate into inflammatory macrophages or DC-like cells and partake in both

immune activation and resolution processes (Guilliams *et al.*, 2018). These functional adaptations are relevant in studying CAP, where monocyte reprogramming under inflammatory pressure may shape the balance between pathogen clearance and immune tolerance. Understanding the effector roles of these immune cells provides essential context for interpreting the DEGs and enriched pathways identified in this study.

In respiratory inflammation, recruitment of $CD11b^{+}$ monocytes to the lungs occurs, where they adopt antigen-presenting and pro-inflammatory functions while retaining Lymphocyte Antigen 6 Complex (Ly6C) expression, confirming their monocytic origin (Lambrecht and Hammad, 2009). Chemokines such as CCL2, CCL3, and CCL7, released by inflamed alveolar macrophages, attract $CCR2^{+}$ monocytes towards sites of infection or damage (Arunachalam *et al.*, 2020; Hadjadj *et al.*, 2020; Jakubzick *et al.*, 2017; Knoll *et al.*, 2021; Lucas *et al.*, 2020). Recruited monocytes contribute to antigen presentation via Major Histocompatibility Complex (MHC) molecules and secrete both pro- and anti-inflammatory cytokines, including IL-1β, IL-6, TNF-α, and IL-10, thus adapting immune responses to the pathogen and the host context (Benoit *et al.*, 2008; Chaplin, 2010; K. L. Wong *et al.*, 2011).

The efficiency of antigen presentation is closely linked to surface Human Leukocyte Antigen (HLA)-DR isotype expression, which is dynamically regulated during infection and immune suppression. In severe inflammatory states such as CAP, monocytes have been shown to downregulate HLA-DR expression, indicating a shift toward an immunoregulatory state (Knoll *et al.*, 2021; Schulte-Schrepping *et al.*, 2020). In the present study, HLA-DR, IL-1β, TNF, and other inflammation-related markers emerged as differentially expressed features, reinforcing their roles in the balance between immune activation and tolerance in CAP.

In antiviral and bacterial infections of the lung, monocytes also contribute via production of type I IFNs, which induce IFN-stimulated genes (ISGs) such as *ISG15*, IFN- Induced Protein with Tetratricopeptide Repeats (*IFIT*) *1*, and Signal Transducer and Activator of Transcription (*STAT*) *2*, limiting pathogen replication and promoting

immune activation (Hambleton *et al.*, 2013; M.-T. Wong and Chen, 2016). Illustrating the context-dependent nature of monocyte reprogramming, some pathogens, including respiratory coronaviruses, may bypass IFN signalling while still provoking inflammatory cytokine release (Funk *et al.*, 2012; Knoll *et al.*, 2021). In this study, elevated expression of several ISGs in LPS-stimulated monocytes from CAP patients was observed, aligning with these findings and reinforcing the dual antiviral and inflammatory roles of monocytes in respiratory infections.

Recent work also underscores the importance of immunometabolism in shaping monocyte function. Inflammatory monocytes can undergo metabolic reprogramming, shifting toward glycolysis or fatty acid oxidation in response to severe respiratory infections, including CAP and COVID-19, a shift characterised by increased expression of enzymes such as Carnitine Palmitoyl transferase (*CPT*) *1*, and changes in lipid metabolism that amplify cytokine production (Codo *et al.*, 2020; Dias *et al.*, 2020; Thompson *et al.*, 2021).

This functional diversity from inflammatory activation to metabolic adaptation and tolerance is central to interpreting transcriptomic shifts observed in this study's dataset and supports the hypothesis that immune tolerance in CAP may reflect a transcriptionally regulated rebalancing of monocyte behaviour, rather than a simple failure of immune activation.

2.1.3 LPS-induced immune suppression

The canonical ligand for TLR4, LPS, is essential for the initiation and shaping of the critical innate immune pathogen control response to Gram-negative bacteria. The LPS ligand triggers a proinflammatory cascade through TLR4 engagement, activating Nuclear Factor Kappa-Light-Chain-Enhancer of Activated B-Cells (NF-κB) and IRF3 signalling and resulting in systemic cytokine release, such as TNF-α, IL-6, IL-1β, and type I IFNs (van der Poll *et al.*, 2017). The resulting inflammation can induce widespread tissue injury and endothelial dysfunction, especially in the lungs and

vascular system, as observed in CAP and sepsis (Kumar, 2022). As a mitigating damage response, compensatory anti-inflammatory processes are initiated, such as immune cell reprogramming, reduced cytokine production, and epigenetic silencing of proinflammatory genes, a state of the immune system also known as innate immune tolerance (Biswas and Lopez-Collazo, 2009; Foster and Medzhitov, 2009).

Innate immune tolerance serves as a regulatory mechanism that balances immune overactivation while preserving essential antimicrobial functions (Foster *et al.*, 2007; Watson and Kim, 1963). This tolerance is recognised as a dynamic and context-dependent adaptation, extending beyond sepsis into non-septic inflammatory conditions, including atherosclerosis, rheumatoid arthritis, multiple sclerosis, and diabetes (Bernard *et al.*, 2023; Cavaillon *et al.*, 2020; Funes *et al.*, 2022; Nakatsuji *et al.*, 2021). The immunological process is characterised by transcriptional and metabolic rewiring of myeloid cells, notably monocytes and macrophages, involving both extrinsic (cytokine secretion) and intrinsic (chromatin state, cellular metabolism) factors (Domínguez-Andrés *et al.*, 2019; Kelly and O'Neill, 2015; Mishra and Ivashkiv, 2024; Qi *et al.*, 2021).

In the CAP context, emerging evidence highlights that circulating monocytes undergo substantial functional reprogramming in response to acute infection. Several studies have shown that monocytes from CAP patients exhibit a hyporesponsive phenotype upon *ex vivo* LPS stimulation, characterised by diminished production of TNF-α, IL-6, IL-1β, and IL-10 (Brands *et al.*, 2021; Christ *et al.*, 2018; Kaufmann *et al.*, 2018). This state may persist for weeks after resolution of infection, with IL-6 expression particularly affected, suggesting that immune tolerance is not only a transient effect of inflammation but may involve longer-term reprogramming at the progenitor level (Brands *et al.*, 2021; Dobrovolskaia *et al.*, 2003; Medvedev *et al.*, 2000).

In terms of epigenetic mechanisms, tolerant monocytes have been shown to exhibit altered DNA methylation patterns and histone modifications, including enrichment of suppressive marks such as Histone 3 Lysine 9 Di-Methylation and Lysine 27

Trimethylation, respectively (H3K9me2 and H3K27me3) at proinflammatory gene promoters (El Gazzar *et al.*, 2009; Foster *et al.*, 2007). Recent epigenomic studies in CAP have corroborated these patterns. For instance, Brands *et al.* (2021) reported hypermethylation of DNase-HS-Chr22 associated with cholesterol biosynthesis genes and reduced cytokine output, along with hypomethylation of genes linked to chromatin remodelling and inflammatory repression. These findings indicate that LPS-tolerant cells have a mechanism to control chromatin accessibility and transcription factor recruitment which enables antimicrobial gene expression but suppresses excessive inflammation.

The process of metabolic remodelling is also shown to be a vital characteristic of LPS-induced tolerance. Cells undergo metabolic changes toward glycolysis (Warburg effect) after TLR4 activation through Hypoxia-Inducible Factor (HIF)-1α stabilization which activates IL-1β transcription and proinflammatory gene expression (Tannahill *et al.*, 2013). The metabolic profile of tolerant cells undergoes a transformation from its initial state. The trained immunity models show dependence on oxidative phosphorylation and fatty acid metabolism, but tolerance models focus on energy conservation together with antioxidant defence and specific nutrient transporter and redox regulator upregulation to control immune responses without causing bioenergetic stress. The clinical scenarios of cardiopulmonary bypass and CAP show elevated serum markers human Multidrug Resistance Proteins (MRP)-8/14 and IL-10 together with Bursa (B)-cell Lymphoma (*BCL*) *3* and *STAT3* expression changes in monocytes which indicate that an anti-inflammatory state continues after recovery (Brands *et al.*, 2021).

Tolerant monocytes also downregulate key molecules involved in antigen presentation, such as HLA-DR and Class II Transactivator (*CIITA*), and upregulate suppressive cytokines like IL-10 and Transforming Growth Factor (TGF)-β, further impairing Thymocyte (T)-cell activation (del Fresno *et al.*, 2009; Monneret *et al.*, 2004). Chromatin analyses have demonstrated that only a subset of promoters, mainly of antimicrobial genes, retain acetylation marks and polymerase accessibility

after LPS exposure, while proinflammatory loci remain repressed (Foster *et al.*, 2007). This selective transcriptional control may be how tolerance can reduce harmful inflammation while preserving pathogen clearance.

In patient-derived monocytes, this dynamic is represented by shifts from hyperinflammatory to immunosuppressive states. Shalova *et al.* (2015) showed that the number of differentially expressed genes in monocytes from septic patients dropped from over 2,000 in the early phase to fewer than 80 in the immunosuppressive stage, reflecting a generally repressed transcriptome. HIF-1α has been identified as an essential regulator in this transition, modulating IL-1 receptor signalling and coordinating metabolic reprogramming toward a tolerance-prone phenotype (Tannahill *et al.*, 2013). At the same time, molecules including *SMAD6*, *CD180*, and *HIC1* are identified as putative transcriptional repressors, which modulate the immune response through interaction with histone deacetylases and chromatin regulators such as C-terminal Binding Protein (CtBP) 2 (Park *et al.*, 2019; Van Rechem *et al.*, 2010; You *et al.*, 2017).

LPS tolerance is understood as a uniform immunosuppressive state in most literature, however more recent studies suggest inter-individual variation in tolerance levels and transcriptional responsiveness. In this context, monocyte TNF-α production serves as a practical indicator for distinguishing between immune tolerance and trained immunity and provides a functional reference point for associated transcriptomic and epigenetic variation. These findings open new avenues for understanding how immune tolerance in CAP varies across individuals as a dynamic, patient-specific program with consequences for immune resilience and risk of secondary infections.

These findings provide the framework for the examination of the molecular basis of the multi-layered tolerance, including differential immune regulator expression, antioxidant enzymes, Extracellular Matrix (ECM) remodelling genes, and amino acid transport proteins. Elucidation of these alterations can guide the design of tailored

immunotherapies that either restore tolerance or facilitate recovery, depending on the clinical context.

2.1.4 Immune Tolerance in Sepsis

Phagocytic immune cells are essential components of the innate immune system, as they are responsible for engulfing pathogens, clearing apoptotic cells, and initiating inflammatory responses (Aderem and Underhill, 1999; Gordon, 2007). Among these, monocytes and macrophages act both as effector cells and as regulators of immune memory (Netea *et al.*, 2016). Upon exposure to pathogens or sterile insults, they can undergo durable functional reprogramming, or innate immune memory (Bowdish *et al.*, 2007; Netea *et al.*, 2011, 2016; Saeed *et al.*, 2014). This memory can manifest as either an enhanced pro-inflammatory response (trained immunity) or a dampened state of reactivity (tolerance), with consequences that are context-dependent and can be either protective or pathological (Saeed *et al.*, 2014). The process begins with the recognition of conserved microbial motifs, or Pathogen-Associated Molecular Patterns (PAMPs), such as Gram-negative bacteria surface LPS, and endogenous danger signals, or Damage-Associated Molecular Patterns (DAMPs) (Hayden and Ghosh, 2012; Matzinger, 2002; Takeuchi and Akira, 2010). These signals are detected by Pattern Recognition Receptors (PRRs), including TLRs, leading to the activation of downstream signalling cascades (Takeuchi and Akira, 2010) of which an important, central cascade, is the NF-κB pathway, which promotes the transcription of pro-inflammatory cytokines such as TNF, IL-1β, IL-12, and IL-18, initiating the immune response and recruiting other immune cells to the site of infection (Chan *et al.*, 2012; Deutschman and Tracey, 2014).

The fluctuating patterns between immune activation and suppression in innate memory prove particularly evident during sepsis. This condition shows how a necessary first immune response transitions into a harmful pattern in later stages. During the early phase of sepsis, acute infections trigger an intense inflammatory response which leads to extensive cytokine release and systemic inflammation that

causes tissue damage (van der Poll *et al.*, 2017). To limit further damage, the immune system initiates a counter-regulatory phase, where monocytes and macrophages enter a hypo-responsive state and reduce cytokine output upon subsequent stimulation, an event termed immunoparalysis or sepsis-induced immunosuppression, which may persist long after the resolution of infection, increasing susceptibility to secondary infections and poor outcomes (Angus and Van Der Poll, 2013; Freise *et al.*, 2019; van der Poll *et al.*, 2017). However, while this suppression helps restrain inflammation, unchecked or prolonged immune dysfunction has been associated with a range of chronic conditions including autoimmune disease, metabolic syndromes, and cancer (Biswas and Lopez-Collazo, 2009; Foster and Medzhitov, 2009). The immunological path during sepsis demonstrates how innate immune memory functions through dual capacities, showing how protective host mechanisms sometimes develop into disease-causing processes.

This immunosuppressive phase involves profound changes in antigen-presenting cells, apoptosis-mediated depletion of T-cells, B-cells, and DCs (Boomer *et al.*, 2012; Hotchkiss *et al.*, 2013a, 2013b) and downregulation of HLA-DR on the surface of monocytes (Pastille *et al.*, 2011; van der Poll *et al.*, 2017). These alterations leave patients more vulnerable to secondary infections, alongside lymphocyte exhaustion (Hotchkiss *et al.*, 2013b). In severe cases, ongoing immunosuppression can culminate in Persistent Inflammation, Immunosuppression, and Catabolism Syndrome (PICS) (Gentile *et al.*, 2012; van der Poll *et al.*, 2017). Research into immune tolerance and immunosuppression mechanisms enables the creation of post-sepsis immune deficiency treatment strategies while using trained immunity to boost vaccine efficacy (Netea *et al.*, 2016).

MRPs, particularly MRP-8 and MRP-14, appear to be important drivers of monocyte hyperresponsiveness in sterile inflammation, acting as endogenous TLR4 ligands (Cavaillon *et al.*, 2020; Vogl *et al.*, 2007, 2012), to induce a hyporesponsive state in monocytes similar to LPS tolerance (Austermann *et al.*, 2014; Freise *et al.*, 2019). A

hallmark of this state is the markedly reduced production of cytokines, including TNF-α, IL-1β, IL-6, and IL-10, upon subsequent LPS challenge (Austermann *et al.*, 2014; Freise *et al.*, 2019). Elevated MRP-8 and MRP-14 levels are consistently observed in sterile inflammatory conditions such as the Systemic Inflammatory Response Syndrome (SIRS) and during cardiopulmonary bypass, where they are associated with prolonged immune tolerance (Freise *et al.*, 2019).

At the molecular level, MRP-mediated monocyte tolerance involves two main signalling pathways. First, the Phosphatidylinositol 3-Kinase (PI3K)/Protein Kinase B (AKT)/Glycogen Synthase Kinase (GSK)-3β cascade disrupts NF-κB-dependent expression of pro-inflammatory genes, thus limiting cytokine secretion (Austermann *et al.*, 2014; Freise *et al.*, 2019). Concurrently, the IL-10-triggered STAT3/BCL3 pathway reinforces this hyporesponsive state by upregulating BCL3 and sustaining STAT3 activation, which has been shown to have a diminished tolerance effect when blocked or genetically deleted (Austermann *et al.*, 2014; Freise *et al.*, 2019). Moreover, pharmacological inhibition of GSK-3β mimics monocyte tolerance and has shown promise in improving survival in a mouse model of endotoxin shock (Freise *et al.*, 2019).

Epigenetic mechanisms further contribute to sustaining MRP-induced hyperresponsiveness. Euchromatic Histone-Lysine N-Methyltransferase 2 (*EHMT2*/G9a)-dependent chromatin modifications suppress pro-inflammatory gene expression, underscoring the importance of transcriptional and epigenetic regulation in controlling immune function (Austermann *et al.*, 2014; Freise *et al.*, 2019). Thus, a complex network of interconnected signalling pathways, transcriptional regulators, and epigenetic modifications that jointly determine the inflammatory capacity of monocytes during sterile inflammation is evidenced by recent research (Freise *et al.*, 2019).

2.1.5 CAP: Clinical and Immunological Implications

CAP remains a significant global health burden, with an estimated incidence ranging from 1.5 to 14 cases per 1,000 person-years worldwide (Prina *et al.*, 2015). Its impact is disproportionately severe in older adults and individuals with chronic comorbidities such as diabetes, Chronic Obstructive Pulmonary Disease (COPD), and cardiovascular disease. Compounding these risks, immunosuppression and recent healthcare exposure increase the likelihood of infection with drug-resistant pathogens, complicating clinical outcomes and management (Aliberti *et al.*, 2016; Hassen *et al.*, 2019; B. Liu *et al.*, 2019; Lu *et al.*, 2019; Regunath and Oba, 2025; Tsoumani *et al.*, 2023). In the United States, CAP is the eighth leading cause of death and the foremost infectious cause of mortality. Among patients requiring admission to Intensive Care Units (ICUs), the mortality rate exceeds 20% (Niederman and Torres, 2022; Simonetti *et al.*, 2016; Viasus *et al.*, 2023).

Importantly, CAP also stands as a leading cause of sepsis, a life-threatening condition marked by dysregulated host responses to infection (Angus and Van Der Poll, 2013; Brands *et al.*, 2020; Singer *et al.*, 2016). Sepsis-induced immunosuppression renders patients vulnerable to secondary infections, including hospital-acquired pneumonia. In a striking postmortem analysis of ICU patients who died of sepsis or septic shock, Torres *et al.*, (2014) reported that 76.6% had at least one unresolved septic focus at death, with pneumonia accounting for 41.3% of these foci, nearly half of which had gone undiagnosed during treatment. These findings illustrate the difficulty of identifying ongoing infection in the context of sepsis and highlight the immune system's impaired capacity for clearance under tolerogenic conditions.

Aging increases susceptibility to CAP through immunosenescence and progressive decline in respiratory defences. Diminished T-cell receptor diversity and reduced naïve T-cell output compromise adaptive immune surveillance (Ciabattini *et al.*, 2018; Shaw *et al.*, 2010; Tizazu *et al.*, 2022). Concurrently, age-related structural changes, including weakened cough reflex, impaired mucociliary clearance, and reduced respiratory muscle strength, limit physical pathogen elimination (J. Lee *et*

al., 2017; Tizazu *et al.*, 2022). Comorbidities further elevate the risk of severe complications such as acute respiratory distress syndrome (ARDS) and septic shock (Santesmasses *et al.*, 2020; Z. Wu and McGoogan, 2020). The COVID-19 pandemic highlighted this vulnerability, with older adults facing sharply increased hospitalisation and mortality from SARS-CoV-2–associated pneumonia (J. Lee *et al.*, 2017; Verity *et al.*, 2020; W. Wang *et al.*, 2020). Figure 2.1 illustrates the age-dependent increase in mortality for COVID-19, sepsis, and CAP, underscoring the heightened risk in older populations.

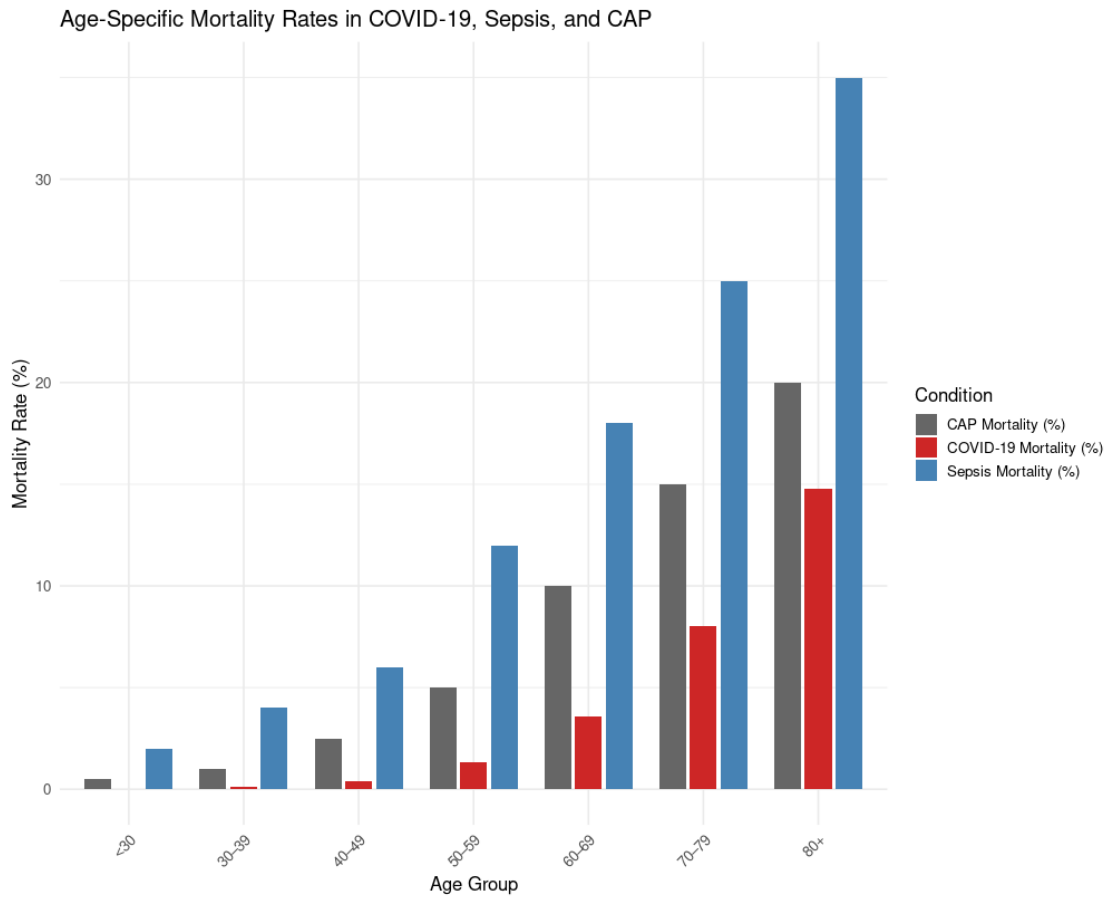

Figure 2.1. Age-specific mortality rates for COVID-19, sepsis, and CAP. *Bar plot displaying estimated mortality by age group for each disease, based on large-scale epidemiological and hospital-based data. COVID-19 mortality rises from ~0.02% (under 30 years) to ~14.8% (≥80 years); sepsis mortality from ~2% to ~35%; and CAP mortality from ~0.5% to ~20%. Data sources: Wu and McGoogan (2020); Verity et al. (2020); Rudd et al. (2020); Angus and van der Poll (2013); Singer et al. (2016); Ramirez et al. (2017); CDC (2024). Figure generated in RStudio (RStudio Team, 2020).*

The pathogenesis of CAP, like sepsis, involves an interplay between pro-inflammatory activation and anti-inflammatory counter regulation. Early immune responses involve an increase of cytokines such as TNF-α and IL-1β, which drive inflammation and pathogen clearance. However, concurrent regulatory responses, such as increased IL-10 and IL-1 Receptor Antagonist (IL-1RA), aim to contain excessive inflammation. When these processes become dysregulated, they may induce a state of immune tolerance marked by diminished leukocyte cytokine production and reduced capacity to control infection (Brands *et al.*, 2020; Hotchkiss *et al.*, 2013b, 2013a; López-Collazo and del Fresno, 2013; van der Poll and Opal, 2008). Notably, endotoxin tolerance has been observed in the early phases of CAP and correlates with ICU admission, multi-organ dysfunction, and worse survival outcomes (Cavaillon *et al.*, 2020; Otto *et al.*, 2022; Pena *et al.*, 2014; Schefold *et al.*, 2008).

Clinically, diagnosing CAP in elderly patients can be challenging, as classical symptoms such as fever, cough, and dyspnoea may be absent or muted. Instead, non-specific features such as delirium, functional decline, or altered mobility may predominate, contributing to delayed recognition and therapeutic intervention (Yoshikawa and Norman, 2017). A blunted febrile response further complicates early diagnosis, making timely antimicrobial therapy more difficult to initiate (Lim *et al.*, 2003; Majumdar *et al.*, 2011; Yoshikawa and Norman, 2017).

Microbial invasion in CAP typically results from aspiration of organisms colonising the oropharynx into the lower respiratory tract. When host defences are overwhelmed by pathogen load or virulence, this results in alveolar inflammation, leukocyte recruitment, and the clinical manifestations of CAP (Regunath and Oba, 2025). Pathogen identification is essential for guiding treatment, primarily because CAP can be caused by various pathogens, including bacteria, viruses, and, rarely, fungi. *Streptococcus pneumoniae* remains the most common bacterial cause, followed by *Haemophilus influenzae*, *Staphylococcus aureus*, *Moraxella catarrhalis*, and various Gram-negative Enterobacteriaceae. Drug-resistant strains, including Methicillin-

Resistant *Streptococcus aureus* (MRSA) and multidrug-resistant *Pseudomonas aeruginosa*, complicate treatment in individuals with prior healthcare exposure or antibiotic use (Gadsby and Musher, 2022; Palmore *et al.*, 2009; Regunath and Oba, 2025; Torres *et al.*, 2014).

Respiratory viruses are also considered major contributors to CAP, a shift enabled by advances in nucleic acid diagnostics, and commonly they are influenza viruses, rhinoviruses, Respiratory Syncytial Virus (RSV), parainfluenza, and human metapneumovirus (Jain *et al.*, 2015). The emergence of SARS-CoV-2 has further emphasised the clinical impact of viral pneumonia, especially in older adults and those with co-infections. Viral CAP is often complicated by bacterial superinfection, amplifying disease severity and immune dysfunction (Regunath and Oba, 2025).

Importantly, recent studies have revealed that monocytes in CAP patients undergo profound transcriptional and functional reprogramming. These cells exhibit hallmark features of LPS-induced immune tolerance, including diminished cytokine output, metabolic shifts, and downregulation of antigen presentation machinery, mirroring the tolerance state observed in sepsis (Brands *et al.*, 2020). This suggests that the mechanisms of monocyte tolerance explored earlier in this chapter are not limited to septic contexts but also play a role in shaping host responses in non-septic pneumonia.

As such, CAP offers a clinically relevant model to explore how monocyte reprogramming and immune tolerance evolve during infection. The following chapter investigates these mechanisms in depth through transcriptomic analysis of monocyte responses in CAP, focusing on TNF-α responsiveness, immune regulatory gene expression, and pathway enrichment following *ex vivo* LPS stimulation.

2.2 Computational Transcriptomics and Network Analysis of Monocyte Responses in CAP

Understanding the complex reprogramming of monocytes in CAP requires not only biological insight but also robust computational frameworks. In recent years, high-throughput RNA-seq has emerged as a powerful technique for dissecting cellular states at the transcriptomic level. When integrated with advanced bioinformatic pipelines, RNA-seq enables the identification of DEGs, inference of pathway activity, and reconstruction of regulatory and protein interaction networks that underlie immune phenotypes. This section outlines the computational strategies employed in the present study to investigate LPS-induced immune modulation in CAP monocytes. Key analytical stages include Quality Control (QC), read alignment, gene quantification, DEG analysis, functional enrichment, and context-specific PPI network construction, to provide a data-driven view of monocyte plasticity, supporting mechanistic hypotheses on immune tolerance in infectious disease.

2.2.1 RNA Sequencing Analysis Pipeline

RNA-seq is a powerful transcriptomic technique that enables comprehensive profiling of RNA molecules in a biological sample (Conesa *et al.*, 2016). In addition to quantifying gene expression levels, RNA-seq reveals alternative splicing events, transcript isoforms, and regulatory interactions central to cellular function and molecular signalling networks (J.-W. Chen *et al.*, 2023; Z. Wang *et al.*, 2009). This section outlines the core stages of RNA-seq data preprocessing as implemented in the present study, from raw read assessment to expression quantification. Together, these preprocessing steps ensure that RNA-seq data are high-quality, interpretable, and biologically meaningful. Accurate trimming, alignment, and quantification enable robust DEG analysis, providing a reliable basis for downstream pathway analysis, immune profiling, and molecular hypothesis testing in CAP-associated monocyte responses.

2.2.1.1 QC of Raw Sequencing Reads

The RNA-seq pipeline begins with stringent QC to ensure that raw sequencing reads are accurate and free of systematic bias (Conesa *et al.*, 2016; Williams *et al.*, 2017). This process evaluates key metrics such as per-base sequence quality, Guanine-Cytosine (GC) content, sequence duplication levels, and the presence of adapter contamination (Andrews, 2010; Soneson and Delorenzi, 2013). Tools like FastQC (Andrews, 2010) generate detailed per-sample QC reports across these parameters, while MultiQC (Ewels *et al.*, 2016) summarises them across multiple datasets to offer a global quality snapshot. QC is essential for identifying sequencing artifacts, RNA degradation, or technical variability that may compromise the integrity of downstream analyses (Conesa *et al.*, 2016). As a general benchmark, Phred scores serve as an established metric for base quality assessment, with a threshold of 20 or higher considered acceptable for most applications (Andrews, 2010; Gondane and Itkonen, 2023).

2.2.1.2 Adapter Removal and Read Trimming

Following QC, adapter removal and quality trimming are performed to eliminate sequencing artifacts and improve mapping accuracy (S. Chen *et al.*, 2018; Del Fabbro *et al.*, 2013). Adapter sequences are synthetic oligonucleotides added during library preparation, and their presence in reads can introduce alignment errors or artificial expression variation (Bolger *et al.*, 2014; Martin, 2011). Several tools are commonly used for adapter trimming and quality filtering in RNA-seq preprocessing, including Trimmomatic (Bolger *et al.*, 2014), Cutadapt (Martin, 2011), AdapterRemoval (Lindgreen, 2012), and fastp (S. Chen *et al.*, 2018). In this study, Trimmomatic was selected for its flexibility in handling single end (SE) reads and its highly tuneable quality filtering options (Bolger *et al.*, 2014). Compared to other widely used tools, Trimmomatic provides a broader range of trimming functionalities, allowing for better customisation to suit complex datasets (Bolger *et al.*, 2014). Its combination of versatility and precision made it the preferred tool for this analysis, where

stringent QC was essential. Post-trimming QC reports confirmed the effective removal of contaminants and improved base-call quality across all samples.

2.2.1.3 Read Alignment to the Reference Genome

With adapter-free, high-quality reads, the next stage is alignment, where reads are mapped to a reference genome or transcriptome to identify their genomic origin, a foundation step for accurate quantification and downstream interpretation (Conesa *et al.*, 2016; Oshlack *et al.*, 2010). Splice-aware aligners are essential in RNA-seq due to the intron-exon architecture of eukaryotic genes (Dobin *et al.*, 2013). In this study, Hierarchical Indexing for Spliced Alignment of Transcripts (HISAT) 2 (D. Kim *et al.*, 2019) was selected for read alignment due to its efficient memory usage, fast performance, and robust ability to detect exon-exon junctions. As a splice-aware aligner specifically developed for RNA-seq workflows, HISAT2 uses a hierarchical indexing strategy based on the Burrows-Wheeler Transform and Ferragina-Manzini index, enabling accurate mapping of reads across introns and splice sites (D. Kim *et al.*, 2019). Its favourable balance between alignment sensitivity and computational demand has made it a standard tool in large-scale transcriptomic studies (Schaarschmidt *et al.*, 2020).

Alternative aligners such as STAR (Dobin *et al.*, 2013) offer ultra-fast performance and high sensitivity for splice junction discovery through a two-pass alignment strategy. However, STAR's higher computational cost and isoform-level precision were not necessary for this study, which focused on gene-level expression changes. Bowtie2 (Langmead and Salzberg, 2012), while also efficient and accurate for contiguous reads, lacks native splice-awareness and is thus less optimal for transcriptome alignment.

HISAT2's accuracy in aligning monocyte transcriptomes under immune stimuli such as LPS, combined with its low resource requirements, ensured consistent, scalable,

and reproducible alignment across all samples (D. Kim *et al.*, 2019; Schaarschmidt *et al.*, 2020).

Aligned reads were stored in Sequence Alignment Map (SAM)/Binary Alignment Map (BAM) formats, which preserve read position, quality, and mapping statistics, serving as structured inputs for quantification and downstream analysis (Gondane and Itkonen, 2023). SAMTools (H. Li *et al.*, 2009) was used due to its standardisation, versatility, and seamless integration with HTSlib (Bonfield *et al.*, 2021), offering reliable performance for essential operations such as sorting, indexing, and format conversion (Bonfield *et al.*, 2021; H. Li *et al.*, 2009). While alternative tools like Picard[1] and BEDTools are also widely used (Ebbert *et al.*, 2016; Quinlan, 2014; Quinlan and Hall, 2010), SAMTools remains the most efficient and commonly adopted utility for high-throughput alignment processing in RNA-seq workflows (Pedersen and Quinlan, 2018).

2.2.1.4 Read Summarisation and Gene-Level Quantification

The final preprocessing step is read summarisation, where mapped reads are assigned to annotated gene features to generate a count matrix, which is a foundational dataset for differential expression analysis (Conesa *et al.*, 2016; Love *et al.*, 2014).

Accurate gene-level quantification is a critical step in RNA-seq analysis, particularly when assessing immune transcriptomes such as those of monocytes (Ranzani *et al.*, 2015; Soneson and Delorenzi, 2013). The choice of quantification tool and annotation database can substantially influence downstream results, especially in regions with alternative splicing or overlapping exons (Frankish *et al.*, 2019; S. Zhao *et al.*, 2015). The *featureCounts* function from the Subread package (Y. Liao *et al.*, 2014) has emerged as a widely adopted tool for gene-level read summarisation due

[1] Part of the Genome Analysis Toolkit; Available from http://broadinstitute.github.io/picard/

to its computational efficiency, flexibility with input formats, and robust handling of complex gene models and exon overlaps (Chandramohan *et al.*, 2013; Y. Liao *et al.*, 2014). It is particularly suited for large-scale RNA-seq datasets, offering a balance between speed and accuracy (Y. Liao *et al.*, 2014).

While alternative tools such as HTSeq (Anders *et al.*, 2015), Salmon (Patro *et al.*, 2017), and Kallisto (Bray *et al.*, 2016) are commonly used, each presents trade-offs. Both HTSeq and *featureCounts* discard ambiguous reads between isoforms, but HTSeq is more sensitive to annotation inconsistencies, which can introduce variability in gene-level estimates (Chandramohan *et al.*, 2013; Y. Liao *et al.*, 2014). In contrast, *featureCounts* maintains robust performance even in the presence of overlapping or incompletely annotated transcripts (S. Zhao *et al.*, 2015). Pseudo-alignment tools like Salmon and Kallisto, while excellent for transcript-level quantification, require additional steps to collapse transcript estimates into gene-level summaries, adding complexity when gene-centric analysis is the primary focus (Sarantopoulou *et al.*, 2021).

2.2.2 DEGs Identification and Analysis

DEG analysis is a fundamental technique in RNA-seq that enables the identification of genes with significant expression changes across different phenotypes (Anders and Huber, 2010; S. Liu *et al.*, 2021; Love *et al.*, 2014). It plays a crucial role in RNA-seq data processing, providing insights into gene regulation, disease mechanisms, and cellular responses, and it is widely employed in various biological research contexts, including studies on both human and plant (J.-W. Chen *et al.*, 2023; Costa-Silva *et al.*, 2023; Emmert-Streib and Glazko, 2011; McDermaid *et al.*, 2019; Rosati *et al.*, 2024). By integrating rigorous normalisation, statistical modelling, and visualisation techniques, DEG analysis has become indispensable for exploring gene responses to biological stimuli, unravelling complex BPs, and generating valuable insights into gene function (Costa-Silva *et al.*, 2023; McDermaid *et al.*, 2019).

The differential expression analysis pipeline typically follows several key steps. The first involves data preprocessing and normalisation to reduce technical variability and improve comparability across samples (S. Liu *et al.*, 2021; Rosati *et al.*, 2024). Commonly used statistical frameworks such as *DESeq2* (Anders and Huber, 2010; Love, 2024; Love *et al.*, 2014), *edgeR* (McCarthy *et al.*, 2012; Robinson and Smyth, 2007), and others model count data using negative binomial distributions and apply distinct normalisation strategies. The *DESeq2* package was selected for its robust handling of non-normal count distributions, mean-variance dependence, and small sample sizes (Lönnstedt and Speed, 2002). *DESeq2* models dispersion across genes, often outperforming alternatives such as *edgeR* (McCarthy *et al.*, 2012; Robinson and Smyth, 2007) and Bayesian methods like *DSS*, *baySeq*, and *ShrinkBayes* (Hardcastle and Kelly, 2010; Van De Wiel *et al.*, 2013; H. Wu *et al.*, 2013), especially in datasets with small sample sizes or over dispersed count data (Rapaport *et al.*, 2013). *DESeq2* (Love *et al.*, 2014) applies a Negative Binomial Generalised Linear Model (GLM) to handle variability in RNA-seq data (McCullagh, 2019). Moreover, *DESeq2* uses a geometric mean-based normalisation (median-of-ratios) to correct for sequencing depth and compositional bias, while *edgeR* implements the Trimmed Mean of M-values method under the assumption that most genes are not differentially expressed (Finotello *et al.*, 2014; Oshlack *et al.*, 2010; Rapaport *et al.*, 2013). In this study, batch correction was not applied, as all samples were sequenced within a single experimental run, eliminating the risk of batch-related technical confounding. This design choice ensured that normalisation procedures were sufficient to account for technical variation and further correction steps, such as surrogate variable analysis (Leek and Storey, 2007) or ComBat (Johnson *et al.*, 2007), were not required.

Alternative approaches such as NOISeq (Tarazona *et al.*, 2011, 2015) and SAMseq (J. Li and Tibshirani, 2013), which do not rely on predefined statistical distributions, offer flexibility for datasets with limited replicates or those sensitive to outliers (J. Li and Tibshirani, 2013; Tarazona *et al.*, 2011). Hybrid methodologies, like the Consexpression approach, combine multiple tools to improve DEG detection by

leveraging consensus analysis across parametric and non-parametric methods, thus enhancing reliability (Costa-Silva *et al.*, 2017, 2023). Once normalised, the data undergoes statistical modelling to identify DEGs, and multiple testing corrections are applied to control False Discovery Rates (FDRs) (S. Liu *et al.*, 2021; Love *et al.*, 2014; Robinson and Smyth, 2007). However, challenges remain in selecting appropriate cutoff thresholds for Logarithm (base 2) of the Fold Change (log_2FC) and *p*-values, as these must be tailored to the specific dataset and experimental conditions (Souza *et al.*, 2018; Tarazona *et al.*, 2011).

Visualisation plays a critical role in making DEG analysis results interpretable and actionable. Common methods include mean–average (MA) plots, which show the relationship between mean expression and log_2FC, and volcano plots, which combine effect size and statistical significance to summarise DEGs intuitively (Andrade, 2019; Evans *et al.*, 2018; Farahbod and Pavlidis, 2019; McDermaid *et al.*, 2019; Rosati *et al.*, 2024; Wodrich *et al.*, 2021). Heatmaps complement these by displaying gene expression patterns across conditions, highlighting clusters and trends within complex datasets (McDermaid *et al.*, 2019). The clarity and validity of these visualisations depend on appropriate scaling, well-defined statistical thresholds, and adequate biological replication to ensure robust interpretation (S. Liu *et al.*, 2021; McDermaid *et al.*, 2019). In this study, these standard visualisation approaches were applied to summarise the monocyte transcriptomic response to LPS stimulation and to support the identification of biologically meaningful DEG signatures.

DEG analysis continues to evolve, with emerging machine learning techniques adding new dimensions to the process. For example, Genetic Algorithm k-Nearest Neighbours aids in gene selection, while Convolutional Neural Networks, which are often trained on graph-based or structured representations of transcriptomic data, are increasingly used to identify critical transcripts (L. Li *et al.*, 2001; Y. Li *et al.*, 2017; Lyu and Haque, 2018; Mostavi *et al.*, 2020; Pratama *et al.*, 2021). These machine learning methods complement traditional statistical models and improve DEG

detection, helping researchers identify biologically significant genes with greater accuracy (J.-W. Chen *et al.*, 2023).

Despite the significant advancements, DEG analysis faces inherent challenges, such as the complexities introduced by biological variability, alternative splicing, and sequencing noise (Soneson and Delorenzi, 2013). As computational methods continue to improve, integrating parametric, non-parametric, and hybrid approaches is expected to further enhance the robustness and accuracy of DEG detection (Costa-Silva *et al.*, 2023).

2.2.3 Pathway Analysis: Gene set, Gene Ontology and Functional Enrichment Analysis

Pathway analysis and functional enrichment are essential methodologies for interpreting gene expression data, enabling insights into biological mechanisms underlying experimental conditions (Bayerlová *et al.*, 2015; J.-W. Chen *et al.*, 2023; Conesa *et al.*, 2016; Gondane and Itkonen, 2023; Q. Huang *et al.*, 2018; Jaakkola and Elo, 2016). These approaches contextualise DEGs within biological pathways, enhancing the interpretation of high-throughput omics studies (J.-W. Chen *et al.*, 2023; Gondane and Itkonen, 2023; T. Wu *et al.*, 2021).

Gene set enrichment approaches help interpret gene expression data by contextualising DEGs within biological pathways. Two major strategies, Over-Representation Analysis (ORA) and GSEA, were employed in this study to capture complementary layers of biological meaning.

ORA, implemented through GO enrichment using the *clusterProfiler* package (T. Wu *et al.*, 2021; S. Xu *et al.*, 2024; G. Yu *et al.*, 2012), identifies functional categories that appear more frequently among differentially expressed genes than expected by chance. This approach emphasises discrete gene lists, making it well-suited for capturing high-confidence signals linked to sharply regulated processes such as immune activation or metabolic shifts (J.-W. Chen *et al.*, 2023; Gondane and Itkonen,

2023). GSEA, by contrast, does not rely on a predefined DEG threshold. Instead, it evaluates whether predefined gene sets are consistently enriched toward the top or bottom of the full ranked expression dataset (Mootha *et al.*, 2003; Subramanian *et al.*, 2005). In this study, non-pre-ranked GSEA was conducted using the standalone software from the Broad Institute (Mootha *et al.*, 2003; Subramanian *et al.*, 2005), using phenotype-based label permutations to uncover coordinated expression programmes. This approach proved especially valuable for detecting subtle yet biologically coherent shifts, such as tolerogenic or IFN-related signatures, that might not reach strict significance in a differential expression framework.

Together, ORA and GSEA allowed for the detection of both sharply overrepresented pathways and more diffuse transcriptional trends, providing a multi-layered view of the BPs engaged during monocyte reprogramming.

Pathway analysis methods can be categorised based on whether they incorporate unstructured gene collections, disregarding known gene and protein interactions (Q. Huang *et al.*, 2018). Conversely, topology-based methods integrate pathway structural organisation, representing pathways as networks of nodes (genes or proteins) and edges (interactions) (Q. Huang *et al.*, 2018). Notable topology-based methods include Signalling Pathway Impact Analysis (SPIA) (Draghici *et al.*, 2007), iPathwayGuide (Ahsan and Drăghici, 2017), Pathway Enrichment Analysis (PWEA) (Ibrahim *et al.*, 2014), and Pathway Regulation Score (PRS) (Reimand *et al.*, 2019). *clusterProfiler* also supports comparative functional profiling, enabling enrichment analyses across experimental conditions (T. Wu *et al.*, 2021; S. Xu *et al.*, 2024).

Statistical testing plays a critical role in pathway analysis, ensuring that observed pathway enrichment is not due to random variation. Common statistical methods include Fisher's exact test, used by DAVID (D. W. Huang *et al.*, 2009), the Kolmogorov-Smirnov test in GSEA (Charmpi and Ycart, 2015), and Wilcoxon signed-rank and Bootstrapping tests (Q. Huang *et al.*, 2018; Nam and Kim, 2008). The PATHChange package integrates multiple statistical approaches, including Bootstrapping, Fisher's exact test, and Wilcoxon signed-rank test (Fontoura *et al.*,

2016; R Core Team, 2023). Additionally, Graphite provides a unified interface for topology-based methods such as TopologyGSA, clipper, DEGraph, and SPIA (Sales *et al.*, 2012).

Several databases provide curated gene sets and pathway annotations to support pathway analysis. Key resources include the Kyoto Encyclopaedia of Genes and Genomes (KEGG) (Kanehisa *et al.*, 2012, 2017), PathwayCommons (Cerami *et al.*, 2012), Reactome (Fabregat *et al.*, 2016, 2018), and WikiPathways (Kelder *et al.*, 2012). The Molecular Signatures Database (MSigDB) (Liberzon *et al.*, 2015) is extensively used for GSEA studies, ensuring access to well-annotated biological pathways. *clusterProfiler* extends its capabilities by integrating custom annotations for disease ontology (G. Yu *et al.*, 2015), gene-disease associations (G. Yu, 2018b), and specialised pathway resources such as Reactome and WikiPathways (Fabregat *et al.*, 2016, 2018; Kelder *et al.*, 2012).

Despite its strengths, pathway enrichment analysis has limitations, including inconsistencies between databases regarding gene composition and biases toward well-characterised pathways (Reimand *et al.*, 2019). Additionally, pathway boundaries can be somewhat arbitrary, affecting enrichment results (Reimand *et al.*, 2019). Tools like GOSemSim help refine GOresults by eliminating redundant terms based on semantic similarity (Ashburner *et al.*, 2000; The Gene Ontology Consortium, 2019; T. Wu *et al.*, 2021; S. Xu *et al.*, 2024, p. 20; G. Yu, 2018b; G. Yu *et al.*, 2012).

Visualisation of pathway enrichment results is crucial for interpretation. *clusterProfiler* implements the *enrichplot* sub-package, leveraging *ggplot2* for customisable graphical representations (Wickham *et al.*, 2019; G. Yu, 2018a). This visualisation framework enhances interpretability by providing flexible customisation options based on the grammar of graphics (G. Yu, 2018a).

By integrating diverse statistical approaches and leveraging curated pathway databases, pathway analysis remains a powerful tool for elucidating biological

mechanisms in genomic studies. The combination of gene set-based and topology-based approaches enables a more comprehensive understanding of cellular processes, ultimately improving the interpretation of high-throughput omics data (J.-W. Chen *et al.*, 2023; Gondane and Itkonen, 2023; Q. Huang *et al.*, 2018; Reimand *et al.*, 2019; T. Wu *et al.*, 2021; S. Xu *et al.*, 2024).

2.2.4 PPI Networks

Proteins operate within complex, interconnected networks rather than in isolation. To capture the functional architecture of the cell, PPI networks are often filtered using transcriptomic data to reflect context-specific expression patterns (Chatr-Aryamontri *et al.*, 2017; Greene *et al.*, 2015). In eukaryotic systems, the construction of condition- or tissue-specific PPI networks increasingly relies on RNA-seq data to include only interactions involving actively transcribed genes under the experimental conditions (Barshir *et al.*, 2014; Bossi and Lehner, 2009; Lopes *et al.*, 2011; Szklarczyk *et al.*, 2023). This refinement enhances biological relevance and interpretability by eliminating interactions involving non-expressed or irrelevant proteins (Greene *et al.*, 2015; Szklarczyk *et al.*, 2023).

Advanced computational frameworks have been developed to integrate interactome and transcriptome data. For example, Murali *et al.* (2014) proposed methods for tailoring global interactomes using expression thresholds from RNA-seq. Szklarczyk *et al.* (2023), through the STRING database, further allow functional enrichment of filtered networks across tissues. Singh *et al.* (2018) and Hollander *et al.* (2021) introduced transcriptome-informed network rewiring models, which trace interaction dynamics under different conditions, shedding light on the plasticity of signalling pathways. Together, these approaches enable more accurate modelling of biologically meaningful networks and reveal regulatory mechanisms that are active in a specific cellular context (Greene *et al.*, 2015).

PPI networks exhibit a scale-free structure, where a small number of hub proteins play a critical role in maintaining network stability (Hollander *et al.*, 2021). These networks also contain tightly connected clusters that often correspond to functional protein complexes (Girvan and Newman, 2002; Hollander *et al.*, 2021). Identifying these complexes is essential, as co-expressed proteins frequently share similar biological functions (Hollander *et al.*, 2021). Structural domain information further aids in predicting stable protein interactions and analysing Domain-Domain Interactions, offering deeper mechanistic insights into protein functionality (Aloy and Russell, 2006; Ozawa *et al.*, 2010; Will and Helms, 2016). Additionally, alternative splicing plays a significant role in shaping PPIs, as most human genes produce multiple isoforms, each capable of interacting with distinct sets of partners (Yang *et al.*, 2016). This highlights the necessity of isoform-specific analysis to fully understand the complexity of protein interaction networks (Buljan *et al.*, 2012; Ellis *et al.*, 2012; Pan *et al.*, 2008; Yang *et al.*, 2016).

Several computational platforms have been developed to facilitate PPI network analysis. The STRING database aggregates protein interaction data from more than 10,000 species, integrating experimental findings, computational predictions, and literature-based associations (Szklarczyk *et al.*, 2023). It compiles information from multiple repositories, including BioGRID (Oughtred *et al.*, 2021), DIP (Salwinski *et al.*, 2004), PDB (Berman *et al.*, 2000), and IntAct (Orchard *et al.*, 2014), as well as functional interaction annotations from KEGG (Kanehisa *et al.*, 2012, 2017), Reactome (Fabregat *et al.*, 2016, 2018), and GO (The Gene Ontology Consortium, 2019). By assigning confidence scores to interactions, STRING allows researchers to evaluate the reliability of predicted associations (Szklarczyk *et al.*, 2023). The latest STRING 12.0 update introduced machine learning-based improvements in co-expression prediction and refined confidence estimation for experimental data (Szklarczyk *et al.*, 2023).

In addition to STRING, other tools provide specialised functionality for PPI analysis. NetworkAnalyst offers a web-based platform for interactive PPI network

exploration, enabling users to input gene or protein lists, build networks from curated datasets, and analyse network topology to identify key hubs (Xia *et al.*, 2014). The platform supports module detection to identify highly interconnected functional subgroups and enrichment analysis to associate networks with biological pathways. NetworkAnalyst also features real-time visualisation capabilities, though it is optimised for networks with fewer than 5,000 nodes to maintain computational efficiency (Xia *et al.*, 2014).

For tissue-specific PPI analysis, DifferentialNet (Basha *et al.*, 2018) integrates experimental interaction data with RNA-seq expression profiles from the Genotype-Tissue Expression consortium (GTEx) (GTEx Consortium, 2013) and the Human Protein Atlas (HPA) (Uhlén *et al.*, 2015). It assigns tissue-specific scores to interactions based on gene expression levels, allowing researchers to investigate how PPIs vary across different tissues (Basha *et al.*, 2018). The tool's Cytoscape.js-powered interface (Franz *et al.*, 2016) enables users to visualise and filter differential interactions based on expression patterns (Basha *et al.*, 2018). This platform is particularly useful for studying context-dependent regulatory mechanisms and exploring proteins with tissue-specific interaction dynamics (Basha *et al.*, 2018).

The computational tools offer essential frameworks to analyse PPI networks across various biological contexts. Researchers can achieve better understanding of protein function and interaction specificity and cellular network dynamics through the combination of experimental data with advanced computational methods.

2.3 Literature Review

As previously presented, LPS plays a dual role in innate immune regulation. It initially activates monocytes via TLR4, triggering robust cytokine release (Ngkelo *et al.*, 2012), however, sustained exposure leads to a tolerant state marked by suppressed pro-inflammatory responses and increased expression of anti-inflammatory mediators (Cavaillon and Adib-Conquy, 2006; Mages *et al.*, 2007). This adaptive

reprogramming, while protective against tissue damage, compromises immune vigilance and has been linked to poor clinical outcomes in sepsis (Cavaillon and Adib-Conquy, 2006; Monguió-Tortajada *et al.*, 2018). Increasing evidence suggests that a similar monocyte-tolerant phenotype may occur in non-septic conditions like CAP, potentially contributing to prolonged recovery, reinfection risk, and impaired immune function (Dorneles *et al.*, 2023; Teixeira *et al.*, 2021). Metabolic shifts, such as altered mitochondrial respiration and glycolysis, appear to underpin these functional changes in monocytes (Lachmandas *et al.*, 2016).

Endotoxin tolerance is an adaptive process where monocytes become hyporesponsive to repeated LPS stimulation, reducing inflammation but potentially compromising host defence. Foundational work by van der Poll *et al.* (1996) showed that a single LPS dose in healthy humans suppressed TNF-α, IL-6, and IL-10 production upon re-exposure, with plasma from treated individuals inhibiting cytokine release in naïve donor blood, implying a role for circulating mediators.

This reprogramming extends beyond cytokines. Weijer *et al.* (2002) reported impaired IFN-γ signalling, reduced IL-12, and downregulated MHC II, indicating broader immunosuppression. Key negative regulators like IL-10 and IL Receptor-Associated Kinase (IRAK)-M have been implicated: van't Veer *et al.* (2007) showed that LPS exposure upregulates IRAK-M and downregulates IRAK-1, curbing TLR signalling and sustaining monocyte unresponsiveness even after IL-10 normalisation.

Epigenetic remodelling also plays a central role. Saeed *et al.* (2014) demonstrated lasting reductions in H3K27ac at tolerised gene loci, dampening cytokine transcription. Novakovic *et al.* (2016) showed that β-glucan treatment could reverse this silencing, restoring immune responsiveness.

On the metabolic front, Tannahill *et al.* (Tannahill *et al.*, 2013) linked succinate accumulation to HIF-1α-mediated IL-1β induction, a process dampened in tolerant cells. Grondman *et al.* (Grondman *et al.*, 2019) found reduced glycolysis, oxidative

phosphorylation, and pentose phosphate activity in tolerised monocytes, functional deficits partially reversible by IFN-γ (Leentjens *et al.*, 2012).

Together, these studies reveal tolerance as a complex cellular adaptation involving epigenetic, transcriptional, and metabolic rewiring. While initially protective, prolonged tolerance in contexts like sepsis or CAP may drive immune dysfunction and poor clinical outcomes (Hotchkiss *et al.*, 2013b).

To investigate these dynamics, a structured literature review was conducted focusing on LPS-induced monocyte tolerance, with attention to transcriptional reprogramming, metabolic alterations, cytokine suppression, and relevance to respiratory infections. Searches were conducted in PubMed and NCBI-GEO using combinations of keywords including "monocytes," "LPS," "immune tolerance," "trained immunity," "endotoxin," and "immune suppression." Inclusion criteria prioritised peer-reviewed, full-text studies published in English and based on RNA-seq or comparable transcriptomic platforms. Exclusion criteria ruled out preprints, reviews, pediatric studies, and research unrelated to infectious tolerance. Manual screening of references from key primary and review articles supplemented database searches to ensure comprehensive coverage. This process yielded a curated body of literature characterising LPS-induced tolerance in human models, highlighting common pathways across septic and non-septic contexts, and revealing a need for deeper investigation into monocyte dysfunction during CAP.

While substantial progress has been made in understanding LPS-induced immune tolerance, the existing literature reveals several limitations that constrain both mechanistic insight and clinical translation in non-septic respiratory infections.

2.3.1 Innate Immune Tolerance

Historically, much of what is known about monocyte immune tolerance has been derived from the study of sepsis and *in vivo* endotoxemia models. These systems have provided critical insights into how dysregulated systemic inflammation, often

triggered by severe infection, leads to a suppressive immune state. For example, Wiersinga *et al.* (2009) demonstrated that monocytes isolated from patients with sepsis caused by *Burkholderia pseudomallei* exhibited significantly reduced production of TNF-α, IL-1β, and IL-8 following LPS stimulation. This functional impairment was accompanied by elevated expression of IRAK-M and diminished levels of IRAK-1, which are molecular markers indicative of an immunosuppressive reprogramming of monocyte function. Importantly, higher IRAK-M levels at admission were associated with increased mortality, underlining the clinical significance of this altered immune state.

Shalova *et al.* (2015) provided further evidence of this phenomenon through transcriptomic profiling of monocytes from septic patients, revealing an early burst of pro-inflammatory cytokine expression followed by a marked downregulation upon repeated stimulation. Notably, while monocytes entered a tolerised state, they maintained essential antimicrobial functions such as phagocytosis and VEGF-A expression. These findings underscored that immune tolerance in sepsis is not a blanket shutdown of function, but a selective reprogramming of immune responses.

Despite the valuable knowledge gleaned from these models, they are limited in scope. *In vivo* endotoxemia models and sepsis cohorts are inherently biased toward systemic inflammation, often relying on high-dose LPS exposure or severe infection (Kox *et al.*, 2011; van 't Veer *et al.*, 2007). These conditions do not mirror the immune dynamics present in localised infections like CAP, which frequently lacks the profound systemic inflammatory shock seen in sepsis. Consequently, findings derived from these models may not fully generalise to respiratory infections that involve more compartmentalised immune responses.

This disconnect is well illustrated by Hoogerwerf *et al.* (2010), who found that local LPS exposure in the lung induces immune priming rather than tolerance, suggesting that the anatomical site of inflammation plays a critical role in shaping immune outcomes. Nevertheless, the impact of spatial context on monocyte reprogramming

has received limited attention in the literature, particularly with respect to infections confined to the pulmonary compartment.

2.3.2 Evidence of Immune Tolerance in CAP

Recent studies have begun to challenge the assumption that monocyte immune tolerance is exclusive to sepsis or endotoxemia. There is now growing recognition that non-septic infections, such as CAP, can also drive a tolerised monocyte phenotype. For instance, Brands *et al.* (2020) showed that patients with CAP exhibited diminished production of TNF-α, IL-1β, IL-6, and IL-10 in response to LPS during the acute phase of illness. Importantly, this blunted response was observed even in CAP patients without sepsis, thereby decoupling immune suppression from systemic inflammation and suggesting a broader relevance of immune tolerance.

Building on this, Brands *et al.* (2021) applied RNA sequencing to LPS-stimulated monocytes from CAP patients, identifying nearly 3,000 DEGs. Their findings revealed widespread transcriptional downregulation of cytokine signalling and antigen presentation pathways during the acute phase, some of which, like IL-6 production, remained impaired even a month post-hospitalisation. The study also pointed to transcriptomic shifts in cholesterol biosynthesis and localised DNA methylation changes, indicating that metabolic and epigenetic reprogramming may underpin the development of immune tolerance in CAP.

Further support for this comes from Otto *et al.* (2022), who analysed the metabolic profiles of monocytes from CAP patients. They observed elevated pyruvate levels and upregulated glycolytic genes, even though cytokine output remained suppressed after LPS stimulation. Interestingly, pyruvate concentrations positively correlated with IL-10 and IL-1β levels, suggesting that the observed metabolic alterations may serve regulatory, rather than purely inflammatory, functions.

2.3.3 Mechanistic Tools and Gaps in CAP Research

To investigate these complex immune alterations, many studies have employed *ex vivo* LPS stimulation models in conjunction with transcriptomic profiling. This approach allows for the dissection of cell-intrinsic regulatory networks in a controlled experimental setting. For example, Pinilla-Vera *et al.* (2016) used *ex vivo* LPS stimulation of alveolar macrophages from healthy individuals and uncovered gene expression profiles enriched for inflammatory, IFN-related, and metabolic pathways. These findings established the validity of this approach in modelling innate immune responses.

In clinical contexts, this methodology has been extended to sepsis and COVID-19. Shalova *et al.* (2015) and Maher *et al.* (2022) used RNA-seq to show that prolonged or repeated LPS exposure in monocytes results in transcriptional suppression of cytokine and IFN signalling pathways, alongside the upregulation of inhibitory regulators such as IRAK-M and the suppression of antigen presentation machinery.

Despite the widespread use of such approaches, CAP remains poorly represented in transcriptomic studies of immune tolerance. Domínguez-Andrés *et al.* (2019) highlighted the potential of integrated omics approaches by combining transcriptomic, epigenetic, and metabolomic data to show that LPS-tolerised monocytes undergo chromatin silencing, diminished glycolytic flux, and mitochondrial dysfunction. Yet few studies have applied similar integrative frameworks to CAP.

Brands *et al.* (2021) remains the most comprehensive CAP study using RNA-seq, but even this dataset has not been widely replicated or extended. The absence of stratified analyses by factors such as sex, cytokine responsiveness, or stage of recovery has hindered efforts to identify robust tolerance signatures or develop personalised therapeutic strategies. The present study aims to address this gap by employing *DESeq2* to analyse LPS- and media-treated monocytes from CAP patients, with stratification by sex and immune phenotype to capture interindividual variation in monocyte responses.

2.3.4 Conceptual and Methodological Limitations

Several conceptual and methodological challenges continue to limit progress in this area. One critical issue is the assumption of homogeneity in immune tolerance. Recent studies suggest that monocyte responses are highly heterogeneous. For instance, Brands *et al.* (2021) reported that IL-6 suppression persisted in some CAP patients even after clinical recovery, indicating that tolerance exists on a continuum shaped by factors such as metabolic status, sex, and prior inflammatory exposure. However, most current analyses apply a group-level lens, which can obscure meaningful interindividual variation.

Another challenge lies in the functional assays used to infer tolerance. *Ex vivo* cytokine production, though widely used, may not reliably reflect systemic immune status. Jansen *et al.* (2023), for example, found that TNF-α levels measured *ex vivo* did not correlate with *in vivo* cytokine responses in healthy volunteers challenged with LPS, raising questions about the translational relevance of these assays, particularly in complex clinical settings like CAP.

Finally, the lack of specific biomarkers for early detection and stratification of immune tolerance in CAP represents a major translational barrier. In sepsis, markers such as HLA-DR, TNF-α, and IL-6 have been used to infer immune suppression (Conway Morris *et al.*, 2018; Monneret *et al.*, 2006), but their utility in CAP remains unproven. The localised and heterogeneous nature of CAP complicates biomarker interpretation, and conventional cytokine-based assays lack the sensitivity to detect subtle shifts in immune function (Menéndez *et al.*, 2012; Póvoa *et al.*, 2024). This hampers the development of targeted immunomodulatory therapies. While experimental interventions such as IFN-γ, β-glucan, and histone deacetylase inhibitors have shown promise in reversing immune tolerance (Leentjens *et al.*, 2012; Novakovic *et al.*, 2016; Ripamonti *et al.*, 2022), there is no consensus on how to identify suitable candidates for such treatments. Developing robust transcriptomic or metabolomic classifiers to flag immune-tolerant patients at risk for poor outcomes

or secondary infections remains an urgent clinical need (W. Chen *et al.*, 2024; Rashid *et al.*, 2024).

2.4 Summary

Monocytes are critical regulators of the innate immune response, capable of both promoting inflammation and initiating immune resolution. Upon exposure to microbial components such as LPS, monocytes can develop a state of immune tolerance, marked by reduced cytokine output, transcriptional reprogramming, and altered metabolic activity. While this phenomenon has been well-documented in sepsis, emerging evidence shows that similar tolerogenic states also arise in non-septic conditions like CAP, even in the absence of systemic inflammation.

In CAP, monocytes have been shown to retain immune-suppressive signatures during and after acute illness, including reduced TNF-α and IL-6 production, suppressed antigen presentation, and shifts in glycolysis and lipid metabolism. Transcriptomic studies highlight widespread downregulation of inflammatory pathways and persistent epigenetic changes, suggesting long-term immune reprogramming. However, CAP remains underrepresented in immune tolerance research, which has traditionally focused on sepsis or endotoxemia models.

To explore these dynamics, this study uses *ex vivo* LPS stimulation and RNA-seq of monocytes from CAP patients, integrating DEG analysis with metadata on cytokine responsiveness and sex. This approach aims to map the molecular architecture of monocyte tolerance in pneumonia and identify context-specific immune alterations with relevance to patient outcomes and therapeutic targeting.

3. METHODOLOGY

This chapter outlines the methodological and computational framework employed to investigate monocyte transcriptional responses during CAP. Given the study's focus on gene expression profiling, particular emphasis was placed on ensuring data quality, analytical reproducibility, and interpretability. The workflow integrates established bioinformatics tools for RNA-seq preprocessing, alignment, and count quantification, followed by robust statistical modelling for DEG analysis. This chapter details each component of the analytical pipeline, including software choices, statistical modelling in R, and downstream functional annotation.

3.1 Methodology Workflow: Pre-processing, Quality Assessment, DEG, and Downstream Analysis

This project utilised a robust technology stack comprising specific libraries, software tools, and their respective versions to ensure reproducibility and uphold data integrity throughout the analysis. The Methodology section details the use of publicly available tools and software, complemented by vignettes for data analysis (Figure 3.1). Importantly, no new software or algorithms were developed, nor was any laboratory work conducted to generate the data analysed in this dissertation.

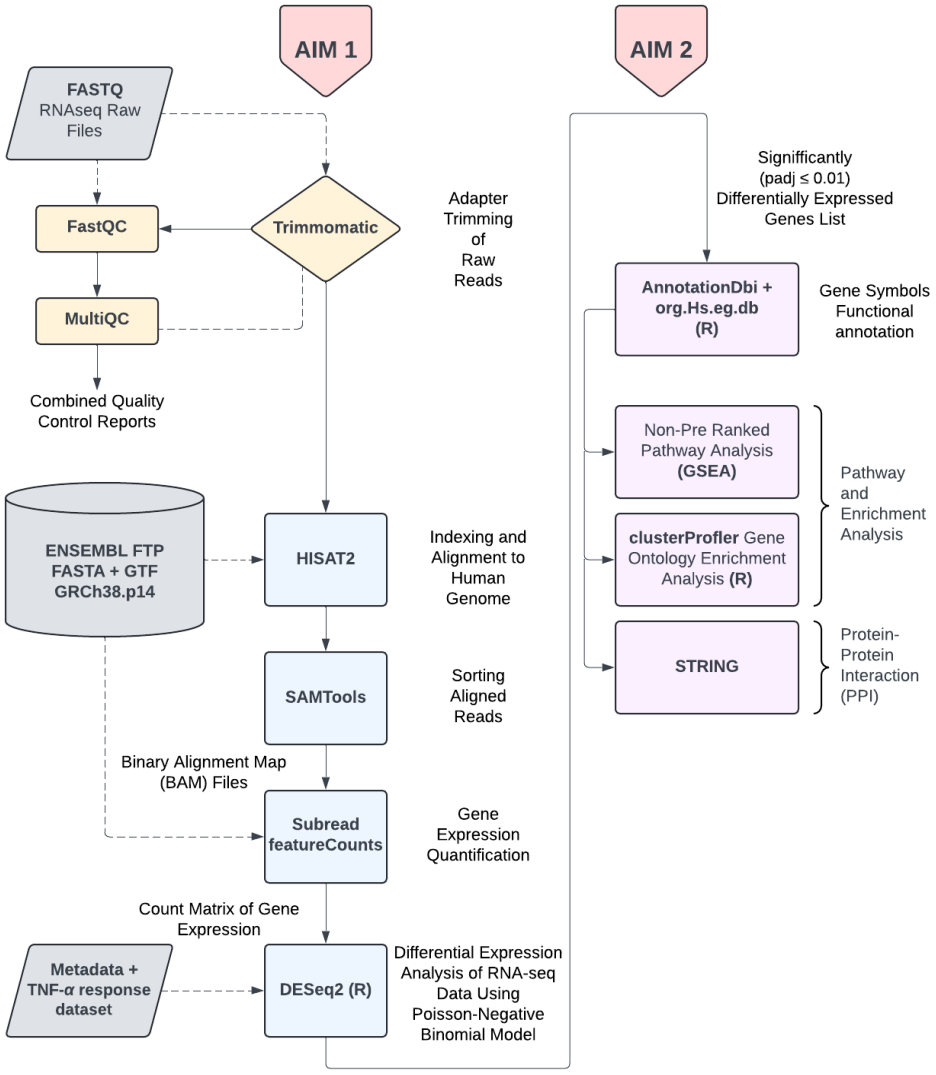

Figure 3.1. RNA-seq Data Pre-processing, Differential Expression Analysis, and Downstream Functional Analysis Pipeline. *The workflow for RNA-seq data processing and analysis consisting of two main objectives. In Aim one (yellow boxes), raw RNA-seq Fast Alignment Search Tool-Quality (FASTQ) files underwent QC using FastQC and MultiQC, followed by adapter trimming with Trimmomatic. Trimmed reads were aligned to the ENSEMBL Assembly and Patch Version 14 (GRCh38.p14) human genome using HISAT2 and sorted with SAMTools. Gene expression was quantified using Subread featureCounts to generate a count matrix, and differential expression analysis was performed using DESeq2 with a Poisson-Negative Binomial model. Aim two (purple boxes) focused on downstream analysis of DEGs, including functional annotation with AnnotationDbi and org.Hs.eg.db, pathway analysis with GSEA, gene ontology enrichment analysis using clusterProfiler, and PPI network analysis with STRING. Grey boxes represented provided or publicly available data, while dotted lines and arrows indicated data flow of supplementary or provided data or outputs from QC steps guiding downstream decisions, such as read trimming. Tools, software, and packages were highlighted in bold. The flowchart was created using the publicly available web-based platform draw.io (JGraph Ltd., n.d.)*

3.2 Study population and Ethics Declaration

The seminal research for this dissertation was a longitudinal, observational cohort study involving hospitalised patients diagnosed with CAP and age-, sex-matched control participants. Blood samples were collected from 75 CAP patients during the acute stage (hospitalisation) and 56 CAP patients one-month post-hospitalisation (recovery stage), along with 41 control subjects without acute infections. All patients and control subjects were age- and sex-matched (Brands *et al.*, 2021). Specifically, the TNF-α dataset comprised 5 high-responder females, 12 low-responder females, 9 high-responder males, and 11 low-responder males (PCA Plot Figure 4.8). To account for confounding and biological heterogeneity, sex was explicitly incorporated as an additive covariate in the *DESeq2* design formula, ensuring that differential expression estimates reflected cytokine-associated transcriptional variation independently of sex-based immune differences.

Participants, aged 18 years or older, were recruited between October 2016 and June 2018 from the Internal Medicine ward or Intensive Care Unit of the Academic Medical Center and BovenIJ Hospital in Amsterdam, the Netherlands. Patients were enrolled within 16 hours of hospital admission and reassessed one month later. Inclusion criteria required a primary clinical suspicion of acute respiratory tract infection, supported by clinical symptoms and radiographic evidence. Exclusion criteria were suspicion of aspiration or hospital-acquired pneumonia, haematologic malignancies, exposure to specific medications, and recent antibiotic use (Brands *et al.*, 2021).

The RNA-sequencing data was obtained from primary monocytes purified from patients and participants enrolled in the clinical study entitled Effect of Leukocyte Dna mEthylation and micRoBIOME Diversity on Host Defence Mechanisms During Community-Acquired Pneumonia - ELDER-BIOME (Brands *et al.*, 2021), which received ethical approval from the medical ethics committee of Amsterdam

University Medical Centre[2]. All procedures adhered to the 2013 Helsinki Declaration (World Medical Association Declaration of Helsinki: Ethical Principles for Medical Research Involving Human Subjects - PubMed, 2013), with written informed consent obtained from all eligible participants, or their legal representatives, prior to their inclusion (Brands *et al.*, 2021).

The RNA-seq data analysed in this dissertation was exclusively subjected to computational and bioinformatics analysis. No involvement in the original data collection or wet laboratory work occurred, and no individual clinical data was incorporated in this analysis.

The study described in this dissertation, submitted under identifier (ID) Centre for Molecular Medicine and Biobanking (CMMB)-2024-00011, was reviewed and endorsed by the Faculty Research Ethics Committee (F/REC) and the principal investigator, Doctor Brendon Scicluna.

3.3 Monocyte Isolation and Purity

Heparinised blood samples were diluted and processed to isolate peripheral blood mononuclear cells (PBMCs) using density-gradient centrifugation[3]. Monocytes were then isolated from PBMCs using magnetic beads coated with antibodies targeting Cluster of Differentiation 14 (anti-CD_{14}) antibodies[4]. Purified monocytes were cultured in 48-well plates at a density of 0.5×10^6 cells per well. The cells were then incubated for 24 hours at 37°C with 5% Carbon Dioxide and 95% humidity in 400 µl of RPMI medium supplemented with 10% foetal calf serum[5], 200 mM glutamax[6], 100 µM pyruvate[7], and 50 µg/ml gentamicin[8]. The cells were treated with 100 ng/ml

[2] NL57847.018.16; clinical trial registration number NCT02928367
[3] GE healthcare, 17-1440-02
[4] Miltenyi Biotec, 130-050-201
[5] Qiagen
[6] Thermo Fisher
[7] Lonza
[8] Invivogen

E. coli LPS or left untreated. After incubation, supernatants were collected and stored at -80°C for subsequent analysis. *Ex vivo* cytokine production, such as for TNF-α after LPS stimulation, was measured by Luminex multiplex assay[9] and BioPlex 200[10].

3.4 DNA and RNA Isolation

Total RNA was isolated from monocyte samples using the AllPrep DNA/RNA Mini Kit[11] following the manufacturer's protocol. RNA quality was evaluated using an Agilent Bioanalyser[12], and all samples exhibited RNA integrity numbers greater than nine. RNA concentrations were quantified using a Qubit® 2.0 Fluorometer[13].

3.5 RNA Sequencing

RNA sequencing libraries were prepared from total RNA samples using the KAPA RNA HyperPrep Kit with RiboErase[14]. Sequencing was performed on the Illumina HiSeq 4000 platform[15], generating SE reads of 50 base pairs (bps) in length, with a target sequencing depth of approximately 40 million reads per sample and a 30x per-base coverage.

3.6 Raw Data Pre-processing and QC

A total of 92 raw FASTQ (Fast Alignment Search Tool - Quality) files were provided, representing 46 media-treated samples and 46 *E. coli* LPS-treated samples. Additionally, two metadata files were included: one distinguishing LPS-treated from

[9] R&D Systems Inc., Minneapolis, MN
[10] BioRad, Hercules, CA
[11] Qiagen
[12] Agilent
[13] Life Technologies, Carlsbad, CA, USA
[14] Roche
[15] Illumina

media-treated monocytes, and the other categorising TNF-α responses within the LPS-treated group, further stratified by sex (female and male).

FastQC V0.12.1 (Andrews, 2010) and MultiQC V1.15 (Ewels *et al.*, 2016) were initially used for QC and visualisation of raw sequencing data. FastQC provided comprehensive metrics on sequence quality, duplication levels, and other quality indicators, generating individual reports for each FASTQ file, which were manually reviewed. After trimming, FastQC was rerun on the processed files to assess improvements in read quality. A total of 184 FastQC HyperText Markup Language (HTML) reports were generated for 92 RNA-seq libraries, covering both pre- and post-Trimmomatic processing. MultiQC aggregated these into summaries for raw and trimmed data, along with a final report combining both. This report provided an overview of sequencing quality, adapter contamination, and data integrity ("multiqc_report.html", can be accessed from the attached FastQC_MultiQC subfolder of the MMB5010_IOANA_NEAMTU_DISSERTATION_SUBMISSION folder).

The downloaded FASTQ files were initially processed to remove Illumina sequencing adaptors, trim low-quality bps, and discard short reads using Trimmomatic (Version 0.39; Bolger *et al.*, 2014).

The adapter trimming process utilised 12 threads for efficient processing and involved removing Illumina adapter sequences with the *ILLUMINACLIP* option and the TruSeq3-SE.fa adapter file, using parameters for seed mismatches (2), palindrome clipping threshold (30), and simple clip threshold (10). To enhance data quality, low-quality bps were trimmed from the start and end of reads with *LEADING* and *TRAILING* thresholds of 3, while a *SLIDINGWINDOW* approach (window size 4, quality threshold 15) ensured consistent read quality throughout. Reads shorter than 36 bps were discarded using the *MINLEN* option.

3.7 Alignment

Following QC, HISAT2 (Version 2.2.1; Kim *et al.*, 2019) was used to align trimmed reads to the human reference genome (Harrison *et al.*, 2024).

Genomic data for *Homo sapiens* from ENSEMBL release 110 was retrieved from the ENSEMBL File Transfer Protocol (FTP) server. This included the DNA sequence file in FAST-All (FASTA) format and the gene annotation file in Gene Transfer Format (GTF), both corresponding to the GRCh38.p14 human genome (Harrison *et al.*, 2024).

Following the creation of the index from the DNA sequence file, using the *hisat2-build* command, HISAT2 was used to align the trimmed reads to the indexed reference genome, with several important parameters applied. These included setting 16 threads for parallel processing (*--threads 16*) to accelerate the alignment. The Phred33 quality score format was specified (*--phred33*), ensuring accurate interpretation of base quality scores. The complementary DNA (cDNA) reads were treated as strand-specific, with the reverse and forward strands indicated (*--rna-strandness RF*). The input files were in SE FASTQ format (*-U*), and the results were output in SAM format (*-S*), with filenames based on the original input file names. Additionally, timing was enabled (*-t*) to provide detailed information for performance monitoring and troubleshooting.

SAM output files generated from HISAT2 alignments were processed using SAMTools (Version 1.9; H. Li *et al.*, 2009). Each SAM file was sorted by genomic coordinates, converted to the BAM format, and compressed.

3.8 Counts Matrix Generation of Gene Expression

Read counts were generated using Subread software package *featureCounts* (Version 2.0.6; Liao *et al.*, 2014). Sorted BAM files were processed, and the resulting gene-

level count matrices were compiled with sample metadata for downstream differential expression analysis.

This tool quantified read counts from sorted BAM files, generating count matrices and sample information files. All files were transferred to a local machine, and *featureCounts* was executed with specified parameters, including the GTF annotation file GRCh38.110.gtf.gz, output file name (*-o subread_counts*), number of threads (*-T 12*), and the attribute used for read summarisation (*-g gene_id*). The command was applied to all sorted BAM files in the directory. After execution, the resulting count matrices and sample metadata were compiled into Comma-Separated Values (csv) files counts.csv and sample_info.csv for downstream analysis.

3.9 Statistical analysis

Statistical analysis was performed using *DESeq2* to identify DEG in RNA-seq datasets. The workflow included data filtering, normalisation, Variance-Stabilising Transformation (VST), PCA, and hierarchical clustering. Gene-level dispersion was modeled using negative binomial GLMs, with $\log_2$FC shrinkage applied to improve effect size estimation. Results were corrected for multiple testing to ensure robustness and interpretability.

3.9.1 Data Preprocessing and Filtering

The RNA-seq data for both analyses (LPS-treated vs. media-treated and high- vs. low-cytokine response based on TNF-α release) underwent stringent filtering to remove low-count observations. Given the data sets' large sizes (56,284 initial observations across 92 samples and across 37 samples, respectively), a threshold of 100 counts was applied to exclude low-abundance features.

The data was also divided into quantile groups based on TNF-α levels after LPS exposure relative to medium controls (high or low responders) using *dplyr* R library.

A boxplot (Figure 4.7) was generated to visualise the distribution of Δ TNF-α levels across defined quantile groups. The Interquartile Range (IQR), lower (Q1), and upper (Q3) quartiles were calculated to define outlier thresholds.

3.9.2 Differential Expression Analysis: QC and VST

The *DESeq2* package (Love, 2024; Love *et al.*, 2014) implemented in R (version 4.0.3; R Core Team, 2023) and Bioconductor (Gentleman *et al.*, 2004), was selected for DEG analysis. This was performed to investigate transcriptomic changes in monocytes under the two experimental conditions. Read counts were imported and stored in a *DESeqDataSet* object using the *DESeqDataSetFromMatrix* function, allowing for internal tracking of experimental design and metadata.

Count normalisation was performed using *DESeq2*'s median-of-ratios method (Anders and Huber, 2010; Love *et al.*, 2014), implemented via the *estimateSizeFactors* function. This adjusted for variation in sequencing depth and RNA composition, ensuring that differential expression reflected true biological differences rather than technical variability (Love *et al.*, 2014). Size factor distributions were also assessed across samples to confirm normalisation effectiveness. normalised column sums revealed a subset of samples (S3013L, S1052M, S3013M, S3032M, and S3019L) with fewer than five million normalised reads; these were flagged for inspection but ultimately retained due to alignment with overall QC metrics.

For variance stabilization and dimensionality reduction, VST was applied using the *vst()* function with *blind=TRUE* to avoid experimental design bias (Love, 2024; Love *et al.*, 2014; McDonnell Genome Institute – Washington University, 2019). The transformation enabled PCA and clustering analyses by improving signal-to-noise ratio in low-count genes. Data sparsity was further evaluated using *DESeq2*'s *plotSparsity()* function to visualise the distribution of zero-count values across genes (Appendix Figure 3) (Love *et al.*, 2014). This confirmed that low-count filtering was effective and ensured the retention of informative features by demonstrating that

many genes were either lowly expressed or highly sample-specific, thus supporting the threshold of excluding transcripts with fewer than 100 counts (Appendix Figure 3).

Raw (Appendix Figures 4 and 5 (A)) and normalised counts (Appendix Figures 4 and 5 (B)) were also plotted across all samples to assess total library sizes and detect potential outliers. Final inspection confirmed that all samples, after normalisation, exceeded the threshold for acceptable depth and were included in downstream analyses.

3.9.3 PCA

Following low-count filtering, the normalised and variance-stabilised dataset was used for PCA and clustering of Regularized log (rlog)-transformed gene expression data (Figures 4.1, 4.8, and Appendix Figure 14) (Giuliani, 2017; Love *et al.*, 2014; Slowikowski, 2016; Wickham, 2016; Wickham *et al.*, 2019). PCA was applied to the variance-stabilised data to capture the main axes of variation, reduce mean-variance dependence, and help control for potential experimental bias, in line with standard *DESeq2* practice (Love, 2024). The loadings for the principal components were calculated, and the *plotPCA* function was used to visualise how samples clustered based on gene expression profiles, with *ggplot2* (*tidyverse* Version 2.0.0; Wickham *et al.*, 2019) and *ggrepel* (Version 0.9.5; Slowikowski, 2016) enhancing clarity (Figures 4.1, 4.8 and Appendix Figure 2).

Additionally, a scree plot (Appendix Figure 1) was generated to show the proportion of variance explained by each principal component in the LPS vs. media dataset, using eigenvalues in descending order to help determine the first two principal components were sufficient in capturing most of the data's variability (Giuliani, 2017; Love, 2024; Slowikowski, 2016; Wickham *et al.*, 2019).

3.9.4 Heatmaps and Clustering

Heatmaps (Appendix Figure 14) were generated using the *pheatmap* library (Version 1.0.12; Kolde, 2010) to visualise hierarchical clustering based on both experimental findings. Dendrograms were included to illustrate the relationships between samples, highlighting clustering patterns and trends in the variance-stabilised gene expression data (Kolde, 2010).

3.9.5 Dispersion Estimation, log_2FC Shrinkage and Statistical Testing

To estimate gene-wise dispersion and log_2FCs, the *DESeq2* model incorporated the experimental design formula alongside a negative binomial GLM (McCullagh and Nelder, 1989; McCullagh, 2019). Initial dispersion estimates were obtained using a method-of-moments approach, based on within-group means and variances, and then refined using the Cox-Reid Adjusted Profile Likelihood (APL) method (Appendix Figure 6) (Cox and Reid, 1987; Landau and Liu, 2013; Love *et al.*, 2014; McCarthy *et al.*, 2012). This two-step estimation approach captured gene-specific variability while reducing overfitting, particularly for low-count genes, and ensured the robustness of the statistical model.

Log_2FC shrinkage was applied to stabilise effect size estimates and reduce biases associated with low-count or high-variance genes (Love *et al.*, 2014). Three shrinkage methods were evaluated using the *lfcShrink()* function on the LPS vs. media dataset: Normal, the *DESeq2* default, which uses maximum likelihood estimation (Love *et al.*, 2014), Adaptive Shrinkage in R (*Ashr*), which uses an empirical Bayes framework to adaptively apply shrinkage based on gene-level properties (Stephens *et al.*, 2016), and Adaptive Prior Estimation for Generalised Linear Models (*Apeglm*), a Bayesian method that estimates gene-specific priors (A. Zhu *et al.*, 2019).

While *Apeglm* offers high precision and robust control of extreme values, its strong assumptions and computational complexity can hinder reproducibility (A. Zhu *et al.*,

2019). In contrast, MA plots (Appendix Figures 7, 8 and 9) visualising log_2FCs against mean normalised counts demonstrated that *Ashr* offered the most stable FC estimates, particularly in low-count genes, without excessive shrinkage. *Ashr* demonstrated a balance of flexibility and precision, applying greater shrinkage to low-count or highly variable genes while preserving meaningful FC estimates in more stable genes (Stephens *et al.*, 2016).

Differential expression analysis was conducted using the *DESeq2* package integrating a Wald test (Appendix Table 1) (Love, 2024; Love *et al.*, 2014; Smyth, 2004) to determine whether log_2FCs in gene expression between conditions differed significantly from zero (Cule *et al.*, 2011; Love *et al.*, 2014; Park *et al.*, 2019). A negative binomial model was used to estimate gene-specific dispersion, and sequencing depth was normalised using size factor estimation. Genes with low mean counts were filtered through independent filtering, and Cook's distance was applied to flag potential outliers (Cook and Weisberg, 1982), with significance assessed via Benjamini-Hochberg correction to control the FDR (Benjamini and Hochberg, 1995). Batch correction was not applied, as all samples were sequenced in a single batch.

To improve the reliability of log_2FC estimates, particularly for genes with low counts or high variability, *Ashr* shrinkage (Stephens *et al.*, 2016) was applied using the *lfcShrink()* function. *Ashr* adaptively controls the amount of shrinkage based on gene-level characteristics and was selected for its ability to minimise over-shrinkage while maintaining precision in effect size estimation. Based on its performance, *Ashr* was used for both the LPS vs. media and TNF-α responder datasets, ensuring consistency across comparisons and reducing false positives.

A stricter Adjusted *p*-value threshold (*padj* ≤ 0.01) was applied to define high-confidence DEGs. Results were exported as .csv files using the *dplyr* package from the *tidyverse* (Version 2.0.0; Wickham *et al.*, 2019), allowing integration into downstream annotation and visualisation workflows.

Dispersion modelling and diagnostic visualisations were guided using standard *DESeq2* workflows and tutorials provided by the Harvard Chan Bioinformatics Core (Piper, 2017).

3.10 Visualisation and Significance Assessments

To enhance the summary and visualisation of differential expression results, additional MA plots highlighting significant expression patterns were generated to assess the effect of *Ashr*-type shrinkage in reducing noise from low-count genes (Appendix Figures 8 and 9) (Stephens *et al.*, 2016).

Next, to optimise the visualisation of significant gene expression changes between conditions, volcano plots were generated using the *EnhancedVolcano* package (Version 1.18.0; Blighe *et al.*, 2023) for all data points in each dataset and not filtered by significance. The plots (Figures 4.2 and 4.9) highlighted genes by $\log_2$FCs and *p*-values, labelling those with the largest FCs and strongest significance for clearer interpretation (20,576 and 18,195 plotted variables for the media vs. LPS and for the high vs. low response datasets, respectively).

For downstream analyses, gene-level results were filtered to exclude noise observed in MA plots by excluding entries with missing identifiers and applying a significance threshold of *padj* ≤ 0.01. Genes with missing *symbol* or *ensgene* annotations and low expression (baseMean ≤ 50) were removed. The *na.omit()* function was used in combination with logical filtering to ensure only well-annotated, biologically relevant genes were retained for functional enrichment and visualisation. Each dataset was then sorted and divided into upregulated ($\log_2$FC > 0) and downregulated ($\log_2$FC < 0) genes.

PPI networks were then constructed using the STRING database (Version 11.5; Szklarczyk *et al.*, 2023) for both up- and downregulated subsets of each dataset (Figures 4.3, 4.10 and 4.11). For each pairwise comparison, DEGs were filtered by statistical significance and direction of change ($\log_2$FC > 0 for upregulated; $\log_2$FC <

0 for downregulated). Each subset was then ranked by absolute log_2FC to prioritise transcripts showing the strongest transcriptional responses. The top 100 upregulated and top 100 downregulated genes were selected for STRING-based PPI analysis (Szklarczyk *et al.*, 2023).

This fixed list length was chosen to balance biological coverage with network clarity. Including more genes markedly increased redundancy and network density, producing saturated PPI maps that obscured pathway structure and hindered functional interpretation. By contrast, the top 100 ensured retention of key regulators (e.g., *IL-6*, *TNF*, *IL-1B*) while keeping networks tractable and comparable across conditions.

It is acknowledged that this effect size-based ranking can omit biologically important genes with moderate FCs but strong significance or known roles. For example, *NFKB1* (log_2FC = 0.62; *padj* = 1.01×10^{-7}) ranked 484th and was thus excluded despite its relevance in inflammatory signalling.

The minimum interaction confidence score in STRING was adjusted empirically for each network to maintain informative connectivity while avoiding excess low-confidence edges. Thresholds from medium (≥ 0.4) to high (≥ 0.9) were tested, and the final cutoff for each PPI was selected to balance hub visibility, network density, and interpretability. Final networks were exported at high resolution for figure preparation and downstream annotation.

3.12 Pathway and Enrichment Analysis

For pathway analysis, gene symbols were mapped to ENSEMBL IDs (Harrison *et al.*, 2024) using the *mapIds* function from the R *AnnotationDbi* package (Version 1.66.0; Pagès, 2017), ensuring effective integration of gene annotations into datasets. The *org.Hs.eg.db* package (Version 3.17.0; Carlson, 2017) was used to convert gene symbols from the differential expression table into ENSEMBL IDs (Harrison *et al.*,

2024), storing them in a new data frame column, with multiple ENSEMBL IDs for a single gene symbol concatenated into a comma-separated string.

GO enrichment analysis (Harris *et al.*, 2004) was performed using the *clusterProfiler* R package (Version 4.8.3; T. Wu *et al.*, 2021; Xu *et al.*, 2024; Yu *et al.*, 2012) to investigate the functional roles of DEGs. The *enrichGO* function identified enriched GO terms across the three specified ontologies: BP, Cellular Component (CC), and Molecular Function (MF) (Ashburner *et al.*, 2000; The Gene Ontology Consortium, 2019; T. Wu *et al.*, 2021; S. Xu *et al.*, 2024; G. Yu *et al.*, 2012).

The top ten most significantly enriched GO terms were selected for each of the three GO domains (Biological Process (BP), Cellular Component (CC), and Molecular Function (MF)) and visualised in bar plots (Figures 4.4, 4.5, 4.12, and 4.13). This ranking by adjusted p-value provided a clear summary of the most statistically significant and biologically relevant terms linked to the DEGs in both datasets. The top ten threshold was deliberately applied to maximise figure interpretability while focusing on key overrepresented pathways. Detailed domain-specific bar plots are also provided in the Appendix (Appendix Figures 10 and 11), facilitating comprehensive functional categorisation and highlighting critical biological roles modulated by LPS stimulation and TNF-α responsiveness.

To ensure a robust interpretation of the biological significance of the DEGs, GO enrichment findings were further corroborated through non-pre-ranked GSEA (Version 4.3.3; Mootha *et al.*, 2003; Subramanian *et al.*, 2005) using. gct gene expression matrices and. cls phenotype labels (Appendix Figures 12, 13, 15, 16). Analyses were performed using Molecular Signatures Database (MSigDB, v2024.1), specifically the Hallmark gene set database (Version 2024; Liberzon *et al.*, 2015) and the ImmuneSigDB human collection (Version 2024.1; Godec *et al.*, 2016). Default parameters were applied, with human ENSEMBL gene IDs used for mapping (Harrison *et al.*, 2024), and 1,000 phenotype permutations were run for statistical testing. To identify enriched pathways, results were filtered for significance based on nominal p-values < 0.01. In the LPS vs. media comparison, this was coupled with

stringent FDR correction (FDR q-value < 0.01) to identify the most robust transcriptional programmes.

For the TNF-α high vs. low responder dataset, interpretation criteria were adapted to reflect dataset-specific constraints. While nominal $p < 0.01$ remained the primary significance threshold, the FDR cut-off was relaxed to < 0.25, consistent with established GSEA guidelines (Subramanian *et al.*, 2005), to allow detection of moderately enriched gene sets in smaller sample groups. In addition, pathways with FDR > 0.25 but Normalised Enrichment Score (NES) > |1.6| and nominal $p < 0.01$ were retained as exploratory findings. This reflected the limited statistical power due to smaller group sizes (Subramanian *et al.*, 2005), particularly in the high-responder cohort (n = 14), and the redundant, overlapping structure of immune-related gene sets, which can obscure enrichment under strict correction. This broader reporting strategy facilitated identification of biologically meaningful but borderline-significant pathways, especially within tightly regulated immune and metabolic circuits.

Due to limitations in the GSEA output format, gene intersections and contextual evaluations were performed manually and are not available as structured output tables or plots. Supplementary GSEA output can be reviewed in the GSEA subfolder of the MMB5010_IOANA_NEAMTU_DISSERTATION_SUBMISSION folder.

3.13 Technology Stack and Computational Environment

This project employed a reproducible, modular computational workflow combining command-line tools, R-based statistical analysis, and graphical enrichment platforms. The pipeline was executed on a Linux-based system with environment isolation via Conda, ensuring compatibility across software dependencies and enabling version-controlled analysis from raw RNA-seq data through to functional interpretation.

3.13.1 Environment Setup

All terminal commands, bash and shell scripts were executed within a Conda environment (Version 24.5.0; Anaconda Software Distribution, 2024). The operating system used was Linux Ubuntu 22.04.3 Long Term Support (LTS), with kernel version 5.15.0-83-generic.

3.13.2 Terminal Binaries

The terminal binaries were installed and configured as outlined in the README.txt file provided (Supporting Document). FastQC (Version 0.12.1; Andrews, 2010) and MultiQC (Version 1.15; Ewels *et al.*, 2016), were used for QC and data aggregation. Trimmomatic (Version 0.39; Bolger *et al.*, 2014) was employed for trimming Illumina Next-Generation Sequencing (NGS) data, while HISAT (Version 2.2.1; Kim *et al.*, 2019), was used for spliced alignment of transcripts. Additionally, SAMTools (Version 1.9; H. Li *et al.*, 2009) facilitated manipulation of HTS data. Finally, Subread (Version 2.0.6; Liao *et al.*, 2014) for read counting genomic features helped build the count matrix of gene expression.

3.13.3 R Setup, DEG Analysis and Downstream Analysis Software

The DEG analysis for this project was performed in RStudio (RStudio Team, 2020) using R version 4.0.3 (R Core Team, 2023), focusing on Media vs. LPS-treated monocytes and LPS-treated monocytes with TNF-α measurements, following the *DESeq2* Vignette (Love, 2024). *DESeq2* (Love *et al.*, 2014) was employed to identify DEGs, and specific versions of key R packages from CRAN, Bioconductor, and GitHub were used to ensure workflow reproducibility. These packages were critical for tasks such as data processing, annotation, visualisation, and functional analysis, supporting key stages like differential expression calculation and pathway enrichment. The core libraries used in the analysis were: CRAN packages *tidyverse*

(Version 2.0.0; Wickham *et al.*, 2019) and *ggrepel* (Version 0.9.5; Slowikowski, 2016), and BiocManager (Version 3.17; Morgan and Ramos, 2025) packages *DESeq2* (Version 1.40.2; Love *et al.*, 2014), *pheatmap* (Version 1.0.12; Kolde, 2010), *EnhancedVolcano* (Version 1.18.0; Blighe *et al.*, 2023), *AnnotationDbi* (Version 1.66.0; Pagès, 2017), *org.Hs.eg.db* (Version 3.17.0; Carlson, 2017), and *clusterProfiler* (Version 4.8.3; T. Wu *et al.*, 2021; Xu *et al.*, 2024; Yu *et al.*, 2012).

GSEA analyses were performed using the GSEA software (Version 4.3.3; Mootha *et al.*, 2003; Subramanian *et al.*, 2005).

3.14 Summary

This project employed a comprehensive computational and analytical framework to process and analyse RNA-seq data from a cohort study investigating CAP. Computational analyses were performed in a Conda environment with R on Ubuntu Linux, employing tools such as FastQC, MultiQC, Trimmomatic, HISAT2, SAMTools, and Subread's *featureCounts* for data preprocessing and alignment. DEG analysis was conducted in RStudio using CRAN and BiocManager libraries *tidyverse*, *ggrepel*, *DESeq2*, *pheatmap*, *EnhancedVolcano*, *AnnotationDbi*, *org.Hs.eg.db* and *clusterProfiler*.

The study analysed blood samples from 92 acute or recovery-stage participants with monocytes isolated, treated with either media or LPS, and sequenced on the Illumina HiSeq 4000 platform.

The pipeline involved performing QC, trimming, and aligning to the GRCh38.p14 genome, followed by generating expression count matrices to ensure high-quality data for subsequent analyses.

Differential expression analysis normalised data, filtered low-abundance features, and utilised $\log_2$FC shrinkage to ensure statistical robustness. Exploratory analyses, including PCA and hierarchical clustering of variance-stabilised data, identified patterns of variation, while MA and volcano plots highlighted significant gene expression changes.

Pathway enrichment analyses, conducted with tools like *clusterProfiler* and GSEA, and protein network analysis in STRING, identified key BPs, CCs, MFs, and PPIs influenced by LPS treatment.

This rigorous and reproducible pipeline revealed insights into the molecular mechanisms of CAP, enhancing the understanding of immune responses and associated pathways.

4. RESULTS AND DISCUSSION

To understand the transcriptional behaviour of monocytes during CAP, both biological profiling and rigorous computational processing were employed. Thus, the Results and Discussion chapter combines whole-transcriptome RNA-seq with rigorous transcriptomic analysis with robust statistical modelling to explore how innate immune activation unfolds at both the population (LPS vs. Media) and individual levels (TNF-α High vs. Low responders, stratified by sex). This chapter also details the bioinformatics and statistical frameworks that underpin these findings, including QC, sequence alignment, and DEG analysis using *DESeq2*, providing a comprehensive view of monocyte functional diversity during CAP, grounded in methodologically sound and biologically interpretable results.

4.1 Monocyte Functionality during CAP

Understanding the functional heterogeneity of monocytes during CAP is critical for dissecting how innate immune responses shape disease severity, recovery, and long-term immune balance. This section examines the activation dynamics of CAP-derived monocytes exposed *ex vivo* to LPS, a model for Gram-negative bacterial inflammation, and demonstrates both a conserved inflammatory signature and patient-specific immune strategies defined by differences in TNF-α production.

The integrated analysis combined transcriptomics, pathway enrichment, PPI networks, and sex-aware statistical modelling to unravel both shared and individualised transcriptional programmes that govern how monocytes respond to inflammatory stress. Across all donors, monocytes mounted a robust, consistent response to LPS, characterised by strong activation of type I IFN-related genes, key cytokines, and other pro-inflammatory signals. Concurrently, genes involved in immune regulation and tissue repair were downregulated, reflecting a shift towards acute inflammatory activation.

However, when monocytes were stratified according to TNF-α output, distinct patterns of immune activation emerged. High TNF-α responders exhibited an amplified inflammatory transcriptional profile but showed reduced expression of genes associated with metabolism and cellular repair processes, suggesting a biological prioritisation of immune aggression over maintenance of metabolic and structural homeostasis. In contrast, low TNF-α responders retained transcriptional programmes that support communication with surrounding tissues and sustained immune regulatory circuits, indicating a more balanced or tolerance-oriented immune strategy.

Together, these findings highlight the complex interplay between conserved innate immune pathways and individual variability in monocyte behaviour during CAP. This variability may partly explain differences in disease severity, clinical trajectories, and therapeutic responses among patients, underscoring the importance of understanding patient-specific immune profiles for precision management of inflammatory diseases.

4.1.1 Global Transcriptional Reprogramming of Monocytes Induced by LPS Stimulation

To characterise the transcriptional reprogramming induced by LPS, a comparative RNA-seq analysis was performed between primary monocytes isolated from CAP patients, stimulated *ex vivo* with LPS to further probe their transcriptional responsiveness, and those cultured in media alone.

PCA confirmed clear treatment-driven separation, with PC1 explaining 27.97% of the total variance (Figure 4.1). This dominant axis distinguished LPS-treated monocytes from unstimulated controls, while PC2 (13.2% variance) captured donor-specific variation, highlighting inter-individual immune responsiveness. Two media-treated samples (S3013M, S1018M) clustered with the LPS group: S3013M exhibited severe technical artefacts (96.2% duplicate reads), while S1018M may

reflect subtle biological priming or residual inflammation, underscoring both technical and physiological sources of variance in human RNA-seq datasets (Appendix Figure 1, Figure 4.16).

Figure 4.1. PCA plot of LPS-treated vs. Media-treated monocyte transcriptomes. *Plot illustrating separation based on gene expression profiles, with PC1 explaining 27.97% of the total variance, delineating the two treatment groups. Most samples clustered distinctly according to their treatment, except for two media-treated samples, S1018M and S3013M, which aligned with the LPS-treated group. PC2 captured an additional 13.2% of the variance.*

DEG analysis revealed extensive transcriptional shifts: of the 20,576 genes with non-zero counts, 7,033 met the significance threshold (*padj* ≤ 0.01), comprising 3,878 upregulated and 3,155 downregulated genes. The volcano plot (Figure 4.2) illustrates this genome-wide reprogramming, highlighting transcripts with both large effect sizes ($\log_2$FC) and robust statistical support ($-\log_{10}$ *padj*). Notably, key mediators of inflammatory signalling (such as *IFNB1*, *IL-6*) were strongly induced, while negative regulators of immune tolerance and transcriptional repression (*SMAD6*, *HIC1*, *CD180*) were significantly suppressed.

To contextualise these expression changes functionally, PPI networks were constructed using STRING for the top 100 up- and downregulated genes. The upregulated network revealed tightly interconnected hubs enriched for cytokine-cytokine receptor interactions, type I IFN responses, and pathogen-sensing pathways, reflecting an intensified inflammatory and antiviral-like state. Conversely, the downregulated network mapped dispersed modules comprising transcriptional repressors and tolerance-associated nodes, whose suppression suggests intentional removal of molecular brakes to sustain a robust pro-inflammatory programme.

GO and GSEA further confirmed this dual signature: LPS exposure amplified innate immune activation, hypoxia adaptation, and pathogen-recognition pathways, while downregulating chromatin remodelling, transcriptional fine-tuning, and tolerance-maintaining programmes. Together, these data delineate a coordinated reprogramming in which monocytes prioritise pathogen clearance and cytokine production at the cost of regulatory restraint, a transcriptional architecture aligning with the hallmark immune dysregulation observed in severe CAP.

4.1.1.1 DEG Reveals Robust Innate Immune Activation and Suppressed Tolerance

Comparative transcriptomic profiling of primary CAP patients-derived human monocytes exposed to LPS versus unstimulated (media-treated) controls revealed

extensive transcriptional reprogramming, indicative of a robust innate immune activation coupled with suppression of regulatory circuits, which is a dynamic particularly relevant to the pathophysiology of CAP.

Out of the 20,576 genes with non-zero read counts, all were assigned nominal p-values and $\log_2$FC estimates, with 7,033 genes meeting the multiple-testing adjusted threshold (*padj* ≤ 0.01): 3,878 upregulated (approximately 19%) and 3,155 downregulated (approximately 15%) in LPS-treated monocytes. This global shift is visually summarised in the volcano plot (Figure 4.2), which displays genes distributed by $\log_2$FC and $-\log_{10}$ nominal *p*-value. Genes in the upper-right and upper-left quadrants represent transcripts with the largest absolute FCs and strongest nominal statistical signal; genes exceeding the adjusted threshold (*padj* ≤ 0.01) are highlighted.

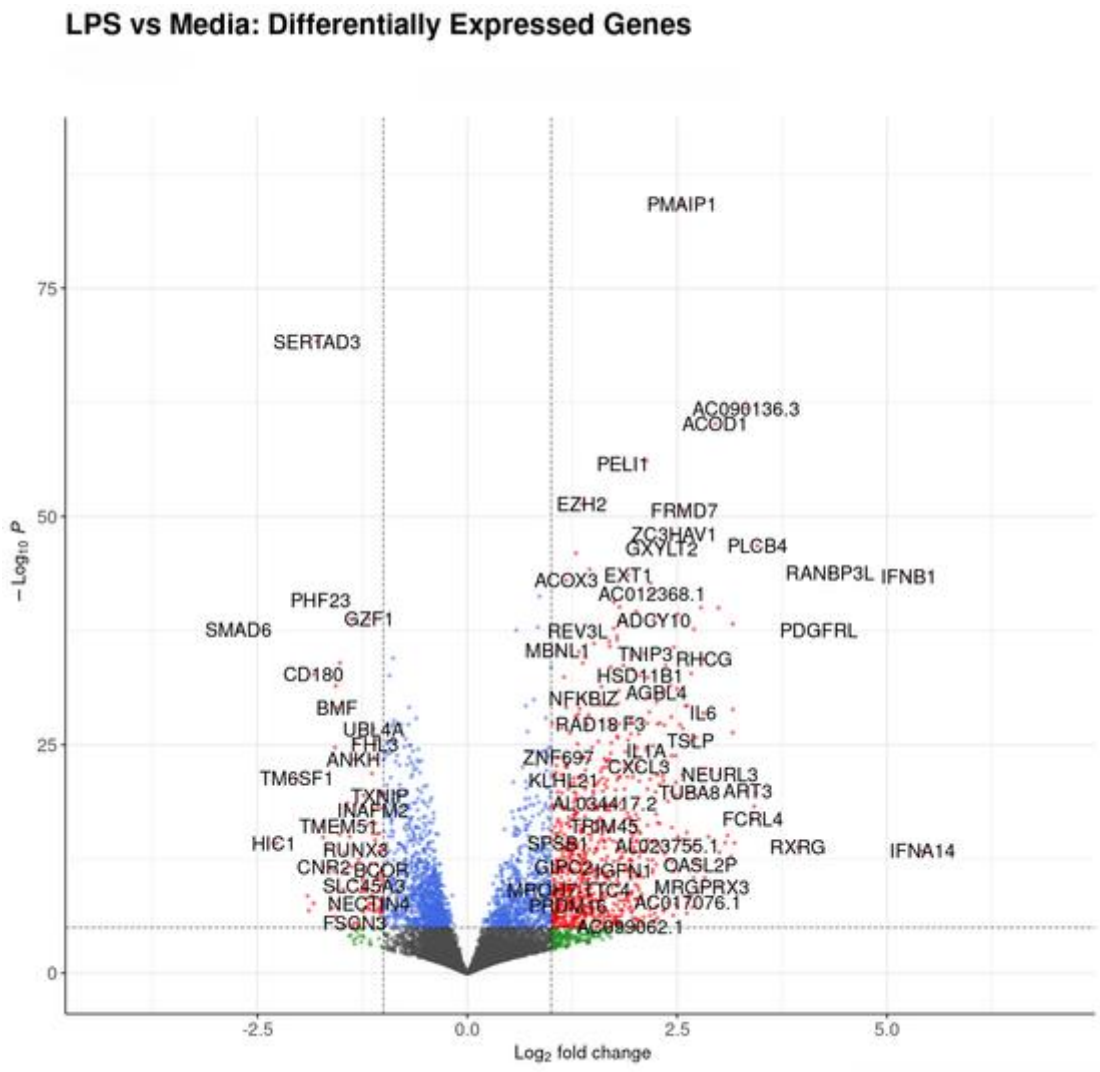

Figure 4.2 Volcano plot showing all 20,576 genes tested in LPS-treated vs. media-treated monocytes. *The x-axis shows log_2FC; the y-axis shows $-log_{10}$ nominal p-value. Genes with the largest positive FCs and highest nominal significance appear in the upper right quadrant; genes with large negative FCs and highest nominal significance appear in the upper left quadrant. Colour coding indicates thresholds: grey for non-significant genes, green for genes meeting only the log_2FC threshold, blue for genes meeting only the nominal p-value threshold, and red for genes meeting both log_2FC and the padj threshold.*

Notably upregulated genes included critical mediators of the classical pro-inflammatory and antiviral response. *IFNB1* and *IFNA14* emerged as among the most strongly upregulated transcripts, reinforcing activation of the type I IFN axis. This axis is known to bridge pathogen detection with both antiviral defences and

resolution of bacterial inflammation through Toll/IL-1 Receptor-Domain-containing Adaptor-Inducing Beta IFN (TRIF)-IRF3-dependent signalling downstream of TLR4 engagement (Bernard *et al.*, 2023; Kawai and Akira, 2007; Pestka *et al.*, 2004). *IL-6*, a canonical inflammatory cytokine central to the acute-phase response and lung pathology in CAP, was also significantly elevated (Tanaka *et al.*, 2014).

Additional upregulated genes such as Retinoid X Receptor Gamma (*RXRG*), which modulates monocyte cytokine output and inflammatory state (Núñez *et al.*, 2010), Platelet-Derived Growth Factor Receptor Like (*PDGFRL*), and Fc Receptor Like 4 (*FCRL4*), a marker linked to innate-like transcriptional programmes in tissue-like B cells and macrophages (Siewe *et al.*, 2017; Xue *et al.*, 2014), point towards broad engagement of transcription factors and surface receptors implicated in monocyte differentiation, migration, and functional plasticity under inflammatory stress.

In contrast, the downregulated gene set included several well-established negative regulators of inflammation and chromatin dynamics, underscoring a shift away from homeostatic repression. *SMAD6*, *HIC1* and *CD180* were among the most significantly suppressed transcripts. *SMAD6* and *HIC1* serve as transcriptional repressors within TGF-β and CtBP2-mediated pathways, dampening NF-κB activity and limiting inflammatory gene expression (X. Lin *et al.*, 2003; Park *et al.*, 2019; Stankovic-Valentin *et al.*, 2007; Van Rechem *et al.*, 2010). *CD180*, a negative modulator of TLR4 signalling and IFN production, when downregulated, removes a brake on the pro-inflammatory cascade, potentially exacerbating lung tissue damage in CAP (Divanovic *et al.*, 2005; You *et al.*, 2017).

Other notable downregulated transcripts such as Transmembrane Protein 51 (*TMEM51*) and Phosphatase and Actin Regulator 3 (*PHACTR3*), though less extensively characterised, may participate in regulatory networks balancing cytoskeletal remodelling and transcriptional control under pathogen stress.

Overall, this large-scale reconfiguration of the monocyte transcriptome reflects a coordinated boost in pathogen recognition, cytokine secretion, and IFN responses,

simultaneously coupled with an intentional silencing of tolerance-associated and energy-consuming housekeeping pathways. This dual modulation aligns with the hallmark imbalance of effective pathogen clearance and excessive inflammatory injury that defines severe bacterial pneumonia.

4.1.1.2 PPI Networks Highlight Functional Hubs Driving Inflammation and Immune Regulation

To contextualise the extensive list of DEGs within a functional interaction landscape, STRING was employed to generate PPI networks for the top 100 upregulated and top 100 downregulated transcripts. This approach prioritised genes with the strongest absolute log_2FCs, ensuring that the resulting networks captured the dominant signals orchestrating monocyte reprogramming under LPS stimulation, a transcriptional scenario directly relevant to the host immune imbalance observed in severe CAP.

The upregulated PPI network (Figure 4.3 (A)) unveiled a dense core of cytokines, chemokines, and IFNs interlinked through high-confidence edges representing experimental evidence, curated pathway co-membership, co-expression patterns, and text-mined associations. Central hubs included IFNB1, TNF, and multiple ILs (IL-6, IL-1A, IL-2RA, IL-23A), supported by chemokines such as CCL4, CCL20, and CCL3L1. These nodes form tightly connected modules which reflect simultaneous activation of pathogen-sensing cascades and recruitment of downstream effector cells, which is a classic pattern in the inflammatory storm underlying lung injury during bacterial pneumonia.

One notable cluster within the upregulated network featured an antiviral defence module: genes such as HERC5, HERC6, IFIH1, and IFIT5 were densely connected, indicating a robust type I ISG signature. While canonical in viral infections, this ISG network is increasingly recognised for its dual role in modulating bacterial responses, resolving excessive inflammation, and promoting tissue repair (Bernard *et al.*, 2023;

Pestka *et al.*, 2004). This cluster suggests that LPS-exposed monocytes partially mimic an antiviral state, likely reflecting TRIF-IRF3 pathway activation downstream of TLR4.

Additional upregulated nodes, such as Rat Sarcoma Virus-Related Nuclear Protein Binding Protein 3 Like (RANBP3L) and Phospholipase C Beta 4 (PLCB4) although highly expressed (as seen in the volcano plot, Figure 4.2), showed sparse connectivity within STRING's confidence-based network, implying that their roles may be more peripheral or context-dependent under LPS-induced stress.

The downregulated PPI network (Figure 4.3 (B)) exhibited a more modular, less densely interconnected topology, consistent with the nature of negative regulators and tolerance factors which often modulate transcription and chromatin accessibility rather than forming large signalling hubs. Key nodes included SMAD6, HIC1, and CD180, each embedded within distinct but overlapping clusters that converge functionally to restrain uncontrolled inflammation.

Specifically, SMAD6 anchored a module of TGF-β/BMP pathway repressors, connecting with SMAD7, ID1, TGFBR1, and CTBP2. This module illustrates the monocyte's homeostatic circuit for dampening NF-κB-mediated transcription during steady state or controlled pathogen clearance. HIC1 and its known CtBP interactors (CTBP1, CTBP2) formed a subnetwork suggesting tight epigenetic regulation of inflammatory genes and DNA damage responses, mechanisms frequently disrupted in hyperinflammatory lung conditions (Stankovic-Valentin *et al.*, 2007; Van Rechem *et al.*, 2010).

A secondary module, pivoting on Early Growth Response 2 (EGR2), connected transcriptional modulators (Runt-Related Transcription Factor 3 (RUNX3), Sphingosine-1-Phosphate Receptor 1, IL-21R) that coordinate signal transduction and gene regulation, suggesting that suppression of this cluster reduces the cell's transcriptional plasticity under stress.

Notably, CD180, a unique TLR co-receptor, bridged the tolerance module to a small antioxidant cluster involving Haeme Oxygenase 1 (HMOX1) and Ubiquitin Like Modifier Activating Enzyme 4A (UBL4A). This arrangement hints at a protective axis linking innate immune restraint with cellular stress mitigation, a function critical for limiting tissue damage in the CAP-inflamed lung environment (Divanovic *et al.*, 2005; You *et al.*, 2017).

All tolerance clusters funnelled functionally toward a chemokine hub, CCL2, serving as a final integrator of pro-inflammatory signals and monocyte recruitment. The positioning of CCL2 highlights how the suppression of repressors amplifies chemokine-driven inflammation, which is a plausible contributor to alveolar infiltration and lung tissue injury during CAP.

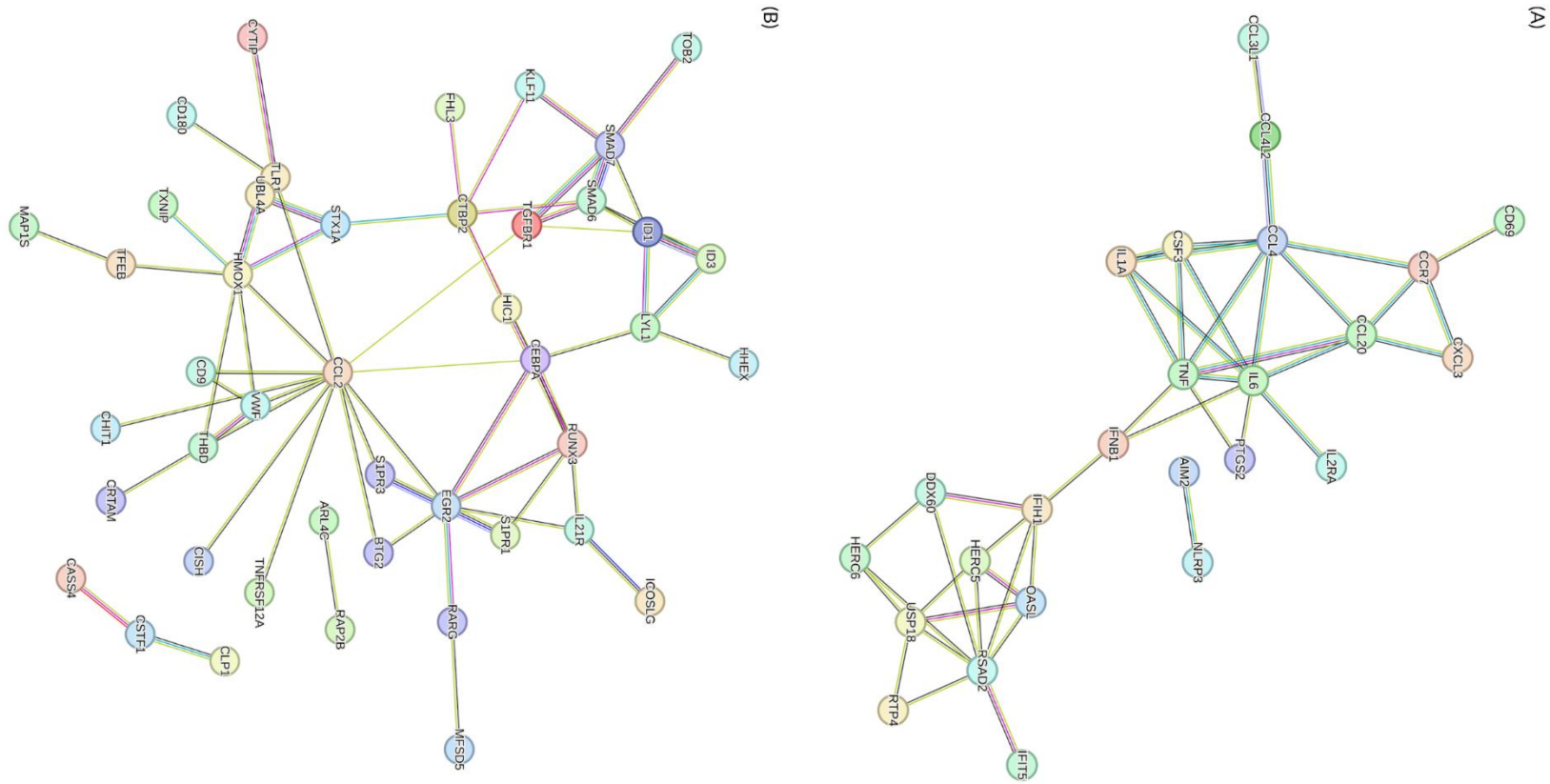

Figure 4.3. STRING PPI networks for top 100 (A) upregulated and (B) downregulated genes in the LPS vs. Media dataset. *Each node represents a protein encoded by a DEG. Edges represent high-confidence interactions based on STRING evidence types: green (gene neighborhood), red (experimental), blue (co-expression), purple (curated databases), yellow (text mining), and light blue (homology) (Szklarczyk et al., 2023).*

Taken together, the STRING network analysis visualises how LPS exposure rewires monocyte interactions: upregulated clusters reinforce cytokine storms and antiviral mimicry, while downregulated modules remove transcriptional and post-translational brakes. This supports a functional model of monocyte behaviour where pathogen clearance is prioritised at the cost of controlled inflammation, aligning with the immunopathological hallmarks of severe CAP. In such pathophysiological context, this imbalance explains how overactivated monocytes amplify alveolar inflammation, promote neutrophil infiltration, and contribute to the destructive cytokine milieu that exacerbates lung injury.

Moreover, by mapping both pro-inflammatory and tolerance-suppressing gene networks, the STRING-derived topology highlights potential targets for therapeutic intervention aimed at restoring immune equilibrium, for instance, modulating the TGF-β/SMAD axis or re-engaging negative TLR co-receptors could temper hyperinflammation without impairing host defence.

4.1.1.3 GO Enrichment Indicates Coordinated Activation of Host Defence and Suppression of Homeostatic Programmes

To interpret the biological processes, molecular functions, and subcellular localisations modulated by LPS exposure in CAP monocytes, a comprehensive GO enrichment analysis was conducted using the *clusterProfiler* package (T. Wu *et al.*, 2021; S. Xu *et al.*, 2024; G. Yu *et al.*, 2012). This three-tiered approach of examining BP, CC and MF ontologies (Full term lists are provided in Appendix Figure 11), provided a systematic view of how innate immune transcriptional programmes are remodelled during bacterial challenge, highlighting features critical to the excessive inflammation and dysregulated host response seen in severe CAP.

For upregulated genes (Figure 4.4), the BP ontology, clearly demonstrated robust activation of host defence pathways. Terms such as regulation of response to biotic stimulus, positive regulation of defence response, and activation of innate immune

response were among the most significantly enriched, reflecting classical pathogen-sensing and effector mechanisms (Ashburner *et al.*, 2000; The Gene Ontology Consortium, 2019; Medzhitov and Janeway, 2000). Notably, the term response to virus was highly enriched despite the bacterial nature of LPS, signifying the canonical cross-activation of antiviral ISGs downstream of the TRIF-IRF3 axis (Kawai and Akira, 2007; Negishi *et al.*, 2018; Pestka *et al.*, 2004). This supports the observation from STRING that LPS-treated monocytes partially engage an IFN-driven antiviral module, which may paradoxically modulate bacterial clearance and tissue repair in the CAP context (Bernard *et al.*, 2023).

Additional BP terms such as pattern recognition receptor signalling pathway underscored the engagement of TLRs, Retinoic Acid-Inducible Gene (RIG)-I-like receptors (RLRs), and C-type Lectin Receptors (CLRs), all central to pathogen detection and immune activation (Brubaker *et al.*, 2015; Takeuchi and Akira, 2010).

Within the CC ontology, enrichment pointed to profound remodelling of the monocyte's endo-lysosomal system and cell-matrix interactions. Highly ranked terms included lysosomal membrane, vacuolar membrane, and late endosome, consistent with enhanced phagocytosis, antigen processing, and pathogen killing (Flannagan *et al.*, 2012; Sancak *et al.*, 2008). Enrichment of focal adhesion and cell-substrate junction implied increased migratory and adhesive capacity, facilitating monocyte recruitment and infiltration into inflamed pulmonary tissue, a hallmark of alveolar exudation and lung injury in pneumonia (Jakubzick *et al.*, 2017; Lämmermann and Germain, 2014; Ley *et al.*, 2007).

The MF ontology further validated the activation of complex signalling cascades. Terms such as cytokine receptor binding and cytokine activity reflected elevated expression of interleukins (e.g., *IL-6*), IFNs (*IFNB1*, *IFNA14*), and chemokines driving paracrine amplification (Borden, 2019; Pestka *et al.*, 2004). Terms including phospholipid binding and phosphatidylinositol binding implicated PI3K/AKT pathways, which interface with NF-κB and MAPK cascades to sustain inflammatory gene transcription (Bilanges *et al.*, 2019; Vanhaesebroeck *et al.*, 2012). Enrichment

of protein serine kinase activity and MAP kinase kinase kinase activity corroborated the intense kinase-driven signal propagation characteristic of activated monocytes under endotoxin stress (Fox *et al.*, 2020; Y. Wu *et al.*, 2020).

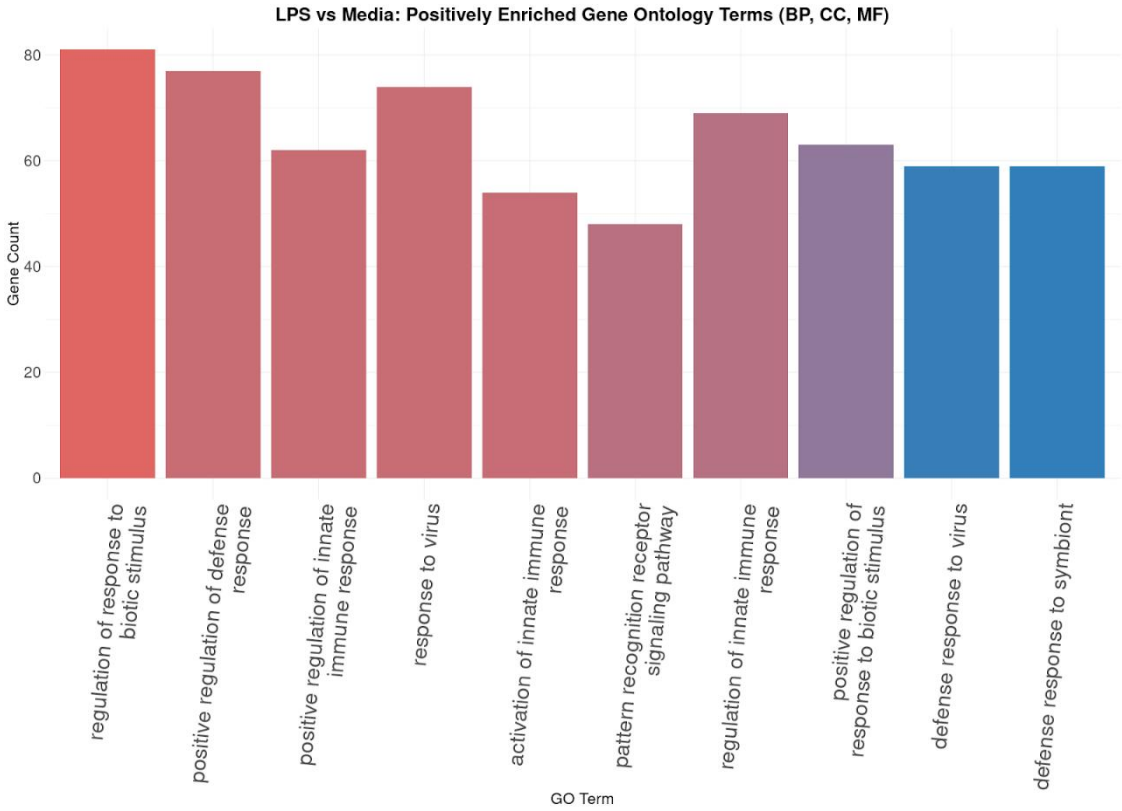

Figure 4.4. The top 10 most significantly positively enriched GO terms across all three ontologies. *Most positively enriched GO BP, CC and MF terms for LPS-stimulated monocytes, highlighting activation of innate immune and antiviral programmes relevant to CAP. All terms meet the significance threshold (padj < 0.01). Colour coding indicates statistical significance, with a gradient from blue (less significant) to red (most significant) representing increasing $-\log_{10}$ adjusted p-values.*

Conversely, the downregulated gene set revealed a coordinated suppression of processes integral to chromatin remodelling, transcriptional fine-tuning, and cellular housekeeping, reflecting a functional pivot away from resource-intensive homeostasis toward aggressive host defence (Novakovic *et al.*, 2016; Saeed *et al.*, 2014). Within BP, prominent negative terms included histone modification, peptidyl-lysine modification, DNA-templated transcription elongation, and RNA splicing

(Foster *et al.*, 2007; Ramirez-Carrozzi *et al.*, 2009; Shalgi *et al.*, 2014). This repression likely constrains epigenetic plasticity and transcriptional checks, promoting sustained inflammatory transcription at the expense of tolerance mechanisms, a pattern aligned with excessive lung inflammation in CAP.

In CC, downregulation of nuclear speck, PML body, and RNA polymerase II transcription regulator complex indicated silencing of nuclear compartments critical for mRNA maturation and chromatin organisation (Bernardi and Pandolfi, 2007; Spector and Lamond, 2011; Q. Zhou *et al.*, 2012). The MF domain echoed this suppression: ubiquitin-like protein ligase activity, SMAD binding, and DNA-binding transcription factor binding were significantly depleted, highlighting reduced post-translational control and feedback inhibition (Ebner *et al.*, 2017; Hata *et al.*, 1998; Pickart and Eddins, 2004).

Together, these enrichment patterns demonstrate that LPS-exposed monocytes adopt a transcriptional state optimised for pathogen sensing, chemokine production, and inflammatory signalling, while simultaneously silencing pathways that maintain tolerance and regulate chromatin dynamics. Mechanistically, the downregulation of *SMAD6*, *HIC1*, and *CD180* within this suppressed landscape underscores the loss of key molecular brakes that would otherwise limit TLR-driven activation and excessive cytokine release (Divanovic *et al.*, 2005; Stankovic-Valentin *et al.*, 2007; You *et al.*, 2017).

This dual reprogramming of enriched and depleted GO terms aligns with the core immunopathology of severe CAP: robust clearance of pathogens at the cost of tissue-damaging inflammation, driven by monocyte hyperactivation and loss of immune tolerance.

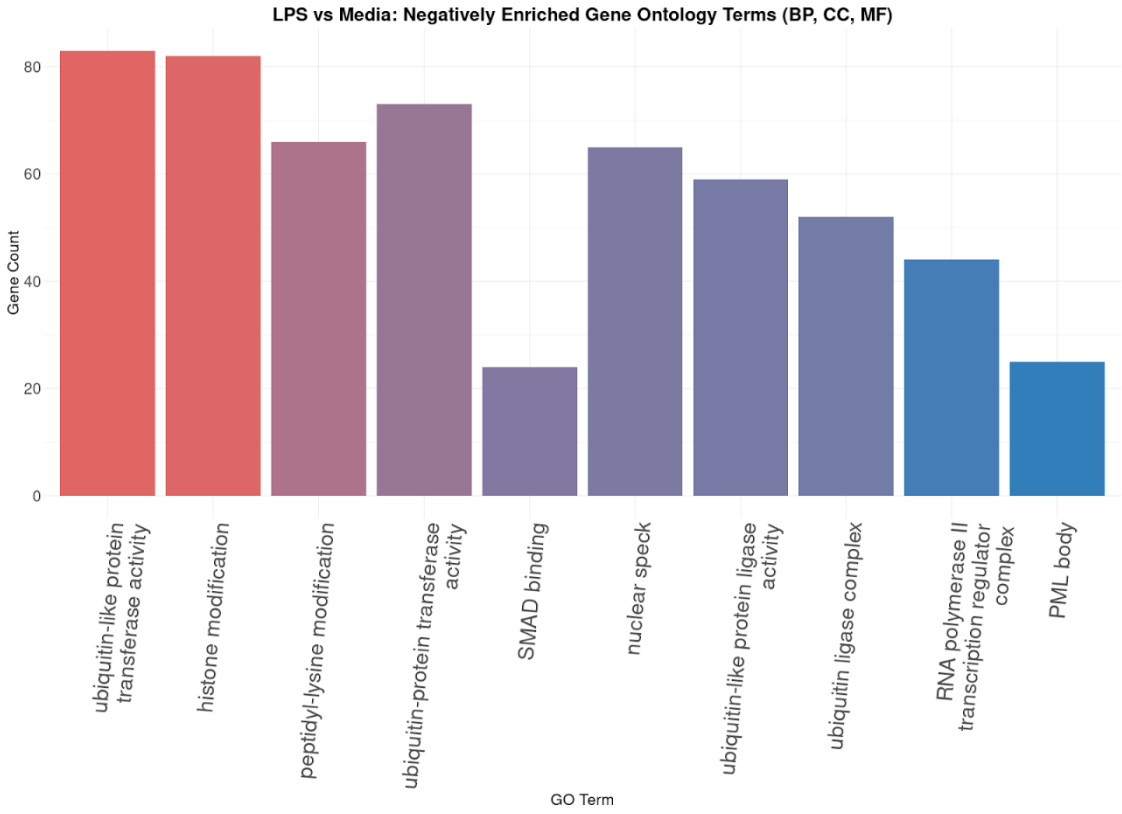

Figure 4.5. The top 10 most significantly negatively enriched GO terms across all three ontologies. *Most negatively enriched GO terms across the BP, CC and MF domains for LPS-stimulated monocytes compared to controls. Terms highlight coordinated downregulation of pathways related to transcriptional regulation, post-translational modification, and nuclear organisation, consistent with suppression of tolerance-associated programmes in CAP. Colour coding indicates statistical significance, with a gradient from blue (less significant) to red (most significant) representing increasing $-\log_{10}$ adjusted p-values.*

4.1.1.4 GSEA Validates Hallmark Pathways and Identifies Key Regulatory Drivers

To expand upon the differential expression and GO enrichment findings, a non-pre-ranked GSEA was performed using the MSigDB Hallmark (Liberzon *et al.*, 2015) and ImmuneSigDB (Godec *et al.*, 2016) collections. This approach enabled systematic interrogation of pathway-level shifts orchestrated by LPS exposure in monocytes, serving as a proxy for the immunological cascade underlying severe CAP.

The Hallmark pathway analysis revealed a striking pattern: 41 out of 50 Hallmark pathways were significantly enriched in the LPS-treated phenotype (Appendix Figure 12 (A)). Among these, TNF-α Signalling via NF-κB, Inflammatory Response, IL-2/STAT5 Signalling, and Hypoxia were the most robustly upregulated, exhibiting nominal *p*-values ≤ 0.002 and, for most, complete permutation saturation (*p*-value = 0) (Figure 4.6). These pathways reflect canonical inflammatory and stress adaptation axes that prepare monocytes to clear pathogens but risk collateral tissue injury in the alveolar microenvironment (Bernard *et al.*, 2023). Conversely, nine pathways were enriched in media-treated cells (Appendix Figure 12 (B)), marking biological processes suppressed by LPS, many of which overlap with tolerance or homeostatic maintenance.

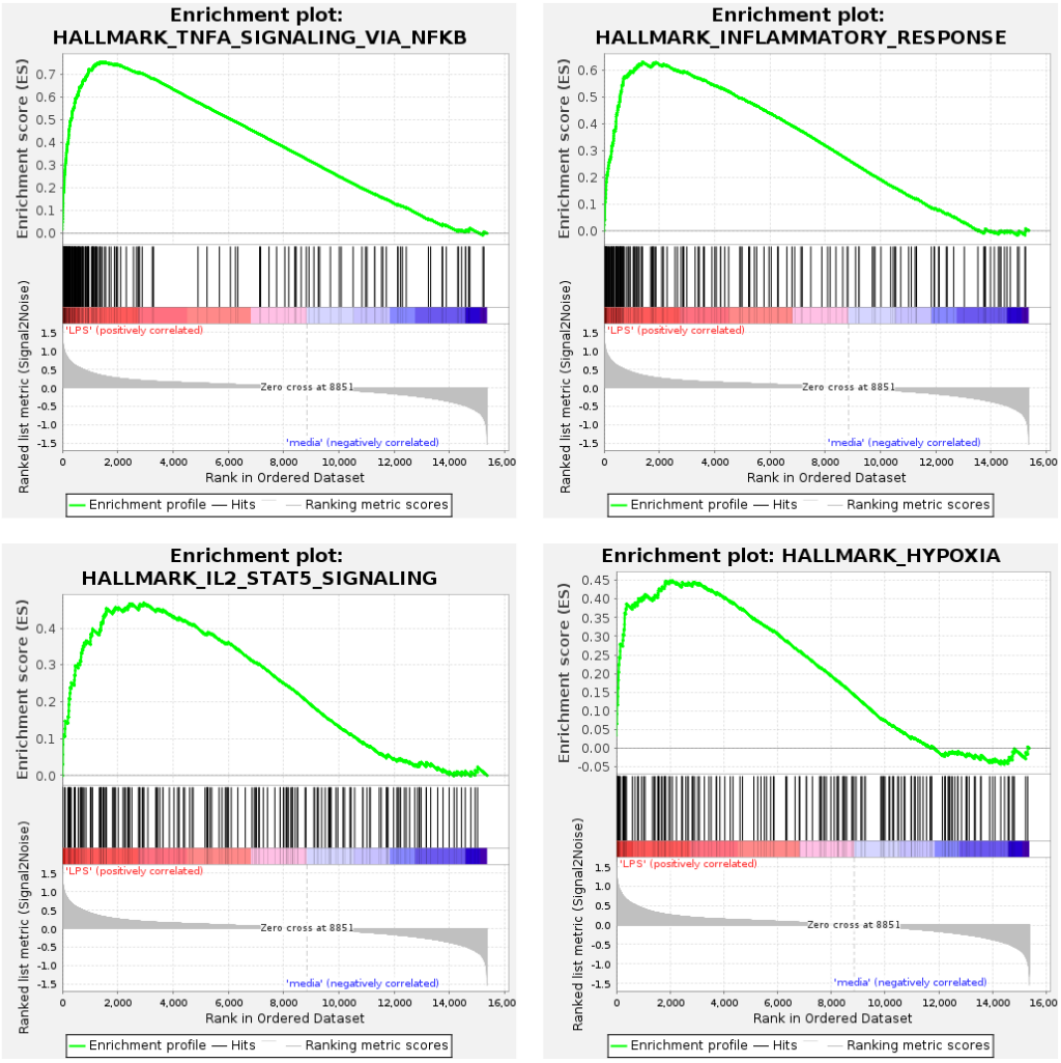

Figure 4.6. GSEA enrichment plots for the four most upregulated Hallmark pathways in LPS-treated monocytes. *Each panel shows the running Enrichment Score (ES, green line), the positions of pathway genes in the ranked gene list (black vertical lines), and the ranking metric (grey plot). The peak of the ES curve reflects the point of maximum enrichment. Pathways shown: TNF-α Signalling via NF-κB (normalised ES (NES) = 2.12), Inflammatory Response (NES = 2.14), IL-2/STAT5 Signalling (NES = 2.01), and Hypoxia (NES = 2.10).*

Within ImmuneSigDB, 2,890 gene sets were enriched in the LPS condition and 1,982 in controls (Appendix Figure 13). This further confirmed that LPS globally rewires transcriptional programmes, amplifying innate immune, cytokine, and metabolic signals while attenuating alternative activation pathways.

Core enrichment gene sets were extracted to pinpoint specific regulators driving these dominant pathways. Across the four top Hallmark pathways (TNF-α Signalling via NF-κB, Inflammatory Response, IL-2/STAT5 Signalling, Hypoxia), leading-edge analysis identified overlapping genes, highlighting shared transcriptional backbones. *KLF6* was uniquely detected in all four pathways, positioning it as a master amplifier of the LPS-induced response. KLF6 is known to coactivate NF-κB, promote M1 macrophage polarisation, repress anti-inflammatory regulators (Peroxisome Proliferator-Activated Receptor (PPAR)-γ, BCL6), and enhance HIF-1α signalling under hypoxic stress, each of which compounds alveolar inflammation in pneumonia (Date *et al.*, 2014; G.-D. Kim *et al.*, 2016, 2019, 2020; Syafruddin *et al.*, 2020).

Other genes with high recurrence included *IL-6* and *TNF*, the quintessential pro-inflammatory cytokines that drive fever, leukocyte recruitment, and endothelial activation in CAP (Bernard *et al.*, 2023). Leukaemia Inhibitory Factor (*LIF*) appeared prominently in both Inflammatory Response and IL-2/STAT5 Signalling, illustrating its dual function in modulating Treg differentiation to counterbalance *IL-6*-mediated TH17 polarisation, a critical "tug-of-war" that shapes lung inflammation severity (Gao *et al.*, 2009; Metcalfe *et al.*, 2015). TNF Ligand Superfamily Member (*TNFSF*) 9 and TNF Receptor Superfamily Member (*TNFRSF*) 9, encoding ligand and receptor pairs modulating T-cell co-stimulation, also bridged multiple pathways, highlighting crosstalk between monocyte and lymphocyte compartments during infection resolution or exacerbation (Cho *et al.*, 2021; Eissner *et al.*, 2004). Notably absent from these upregulated pathways were classic tolerance-associated repressors such as *SMAD6*, *HIC1*, and *CD180*. This omission aligns with their negative enrichment in the GO analysis and STRING downregulated PPI cluster (Figures 4.3 (B), 4.5). Their silencing removes inhibitory checkpoints on NF-κB and TLR pathways, predisposing monocytes to sustained pro-inflammatory transcription, which is a well-documented driver of alveolar damage in severe CAP (Novakovic *et al.*, 2016; Saeed *et al.*, 2014).

ImmuneSigDB enrichment patterns added functional context and stimulus specificity. For example, gene sets derived from anti-TREM-1 activation (Dower *et*

al., 2008) and TLR-7/8 agonists like R848 or Gardiquimod (Amit *et al.*, 2009; Napolitani *et al.*, 2005) were enriched in media-treated controls but downregulated in LPS-treated cells. This illustrates how LPS dampens alternative activation routes to prioritise canonical TLR4-NF-κB-IRF3 responses, which is a phenomenon that contributes to an unbalanced inflammatory milieu in pneumonia (You *et al.*, 2017).

Conversely, gene sets from *IL-10* knockout macrophages (El Kasmi *et al.*, 2007) were strongly enriched in the LPS condition, confirming that negative feedback loops are disengaged when anti-inflammatory signals are removed, mirroring the suppression of *SMAD6* and *HIC1* (X. Lin *et al.*, 2003; Park *et al.*, 2019). This shows how LPS not only triggers pro-inflammatory pathways but also actively silences mechanisms that would otherwise limit tissue damage.

Taken together, the GSEA confirms that LPS reprogrammes monocytes into a hyper-responsive state primed for robust cytokine secretion, pathogen killing, and hypoxia adaptation, at the cost of losing transcriptional brakes that maintain immune homeostasis. This transcriptional signature mechanistically supports the concept that monocyte overactivation is a double-edged sword in CAP: essential for bacterial clearance but equally capable of driving alveolar exudation, oedema, and lung injury when unchecked (Bernard *et al.*, 2023; Medzhitov and Horng, 2009; Pearce and Pearce, 2013).

4.1.1.5 Integrated Model: Ex Vivo LPS Challenge Highlights the Transcriptional Basis of Immune Dysregulation in CAP

Together, the differential expression analysis, PPI networks, GO enrichment, and GSEA converge to delineate a coherent model of how LPS reprogrammes human monocytes, which is a model with direct implications for the immunopathology of CAP.

First, the global transcriptomic shifts reveal that approximately one-third of the actively transcribed genome is significantly modulated by LPS stimulation, with a

near-even split between upregulated effectors and downregulated regulatory elements. Volcano and MA plots (Figures 4.2 and Appendix Figure 8) illustrate this distribution visually, pinpointing genes with both large effect sizes and robust statistical support. STRING PPI networks (Figures 4.3 (A) and (B)) further contextualise these DEGs by uncovering clusters of tightly interacting proteins that cooperate to drive either inflammation or immune suppression.

The upregulated module, anchored by central cytokines (*IFNB1*, *IFNA14*, *IL-6*, *TNF*) and transcriptional amplifiers like *KLF6*, orchestrates an aggressive inflammatory and antiviral response. These genes appear consistently in leading-edge sets across the top enriched Hallmark pathways (TNF-α Signalling via NF-κB, Inflammatory Response, IL-2/STAT5 Signalling, and Hypoxia), as confirmed by GSEA (Appendix Figure 12 (A)). Their simultaneous representation in GO BP terms such as positive regulation of defence response, response to virus, and pattern recognition receptor signalling pathway (Figure 4.4) reinforces this interpretation. CC terms like lysosomal membrane and late endosome indicate boosted endo-lysosomal processing, a hallmark of activated monocytes primed for pathogen engulfment and antigen presentation (Flannagan *et al.*, 2012). MF terms such as cytokine receptor binding and protein serine kinase activity point to robust engagement of signalling cascades controlling gene expression, cell migration, and tissue infiltration (Fox *et al.*, 2020; Vanhaesebroeck *et al.*, 2012).

Concurrently, the repression of tolerance-associated genes (*SMAD6*, *HIC1*, *CD180*) and chromatin modifiers (*ID1*, *SMAD7*) reveals a strategic silencing of molecular brakes that would normally dampen NF-κB and TLR-driven transcription. GO BP and MF terms such as SMAD binding, histone modification, and ubiquitin-like protein ligase activity (Figure 4.5) demonstrate this suppression at multiple regulatory layers: transcriptional repression, post-translational modification, and chromatin remodelling (Foster *et al.*, 2007; Novakovic *et al.*, 2016; Saeed *et al.*, 2014). STRING PPI networks visualise these regulators as interconnected nodes clustered with

TGFBR1 and *CTBP2*, pivotal molecules for tolerance maintenance via TGF-β/SMAD pathways (X. Lin *et al.*, 2003; Park *et al.*, 2019; Van Rechem *et al.*, 2010).

ImmuneSigDB results reinforce this duality: LPS strongly upregulates gene sets associated with pro-inflammatory macrophage states, especially in contexts lacking counter-regulation by *IL-10* or alternative TLR agonists (El Kasmi *et al.*, 2007; Napolitani *et al.*, 2005). Simultaneously, it downregulates pathways typically enhanced by TREM-1 activation or TLR7/8 stimulation, confirming that TLR4 signalling dominates and suppresses competing innate routes (Amit *et al.*, 2009; Dower *et al.*, 2008).

Mechanistically, this transcriptional blueprint mirrors the paradox at the heart of CAP pathophysiology: Monocytes are reprogrammed to maximise pathogen recognition, engulfment, and inflammatory cytokine release, ensuring effective bacterial clearance. However, the concurrent suppression of tolerance regulators prevents timely de-escalation of this response, predisposing the lung microenvironment to excessive neutrophil recruitment, endothelial leakage, and alveolar damage (Bernard *et al.*, 2023; Medzhitov and Horng, 2009). This explains why patients with severe pneumonia often exhibit an uncontrolled cytokine storm even as bacterial loads decline, a signature captured in this model at the single-cell transcriptome level.

Critically, the identification of a type I IFN-dominated antiviral module within the LPS-induced network (Figure 4.3 (A)) aligns with the dual role of IFNs in bacterial infections: they aid pathogen clearance but also drive immunoregulatory crosstalk that can either resolve or prolong inflammation, depending on context (Bernard *et al.*, 2023; Monroe *et al.*, 2010; Pestka *et al.*, 2004). This highlights why therapeutic modulation of IFN pathways remains a double-edged sword in bacterial pneumonia.

In summary, this integrative analysis shows that LPS-stimulated monocytes adopt a transcriptional state primed for maximal host defence but with suppressed regulatory feedback, creating a fertile ground for hyperinflammation if left

unchecked. These findings provide a molecular explanation for the immunological imbalance observed in severe CAP and offer clear targets, such as *KLF6*, *IL-6*, and *SMAD6*, for future therapeutic intervention to restore immune homeostasis without compromising pathogen control.

4.1.2 Stratification of Monocyte Transcriptomes by TNF-α Response Magnitude

While LPS exposure consistently triggered a broad pro-inflammatory and IFN-driven transcriptional programme across all donors (Section 4.1.1), substantial inter-individual variation emerged in the magnitude of cytokine release. To capture this heterogeneity, monocytes were stratified based on TNF-α output, a canonical marker of monocyte activation and clinical severity in endotoxemia and pneumonia (Bradley, 2008; Parameswaran and Patial, 2010).

Samples were ranked by TNF-α concentration following LPS stimulation and grouped into quartiles: the top 25% (75-100% quartile) defined high responders, while the bottom 25% (0-25% quartile) defined low responders (Figure 4.7).

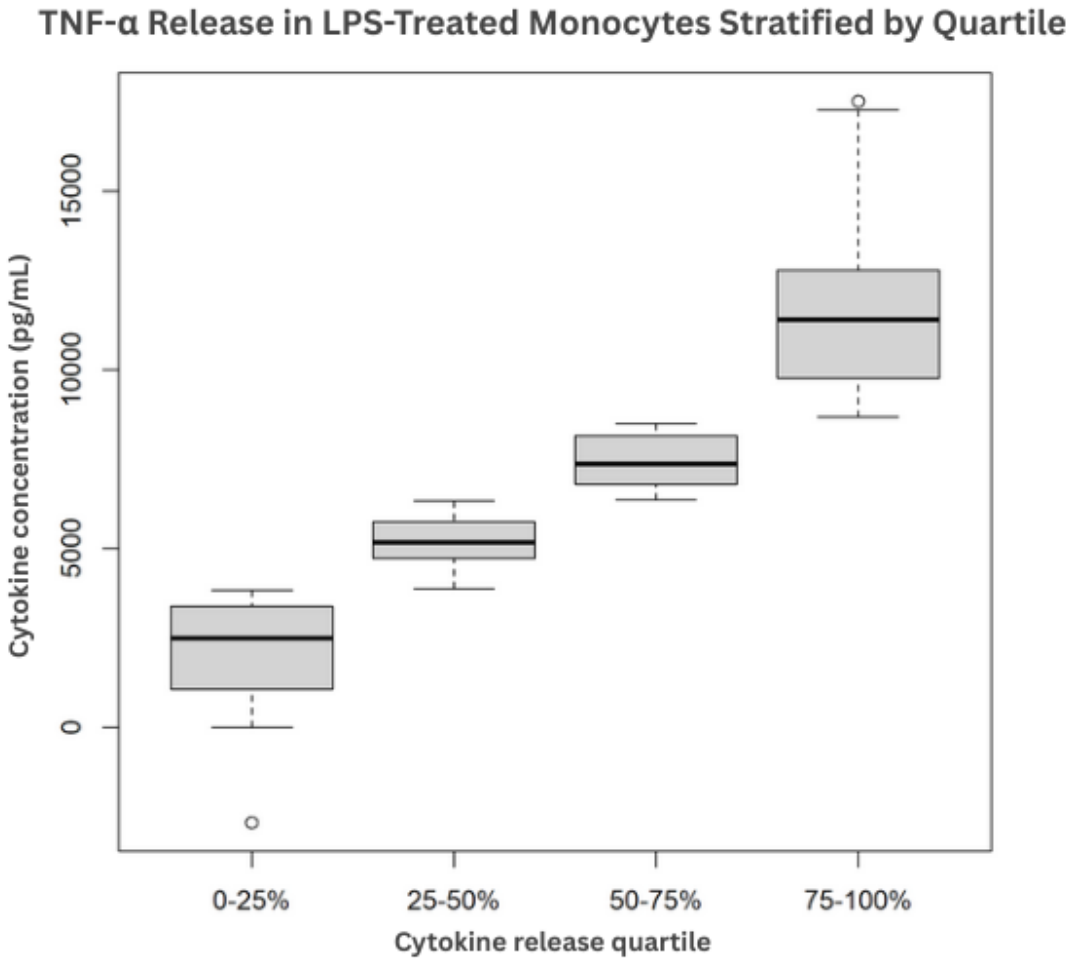

Figure 4.7. TNF-α release in LPS-treated monocyte samples stratified by quartiles. *TNF-α release in LPS-treated monocyte samples, grouped into quartiles: 0-25% (low responders), 25-50%, 50-75%, and 75-100% (high responders). Samples in the top quartile were defined as high responders and those in the bottom quartile as low responders for downstream transcriptomic analysis.*

Dimensionality reduction and correlation-based clustering consistently demonstrated that TNF-α release closely aligned with global expression variation, while sex emerged as a secondary but significant axis of variance; accordingly, sex was retained as an additive covariate in all downstream analyses (Methodology Section 3.2). Specifically, PCA of rlog-transformed gene expression data (Figure 4.8) revealed two distinct clusters along PC1, explaining 20.34% of total variance and reflecting TNF-α response levels, indicating broad transcriptional reprogramming

linked to cytokine output. PC2 accounted for an additional 12.55% of variance and stratified samples by sex, a trend consistent with documented sex-based immune differences (Klein and Flanagan, 2016; Márquez *et al.*, 2020). Correlation-based clustering and a Pearson correlation heatmap of rlog-transformed data (Appendix Figure 14) further reinforced this structure, showing strong intra-group similarity (correlation coefficients ~0.88-1.0) and clear inter-group separation, confirming robust and reproducible gene expression patterns underlying inflammatory responsiveness. This integrated approach validated that TNF-α output is a primary driver of monocyte transcriptomic heterogeneity, with sex acting as a modulating factor, thereby justifying its inclusion as a covariate in the final *DESeq2* model to ensure precise, bias-adjusted detection of cytokine-associated signatures (Love, 2024).

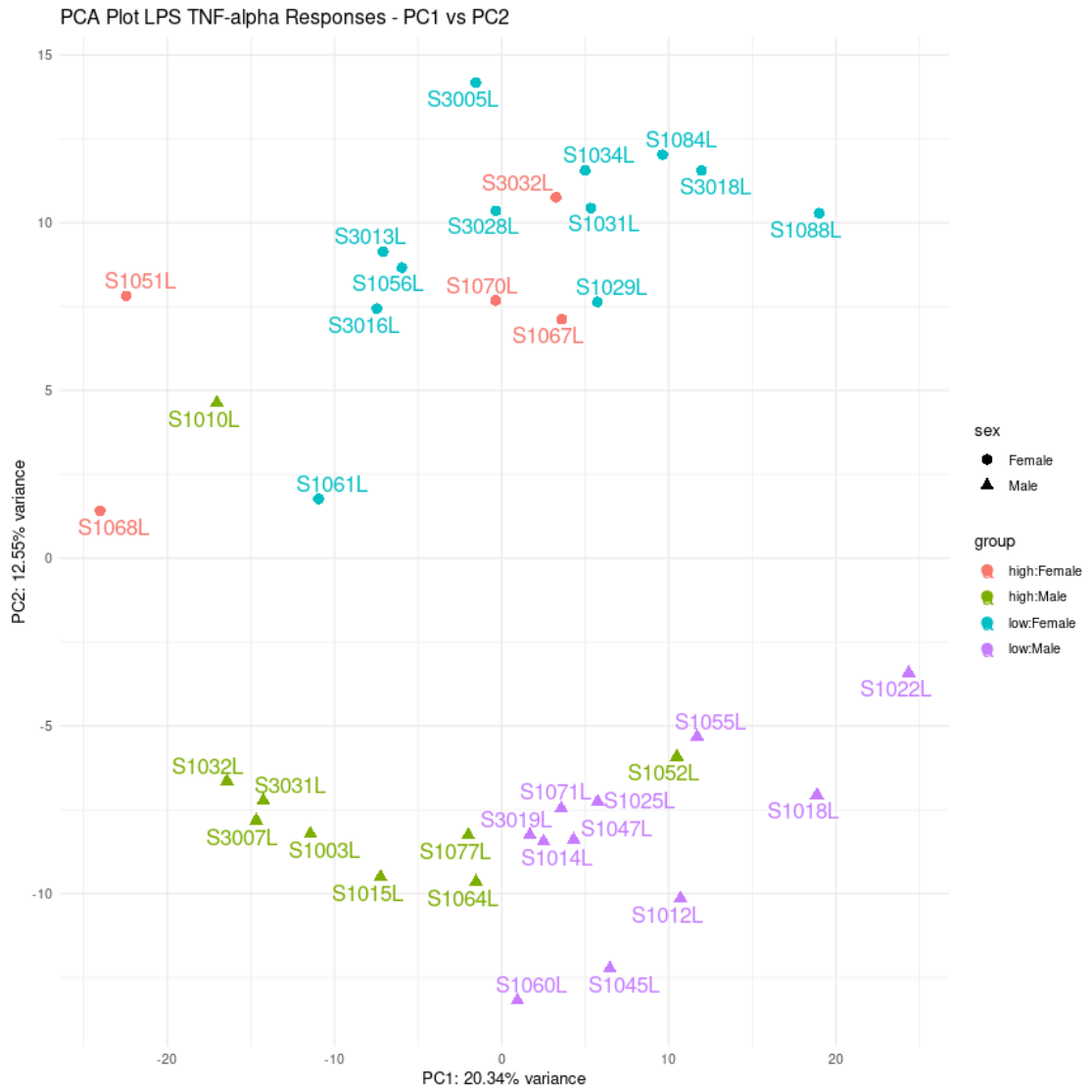

Figure 4.8. PCA of TNF-α response in LPS-treated monocytes. *PC1 (20.34%) distinguishes high and low TNF-α responders; PC2 (12.55%) stratifies samples by sex. colours indicate groups: red (high-female), green (high-male), blue (low-female), purple (low-male). Circles represent female samples; triangles represent male samples.*

Comparison of high versus low TNF-α responders revealed a focused but biologically relevant DEG signature (Volcano Plot, Figure 4.9). High responders upregulated genes linked to antigen processing and presentation, type I IFN signalling, and cytokine receptor pathways, amplifying transcriptional programmes for pathogen recognition and inflammatory escalation. In contrast, low responders maintained higher expression of genes governing ECM organisation, solute transport, and redox

homeostasis, indicating a more restrained, tissue-preserving profile that prioritises structural integrity and metabolic resilience. PPI networks (STRING, Figures 4.10-4.11) and pathway enrichment analyses (GO, Figures 4.12-4.13) corroborated these divergent states: high responders formed dense immune activation hubs, whereas low responders engaged integrated metabolic-redox modules that may mitigate excessive inflammation. Collectively, these findings demonstrate that stratifying by TNF-α output uncovers distinct monocyte immune programmes, one favouring robust inflammatory amplification, the other supporting tolerance and repair, offering mechanistic insight into inter-individual variation in susceptibility to hyperinflammatory injury and recovery following endotoxin challenge.

4.1.2.1 DGE Between High and Low TNF-α Responders

Differential expression analysis comparing TNF-α high and low responders, adjusted for sex stratification and refined using *Ashr* shrinkage with contrast, revealed a focused yet biologically meaningful transcriptional response (Love *et al.*, 2014; Stephens *et al.*, 2016). Of the 18,195 genes tested, all were assigned nominal *p*-values and $\log_2$FC estimates, with 555 genes additionally meeting the multiple-testing corrected threshold (*padj* ≤ 0.01): 228 upregulated (41%) and 327 downregulated (59%) in high responders (Appendix Table 1). *Ashr* shrinkage stabilised $\log_2$FC estimates and improved interpretability, yielding a robust view of TNF-α–associated transcriptional variation. A volcano plot visualises the full distribution (Figure 4.9): genes are plotted by $\log_2$FC and $-\log_{10}$ nominal *p*-value, with points exceeding the adjusted threshold (*padj* ≤ 0.01) highlighted at the plot's extremes.

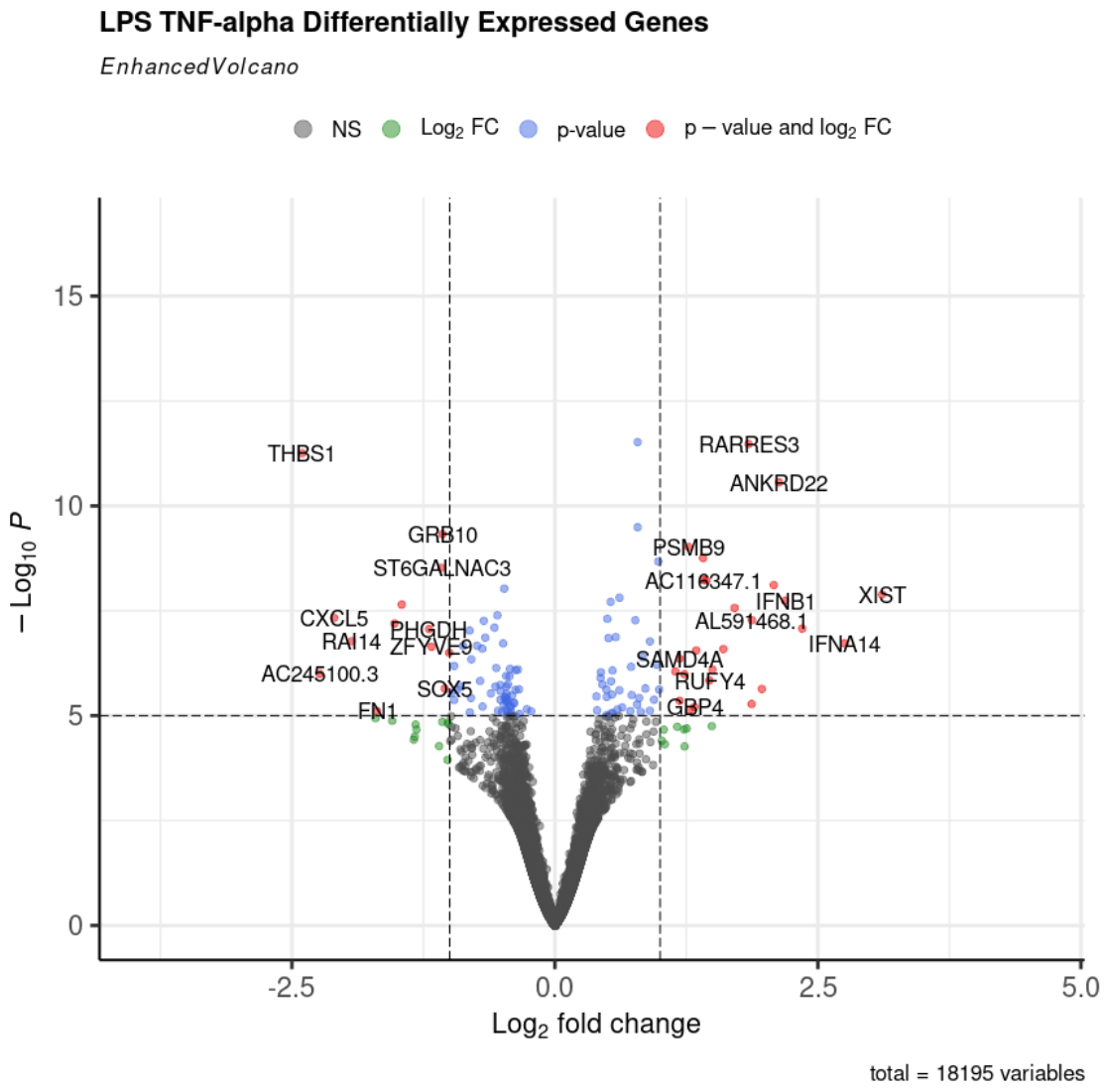

Figure 4.9. Volcano plot showing all 18,195 genes tested in TNF-α high vs. low responders. *The x-axis displays log₂FCs; the y-axis shows −log₁₀ nominal p-value. Notable upregulated genes in high responders include IFNB1, IFNA14, ANKRD22, and XIST; prominent downregulated genes include THBS1, CXCL5, RAI14, and FN1. Genes passing the multiple testing adjusted threshold (padj ≤ 0.01) are highlighted in red at the plot's extremities.*

Upregulated genes included *IFNB1* and *IFNA14*, canonical type I IFNs central to LPS-induced activation and antiviral defence (Klassert *et al.*, 2017). Ankyrin Repeat Domain (*ANKRD*) 22 and Calcium Homeostasis Modulator Family Member (*CALHM*) 6, both IFN-inducible and linked to inflammatory signalling, were also elevated

(Danielli *et al.*, 2023; Zang *et al.*, 2023). Guanylate Binding Protein (*GBP*) 5, another IFN-stimulated gene involved in inflammasome regulation (Zwack *et al.*, 2017) was similarly upregulated. The long non-coding RNA X-Inactive Specific Transcript (*XIST*) showed increased expression, reflecting sex-based transcriptional differences (Carrel and Willard, 2005).

Conversely, TNF-α high responders showed significant downregulation of immune and matrix remodelling genes. Thrombospondin (*THBS*) 1 and *MMP9*, which mediate leukocyte trafficking and ECM breakdown, were strongly suppressed (He *et al.*, 2022). The chemokine *CXCL5*, which recruits neutrophils, was also downregulated (Mei *et al.*, 2010). *FN1*, encoding Fibronectin, a key ECM component for monocyte adhesion and tissue remodelling (Rudnik *et al.*, 2021), was likewise reduced. Together, this implies a restrained inflammatory and migratory phenotype despite elevated TNF-α.

4.1.2.2 PPI Network Analysis Reveals Functional Clusters in High and Low TNF-α Responders

STRING analysis of the top 100 upregulated genes (Figure 4.10) revealed a dense network anchored by IFN signalling, antigen processing, and cytokine-mediated activation. IFNB1 was a major hub linked to Proteasome Subunit (PSM)-B9, TNFSF10, and Beta-2-Microglobulin (B2M) (Qureshi *et al.*, 2023; Schmid *et al.*, 2010). A proteasome module centred on Proteasome Activator Subunit (PSME) 2 incorporated PSMB8, PSMB10, PSME1, PSMA4, Ubiquitin-Conjugating Enzyme (UBE) 2L6, and IFN-Induced Protein (IFI) 35 (Bae and Lee, 2018; Javed *et al.*, 2016). A cytokine receptor cluster centred on CD40 connected to IL-27, IL-12RB1, IL-15, CD72, and IL-15RA (de Jong *et al.*, 1998; Hall *et al.*, 2012; van Kooten and Banchereau, 2000; Waldmann, 2006). IRF8 linked IFN and cytokine modules, while GBP5 bridged to CD274, reinforcing trained immunity and inflammasome control (B.-H. Kim *et al.*, 2016; S. Ma *et al.*, 2023).

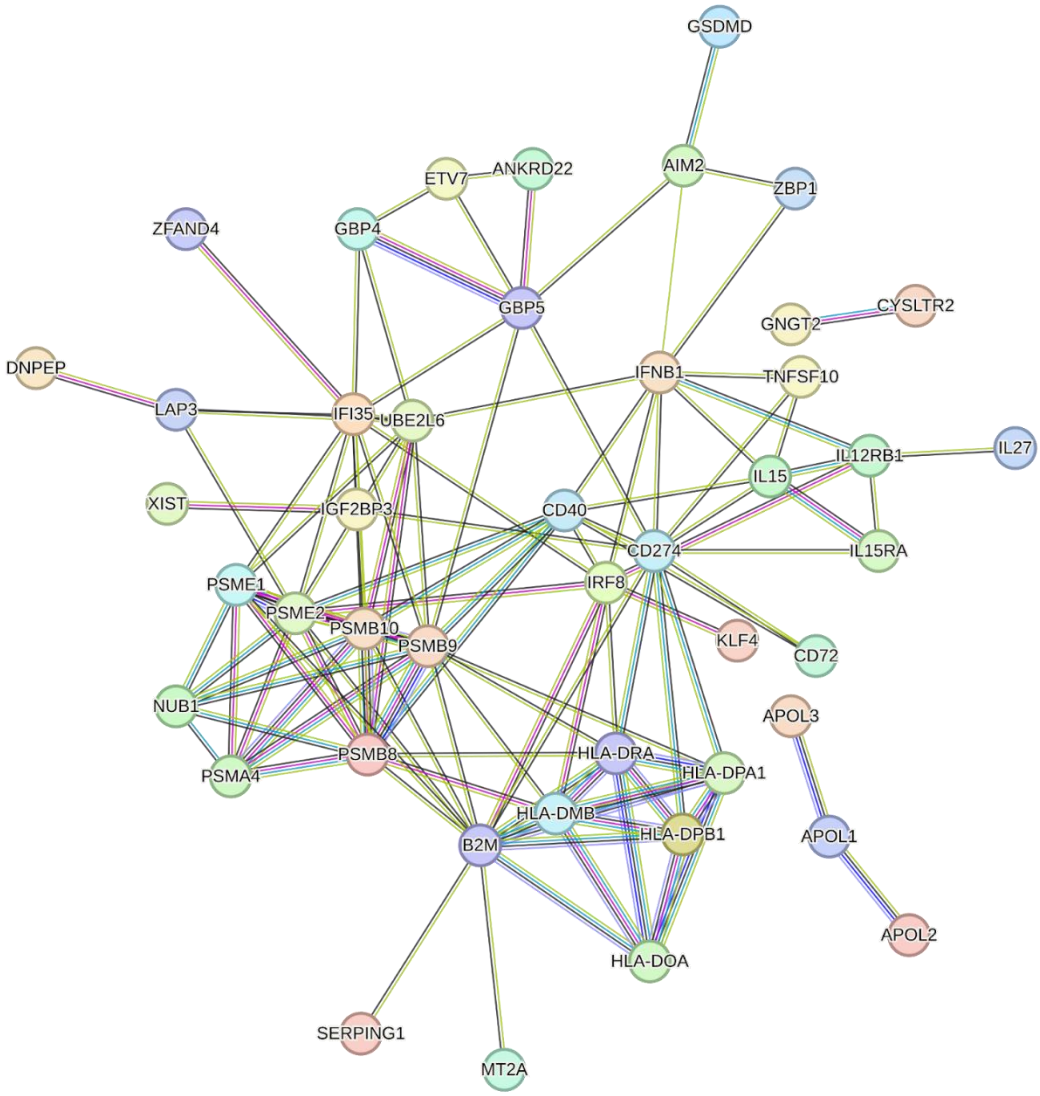

Figure 4.10. STRING PPI network of the top 100 upregulated genes in TNF-α high responders. *Nodes represent proteins encoded by significantly upregulated genes (padj ≤ 0.01, baseMean > 50), and edges reflect high confidence predicted or known interactions derived from the STRING database. Edge types include experimental evidence, curated databases, gene co-expression, and text mining. Central hubs such as IFNB1, PSME2, HLA-DPA1, IL-15, CD40 and TNFSF10 are highlighted by multiple high-confidence connections, forming functional modules related to IFN signalling, immunoproteasome assembly, cytokine receptor engagement, and antigen presentation. The network visualisation emphasises the structured nature of transcriptional activation in TNF-α high responders, with interconnected immune signalling pathways.*

STRING analysis of the top 100 downregulated genes (Figure 4.11) revealed two clusters: an upper immune/tissue remodelling module and a lower metabolic/redox module. The immune cluster was anchored by Insulin Receptor Substrate (IRS) 1, CXCL5, FN1, MMP9, MMP14, with links to Fibroblast Growth Factor Receptor (FGFR) 1, VEGFR1, MET, and IL-7R (Alexander *et al.*, 2015; Mansour *et al.*, 2006; Salminen *et al.*, 2021; W. Xu *et al.*, 2019; Y. Zhou *et al.*, 2024). CXCL5 connected with CXCL1, CCL20, IL-1R2, IL-7R, MMP9, MMP14, and A Disintegrin and Metalloproteinase with Thrombospondin Motif (ADAMTS) 2, highlighting dampened infiltration/remodelling capacity (Etich *et al.*, 2019; Fingleton, 2017; Gill and Parks, 2008; Visse and Nagase, 2003).

The metabolic cluster, anchored by Solute Carrier Family 1 Member (SLC1A) 5, Glutamate-Cysteine Ligase Modifier Subunit (GCLM), Malic Enzyme (ME) 1, and Phosphoserine Aminotransferase (PSAT) 1, included SLC7A11, SLC38A1, BCAT1, Thioredoxin Reductase (TXNRD) 1, ChaC Glutathione Specific Gamma-Glutamylcyclotransferase (CHAC) 1, Sestrin (SESN) 2, and DNA Damage Inducible Transcript (DDIT) 4 (T. Liu *et al.*, 2023; Tang *et al.*, 2023; J. Zhao *et al.*, 2020). Downregulation suggests reduced oxidative stress resilience and metabolic adaptability, matching an energetically restrained monocyte state.

Bridging nodes (MMP9, FN1, Peroxisome Proliferator-Activated Receptor (PPAR) D, Acyl-CoA Synthetase Long Chain Family Member (ACSL) 1, BCAT1, SLC1A5) integrated ECM remodelling, nutrient sensing and stress adaptation, underscoring how high responders simultaneously dampen cytokine effectors and metabolic pathways, which is a transcriptional signature of tolerance and energy conservation following LPS challenge.

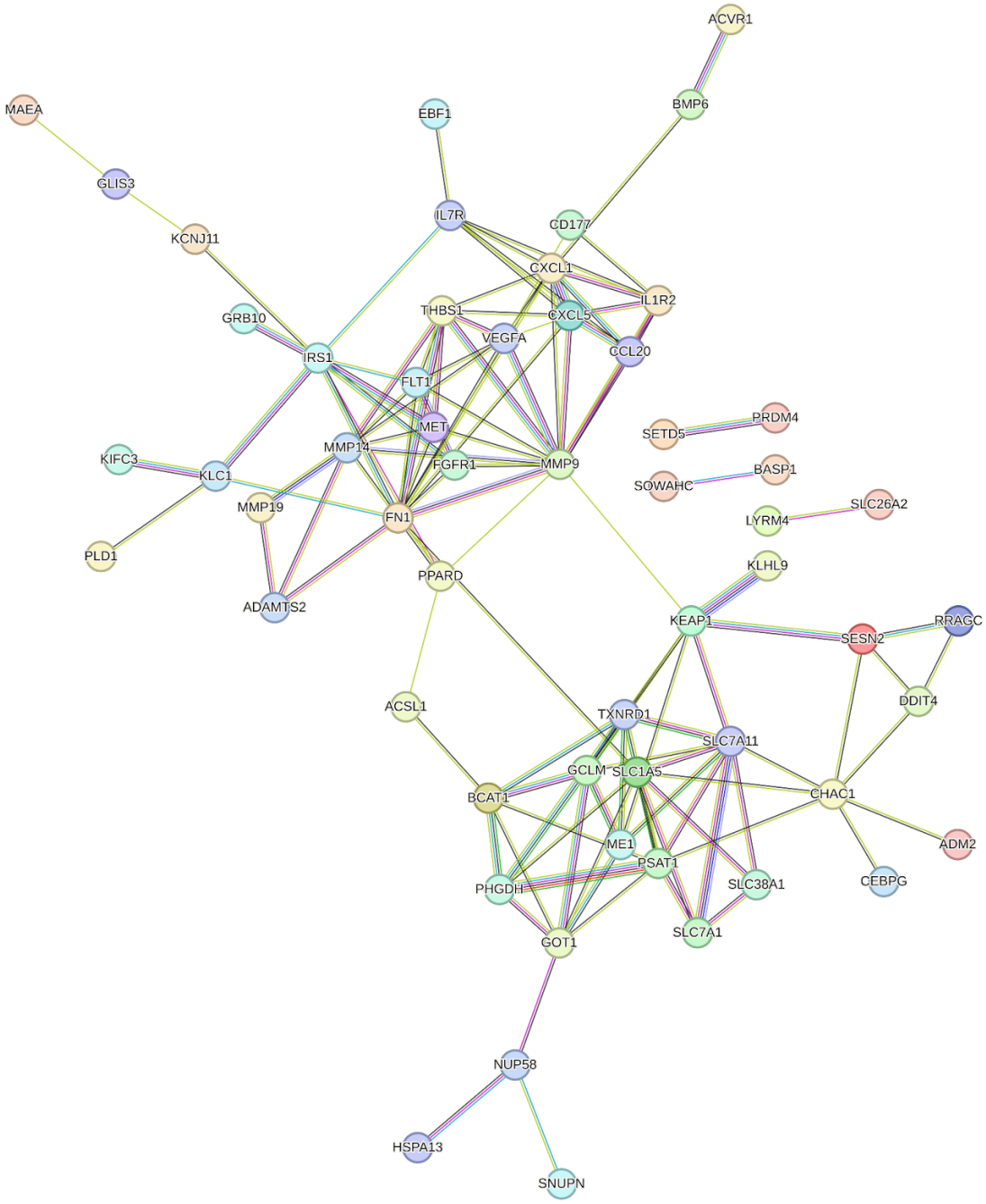

Figure 4.11. PPI network of the top 100 downregulated genes in TNF-α high responders. *Nodes represent proteins encoded by significantly downregulated genes (padj ≤ 0.01; baseMean > 50), with edges reflecting known or predicted interactions derived from experimental evidence, curated databases, text mining, co-expression, and gene neighborhood. Two major clusters are evident: an upper immune-associated cluster centered around CXCL5, MMP9, IRS1, and FN1, and a lower metabolism- and redox-associated cluster anchored by SLC1A5, GCLM, and ME1. Central nodes connecting the clusters include MMP9, FN1, PPARD, and BCAT1.*

4.1.2.3 Integrated Expression Profiles Reveal Divergent Immune and Metabolic States

The volcano plot comparing TNF-α high and low responders revealed a robust upregulation of type I IFN-stimulated genes (ISGs) in individuals with elevated cytokine release (Figure 4.9). Among these, *IFNB1* and *IFNA14* emerged as two of the most significantly upregulated transcripts in the dataset, consistent with their well-established roles as pivotal mediators of LPS-induced antiviral responses and innate immune activation (Klassert *et al.*, 2017). Their consistent recurrence across multiple contrasts, including the broader LPS vs. media comparison, underscores their dominant function as central effectors of monocyte activation under inflammatory stress within this donor cohort, highlighting the centrality of a type I IFN-driven immune activation program under LPS stimulation.

Beyond *IFNB1* and *IFNA14*, significant upregulation of several additional IFN-inducible transcripts was detected in high responders, including *ANKRD22*, *CALHM6*, and *GBP5*. While *ANKRD22* has been previously linked to inflammatory cytokine production (Danielli *et al.*, 2023) and *CALHM6* to immune cell activation and membrane remodelling (S. Zhang *et al.*, 2024) their co-expression in the context of elevated TNF-α production constitutes a novel feature of the transcriptional program captured in the dataset. *GBP5*, known to participate in inflammasome activation and cytosolic bacterial sensing (Man *et al.*, 2017), was embedded within a broader network of innate effector genes, suggesting that monocytes in high responders are transcriptionally primed for robust pathogen sensing and inflammasome activity.

The long non-coding RNA *XIST* also appeared among the upregulated transcripts in high responders. This upregulation reflects the inclusion of sex as a covariate in the *DESeq2* model and validates appropriate control for sex-specific transcriptional effects (Carrel and Willard, 2005; Disteche, 2016) rather than direct involvement in inflammatory signalling, reinforcing the methodological rigor of the dataset analysis.

PPI network analysis of the top 100 upregulated genes in TNF-α high responders revealed a highly interconnected module centred on IFNB1 (Figure 4.10). This core cluster directly linked IFNB1 to PSMB9, TNFSF10, and B2M, forming a signalling axis aligned with type I IFN responses and enhanced antigen presentation (Qureshi *et al.*, 2023; Schmid *et al.*, 2010). The immunoproteasome subunits PSMB9, PSMB8, and PSME2, well documented for their role in endogenous antigen processing (Groettrup *et al.*, 2010) were co-upregulated, revealing strong activation of proteasomal machinery to support efficient peptide generation for MHC class I presentation and sustained immunological vigilance in high responders.

A second interconnected subnetwork centred around PSME2 was enriched for proteasome and ubiquitin pathway genes, including PSMB10, PSME1, PSMA4, UBE2L6, and IFI35. The presence of these components aligns with established functions in antigenic peptide processing (Bae and Lee, 2018; Javed *et al.*, 2016; Vigneron and Van den Eynde, 2014) and confirms that high TNF-α responders in the dataset exhibit an enhanced proteolytic capacity coupled to robust antigen presentation, further supporting cytotoxic T-cell activation (Rock *et al.*, 2002).

Parallel to the IFN and proteasome modules, a cytokine receptor signalling cluster anchored by CD40 connected directly to IL-27, IL-12RB1, and IL-15, consistent with a coordinated transcriptional program for T-cell co-stimulation and cytokine-mediated amplification (van Kooten and Banchereau, 2000). Additional linkages to CD72 and IL-15RA expand this cluster, indicating integration between antigen-presenting cell maturation signals and effector lymphocyte activation pathways (Waldmann, 2006). Within this network, IRF8 occupied a bridging position, connecting the IFNB1 and CD40-driven modules; while its induction by type I IFNs is well established (S. Ma *et al.*, 2023; Moorman *et al.*, 2022), the bridging role highlighted here illustrates how IFN signalling and cytokine receptor pathways converge in monocytes with high TNF-α production, reinforcing a tightly coordinated innate and adaptive immune interface.

The GBP family, particularly GBP4 and GBP5, formed a distinct subnetwork linking to CD274, Serpin Family G Member (SERPING) 1, and Apolipoprotein L (APOL) 1-APOL3 genes. These connections imply upregulation of cytosolic bacterial sensing, inflammasome regulation, and checkpoint control (B.-H. Kim *et al.*, 2016), indicating that the transcriptional landscape in high responders balances robust pathogen elimination with mechanisms that may limit excessive tissue-damaging inflammation.

Consistent with the pronounced activation of antigen processing, upregulation of several HLA class II molecules was also detected, including HLA-DPA1, HLA-DPB1, HLA-DOA, HLA-DMB, and HLA-DRA. These genes clustered closely with CD274 and B2M, supporting a dual enhancement of both MHC class I and II presentation machinery. This suggests that monocytes in high responders are transcriptionally configured for broad-spectrum antigen presentation, capable of priming both cytotoxic and T-helper cell responses (J. Lee *et al.*, 2017). Notably, HLA-DRA, a marker of sepsis-induced immunosuppression (Cajander *et al.*, 2016) was upregulated alongside these immune activation modules, underscoring the complexity of transcriptional states balancing immune defence and regulation under inflammatory stress.

In contrast, low responders exhibited a distinct gene expression signature characterised by relatively higher expression of a defined subset of genes involved in immune regulation, leukocyte trafficking, and ECM remodelling (Figures 4.9 and 4.11). Among the most significantly downregulated genes in high responders, and thus more highly expressed in low responders, were *THBS1*, *CXCL5*, *MMP9*, and *FN1* (He *et al.*, 2022; Mei *et al.*, 2010; Rudnik *et al.*, 2021). These genes have established roles in tissue remodelling and cancer progression. For example, overexpression of *Connective Tissue Growth Factor (CTGF)*, *FN1*, *IL-6*, *THBS1*, and *WISP1* has been linked to reduced survival in gastric cancer (Khoshdel *et al.*, 2024). *CXCL5*, a key regulator of neutrophil recruitment and angiogenesis, has been shown to promote tumour progression (C. Chen *et al.*, 2019; W. Zhang *et al.*, 2020; Z. Zhou *et al.*, 2019).

Similarly, *THBS1* facilitates angiogenesis and tumour spread through cell–matrix interactions (S. Zhang *et al.*, 2021), while FN1 enhances tumour cell adhesion, migration, and invasion (Cajander *et al.*, 2016).

The volcano plot confirmed that ECM remodelling and immune trafficking genes are relatively more abundant in low responders. PPI analysis revealed two interconnected clusters: the first dominated by MMP9, MMP14, FN1, and THBS1, coordinating ECM remodelling and leukocyte infiltration (Fingleton, 2017; Gill and Parks, 2008; Visse and Nagase, 2003), with CXCL5 linking to other chemokines (Cabral-Pacheco *et al.*, 2020; Mei *et al.*, 2010). Additional hubs such as IRS1, FGFR1, FLT1, and MET integrated growth factor signalling with ECM dynamics (Alexander *et al.*, 2015; Mansour *et al.*, 2006; Salminen *et al.*, 2021; W. Xu *et al.*, 2019; Y. Zhou *et al.*, 2024).

STRING visualisation (Figure 4.11) reinforced THBS1, FN1, and CXCL5 as central in the ECM remodelling module, implying sustained monocyte migration, leukocyte trafficking, and dynamic tissue interaction (Gill and Parks, 2008; Rudnik *et al.*, 2021; Zhong *et al.*, 2024). A second cluster, centred on SLC1A5 and encompassing SLC7A11, SLC38A1, PSAT1, ME1, GCLM, and BCAT1, indicated sustained Nicotinamide Adenine Dinucleotide Phosphate (NADPH) production, serine biosynthesis, and antioxidant defence (T. Liu *et al.*, 2023; J. Zhao *et al.*, 2020). TXNRD1, CHAC1, and stress-responsive genes DDIT4, SESN2, CEBPG, and ADM2 reinforced redox balance (Schmidlin *et al.*, 2019; Tang *et al.*, 2023).

The metabolic and ECM modules were bridged by MMP9, FN1, PPARD, ACSL1, BCAT1, and SLC1A5, demonstrating that low responders coordinate ECM remodelling with nutrient sensing and stress adaptation within an integrated architecture (Hotamisligil, 2017; H. S. Lee and Kim, 2022).

Incorporation of sex as a covariate was essential for resolving these profiles. Consistent with prior observations, female donors exhibited heightened ISG expression, including *IFNB1*, *IFNA14*, *GBP5*, and *IRF8* (Gettler *et al.*, 2019; La Mata *et*

al., 2023; Quin *et al.*, 2024), while low responders, mostly male, maintained higher expression of *THBS1*, *CXCL5*, *FN1*, and *SLC1A5*, suggesting a sex-influenced immunoregulatory and metabolically adaptive state (Klein and Flanagan, 2016; Schurz *et al.*, 2019; Taneja, 2018). The prominence of *XIST* among key transcripts confirmed successful adjustment for sex differences without obscuring core IFN-driven signatures.

Together, these data describe how TNF-α high responders maintain a coordinated IFN-driven immune activation program, while low responders preserve a distinct matrix-remodelling and metabolic resilience profile, modulated in part by sex-specific transcriptional influences.

4.1.2.4 Pathway Enrichment Analysis Highlights Divergent Immune and Metabolic Programmes

Building on the transcriptional shifts observed in the global LPS vs. media comparison, this section examines how variation in TNF-α responsiveness corresponds to distinct pathway-level immune states. Using the combined enrichment approach (Section 3.12), which integrates GO term overrepresentation and non-pre-ranked GSEA for Hallmark and ImmuneSigDB gene sets, the analysis highlighted functional programmes distinguishing high and low cytokine responders after LPS stimulation.

Although overall differential expression between responder groups was narrower than in the broader LPS response, pathway enrichment revealed clear mechanistic contrasts. High responders showed strong positive enrichment of adaptive immune processes (Figure 4.12), especially antigen presentation, with top GO terms including MHC protein complex, MHC class II complex, and peptide antigen assembly, driven by upregulation of *HLA-DPA1*, *HLA-DPB1*, *HLA-DOA*, *HLA-DMB*, and *HLA-DRA* (Madej *et al.*, 2017; Rayees *et al.*, 2020; Tiemeijer *et al.*, 2023). This pattern co-occurred with elevated *IFNB1*, *IL-27*, and *CD40*, suggesting monocytes in high

responders are transcriptionally primed for robust antigen presentation and T-cell activation (Schenten and Medzhitov, 2011; Takeuchi and Akira, 2010). Enrichment of leukocyte and lymphocyte proliferation terms further supported heightened immune coordination. Notably, the presence of the adaptive immune response term based on somatic recombination, while functionally executed by lymphocytes, likely reflects the supportive transcriptional milieu provided by monocytes (Notarangelo *et al.*, 2016).

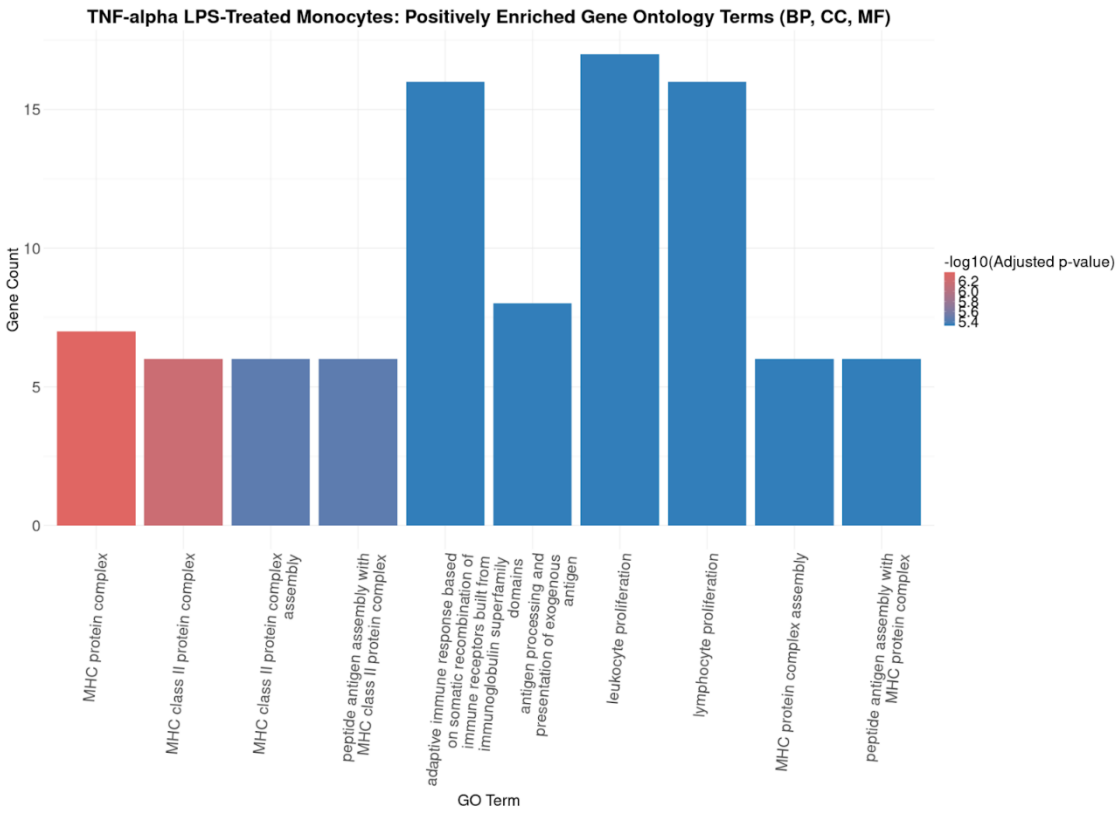

Figure 4.12. Top 10 most significantly positively enriched GO terms in TNF-α high responders relative to low responders. *Each bar represents a GO term enriched among genes upregulated in high responders, with bar height indicating the number of DEGs contributing to the term. The x-axis lists GO terms, ordered by significance, and the y-axis displays gene counts. A color gradient from red to blue encodes enrichment strength, where red indicates higher significance ($-\log_{10}$ x padj ≈ 6.2) and blue denotes lower significance ($-\log_{10}$ x padj ≈ 5.4). Positively enriched terms highlight antigen presentation, MHC complex assembly, and adaptive immune activation.*

In contrast, negatively enriched terms in high responders (Figure 4.13) indicated suppression of pathways related to cellular transport, metabolism, and redox adaptation. Downregulation of *SLC1A5*, *SLC7A11*, and *SLC38A1* suggested constrained nutrient import (O'Neill *et al.*, 2016), while decreased *GCLM*, *SESN2*, and *TXNRD1* implied reduced antioxidant capacity (Mills *et al.*, 2016; Nathan and Cunningham-Bussel, 2013). Reduced expression of ECM remodelling and adhesion factors such as *FN1*, *MMP9*, and *THBS1* further highlighted a profile favouring immune effector activation over tissue interaction or metabolic adaptability (Marangio *et al.*, 2022).

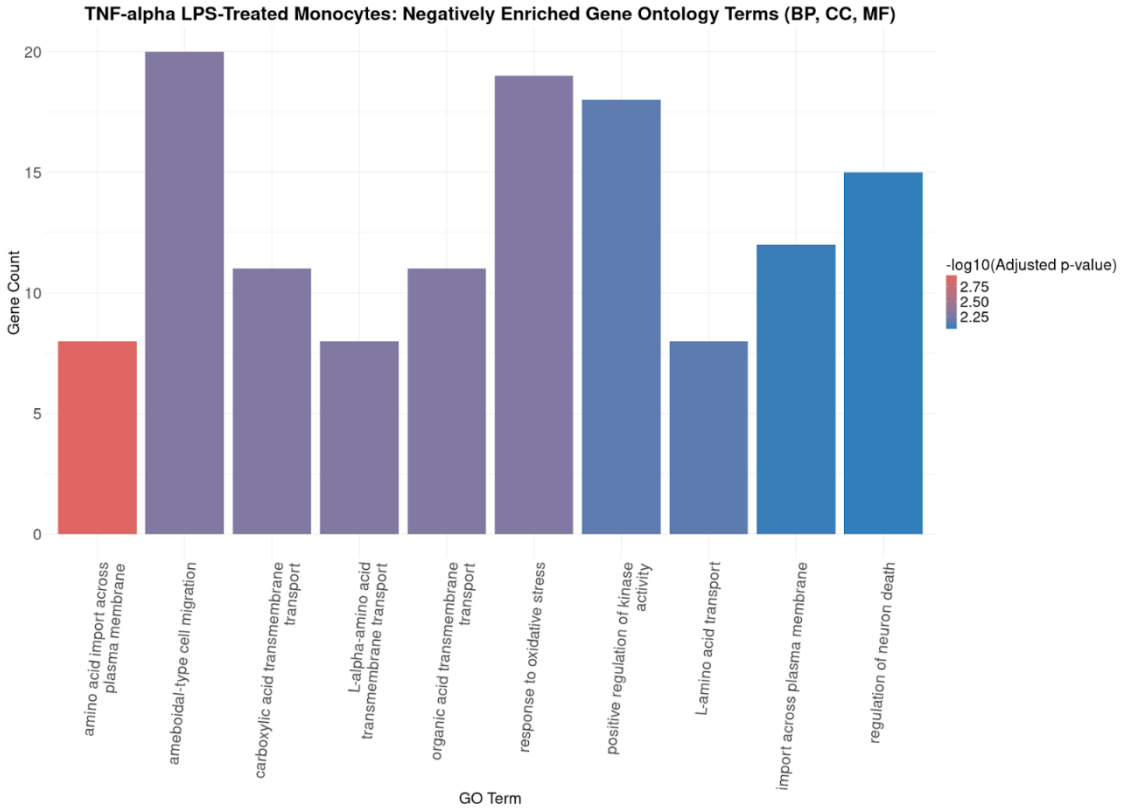

Figure 4.13. Top 10 most significantly negatively enriched GO terms in TNF-α high responders relative to low responders. *The bar plot displays the most enriched GO terms among downregulated genes in high responders. Each bar denotes a GO term, with bar height corresponding to the number of DEGs annotated to that term. GO terms are sorted on the x-axis by statistical significance, while gene counts appear on the y-axis. A red-to-blue color scale indicates enrichment strength, with red reflecting higher significance ($-\log_{10}$ x padj ≈ 2.75) and blue lower significance ($-\log_{10}$ x padj ≈ 2.25). These terms reflect reduced expression of genes involved in amino acid transport, oxidative stress response, and chemotaxis.*

These patterns parallel the global LPS vs. media response (Section 4.1.1.2), where LPS broadly activated innate and antiviral pathways while suppressing housekeeping programmes. TNF-α stratification refined this, revealing that high responders selectively amplify antigen presentation, IFN signalling, and cytokine co-stimulation while further repressing metabolic transport, redox buffering, and motility. Low responders, meanwhile, retained higher expression of amino acid transport, oxidative stress control, and ECM remodelling genes, including *THBS1*, *FN1*, *CXCL5*, and *SLC1A5*, indicating a phenotype focused on tissue interaction and controlled inflammation rather than escalated immune activation.

PPI network analysis supported these functional profiles: high responders showed dense modules centred on IFNB1, CD40, PSMB9, and HLA molecules, indicative of an organised immune amplification axis. Low responders displayed networks anchored by solute carriers and ECM regulators, reflecting maintained immunometabolic flexibility and structural adaptability.

Biologically, these patterns suggest high responders exhibit features of trained immunity, an epigenetically primed, heightened innate response (Netea *et al.*, 2016), while low responders show a more tolerant state aimed at preventing excessive inflammation (O'Neill *et al.*, 2016). The suppression of metabolic and redox genes in high responders implies reallocation of resources toward immediate immune activation at the expense of resilience and repair. Conversely, low responders maintain a bioenergetically favourable state supporting long-term function.

Importantly, stratification by TNF-α production uncovered how within the LPS-driven activation, monocytes diverge into distinct states balancing immune escalation and tolerance (M. N. Lee *et al.*, 2014). High responders upregulated genes for MHC class II assembly, type I IFN signalling, and cytokine co-stimulation but repressed amino acid transporters (*SLC1A5*), redox regulators (*GCLM*, *TXNRD1*), and ECM components (*THBS1*, *FN1*) (Cheng *et al.*, 2014), indicating trade-offs favouring pathogen clearance over metabolic flexibility (Mohammadnezhad *et al.*, 2022; O'Neill *et al.*, 2016; Pearce and Pearce, 2013). Low responders, with sustained

expression of *CXCL5*, *FN1*, *MMP9*, and solute carriers, maintained pathways supporting stress tolerance and tissue integrity (W. Lin *et al.*, 2020; Q. Wu *et al.*, 2021; Xue *et al.*, 2014).

These enrichment profiles echo the global LPS vs. media patterns but demonstrate how TNF-α responsiveness layers additional variation onto shared innate programmes (Domínguez-Andrés *et al.*, 2019; Netea *et al.*, 2016).

Adjusting for sex as a covariate was critical to prevent confounding by sex-linked transcriptional differences, especially in type I IFN and MHC pathways (Klein and Flanagan, 2016; López-Collazo and del Fresno, 2013; Márquez *et al.*, 2020). For example, *XIST*, an X-chromosome inactivation marker, was upregulated in high responders partly due to female overrepresentation (Disteche, 2012; Schurz *et al.*, 2019). By accounting for sex, the analysis robustly isolated true cytokine-driven effects: MHC protein complex and adaptive immune terms remained significantly enriched, while stable metabolic gene expression in low responders (*SLC1A5*, *THBS1*, *GCLM*) confirmed an authentic regulatory orientation, not merely a demographic artefact (Taneja, 2018; Wilkinson *et al.*, 2022).

In sum, this sex-adjusted enrichment framework clarifies that individual transcriptional states, and not demographic bias, shape divergent monocyte trajectories after LPS challenge. Recognising these patterns informs precision approaches for immune modulation, accounting for interindividual and sex-based variation (S. Xu *et al.*, 2024).

4.1.2.5 GSEA Highlights Distinct Hallmark and Immune Signatures in TNF-α Responder Phenotypes

GSEA of Hallmark and ImmuneSigDB gene sets revealed phenotype-specific transcriptional programmes distinguishing the low and high TNF-α responder groups. In the low responders (n = 23), Hallmark analysis (Figure 4.14) identified significant enrichment (FDR < 0.25) for pathways including Androgen Response,

PI3K/AKT/mTOR Signalling, Mitotic Spindle, and UV Response DN, implicating increased proliferative signalling and hormonal regulation (Saxton and Sabatini, 2017). Additionally, TGF-β Signalling and Coagulation demonstrated high NES (> 1.6) with nominal $p < 0.01$, suggesting biological relevance despite narrowly missing FDR significance (Wynn and Vannella, 2016). Complementary ImmuneSigDB analysis highlighted broader immune activation in the low group, with 85 gene sets enriched at $p < 0.01$ and 271 at $p < 0.05$. Top-ranked immune programmes (NES > 1.87) pointed to robust activation of IFN-responsive microglia, $CD4^+$ T-cell polarization, and monocyte-driven pathways (Prinz and Priller, 2014; J. Zhu *et al.*, 2010). These findings support a phenotype characterised by sustained proliferative and regulatory signals alongside flexible immune readiness.

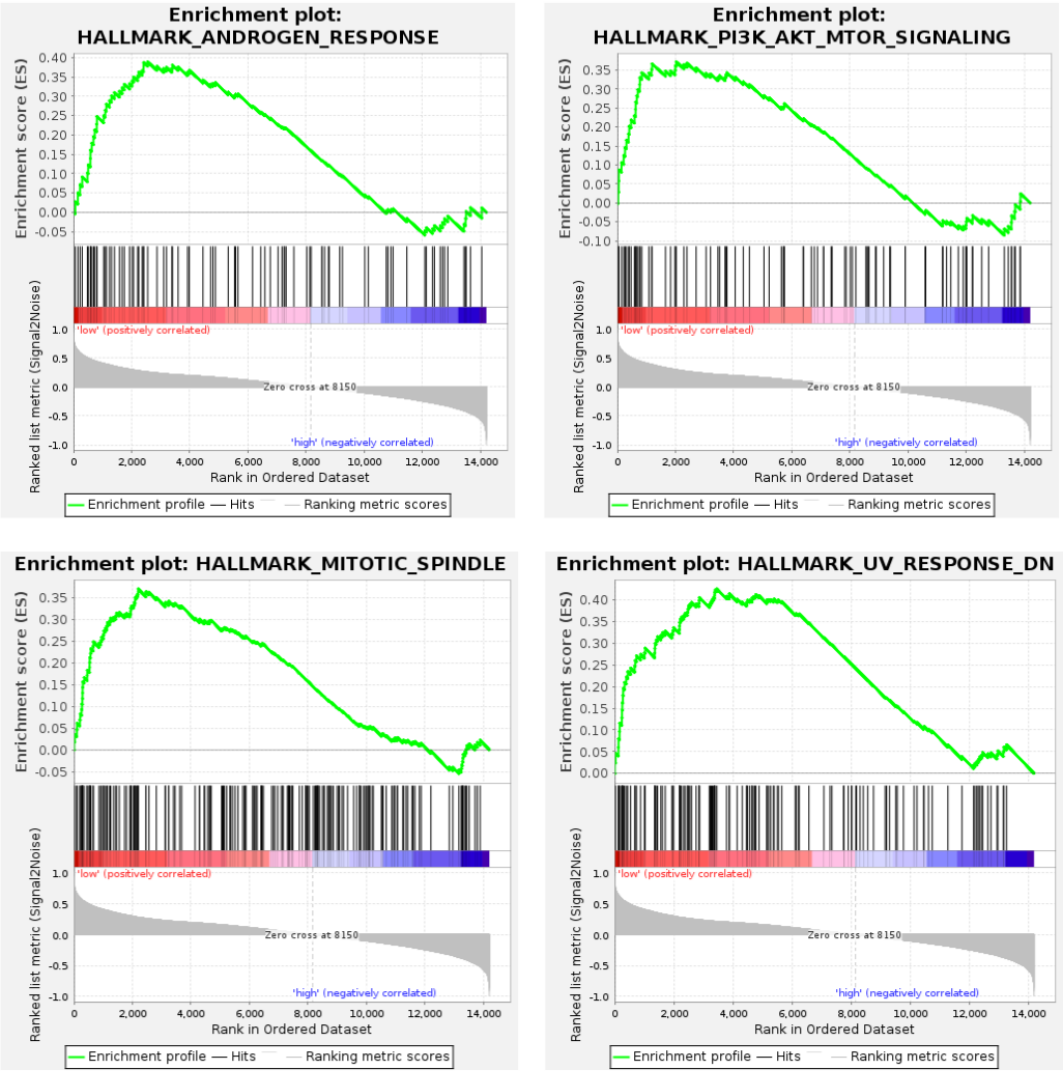

Figure 4.14. Hallmark GSEA enrichment plots for the four most upregulated pathways in TNF-α low responder monocytes following LPS stimulation (n = 23). *Each panel displays the running Enrichment Score (green line), the locations of pathway genes in the ranked list (black vertical lines), and the ranking metric (grey plot). The peak of the ES curve indicates the point of maximum enrichment for each pathway. Shown pathways include Androgen Response (NES = 1.56; FDR = 0.21), PI3K/AKT/mTOR Signalling (NES = 1.60; FDR = 0.26), Mitotic Spindle (NES = 1.57; FDR = 0.25), and UV Response DN (NES = 1.66; FDR = 0.24). Collectively, these enrichments highlight increased proliferative signalling and hormonal modulation characteristic of the low responder phenotype.*

In contrast, the high responders (n = 14) showed a distinct enrichment profile (Figure 4.15). Hallmark pathways such as Oxidative Phosphorylation, IFN Alpha Response, Adipogenesis, and Fatty Acid Metabolism met FDR < 0.25, indicating a shift toward metabolic activation and focused immunomodulation (O'Neill *et al.*, 2016). ImmuneSigDB analysis similarly revealed suppression of broader immune pathways, with 31 gene sets enriched at p < 0.01, including negatively enriched (NES < -1.9) signatures for IFN-γ signalling, microglial activation, and TH17 polarization (Sica and Mantovani, 2012). These results suggest that despite high TNF-α production, these monocytes prioritise a streamlined IFN-driven axis tied closely to antigen presentation while constraining other inflammatory circuits.

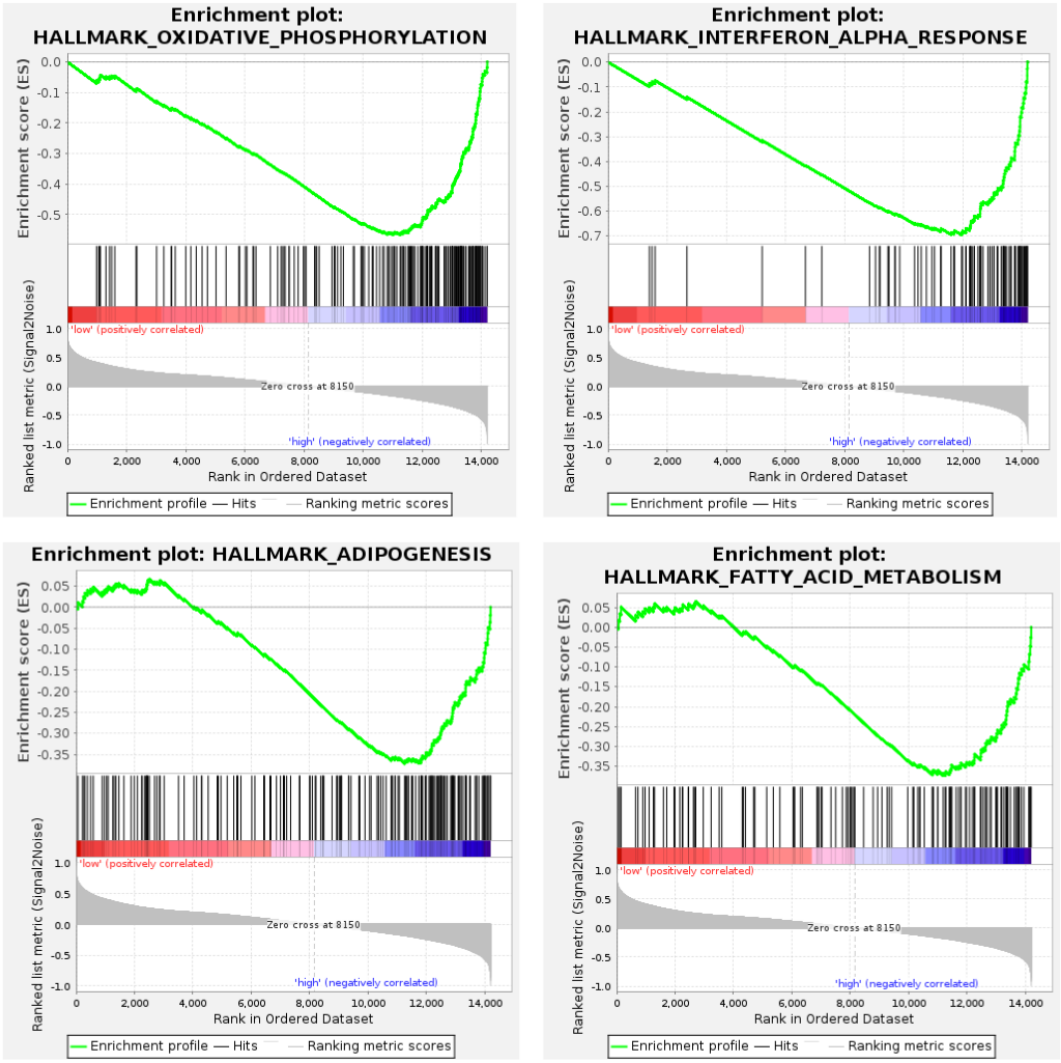

Figure 4.15. Hallmark GSEA enrichment plots for the four most upregulated pathways in TNF-α high responder monocytes following LPS stimulation (n = 14). *Each panel shows the running Enrichment Score (ES, green line), the positions of pathway genes in the ranked gene list (black vertical lines), and the ranking metric (grey plot). The peak of the ES curve indicates the point of maximum enrichment. Shown pathways include Oxidative Phosphorylation (NES = –1.64; FDR = 0.19), IFN Alpha Response (NES = –1.64; FDR = 0.13), Adipogenesis (NES = –1.57; FDR = 0.15), and Fatty Acid Metabolism (NES = –1.51; FDR = 0.17). These enrichments highlight a metabolic and IFN-focused transcriptional program that distinguishes the high responder phenotype.*

Together, these results delineate contrasting molecular states: low responders show transcriptional signatures combining proliferative pathways, PI3K/mTOR signalling, and immune regulatory circuits, supporting a phenotype geared toward tissue integrity, metabolic flexibility, and containment-focused monocyte behaviour (Martinez *et al.*, 2006; Wynn and Vannella, 2016). The co-enrichment of TGF-β Signalling and Coagulation further implies readiness for immune resolution and repair rather than broad inflammatory escalation.

High responders, in contrast, exhibit a focused transcriptional profile dominated by type I IFN signalling, enhanced antigen presentation, and oxidative metabolism, but with suppressed nutrient transport and antioxidant genes, highlighting a trade-off: immune intensity sustained by downregulating cellular maintenance pathways (Mills *et al.*, 2016; Schreiber *et al.*, 2011; Schultze *et al.*, 2015). This suggests these cells allocate resources to rapid immune escalation at the expense of resilience to oxidative or metabolic stress.

The combined Hallmark and ImmuneSigDB enrichment, in agreement with differential expression and GO analyses, supports the broader hypothesis that TNF-α responsiveness stratifies monocytes along an axis balancing “high-alert” trained immunity against a more tolerant, regulatory state (Domínguez-Andrés *et al.*, 2019; Netea *et al.*, 2016). This divergence may contribute to inter-individual differences in susceptibility to inflammation-mediated damage or chronic immune dysfunction following LPS exposure.

4.1.2.6 Biological Implications of Sex Differences in Monocyte TNF-α Responsiveness

Beyond statistical adjustment, interpreting the biological consequences of sex differences in monocyte function provides critical insight into the immune landscape underlying TNF-α responsiveness. Sex is a well-established modulator of immune responses across both innate and adaptive systems (Klein and Flanagan, 2016;

Márquez *et al.*, 2020), and monocytes in particular exhibit pronounced sex-specific variation in pattern recognition receptor signalling, cytokine output, and chromatin accessibility (Gal-Oz *et al.*, 2019; Márquez *et al.*, 2020; Song *et al.*, 2021).

In the context of TLR4 signalling, the key pathway triggered by LPS and upstream of TNF-α production, female immune cells demonstrate greater responsiveness, characterised by enhanced activation of NF-κB and IRF transcriptional cascades and elevated production of cytokines such as TNF-α, IL-6, and type I IFNs (Furman *et al.*, 2014; Seibl *et al.*, 2003). These sex-based differences are shaped by both genetic factors, like X-linked immune gene dosage (Amarasinghe *et al.*, 2023; Youness *et al.*, 2023), and hormonal regulation, with oestrogen known to enhance, and testosterone to suppress, TLR4-mediated myeloid activation (Libert *et al.*, 2010; Straub, 2007).

This sexually dimorphic immune wiring has direct relevance to TNF-α responses. Multiple studies show that females often produce higher levels of TNF-α upon immune challenge but exhibit greater resilience to its pathogenic effects, (Kovats, 2015; Márquez *et al.*, 2020), highlighting the importance of not only cytokine magnitude but also regulatory context (Dunn *et al.*, 2024). In inflammatory conditions like sepsis, males consistently suffer greater morbidity and mortality, often attributed to unchecked TNF-mediated tissue damage despite equal or lower cytokine production (Angele *et al.*, 2014; van der Poll *et al.*, 2017).

These findings resonate with the transcriptomic pattern observed in this study: high responders were enriched for female donors and exhibited elevated expression of *XIST* and IFN-responsive genes (Gal-Oz *et al.*, 2019; So *et al.*, 2021), raising the possibility that intrinsic sex-based transcriptional baselines shape TNF-α response thresholds (Song *et al.*, 2021; Zong *et al.*, 2021).

Crucially, after correcting for sex as a covariate in the *DESeq2* model, the persistence of transcriptional modules linked to antigen presentation, IFN signalling, and co-stimulatory receptor expression confirms that high responder status reflects a

biologically distinct immune trajectory (Márquez *et al.*, 2020; Song *et al.*, 2021). Similarly, the stability of metabolic, redox, and ECM-related gene expression in low responders, despite a higher proportion of male donors, reinforces the interpretation that this group is transcriptionally configured for immune restraint and metabolic maintenance, independent of sex-linked bias (Feng *et al.*, 2024; Ucar *et al.*, 2017). These findings illustrate the necessity of sex-aware transcriptomic profiling in immunogenomics (Klein and Flanagan, 2016; Taneja, 2018). Failure to account for sex as a biological variable risks conflating immune programming with demographic composition (Libert *et al.*, 2010). Moreover, understanding how sex-linked immunobiology intersects with cytokine responsiveness may aid in the design of tailored interventions for inflammatory diseases even beyond CAP, including sepsis, rheumatoid arthritis, and COVID-19, where TNF-α plays a key role and sex-discordant clinical outcomes are well documented (Feng *et al.*, 2024; Takahashi *et al.*, 2020; Taneja, 2018).

4.2 Data Preprocessing and Bioinformatics

RNA HTS data requires rigorous preprocessing to ensure analytical integrity and reproducibility. In this study, a standardised computational pipeline was employed to assess sequencing quality, remove technical artifacts, align reads to the human genome, and quantify gene-level expression. These steps ensured that downstream statistical comparisons reflected biological variation rather than noise or bias. The sections below detail this workflow, from initial raw read assessment to DEG modelling.

Efficient and reproducible bioinformatics workflows are essential to ensure the integrity of HTS data (Conesa *et al.*, 2016). This section describes the preprocessing and quality assurance steps applied to the RNA-seq libraries, detailing QC, trimming, alignment to the reference genome, and preparation of count matrices for downstream statistical analysis.

4.2.1 Quality Control and Pre-Processing

Initial FastQC reports revealed mild residual Illumina adapter sequences and typical 3′-end quality drop-offs. Adapter and low-quality base trimming were therefore applied, conservatively removing less than 5% of bases per sample. Post-trimming FastQC and MultiQC assessments confirmed effective adapter removal and improved per-base quality, ensuring high-confidence alignment. In total, 184 individual FastQC reports (92 raw and 92 trimmed) were generated and summarised with MultiQC, providing comprehensive pre- and post-processing quality metrics.

The quality assessment of RNA sequencing data, as summarised from MultiQC reports, indicated that the overall data quality was acceptable: the majority of FASTQ files met essential quality standards based on GC content, read length consistency, and sequence quality metrics. No samples were excluded from downstream analyses; all files were retained, as all datasets met the minimum thresholds required for robust alignment and differential expression analysis.

The average read length was consistent across all samples at 51 bps, with only one exception (3016M_trim at 50 bp), and the median read length remained stable. GC content across all FASTQ files ranged from 50% to 57%. Several samples, including 1017L_raw, exhibited the lowest GC content at 50%, while the highest value of 57% was observed in both 1052M_trim and 1052M_raw. While sequence duplication levels showed notable variability, ranging from 40.9% (3016M_trim) to 96.2% (3013M_trim), these levels are expected in RNA-Seq data due to transcript abundance and technical biases (Andrews, 2010; Conesa *et al.*, 2016). The total number of sequences also varied, with the lowest counts around 20.4 million (such as 1022M_trim) and the highest reaching up to 64% of total reads (3013M_raw). Additionally, FastQC module failure rates across samples ranged from 0% in most files to 18% in select cases, indicating localised issues but not compromising the overall dataset quality. Despite these differences, the data quality was deemed robust and suitable for downstream analyses such as DEG, aligning with quality

expectations outlined in the FastQC Documentation from the Babraham Institute (Andrews, 2010) and compiled through MultiQC summaries (Ewels *et al.*, 2016).

The sequence count analysis (Figure 4.16), encompassing both raw and trimmed reads, demonstrated highly consistent results across all FASTQ files. FASTQ files were categorised based on the proportion of single reads, with the remaining percentage representing duplicate reads. Within the 0%-20% range, 28 FASTQ files, including 3013M (3.9% and 3.8% unique raw and trimmed reads, respectively) and 3013L (4.5% and 4.4% unique raw and trimmed reads, respectively), exhibited the lowest percentages of single reads. Most of the dataset, consisting of 152 FASTQ files, fell within the 20%-40% range, again showing a high degree of comparability between raw and trimmed reads. Finally, four samples, including 1022M and 3016M (each with both raw and trimmed FASTQ files), fell within the 40%-60% unique read range, with 3016M showing the highest single-read percentage (54.2% for raw, 59.1% for trimmed reads). No FASTQ files displayed single-read percentages within the 60%-100% range. Overall, these results suggest highly variable sequence duplication rates across FASTQ files, a common feature in RNA-seq datasets that may reflect either technical artifacts or biological abundance (Conesa *et al.*, 2016). As duplication rates did not compromise overall quality metrics, all samples were retained for downstream analysis.

Figure 4.16. Unique and duplicate read proportions across FASTQ files before and after trimming. *Stacked bar plot showing the proportion of unique (blue) and duplicate (grey) reads for each sample. Sample IDs on the x-axis indicate treatment condition (suffix "M" for media-treated, "L" for LPS-treated) and are ordered by increasing numerical ID. For each sample, two horizontally aligned bars represent the raw data (top) and the same sample after adapter trimming (bottom).*

All 184 FASTQ files successfully passed the sequence QC assessment, with quality scores consistently falling within the high confidence "green" zone (Figure 4.17). Across all samples, base-wise mean quality scores were consistently high (Phred ~40), indicating excellent sequencing quality suitable for downstream analyses. Minor deviations in a few files (such as 3016M) did not affect overall data quality.

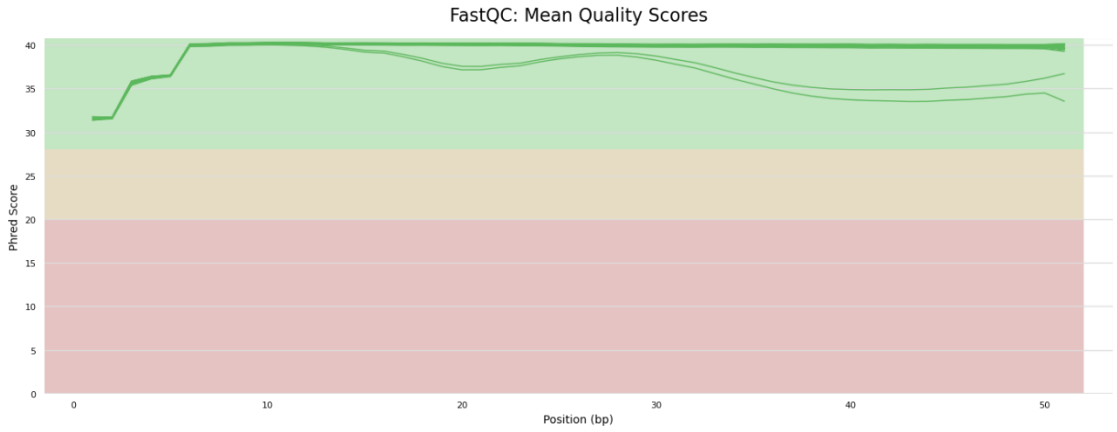

Figure 4.17. Base-wise mean Phred quality scores across all FASTQ files. Line plot showing the average Phred quality score at each base position (1-50) for 184 FASTQ files. *The x-axis represents base position along the read, and the y-axis indicates the mean Phred score. The solid green line traces the average quality per base, with slight tapering toward the 3′ end. Background shading reflects FastQC confidence zones: green (>30, high quality), orange (20-30, moderate), and red (<20, low). All base positions fall within the high-quality range.*

4.2.1.1 Per Sequence Quality Scores and Per Base Sequence Content

All FASTQ files met per-sequence quality standards (Appendix Figure 15). In the Per Base Sequence Content module, 180 FASTQ files generated warnings and four files (sample 3013 under both treatment conditions, raw and trimmed) failed due to known sequence bias at the 5′ end, consistent with random hexamer priming during library preparation (Andrews, 2010). Such imbalances can increase the risk of unmapped reads due to mismatches; however, alignment rates remained high (>95% for all libraries), indicating that this bias did not substantially impact mapping efficiency. Previous studies (Hansen *et al.*, 2010; Tarazona *et al.*, 2011) have similarly shown that sequence-specific priming bias has minimal effect on gene-level

quantification when standard RNA-seq normalisation is applied. Therefore, all files were retained for downstream analysis; no explicit correction for residual quality biases was applied, but standard trimming, alignment, and feature-level quantification ensured consistent processing across samples.

4.2.1.1 Per Sequence GC and per base N Content

In the Per Sequence GC Content analysis (Figure 4.18), 16 FASTQ files, comprising paired raw and trimmed versions of 8 individual samples, were flagged as failed, while 22 FASTQ files, corresponding to 11 sample pairs, received warnings. In all flagged cases, both raw and trimmed FASTQ files from each sample exhibited identical patterns, with no differences observed between them, as confirmed by MultiQC aggregation and FastQC reports. Although notable deviations from the expected normal distribution were observed, failed files generally remained centred near the mean GC content but displayed sharper peaks toward the right side of the distribution, suggestive of potential contamination or technical bias during library preparation, such as adapter dimers or abnormal base composition (Andrews, 2010). According to FastQC criteria, warnings are triggered when over 15% of reads deviate from the normal distribution, while failures occur beyond a 30% deviation threshold (Andrews, 2010). Despite these observations, 146 FASTQ files passed the module, indicating that the majority of the dataset-maintained GC content within acceptable ranges.

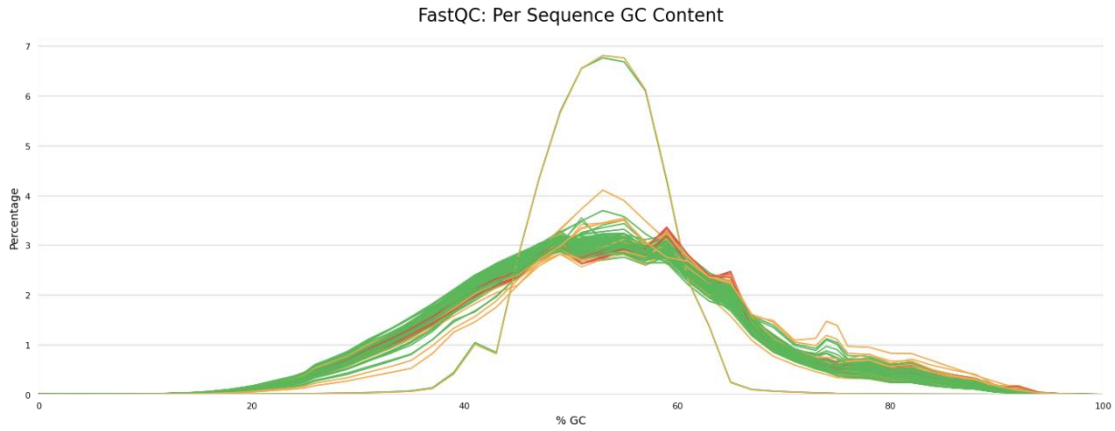

Figure 4.18. Per sequence GC content across all FASTQ files. *Per-sequence GC content distribution for 184 FASTQ files; each line represents a single file. Line colours indicate FastQC evaluation: green (pass), orange (warning), red (fail). Warnings were flagged in 22 files (e.g., 1018M, 1052L, 1060M, 1084M, 3013M_trim, 3018L, 3032M), while 16 files failed (e.g., 1051L, 1055M, 1056L, 1064M, 3015M), according to FastQC thresholds (Andrews, 2010). The tall, narrow GC peak distinct from the main distribution reflects two high-duplication samples, 3013L and 3013M.*

In the Per Base N (ambiguous nucleotide) Content analysis (Appendix Figure 16), approximately half of the FASTQ files, corresponding to the trimmed reads, showed 0% N content at base position 1. In contrast, the raw reads displayed up to 0.54% N content at base 1, which sharply dropped to between 0.01% and 0% from base 2 onwards. This difference highlighted the effect of trimming on improving sequence quality by removing uncertain base calling at the start of the reads.

4.2.1.1 Sequence Length Distribution and Duplication levels

For the Sequence Length Distribution module (Appendix Figure 17), 92 raw read FASTQ files passed the assessment, as they all exhibited consistent lengths of 51 bps. However, 92 trimmed read FASTQ files received warnings due to variability in sequence lengths, with the plot showing an abrupt upward curve at exactly 50 bp on the x-axis. According to the FastQC documentation (Andrews, 2010), this module can raise a warning when all sequences are not of the same length. The discrepancy is attributed to the 3016M_trim sample being 50 bp long, while the other trimmed

reads are 51 bp. Even within libraries that generally maintain uniform sequence lengths, some pipelines may trim sequences to remove poor-quality base calls from the ends, which explains the observed length variation in the trimmed FASTQ files (Andrews, 2010).

As previously discussed on the general statistics (Section 4.2.1.1), where the 3016M raw and trimmed FASTQ files had the lowest percentage of duplicate reads (40.9% for 3016M_trim and 45.8% for 3016M_raw), 182 of 184 FASTQ files failed the Sequence Duplication Levels module. Only the 3016M raw and trimmed FASTQ files were flagged with warnings rather than failures (Appendix Figure 18). According to the FastQC documentation, this module issues a warning if more than 20% of sequences are non-unique, and a failure occurs if this number exceeds 50% (Andrews, 2010).

The module assumes a diverse, unenriched library, and deviations from this can result in duplicate sequences due to either technical issues, such as PCR artifacts, or biological duplicates, where identical sequences are naturally present in the sample (Fu *et al.*, 2018; Sims *et al.*, 2014). However, in RNA-Seq libraries, the varying levels of transcript abundance can lead to over-sequencing of highly expressed transcripts, causing a high level of duplication (Andrews, 2010). These duplicates were not necessarily indicative of technical issues but could reflect the nature of RNA-seq data, where duplicates can arise from biologically relevant regions rather than technical errors (Andrews, 2010). Thus, while high duplication levels were flagged in most FASTQ files, they were expected in RNA-seq libraries and were not a concern to impact downstream alignments and DEG analysis.

4.2.1.1 Overrepresented Sequences and Adaptor content

In the Overrepresented Sequences analysis, 28 FASTQ files passed, 155 FASTQ files received warnings, and 1 sample (3005L_raw) failed (Appendix Figure 19). This module evaluated the total amount of overrepresented sequences in each library.

According to the FastQC documentation (Andrews, 2010), a warning is issued if any sequence represents more than 0.1% of the total, while a failure occurs if a sequence exceeds 1% of the total. Overrepresented sequences may indicate biological significance, contamination, or lack of library diversity. While this module can help flag potential issues, some overrepresentation is expected in RNA-seq libraries, especially in cases where highly expressed sequences dominate, such as small RNA libraries, where sequences are not randomly fragmented (Andrews, 2010). Thus, the deviations were likely reflective of the nature of RNA-seq data rather than true contamination.

In the Adapter Content analysis module (Appendix Figure 20), all 184 FASTQ files passed, indicating no significant adapter contamination. This module specifically tracked known adapter sequences in the library, showing a cumulative percentage of their presence at each position in the read. Unlike the K-mer Content module, which may be dominated by overrepresented K-mers, this analysis focused solely on adapter K-mers, helping determine if trimming was needed (Andrews, 2010). The results showed minimal adapter content across all FASTQ files, suggesting effective trimming or no contamination.

Trimmed reads were aligned to the human genome using HISAT2 (D. Kim *et al.*, 2019), and gene-level counts were then generated with *featureCounts* (Y. Liao *et al.*, 2014) for downstream differential expression analysis in *DESeq2*.

4.2.2 Statistical Analysis in R: DEG Analysis using *DESeq2*

Following data preprocessing, statistical analysis was conducted in R using the *DESeq2* package to identify DEGs across experimental conditions. This section outlines the analytical framework used to normalise data, assess quality metrics, estimate dispersion, and evaluate $\log_2$FCs in gene expression. Each step was tailored to account for dataset-specific features and to ensure robust inference.

4.2.2.1 Analytical Framework and QC for RNA-seq Differential Expression

Size factor distributions were assessed across both datasets to confirm normalisation effectiveness (Figure 4.19 (A) and (B); Raw and normalised counts scatter plots for both datasets can be reviewed in Appendix Figures 4 and 5). Most values clustered tightly around 1.0, indicating consistent sequencing depth and library sizes. A limited number of samples exhibited deviations, including S3013L and S3013M, which displayed low total read counts (<5 million reads). However, normalisation brought these samples into alignment, and all passed quality thresholds for inclusion.

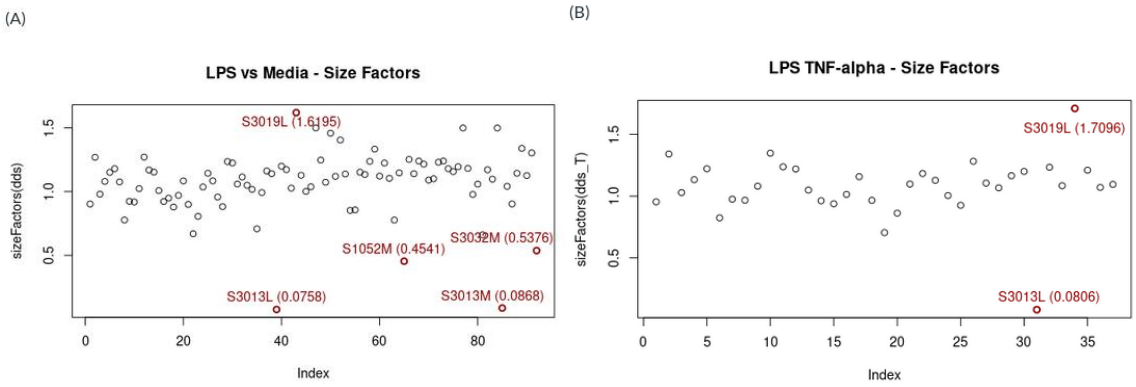

Figure 4.19. Size factor distributions. *(A) Size factors estimated for the full LPS-treated vs. media-treated monocyte dataset (dds object, n = 92 samples). (B) Size factors estimated for the TNF-α high vs. low responder subset (dds_T object, n = 37 samples). In both panels, size factors are plotted by sample index (x-axis) against estimated value (y-axis). Most samples cluster near 1.0, with mild deviations in S3013L, S1052M, S3013M, S3032M, and S3019L in the LPS vs. media dataset, and in S3013L and S3019L among the TNF-α responder groups.*

Overall, this QC confirmed that trimmed, normalised datasets were suitable for robust DEG and enrichment analysis.

4.2.2.2 Dispersion Estimators of Alternative log_2FC Shrinkage

Accurately estimating gene-wise dispersion is a critical step in modelling RNA-seq count data because it directly impacts the precision and interpretability of log_2FCs (Love *et al.*, 2014). To ensure stable and biologically meaningful results across datasets of different sizes and complexities, this section presents the per-gene dispersion estimates and explains how the fitted trends were evaluated and how shrinkage approaches were compared and selected.

Dispersion plots were generated for both the LPS vs. media and the TNF-α responder datasets, showing gene-wise dispersion as a function of mean normalised counts (Appendix Figure 6) (Love, 2024). As expected, variance decreased with increasing expression, matching well-established RNA-seq patterns (B.-Y. Liao and Zhang, 2006) and supporting the filtering of low-count transcripts in pre-processing. For the LPS vs. media dataset (n = 92), the dispersion plot (Appendix Figure 6 (A)) showed a clear decline from high dispersion (~10^{1}) at low counts to ~10^{-1} at high counts. The final adjusted estimates (blue points) tracked closely along the fitted red trendline, indicating a robust and stable model fit. A minority of very low-expression genes exhibited extremely low dispersion values (~10^{-6}), likely representing biologically inactive or noise-driven transcripts. About 10% of genes were flagged by Cook's distance as influential outliers (Appendix Table 1) (Love *et al.*, 2014), but all retained interpretable variance estimates and were not excluded.

In the TNF-α responder dataset (n = 37), dispersion estimates likewise decreased steadily with increasing expression and showed tighter clustering around the trendline than in the larger dataset, reflecting the reduced sampling variance due to the smaller cohort size (Appendix Figure 6 (B)) (D. Yu *et al.*, 2013). Few under-dispersed genes were observed, and no significant outliers were detected, validating the normalisation and modelling assumptions (G. Chen *et al.*, 2019).

To further evaluate performance, MA plots were generated for the LPS vs. media dataset comparing log_2FC shrinkage methods side-by-side: *Normal*, *Apeglm*, and *Ashr* (Appendix Figure 7) (Love, 2024). The Normal shrinkage plot showed excessive

scatter for low-count genes, demonstrating unstable estimates and a tendency to over-correct, especially for genes with sparse data (Love *et al.*, 2014; A. Zhu *et al.*, 2019). Although straightforward to apply, this method introduced bias, particularly in low-expression ranges. The *Apeglm* method produced a more balanced distribution, better centring high-variance genes, but at times shrank estimates too aggressively in sparsely covered regions and required greater computational cost (A. Zhu *et al.*, 2019). By comparison, the *Ashr* shrinkage method gave the most refined distribution: it adaptively adjusted shrinkage based on each gene's local variance, resulting in fewer extreme $\log_2$FCs at low counts and improved centrality overall (Stephens *et al.*, 2016). This balance made *Ashr* particularly well suited for stabilising effect estimates in both high-power and low-sample contexts.

Consistent visual and statistical evidence supported *Ashr* as the default shrinkage method for both the global LPS comparison and the TNF-α stratification. Summary statistics for all models are detailed in Appendix Table 1.

For the LPS vs. media dataset, 20,576 genes with nonzero read counts were analysed. At $p \leq 0.1$, about 18% were significantly upregulated and 15% downregulated, demonstrating a robust global transcriptional response to LPS stimulation. No genes were excluded for low mean counts, and approximately 10% were flagged as outliers by Cook's distance, all of which retained interpretable estimates. Applying *Ashr* shrinkage and filtering at $padj \leq 0.01$, 4,490 DEGs were retained, with 55% upregulated and 45% downregulated, and no outliers remaining, thus supporting *Ashr*'s ability to stabilise high-variance estimates and yield a robust profile of monocyte activation after LPS challenge (Stephens *et al.*, 2016).

In the TNF-α high vs. low responder comparison (18,195 genes), the inclusion of sex as a covariate proved critical for revealing genuine biological signals. Without covariates, the Wald test identified 878 upregulated (4.83%) and 1,169 downregulated (6.43%) genes, while flagging 2,066 outliers (11.36%) and excluding 3,507 (19.27%) low-count features. Adding sex to the model refined these estimates to 1,021 upregulated (5.61%) and 1,322 downregulated (7.27%) genes, with outliers

dropping to just 36 (0.2%) and low-count exclusions rising moderately to 4,930 (27.09%). *Ashr* shrinkage applied to this sex-adjusted model produced a conservative final set of 555 DEGs: 228 upregulated (41%) and 327 downregulated (59%), with no flagged outliers or additional exclusions. This illustrates how sex adjustment and empirical shrinkage together clarify biologically meaningful patterns, especially for immune genes sensitive to sex-linked regulatory effects.

Comparatively, the LPS vs. media dataset revealed a broad, high-powered innate immune activation, while the smaller TNF-α dataset uncovered a more focused and regulatory immune signature, made clearer by proper covariate adjustment and robust shrinkage. *Ashr* consistently outperformed the raw Wald estimates by reducing false positives and stabilising FC magnitudes, especially for genes with low read counts and high dispersion, aligning with its proven utility in small-sample RNA-seq contexts (Appendix Table 1; Love *et al.*, 2014; Stephens *et al.*, 2016).

4.3 Summary

This study examines the transcriptional behaviour of human monocytes in CAP, focusing on responses to *ex vivo* LPS stimulation. RNA-seq data from 92 samples were analysed to characterise shared and individual patterns of immune activation using DEG, pathway enrichment, PPI mapping, and sex-aware modelling.

LPS induced a robust and conserved transcriptional program across patients, with upregulation of inflammatory mediators, IFN-stimulated genes, and TNF-α/IL-2/STAT5 pathways. Simultaneously, chromatin remodelling and mitochondrial functions were suppressed, consistent with a shift toward inflammatory priming. Key transcription factors like *KLF6* and *IFNB1* emerged as central regulators.

Stratifying by TNF-α output revealed two distinct phenotypes. High responders showed elevated expression of antigen presentation genes and IFN-regulated transcripts, such as *CD40*, *PSMB9* and *IRF8*, indicating immune priming. Low responders-maintained expression of ECM and metabolic regulators, suggesting a regulatory or tolerance-like state. This divergence reflected strategic differences, not just magnitude.

The computational pipeline, based on *DESeq2* and *Ashr* shrinkage, ensured robust FC estimation. Sex was included as a covariate, and QC confirmed dataset integrity. These findings highlight how monocyte heterogeneity in CAP shapes immune responses and may influence recovery trajectories.

5. CONCLUSION

In conclusion, while LPS exposure of monocytes triggered a robust, shared transcriptional response, the study further sought to resolve whether inter-individual variation in cytokine production, specifically TNF-α, could uncover divergent immune strategies within this cohort. Stratifying monocytes based on TNF-α output served as a biologically grounded approach to interrogate transcriptional immune diversity.

High TNF-α responders appear to prioritise rapid antigen presentation and inflammatory signalling, while low responders maintain metabolic adaptability and immune-regulatory features consistent with tolerance. These findings offer mechanistic insight into how monocyte states might influence recovery, risk of hyperinflammation, or immunoparalysis in the clinical course of CAP.

5.1 Limitations

Analytical and computational limitations must be acknowledged. RNA-seq captures messenger RNA abundance, but not protein levels, post-translational modifications, or true cellular function (S. Zhang *et al.*, 2024). This is especially relevant to immune tolerance, which frequently involves epigenetic imprinting, altered signalling thresholds, or shifts in protein turnover, phenomena invisible to transcriptomic profiling alone (Khan *et al.*, 2019).

Although TNF-α release was quantified via Luminex, no multiplex cytokine profiling or orthogonal functional assays were conducted to validate immune states inferred from gene expression (Jansen *et al.*, 2023). Consequently, conclusions about regulatory phenotypes remain indirect. The decision to stratify samples by TNF-α output, while biologically justified as it is a key effector of innate activation (Guillemin *et al.*, 2021), imposed a unidimensional lens on immune heterogeneity. TNF-α alone does not fully represent the diversity of monocyte states, particularly those defined by IL-10 suppression, IFN-related antiviral signatures, or reparative programmes

(Shalek *et al.*, 2014). As such, framing low TNF-α responders as “tolerant” is interpretive, as their gene programmes could equally reflect delayed kinetics, cell state heterogeneity, or alternative activation (Shalek *et al.*, 2014).

Computationally, the use of a strict expression cutoff (baseMean ≤ 50) and adjusted significance threshold (*padj* ≤ 0.01) improved specificity but likely excluded low-abundance transcripts critical to immune regulation, including microRNAs, long non-coding RNAs, and transcriptional repressors (Conant and Wagner, 2003; Diederichs and Haber, 2007; Lorente-Sorolla *et al.*, 2019). These elements are often central to the establishment and maintenance of immune tolerance, representing a blind spot in this analysis. Moreover, gene-level aggregation precluded investigation of isoform switching, splicing variation, and RNA editing, all important mechanisms in monocyte plasticity (Hotchkiss *et al.*, 2013a; M. N. Lee *et al.*, 2014).

The sample size of the TNF-α high responder group (n = 14) limited statistical power, particularly for detecting nonlinear expression patterns or subtle transcriptional shifts. Although shrinkage estimators and covariate adjustments were applied to stabilise dispersion estimates and account for known confounders such as sex, smaller group sizes inherently reduce model sensitivity by limiting statistical power to detect subtle or nonlinear patterns of differential expression (Sureshchandra *et al.*, 2021). This is especially critical in immune transcriptomics, where effect sizes may be modest and inter-individual variability high, increasing the risk of false negatives and potentially overlooking biologically relevant transcriptional programmes. Additionally, while all samples were processed within a single batch and batch correction was not required, residual confounders, such as RNA integrity, cell viability, or individual variability, may still influence expression differences (Sureshchandra *et al.*, 2021).

Importantly, the analysis was cross-sectional. Although drawn from a longitudinal cohort, all transcriptomic profiling occurred at a single post-stimulation timepoint. As immune tolerance is dynamic, often defined by blunted secondary responses or persistence of regulatory signatures, this static view precludes temporal resolution.

Without repeated measures or time-course designs, the classification of low responders as "tolerised" remains inferential rather than demonstrated.

Finally, although sex was modelled as an additive covariate to reduce confounding, this approach does not capture interaction effects between sex and cytokine responsiveness. Given that high responders skewed female and showed enriched type I IFN activity and X-linked gene expression, non-additive interactions may play a mechanistic role in shaping tolerance trajectories (Klein and Flanagan, 2016; Takahashi *et al.*, 2020).

5.2 Future Work

This study provides a foundation for understanding how monocyte transcriptional states can shape, reflect, or predict immune tolerance during CAP. However, the insights it offers are not an endpoint, but a launchpad for clinically transformative research that could improve patient outcomes and ultimately save lives.

Future work must begin with functional validation of the transcriptional states uncovered in this analysis. While *ex vivo* LPS stimulation provides a controlled snapshot of monocyte behaviour, further studies are needed to determine whether the identified transcriptional signatures correspond to immune function *in vivo*, and whether they can predict responses to diverse pathogens, disease stages, or treatment regimens. Incorporating proteomic and cytokine profiling will be essential to confirm whether DEG translates into altered protein output, distinguishing immune tolerance from transcriptional silence caused by other regulatory mechanisms.

The identification of inflammatory-primed and tolerance-oriented monocyte states presents a powerful framework for early immune stratification. If key transcripts or proteins such as HLA-DR, CD40, *SLC1A5*, or *TXNRD1* can be validated as biomarkers, they could be developed into clinical assays to classify patients early in the disease course. Such tests could allow clinicians to identify high-risk individuals

before clinical deterioration, enabling earlier ICU admission, timely initiation of immune-modulatory therapy, or tailored support to prevent immune collapse. These strategies hold promise for preventing sepsis progression and could help reduce mortality in CAP, offering a direct, data-driven path to saving lives.

Equally important, this study demonstrates the utility and flexibility of bioinformatics approaches in uncovering hidden layers of immune variation. The computational pipeline developed here, from QC and DEG modelling using *DESeq2*, to functional annotation and PPI network analysis, can be adapted to other infections or immune-mediated conditions. This scalable, reproducible framework could serve as a foundation for studying immune tolerance in settings like sepsis, COVID-19, or chronic inflammation, positioning computational immunology as a central tool for translational discovery.

Future studies should also move beyond single time-point analyses. Longitudinal sampling across acute, resolving, and recovery phases would allow dynamic modelling of immune adaptation, revealing whether tolerance is transient, permanent, or reversible. Combining bulk transcriptomics with single-cell RNA-seq, Assay for Transposase-Accessible Chromatin (ATAC)-seq, or other epigenetic profiling techniques could expose the chromatin-level mechanisms that fix or rewire monocyte programmes and help differentiate trained immunity from immunoparalysis. This would deepen our understanding of innate immune memory and its impact on secondary infection risk or vaccine responsiveness.

Lastly, clinical translation will require linking these immune phenotypes to real-world outcomes. Future work must integrate transcriptional data with comorbidity profiles, microbiological findings, disease severity scores, and patient trajectories to determine how immune tolerance states influence recovery, reinfection, or mortality. Only by embedding molecular data within clinical frameworks can these findings evolve into actionable diagnostics or therapeutic strategies.

This bioinformatics study contributes both mechanistic insights into monocyte functional heterogeneity and a scalable analytical blueprint for future translational research. With validation and expansion, its findings could inform early detection of immune tolerance states, improve risk stratification in CAP, and ultimately support more personalised approaches to infection management.

REFERENCES

Aderem, A., & Underhill, D. M. (1999). Mechanisms of phagocytosis in macrophages. *Annual Review of Immunology*, *17*, 593–623. https://doi.org/10.1146/annurev.immunol.17.1.593

Ahsan, S., & Drăghici, S. (2017). Identifying Significantly Impacted Pathways and Putative Mechanisms with iPathwayGuide. *Current Protocols in Bioinformatics*, *57*, 7.15.1-7.15.30. https://doi.org/10.1002/cpbi.24

Alexander, S. P., Davenport, A. P., Kelly, E., Marrion, N., Peters, J. A., Benson, H. E., Faccenda, E., Pawson, A. J., Sharman, J. L., Southan, C., Davies, J. A., & CGTP Collaborators. (2015). The Concise Guide to PHARMACOLOGY 2015/16: G protein-coupled receptors. *British Journal of Pharmacology*, *172*(24), 5744–5869. https://doi.org/10.1111/bph.13348

Aliberti, S., Lonni, S., Dore, S., McDonnell, M. J., Goeminne, P. C., Dimakou, K., Fardon, T. C., Rutherford, R., Pesci, A., Restrepo, M. I., Sotgiu, G., & Chalmers, J. D. (2016). Clinical phenotypes in adult patients with bronchiectasis. *European Respiratory Journal*, *47*(4), 1113–1122. https://doi.org/10.1183/13993003.01899-2015

Allam, C., Mouton, W., Testaert, H., Ginevra, C., Fessy, N., Ibranosyan, M., Descours, G., Beraud, L., Guillemot, J., Chapalain, A., Albert-Vega, C., Richard, J.-C., Argaud, L., Friggeri, A., Labeye, V., Jamilloux, Y., Freymond, N., Venet, F., Lina, G., … Jarraud, S. (2023). Hyper-inflammatory profile and immunoparalysis in patients with severe Legionnaires' disease. *Frontiers in*

Cellular and Infection Microbiology, *13*, 1252515. https://doi.org/10.3389/fcimb.2023.1252515

Aloy, P., & Russell, R. B. (2006). Structural systems biology: Modelling protein interactions. *Nature Reviews Molecular Cell Biology*, *7*(3), 188–197. https://doi.org/10.1038/nrm1859

Amarasinghe, H. E., Zhang, P., Whalley, J. P., Allcock, A., Migliorini, G., Brown, A. C., Scozzafava, G., & Knight, J. C. (2023). Mapping the epigenomic landscape of human monocytes following innate immune activation reveals context-specific mechanisms driving endotoxin tolerance. *BMC Genomics*, *24*(1), 595. https://doi.org/10.1186/s12864-023-09663-0

Amit, I., Garber, M., Chevrier, N., Leite, A. P., Donner, Y., Eisenhaure, T., Guttman, M., Grenier, J. K., Li, W., Zuk, O., Schubert, L. A., Birditt, B., Shay, T., Goren, A., Zhang, X., Smith, Z., Deering, R., McDonald, R. C., Cabili, M., … Regev, A. (2009). Unbiased reconstruction of a mammalian transcriptional network mediating pathogen responses. *Science (New York, N.Y.)*, *326*(5950), 257–263. https://doi.org/10.1126/science.1179050

Anaconda Software Distribution. (2024). *Anaconda Documentation* (Version 24.5.0) [Computer software]. Anaconda Inc. https://docs.anaconda.com/

Anders, S., & Huber, W. (2010). Differential expression analysis for sequence count data. *Genome Biology*, *11*(10), R106. https://doi.org/10.1186/gb-2010-11-10-r106

Anders, S., Pyl, P. T., & Huber, W. (2015). HTSeq—A Python framework to work with high-throughput sequencing data. *Bioinformatics (Oxford, England)*, *31*(2), 166–169. https://doi.org/10.1093/bioinformatics/btu638

Andrade, C. (2019). The P Value and Statistical Significance: Misunderstandings, Explanations, Challenges, and Alternatives. *Indian Journal of Psychological Medicine*, *41*(3), 210–215. https://doi.org/10.4103/IJPSYM.IJPSYM_193_19

Andrews, S. (2010). *FastQC: A quality control tool for high throughput sequence data* (Version 0.12.1) [Computer software]. Babraham Bioinformatics. http://www.bioinformatics.babraham.ac.uk/projects/fastqc

Angele, M. K., Pratschke, S., Hubbard, W. J., & Chaudry, I. H. (2014). Gender differences in sepsis: Cardiovascular and immunological aspects. *Virulence*, *5*(1), 12–19. https://doi.org/10.4161/viru.26982

Angus, D. C., & Van Der Poll, T. (2013). Severe Sepsis and Septic Shock. *New England Journal of Medicine*, *369*(9), 840–851. https://doi.org/10.1056/NEJMra1208623

Arora, S., Dev, K., Agarwal, B., Das, P., & Syed, M. A. (2018). Macrophages: Their role, activation and polarization in pulmonary diseases. *Immunobiology*, *223*(4–5), 383–396. https://doi.org/10.1016/j.imbio.2017.11.001

Arunachalam, P. S., Wimmers, F., Mok, C. K. P., Perera, R. A. P. M., Scott, M., Hagan, T., Sigal, N., Feng, Y., Bristow, L., Tak-Yin Tsang, O., Wagh, D., Coller, J., Pellegrini, K. L., Kazmin, D., Alaaeddine, G., Leung, W. S., Chan, J. M. C., Chik, T. S. H., Choi, C. Y. C., … Pulendran, B. (2020). Systems biological assessment of immunity to mild versus severe COVID-19 infection in humans. *Science*

(New York, N.Y.), *369*(6508), 1210–1220. https://doi.org/10.1126/science.abc6261

Ashburner, M., Ball, C. A., Blake, J. A., Botstein, D., Butler, H., Cherry, J. M., Davis, A. P., Dolinski, K., Dwight, S. S., Eppig, J. T., Harris, M. A., Hill, D. P., Issel-Tarver, L., Kasarskis, A., Lewis, S., Matese, J. C., Richardson, J. E., Ringwald, M., Rubin, G. M., & Sherlock, G. (2000). Gene ontology: Tool for the unification of biology. The Gene Ontology Consortium. *Nature Genetics*, *25*(1), 25–29. https://doi.org/10.1038/75556

Austermann, J., Friesenhagen, J., Fassl, S. K., Petersen, B., Ortkras, T., Burgmann, J., Barczyk-Kahlert, K., Faist, E., Zedler, S., Pirr, S., Rohde, C., Müller-Tidow, C., von Köckritz-Blickwede, M., von Kaisenberg, C. S., Flohé, S. B., Ulas, T., Schultze, J. L., Roth, J., Vogl, T., & Viemann, D. (2014). Alarmins MRP8 and MRP14 induce stress tolerance in phagocytes under sterile inflammatory conditions. *Cell Reports*, *9*(6), 2112–2123. https://doi.org/10.1016/j.celrep.2014.11.020

Bae, S.-C., & Lee, Y. H. (2018). Meta-analysis of gene expression profiles of peripheral blood cells in systemic lupus erythematosus. *Cellular and Molecular Biology (Noisy-Le-Grand, France)*, *64*(10), 40–49.

Barshir, R., Shwartz, O., Smoly, I. Y., & Yeger-Lotem, E. (2014). Comparative Analysis of Human Tissue Interactomes Reveals Factors Leading to Tissue-Specific Manifestation of Hereditary Diseases. *PLOS Computational Biology*, *10*(6), e1003632. https://doi.org/10.1371/journal.pcbi.1003632

Basha, O., Shpringer, R., Argov, C. M., & Yeger-Lotem, E. (2018). The DifferentialNet database of differential protein-protein interactions in human tissues. *Nucleic Acids Research*, *46*(D1), D522–D526. https://doi.org/10.1093/nar/gkx981

Bayerlová, M., Jung, K., Kramer, F., Klemm, F., Bleckmann, A., & Beißbarth, T. (2015). Comparative study on gene set and pathway topology-based enrichment methods. *BMC Bioinformatics*, *16*(1), 334. https://doi.org/10.1186/s12859-015-0751-5

Benjamini, Y., & Hochberg, Y. (1995). Controlling the False Discovery Rate: A Practical and Powerful Approach to Multiple Testing. *Journal of the Royal Statistical Society: Series B (Methodological)*, *57*(1), 289–300. https://doi.org/10.1111/j.2517-6161.1995.tb02031.x

Benoit, M., Desnues, B., & Mege, J.-L. (2008). Macrophage polarization in bacterial infections. *Journal of Immunology (Baltimore, Md.: 1950)*, *181*(6), 3733–3739. https://doi.org/10.4049/jimmunol.181.6.3733

Berman, H. M., Westbrook, J., Feng, Z., Gilliland, G., Bhat, T. N., Weissig, H., Shindyalov, I. N., & Bourne, P. E. (2000). The Protein Data Bank. *Nucleic Acids Research*, *28*(1), 235–242. https://doi.org/10.1093/nar/28.1.235

Bernard, Q., Goumeidane, M., Chaumond, E., Robbe-Saule, M., Boucaud, Y., Esnault, L., Croué, A., Jullien, J., Marsollier, L., & Marion, E. (2023a). Type-I interferons promote innate immune tolerance in macrophages exposed to Mycobacterium ulcerans vesicles. *PLoS Pathogens*, *19*(7), e1011479. https://doi.org/10.1371/journal.ppat.1011479

Bernard, Q., Goumeidane, M., Chaumond, E., Robbe-Saule, M., Boucaud, Y., Esnault, L., Croué, A., Jullien, J., Marsollier, L., & Marion, E. (2023b). Type-I interferons promote innate immune tolerance in macrophages exposed to Mycobacterium ulcerans vesicles. *PLoS Pathogens*, *19*(7), e1011479. https://doi.org/10.1371/journal.ppat.1011479

Bernardi, R., & Pandolfi, P. P. (2007). Structure, dynamics and functions of promyelocytic leukaemia nuclear bodies. *Nature Reviews. Molecular Cell Biology*, *8*(12), 1006–1016. https://doi.org/10.1038/nrm2277

Bilanges, B., Posor, Y., & Vanhaesebroeck, B. (2019). PI3K isoforms in cell signalling and vesicle trafficking. *Nature Reviews. Molecular Cell Biology*, *20*(9), 515–534. https://doi.org/10.1038/s41580-019-0129-z

Biswas, S. K., & Lopez-Collazo, E. (2009). Endotoxin tolerance: New mechanisms, molecules and clinical significance. *Trends in Immunology*, *30*(10), 475–487. https://doi.org/10.1016/j.it.2009.07.009

Blighe, kevin, Rana, S., & Lewis, M. (2023). *EnhancedVolcano: Publication-ready volcano plots with enhanced colouring and labelling* (Version 1.18.0) [Computer software]. Bioconductor. https://bioconductor.org/packages/release/bioc/html/EnhancedVolcano.html

Bolger, A. M., Lohse, M., & Usadel, B. (2014). Trimmomatic: A flexible trimmer for Illumina sequence data. *Bioinformatics (Oxford, England)*, *30*(15), 2114–2120. https://doi.org/10.1093/bioinformatics/btu170

Bonfield, J. K., Marshall, J., Danecek, P., Li, H., Ohan, V., Whitwham, A., Keane, T., & Davies, R. M. (2021). HTSlib: C library for reading/writing high-throughput sequencing data. *GigaScience*, *10*(2), giab007. https://doi.org/10.1093/gigascience/giab007

Boomer, J. S., Shuherk-Shaffer, J., Hotchkiss, R. S., & Green, J. M. (2012). A prospective analysis of lymphocyte phenotype and function over the course of acute sepsis. *Critical Care (London, England)*, *16*(3), R112. https://doi.org/10.1186/cc11404

Borden, E. C. (2019). Interferons α and β in cancer: Therapeutic opportunities from new insights. *Nature Reviews. Drug Discovery*, *18*(3), 219–234. https://doi.org/10.1038/s41573-018-0011-2

Bossi, A., & Lehner, B. (2009). Tissue specificity and the human protein interaction network. *Molecular Systems Biology*, *5*, 260. https://doi.org/10.1038/msb.2009.17

Bowdish, D. M. E., Loffredo, M. S., Mukhopadhyay, S., Mantovani, A., & Gordon, S. (2007). Macrophage receptors implicated in the “adaptive” form of innate immunity. *Microbes and Infection*, *9*(14–15), 1680–1687. https://doi.org/10.1016/j.micinf.2007.09.002

Bradley, J. R. (2008). TNF-mediated inflammatory disease. *The Journal of Pathology*, *214*(2), 149–160. https://doi.org/10.1002/path.2287

Brands, X., Haak, B. W., Klarenbeek, A. M., Butler, J., Uhel, F., Qin, W., Otto, N. A., Jakobs, M. E., Faber, D. R., Lutter, R., Wiersinga, W. J., van der Poll, T., & Scicluna, B. P. (2021). An epigenetic and transcriptomic signature of immune

tolerance in human monocytes through multi-omics integration. *Genome Medicine*, *13*(1), 131. https://doi.org/10.1186/s13073-021-00948-1

Brands, X., Haak, B. W., Klarenbeek, A. M., Otto, N. A., Faber, D. R., Lutter, R., Scicluna, B. P., Wiersinga, W. J., & van der Poll, T. (2020). Concurrent Immune Suppression and Hyperinflammation in Patients With Community-Acquired Pneumonia. *Frontiers in Immunology*, *11*, 796. https://doi.org/10.3389/fimmu.2020.00796

Bray, N. L., Pimentel, H., Melsted, P., & Pachter, L. (2016). Near-optimal probabilistic RNA-seq quantification. *Nature Biotechnology*, *34*(5), 525–527. https://doi.org/10.1038/nbt.3519

Brubaker, S. W., Bonham, K. S., Zanoni, I., & Kagan, J. C. (2015). Innate immune pattern recognition: A cell biological perspective. *Annual Review of Immunology*, *33*, 257–290. https://doi.org/10.1146/annurev-immunol-032414-112240

Buljan, M., Chalancon, G., Eustermann, S., Wagner, G. P., Fuxreiter, M., Bateman, A., & Babu, M. M. (2012). Tissue-specific splicing of disordered segments that embed binding motifs rewires protein interaction networks. *Molecular Cell*, *46*(6), 871–883. https://doi.org/10.1016/j.molcel.2012.05.039

Cabral-Pacheco, G. A., Garza-Veloz, I., Castruita-De la Rosa, C., Ramirez-Acuña, J. M., Perez-Romero, B. A., Guerrero-Rodriguez, J. F., Martinez-Avila, N., & Martinez-Fierro, M. L. (2020). The Roles of Matrix Metalloproteinases and Their Inhibitors in Human Diseases. *International Journal of Molecular Sciences*, *21*(24), 9739. https://doi.org/10.3390/ijms21249739

Cajander, S., Tina, E., Bäckman, A., Magnuson, A., Strålin, K., Söderquist, B., & Källman, J. (2016). Quantitative Real-Time Polymerase Chain Reaction Measurement of HLA-DRA Gene Expression in Whole Blood Is Highly Reproducible and Shows Changes That Reflect Dynamic Shifts in Monocyte Surface HLA-DR Expression during the Course of Sepsis. *PloS One*, *11*(5), e0154690. https://doi.org/10.1371/journal.pone.0154690

Canè, S., Ugel, S., Trovato, R., Marigo, I., De Sanctis, F., Sartoris, S., & Bronte, V. (2019). The Endless Saga of Monocyte Diversity. *Frontiers in Immunology*, *10*, 1786. https://doi.org/10.3389/fimmu.2019.01786

Carlson, M. (2017). *Org.Hs.eg.db* [Computer software]. Bioconductor. https://doi.org/10.18129/B9.BIOC.ORG.HS.EG.DB

Carrel, L., & Willard, H. F. (2005). X-inactivation profile reveals extensive variability in X-linked gene expression in females. *Nature*, *434*(7031), 400–404. https://doi.org/10.1038/nature03479

Cavaillon, J.-M., & Adib-Conquy, M. (2006). Bench-to-bedside review: Endotoxin tolerance as a model of leukocyte reprogramming in sepsis. *Critical Care (London, England)*, *10*(5), 233. https://doi.org/10.1186/cc5055

Cavaillon, J.-M., Singer, M., & Skirecki, T. (2020). Sepsis therapies: Learning from 30 years of failure of translational research to propose new leads. *EMBO Molecular Medicine*, *12*(4), e10128. https://doi.org/10.15252/emmm.201810128

CDC. (2024). *Pneumonia Prevention and Control*. Centre for Disease Control. https://www.cdc.gov/pneumonia/prevention/index.html

Cerami, E., Gao, J., Dogrusoz, U., Gross, B. E., Sumer, S. O., Aksoy, B. A., Jacobsen, A., Byrne, C. J., Heuer, M. L., Larsson, E., Antipin, Y., Reva, B., Goldberg, A. P., Sander, C., & Schultz, N. (2012). The cBio cancer genomics portal: An open platform for exploring multidimensional cancer genomics data. *Cancer Discovery*, *2*(5), 401–404. https://doi.org/10.1158/2159-8290.CD-12-0095

Chan, J. K., Roth, J., Oppenheim, J. J., Tracey, K. J., Vogl, T., Feldmann, M., Horwood, N., & Nanchahal, J. (2012). Alarmins: Awaiting a clinical response. *The Journal of Clinical Investigation*, *122*(8), 2711–2719. https://doi.org/10.1172/JCI62423

Chandramohan, R., Wu, P.-Y., Phan, J. H., & Wang, M. D. (2013). Benchmarking RNA-Seq quantification tools. *Annual International Conference of the IEEE Engineering in Medicine and Biology Society. IEEE Engineering in Medicine and Biology Society. Annual International Conference*, *2013*, 647–650. https://doi.org/10.1109/EMBC.2013.6609583

Chaplin, D. D. (2010). Overview of the immune response. *The Journal of Allergy and Clinical Immunology*, *125*(2 Suppl 2), S3-23. https://doi.org/10.1016/j.jaci.2009.12.980

Charmpi, K., & Ycart, B. (2015). Weighted Kolmogorov Smirnov testing: An alternative for Gene Set Enrichment Analysis. *Statistical Applications in Genetics and Molecular Biology*, *14*(3), 279–293. https://doi.org/10.1515/sagmb-2014-0077

Chatr-Aryamontri, A., Oughtred, R., Boucher, L., Rust, J., Chang, C., Kolas, N. K., O'Donnell, L., Oster, S., Theesfeld, C., Sellam, A., Stark, C., Breitkreutz, B.-J.,

Dolinski, K., & Tyers, M. (2017). The BioGRID interaction database: 2017 update. *Nucleic Acids Research*, *45*(D1), D369–D379. https://doi.org/10.1093/nar/gkw1102

Chen, C., Xu, Z.-Q., Zong, Y.-P., Ou, B.-C., Shen, X.-H., Feng, H., Zheng, M.-H., Zhao, J.-K., & Lu, A.-G. (2019). CXCL5 induces tumor angiogenesis via enhancing the expression of FOXD1 mediated by the AKT/NF-κB pathway in colorectal cancer. *Cell Death & Disease*, *10*(3), 178. https://doi.org/10.1038/s41419-019-1431-6

Chen, G., Ning, B., & Shi, T. (2019). Single-Cell RNA-Seq Technologies and Related Computational Data Analysis. *Frontiers in Genetics*, *10*, 317. https://doi.org/10.3389/fgene.2019.00317

Chen, J.-W., Shrestha, L., Green, G., Leier, A., & Marquez-Lago, T. T. (2023). The hitchhikers' guide to RNA sequencing and functional analysis. *Briefings in Bioinformatics*, *24*(1), bbac529. https://doi.org/10.1093/bib/bbac529

Chen, S., Zhou, Y., Chen, Y., & Gu, J. (2018). fastp: An ultra-fast all-in-one FASTQ preprocessor. *Bioinformatics (Oxford, England)*, *34*(17), i884–i890. https://doi.org/10.1093/bioinformatics/bty560

Chen, W., Guo, W., Li, Y., & Chen, M. (2024). Integrative analysis of metabolomics and transcriptomics to uncover biomarkers in sepsis. *Scientific Reports*, *14*(1), 9676. https://doi.org/10.1038/s41598-024-59400-0

Cheng, S.-C., Quintin, J., Cramer, R. A., Shepardson, K. M., Saeed, S., Kumar, V., Giamarellos-Bourboulis, E. J., Martens, J. H. A., Rao, N. A., Aghajanirefah, A., Manjeri, G. R., Li, Y., Ifrim, D. C., Arts, R. J. W., van der Veer, B. M. J. W.,

Deen, P. M. T., Logie, C., O'Neill, L. A., Willems, P., … Netea, M. G. (2014). mTOR- and HIF-1α-mediated aerobic glycolysis as metabolic basis for trained immunity. *Science (New York, N.Y.)*, *345*(6204), 1250684. https://doi.org/10.1126/science.1250684

Chimen, M., Yates, C. M., McGettrick, H. M., Ward, L. S. C., Harrison, M. J., Apta, B., Dib, L. H., Imhof, B. A., Harrison, P., Nash, G. B., & Rainger, G. E. (2017). Monocyte Subsets Coregulate Inflammatory Responses by Integrated Signaling through TNF and IL-6 at the Endothelial Cell Interface. *Journal of Immunology (Baltimore, Md.: 1950)*, *198*(7), 2834–2843. https://doi.org/10.4049/jimmunol.1601281

Cho, J.-W., Son, J., Ha, S.-J., & Lee, I. (2021). Systems biology analysis identifies TNFRSF9 as a functional marker of tumor-infiltrating regulatory T-cell enabling clinical outcome prediction in lung cancer. *Computational and Structural Biotechnology Journal*, *19*, 860–868. https://doi.org/10.1016/j.csbj.2021.01.025

Christ, A., Günther, P., Lauterbach, M. A. R., Duewell, P., Biswas, D., Pelka, K., Scholz, C. J., Oosting, M., Haendler, K., Baßler, K., Klee, K., Schulte-Schrepping, J., Ulas, T., Moorlag, S. J. C. F. M., Kumar, V., Park, M. H., Joosten, L. A. B., Groh, L. A., Riksen, N. P., … Latz, E. (2018). Western Diet Triggers NLRP3-Dependent Innate Immune Reprogramming. *Cell*, *172*(1–2), 162-175.e14. https://doi.org/10.1016/j.cell.2017.12.013

Christaki, E., & Giamarellos-Bourboulis, E. J. (2014). The beginning of personalized medicine in sepsis: Small steps to a bright future. *Clinical Genetics*, *86*(1), 56–61. https://doi.org/10.1111/cge.12368

Ciabattini, A., Nardini, C., Santoro, F., Garagnani, P., Franceschi, C., & Medaglini, D. (2018). Vaccination in the elderly: The challenge of immune changes with aging. *Seminars in Immunology*, *40*, 83–94. https://doi.org/10.1016/j.smim.2018.10.010

Cilloniz, C., Martin-Loeches, I., Garcia-Vidal, C., San Jose, A., & Torres, A. (2016). Microbial Etiology of Pneumonia: Epidemiology, Diagnosis and Resistance Patterns. *International Journal of Molecular Sciences*, *17*(12), 2120. https://doi.org/10.3390/ijms17122120

Codo, A. C., Davanzo, G. G., Monteiro, L. D. B., De Souza, G. F., Muraro, S. P., Virgilio-da-Silva, J. V., Prodonoff, J. S., Carregari, V. C., De Biagi Junior, C. A. O., Crunfli, F., Jimenez Restrepo, J. L., Vendramini, P. H., Reis-de-Oliveira, G., Bispo Dos Santos, K., Toledo-Teixeira, D. A., Parise, P. L., Martini, M. C., Marques, R. E., Carmo, H. R., … Moraes-Vieira, P. M. (2020). Elevated Glucose Levels Favor SARS-CoV-2 Infection and Monocyte Response through a HIF-1α/Glycolysis-Dependent Axis. *Cell Metabolism*, *32*(3), 498–499. https://doi.org/10.1016/j.cmet.2020.07.015

Conant, G. C., & Wagner, A. (2003). Convergent evolution of gene circuits. *Nature Genetics*, *34*(3), 264–266. https://doi.org/10.1038/ng1181

Conesa, A., Madrigal, P., Tarazona, S., Gomez-Cabrero, D., Cervera, A., McPherson, A., Szcześniak, M. W., Gaffney, D. J., Elo, L. L., Zhang, X., & Mortazavi, A.

(2016). A survey of best practices for RNA-seq data analysis. *Genome Biology*, *17*, 13. https://doi.org/10.1186/s13059-016-0881-8

Conway Morris, A., Datta, D., Shankar-Hari, M., Stephen, J., Weir, C. J., Rennie, J., Antonelli, J., Bateman, A., Warner, N., Judge, K., Keenan, J., Wang, A., Burpee, T., Brown, K. A., Lewis, S. M., Mare, T., Roy, A. I., Hulme, G., Dimmick, I., … Walsh, T. S. (2018). Cell-surface signatures of immune dysfunction risk-stratify critically ill patients: INFECT study. *Intensive Care Medicine*, *44*(5), 627–635. https://doi.org/10.1007/s00134-018-5247-0

Cook, R. D., & Weisberg, S. (1982). Criticism and influence analysis in regression. *Sociological Methodology*, *13*, 313–361.

Costa-Silva, J., Domingues, D., & Lopes, F. M. (2017). RNA-Seq differential expression analysis: An extended review and a software tool. *PloS One*, *12*(12), e0190152. https://doi.org/10.1371/journal.pone.0190152

Costa-Silva, J., Domingues, D. S., Menotti, D., Hungria, M., & Lopes, F. M. (2023). Temporal progress of gene expression analysis with RNA-Seq data: A review on the relationship between computational methods. *Computational and Structural Biotechnology Journal*, *21*, 86–98. https://doi.org/10.1016/j.csbj.2022.11.051

Cox, D. R., & Reid, N. (1987). Parameter Orthogonality and Approximate Conditional Inference. *Journal of the Royal Statistical Society: Series B (Methodological)*, *49*(1), 1–18. https://doi.org/10.1111/j.2517-6161.1987.tb01422.x

Cule, E., Vineis, P., & De Iorio, M. (2011). Significance testing in ridge regression for genetic data. *BMC Bioinformatics*, *12*(1), 372. https://doi.org/10.1186/1471-2105-12-372

Danielli, S., Ma, Z., Pantazi, E., Kumar, A., Demarco, B., Fischer, F. A., Paudel, U., Weissenrieder, J., Lee, R. J., Joyce, S., Foskett, J. K., & Bezbradica, J. S. (2023). The ion channel CALHM6 controls bacterial infection-induced cellular cross-talk at the immunological synapse. *The EMBO Journal*, *42*(7), e111450. https://doi.org/10.15252/embj.2022111450

Date, D., Das, R., Narla, G., Simon, D. I., Jain, M. K., & Mahabeleshwar, G. H. (2014). Kruppel-like Transcription Factor 6 Regulates Inflammatory Macrophage Polarization. *The Journal of Biological Chemistry*, *289*(15), 10318–10329. https://doi.org/10.1074/jbc.M113.526749

de Jong, R., Altare, F., Haagen, I. A., Elferink, D. G., Boer, T., van Breda Vriesman, P. J., Kabel, P. J., Draaisma, J. M., van Dissel, J. T., Kroon, F. P., Casanova, J. L., & Ottenhoff, T. H. (1998). Severe mycobacterial and Salmonella infections in interleukin-12 receptor-deficient patients. *Science (New York, N.Y.)*, *280*(5368), 1435–1438. https://doi.org/10.1126/science.280.5368.1435

Del Fabbro, C., Scalabrin, S., Morgante, M., & Giorgi, F. M. (2013). An extensive evaluation of read trimming effects on Illumina NGS data analysis. *PloS One*, *8*(12), e85024. https://doi.org/10.1371/journal.pone.0085024

del Fresno, C., García-Rio, F., Gómez-Piña, V., Soares-Schanoski, A., Fernández-Ruíz, I., Jurado, T., Kajiji, T., Shu, C., Marín, E., Gutierrez del Arroyo, A., Prados, C., Arnalich, F., Fuentes-Prior, P., Biswas, S. K., & López-Collazo, E. (2009).

Potent phagocytic activity with impaired antigen presentation identifying lipopolysaccharide-tolerant human monocytes: Demonstration in isolated monocytes from cystic fibrosis patients. *Journal of Immunology (Baltimore, Md.: 1950)*, *182*(10), 6494–6507. https://doi.org/10.4049/jimmunol.0803350

Deutschman, C. S., & Tracey, K. J. (2014). Sepsis: Current dogma and new perspectives. *Immunity*, *40*(4), 463–475. https://doi.org/10.1016/j.immuni.2014.04.001

DeWolf, S., Laracy, J. C., Perales, M.-A., Kamboj, M., Van Den Brink, M. R. M., & Vardhana, S. (2022). SARS-CoV-2 in immunocompromised individuals. *Immunity*, *55*(10), 1779–1798. https://doi.org/10.1016/j.immuni.2022.09.006

Dias, S. S. G., Soares, V. C., Ferreira, A. C., Sacramento, C. Q., Fintelman-Rodrigues, N., Temerozo, J. R., Teixeira, L., Nunes da Silva, M. A., Barreto, E., Mattos, M., de Freitas, C. S., Azevedo-Quintanilha, I. G., Manso, P. P. A., Miranda, M. D., Siqueira, M. M., Hottz, E. D., Pão, C. R. R., Bou-Habib, D. C., Barreto-Vieira, D. F., … Bozza, P. T. (2020). Lipid droplets fuel SARS-CoV-2 replication and production of inflammatory mediators. *PLoS Pathogens*, *16*(12), e1009127. https://doi.org/10.1371/journal.ppat.1009127

Diederichs, S., & Haber, D. A. (2007). Dual role for argonautes in microRNA processing and posttranscriptional regulation of microRNA expression. *Cell*, *131*(6), 1097–1108. https://doi.org/10.1016/j.cell.2007.10.032

Disteche, C. M. (2012). Dosage compensation of the sex chromosomes. *Annual Review of Genetics*, *46*, 537–560. https://doi.org/10.1146/annurev-genet-110711-155454

Disteche, C. M. (2016). Dosage compensation of the sex chromosomes and autosomes. *Seminars in Cell & Developmental Biology*, *56*, 9–18. https://doi.org/10.1016/j.semcdb.2016.04.013

Divanovic, S., Trompette, A., Atabani, S. F., Madan, R., Golenbock, D. T., Visintin, A., Finberg, R. W., Tarakhovsky, A., Vogel, S. N., Belkaid, Y., Kurt-Jones, E. A., & Karp, C. L. (2005). Negative regulation of Toll-like receptor 4 signaling by the Toll-like receptor homolog RP105. *Nature Immunology*, *6*(6), 571–578. https://doi.org/10.1038/ni1198

Dobin, A., Davis, C. A., Schlesinger, F., Drenkow, J., Zaleski, C., Jha, S., Batut, P., Chaisson, M., & Gingeras, T. R. (2013). STAR: Ultrafast universal RNA-seq aligner. *Bioinformatics (Oxford, England)*, *29*(1), 15–21. https://doi.org/10.1093/bioinformatics/bts635

Dobrovolskaia, M. A., Medvedev, A. E., Thomas, K. E., Cuesta, N., Toshchakov, V., Ren, T., Cody, M. J., Michalek, S. M., Rice, N. R., & Vogel, S. N. (2003). Induction of in vitro reprogramming by Toll-like receptor (TLR)2 and TLR4 agonists in murine macrophages: Effects of TLR “homotolerance” versus “heterotolerance” on NF-kappa B signaling pathway components. *Journal of Immunology (Baltimore, Md.: 1950)*, *170*(1), 508–519. https://doi.org/10.4049/jimmunol.170.1.508

Domínguez-Andrés, J., Joosten, L. A., & Netea, M. G. (2019). Induction of innate immune memory: The role of cellular metabolism. *Current Opinion in Immunology*, *56*, 10–16. https://doi.org/10.1016/j.coi.2018.09.001

Dorneles, G. P., Teixeira, P. C., Peres, A., Rodrigues Júnior, L. C., da Fonseca, S. G., Monteiro, M. C., Eller, S., Oliveira, T. F., Wendland, E. M., & Romão, P. R. T. (2023). Endotoxin tolerance and low activation of TLR-4/NF-κB axis in monocytes of COVID-19 patients. *Journal of Molecular Medicine (Berlin, Germany)*, *101*(1–2), 183–195. https://doi.org/10.1007/s00109-023-02283-x

Dower, K., Ellis, D. K., Saraf, K., Jelinsky, S. A., & Lin, L.-L. (2008). Innate immune responses to TREM-1 activation: Overlap, divergence, and positive and negative cross-talk with bacterial lipopolysaccharide. *Journal of Immunology (Baltimore, Md.: 1950)*, *180*(5), 3520–3534. https://doi.org/10.4049/jimmunol.180.5.3520

Draghici, S., Khatri, P., Tarca, A. L., Amin, K., Done, A., Voichita, C., Georgescu, C., & Romero, R. (2007). A systems biology approach for pathway level analysis. *Genome Research*, *17*(10), 1537–1545. https://doi.org/10.1101/gr.6202607

Dunn, S. E., Perry, W. A., & Klein, S. L. (2024). Mechanisms and consequences of sex differences in immune responses. *Nature Reviews. Nephrology*, *20*(1), 37–55. https://doi.org/10.1038/s41581-023-00787-w

Ebbert, M. T. W., Staley, L. A., Hoyt, K. L., Pickett, B., Miller, J., Duce, J., Kauwe, J. S. K., & Ridge, P. G. (2016). Evaluating the necessity of PCR duplicate removal from next-generation sequencing data and a comparison of approaches for

the Alzheimer's Disease Neuroimaging Initiative. *BMC Bioinformatics*, *17*(S7), 239. https://doi.org/10.1186/s12859-016-1097-3

Ebner, P., Versteeg, G. A., & Ikeda, F. (2017). Ubiquitin enzymes in the regulation of immune responses. *Critical Reviews in Biochemistry and Molecular Biology*, *52*(4), 425–460. https://doi.org/10.1080/10409238.2017.1325829

Eissner, G., Kolch, W., & Scheurich, P. (2004). Ligands working as receptors: Reverse signaling by members of the TNF superfamily enhance the plasticity of the immune system. *Cytokine & Growth Factor Reviews*, *15*(5), 353–366. https://doi.org/10.1016/j.cytogfr.2004.03.011

El Gazzar, M., Yoza, B. K., Chen, X., Garcia, B. A., Young, N. L., & McCall, C. E. (2009). Chromatin-specific remodeling by HMGB1 and linker histone H1 silences proinflammatory genes during endotoxin tolerance. *Molecular and Cellular Biology*, *29*(7), 1959–1971. https://doi.org/10.1128/MCB.01862-08

El Kasmi, K. C., Smith, A. M., Williams, L., Neale, G., Panopoulos, A. D., Watowich, S. S., Häcker, H., Foxwell, B. M. J., & Murray, P. J. (2007). Cutting edge: A transcriptional repressor and corepressor induced by the STAT3-regulated anti-inflammatory signaling pathway. *Journal of Immunology (Baltimore, Md.: 1950)*, *179*(11), 7215–7219. https://doi.org/10.4049/jimmunol.179.11.7215

Ellery, P. J., Tippett, E., Chiu, Y.-L., Paukovics, G., Cameron, P. U., Solomon, A., Lewin, S. R., Gorry, P. R., Jaworowski, A., Greene, W. C., Sonza, S., & Crowe, S. M. (2007). The CD16+ monocyte subset is more permissive to infection and preferentially harbors HIV-1 in vivo. *Journal of Immunology (Baltimore,*

Md.: 1950), *178*(10), 6581–6589. https://doi.org/10.4049/jimmunol.178.10.6581

Ellis, J. D., Barrios-Rodiles, M., Colak, R., Irimia, M., Kim, T., Calarco, J. A., Wang, X., Pan, Q., O'Hanlon, D., Kim, P. M., Wrana, J. L., & Blencowe, B. J. (2012). Tissue-specific alternative splicing remodels protein-protein interaction networks. *Molecular Cell*, *46*(6), 884–892. https://doi.org/10.1016/j.molcel.2012.05.037

Emmert-Streib, F., & Glazko, G. V. (2011). Pathway analysis of expression data: Deciphering functional building blocks of complex diseases. *PLoS Computational Biology*, *7*(5), e1002053. https://doi.org/10.1371/journal.pcbi.1002053

Etich, J., Koch, M., Wagener, R., Zaucke, F., Fabri, M., & Brachvogel, B. (2019). Gene Expression Profiling of the Extracellular Matrix Signature in Macrophages of Different Activation Status: Relevance for Skin Wound Healing. *International Journal of Molecular Sciences*, *20*(20), 5086. https://doi.org/10.3390/ijms20205086

Evans, C., Hardin, J., & Stoebel, D. M. (2018). Selecting between-sample RNA-Seq normalization methods from the perspective of their assumptions. *Briefings in Bioinformatics*, *19*(5), 776–792. https://doi.org/10.1093/bib/bbx008

Ewels, P., Magnusson, M., Lundin, S., & Käller, M. (2016). MultiQC: Summarize analysis results for multiple tools and samples in a single report. *Bioinformatics (Oxford, England)*, *32*(19), 3047–3048. https://doi.org/10.1093/bioinformatics/btw354

Fabregat, A., Jupe, S., Matthews, L., Sidiropoulos, K., Gillespie, M., Garapati, P., Haw, R., Jassal, B., Korninger, F., May, B., Milacic, M., Roca, C. D., Rothfels, K., Sevilla, C., Shamovsky, V., Shorser, S., Varusai, T., Viteri, G., Weiser, J., … D'Eustachio, P. (2018). The Reactome Pathway Knowledgebase. *Nucleic Acids Research*, *46*(D1), D649–D655. https://doi.org/10.1093/nar/gkx1132

Fabregat, A., Sidiropoulos, K., Garapati, P., Gillespie, M., Hausmann, K., Haw, R., Jassal, B., Jupe, S., Korninger, F., McKay, S., Matthews, L., May, B., Milacic, M., Rothfels, K., Shamovsky, V., Webber, M., Weiser, J., Williams, M., Wu, G., … D'Eustachio, P. (2016). The reactome pathway knowledgebase. *Nucleic Acids Research*, *44*(D1), D481–D487. https://doi.org/10.1093/nar/gkv1351

Farahbod, M., & Pavlidis, P. (2019). Differential coexpression in human tissues and the confounding effect of mean expression levels. *Bioinformatics (Oxford, England)*, *35*(1), 55–61. https://doi.org/10.1093/bioinformatics/bty538

Feng, Z., Liao, M., & Zhang, L. (2024). Sex differences in disease: Sex chromosome and immunity. *Journal of Translational Medicine*, *22*(1), 1150. https://doi.org/10.1186/s12967-024-05990-2

Fingleton, B. (2017). Matrix metalloproteinases as regulators of inflammatory processes. *Biochimica et Biophysica Acta (BBA) - Molecular Cell Research*, *1864*(11), 2036–2042. https://doi.org/10.1016/j.bbamcr.2017.05.010

Finotello, F., Lavezzo, E., Bianco, L., Barzon, L., Mazzon, P., Fontana, P., Toppo, S., & Di Camillo, B. (2014). Reducing bias in RNA sequencing data: A novel approach to compute counts. *BMC Bioinformatics*, *15 Suppl 1*(Suppl 1), S7. https://doi.org/10.1186/1471-2105-15-S1-S7

Flannagan, R. S., Jaumouillé, V., & Grinstein, S. (2012). The cell biology of phagocytosis. *Annual Review of Pathology*, *7*, 61–98. https://doi.org/10.1146/annurev-pathol-011811-132445

Fontoura, C. A. R. S., Castellani, G., & Mombach, J. C. M. (2016). The R implementation of the CRAN package PATHChange, a tool to study genetic pathway alterations in transcriptomic data. *Computers in Biology and Medicine*, *78*, 76–80. https://doi.org/10.1016/j.compbiomed.2016.09.010

Foster, S. L., Hargreaves, D. C., & Medzhitov, R. (2007). Gene-specific control of inflammation by TLR-induced chromatin modifications. *Nature*, *447*(7147), 972–978. https://doi.org/10.1038/nature05836

Foster, S. L., & Medzhitov, R. (2009). Gene-specific control of the TLR-induced inflammatory response. *Clinical Immunology (Orlando, Fla.)*, *130*(1), 7–15. https://doi.org/10.1016/j.clim.2008.08.015

Fox, L. E., Locke, M. C., & Lenschow, D. J. (2020). Context Is Key: Delineating the Unique Functions of IFNα and IFNβ in Disease. *Frontiers in Immunology*, *11*, 606874. https://doi.org/10.3389/fimmu.2020.606874

Frankish, A., Diekhans, M., Ferreira, A.-M., Johnson, R., Jungreis, I., Loveland, J., Mudge, J. M., Sisu, C., Wright, J., Armstrong, J., Barnes, I., Berry, A., Bignell, A., Carbonell Sala, S., Chrast, J., Cunningham, F., Di Domenico, T., Donaldson, S., Fiddes, I. T., … Flicek, P. (2019). GENCODE reference annotation for the human and mouse genomes. *Nucleic Acids Research*, *47*(D1), D766–D773. https://doi.org/10.1093/nar/gky955

Franz, M., Lopes, C. T., Huck, G., Dong, Y., Sumer, O., & Bader, G. D. (2016). Cytoscape.js: A graph theory library for visualisation and analysis. *Bioinformatics (Oxford, England)*, *32*(2), 309–311. https://doi.org/10.1093/bioinformatics/btv557

Freise, N., Burghard, A., Ortkras, T., Daber, N., Imam Chasan, A., Jauch, S.-L., Fehler, O., Hillebrand, J., Schakaki, M., Rojas, J., Grimbacher, B., Vogl, T., Hoffmeier, A., Martens, S., Roth, J., & Austermann, J. (2019). Signaling mechanisms inducing hyporesponsiveness of phagocytes during systemic inflammation. *Blood*, *134*(2), 134–146. https://doi.org/10.1182/blood.2019000320

Fu, Y., Wu, P.-H., Beane, T., Zamore, P. D., & Weng, Z. (2018). Elimination of PCR duplicates in RNA-seq and small RNA-seq using unique molecular identifiers. *BMC Genomics*, *19*(1), 531. https://doi.org/10.1186/s12864-018-4933-1

Funes, S. C., Rios, M., Fernández-Fierro, A., Di Genaro, M. S., & Kalergis, A. M. (2022). Trained Immunity Contribution to Autoimmune and Inflammatory Disorders. *Frontiers in Immunology*, *13*, 868343. https://doi.org/10.3389/fimmu.2022.868343

Funk, C. J., Wang, J., Ito, Y., Travanty, E. A., Voelker, D. R., Holmes, K. V., & Mason, R. J. (2012). Infection of human alveolar macrophages by human coronavirus strain 229E. *The Journal of General Virology*, *93*(Pt 3), 494–503. https://doi.org/10.1099/vir.0.038414-0

Furman, D., Hejblum, B. P., Simon, N., Jojic, V., Dekker, C. L., Thiébaut, R., Tibshirani, R. J., & Davis, M. M. (2014). Systems analysis of sex differences reveals an

immunosuppressive role for testosterone in the response to influenza vaccination. *Proceedings of the National Academy of Sciences of the United States of America*, *111*(2), 869–874. https://doi.org/10.1073/pnas.1321060111

Gadsby, N. J., & Musher, D. M. (2022). The Microbial Etiology of Community-Acquired Pneumonia in Adults: From Classical Bacteriology to Host Transcriptional Signatures. *Clinical Microbiology Reviews*, *35*(4), e0001522. https://doi.org/10.1128/cmr.00015-22

Gal-Oz, S. T., Maier, B., Yoshida, H., Seddu, K., Elbaz, N., Czysz, C., Zuk, O., Stranger, B. E., Ner-Gaon, H., & Shay, T. (2019). ImmGen report: Sexual dimorphism in the immune system transcriptome. *Nature Communications*, *10*(1), 4295. https://doi.org/10.1038/s41467-019-12348-6

Gao, W., Thompson, L., Zhou, Q., Putheti, P., Fahmy, T. M., Strom, T. B., & Metcalfe, S. M. (2009). Treg versus Th17 lymphocyte lineages are cross-regulated by LIF versus IL-6. *Cell Cycle (Georgetown, Tex.)*, *8*(9), 1444–1450. https://doi.org/10.4161/cc.8.9.8348

Geissmann, F., & Mass, E. (2015). A stratified myeloid system, the challenge of understanding macrophage diversity. *Seminars in Immunology*, *27*(6), 353–356. https://doi.org/10.1016/j.smim.2016.03.016

The Gene Ontology Consortium. (2019). The Gene Ontology Resource: 20 years and still GOing strong. *Nucleic Acids Research*, *47*(D1), D330–D338. https://doi.org/10.1093/nar/gky1055

Gentile, L. F., Cuenca, A. G., Efron, P. A., Ang, D., Bihorac, A., McKinley, B. A., Moldawer, L. L., & Moore, F. A. (2012). Persistent inflammation and immunosuppression: A common syndrome and new horizon for surgical intensive care. *The Journal of Trauma and Acute Care Surgery*, *72*(6), 1491–1501. https://doi.org/10.1097/TA.0b013e318256e000

Gentleman, R. C., Carey, V. J., Bates, D. M., Bolstad, B., Dettling, M., Dudoit, S., Ellis, B., Gautier, L., Ge, Y., Gentry, J., Hornik, K., Hothorn, T., Huber, W., Iacus, S., Irizarry, R., Leisch, F., Li, C., Maechler, M., Rossini, A. J., … Zhang, J. (2004). Bioconductor: Open software development for computational biology and bioinformatics. *Genome Biology*, *5*(10), R80. https://doi.org/10.1186/gb-2004-5-10-r80

Gettler, K., Giri, M., Kenigsberg, E., Martin, J., Chuang, L. S., Hsu, N. Y., Denson, L. A., Hyams, J. S., Griffiths, A., Noe, J. D., Crandall, W. V., Mack, D. R., Kellermayer, R., Abraham, C., Hoffman, G., Kugathasan, S., & Cho, J. H. (2019). Prioritizing Crohn's disease genes by integrating association signals with gene expression implicates monocyte subsets. *Genes and Immunity*, *20*(7), 577–588. https://doi.org/10.1038/s41435-019-0059-y

Gill, S., & Parks, W. (2008). Metalloproteinases and their inhibitors: Regulators of wound healing. *The International Journal of Biochemistry & Cell Biology*, *40*(6–7), 1334–1347. https://doi.org/10.1016/j.biocel.2007.10.024

Ginhoux, F., & Jung, S. (2014). Monocytes and macrophages: Developmental pathways and tissue homeostasis. *Nature Reviews Immunology*, *14*(6), 392–404. https://doi.org/10.1038/nri3671

Girvan, M., & Newman, M. E. J. (2002). Community structure in social and biological networks. *Proceedings of the National Academy of Sciences*, *99*(12), 7821–7826. https://doi.org/10.1073/pnas.122653799

Giuliani, A. (2017). The application of principal component analysis to drug discovery and biomedical data. *Drug Discovery Today*, *22*(7), 1069–1076. https://doi.org/10.1016/j.drudis.2017.01.005

Godec, J., Tan, Y., Liberzon, A., Tamayo, P., Bhattacharya, S., Butte, A. J., Mesirov, J. P., & Haining, W. N. (2016). Compendium of Immune Signatures Identifies Conserved and Species-Specific Biology in Response to Inflammation. *Immunity*, *44*(1), 194–206. https://doi.org/10.1016/j.immuni.2015.12.006

Gondane, A., & Itkonen, H. M. (2023). Revealing the History and Mystery of RNA-Seq. *Current Issues in Molecular Biology*, *45*(3), 1860–1874. https://doi.org/10.3390/cimb45030120

Gordon, S. (2007). The macrophage: Past, present and future. *European Journal of Immunology*, *37 Suppl 1*, S9-17. https://doi.org/10.1002/eji.200737638

Greene, C. S., Krishnan, A., Wong, A. K., Ricciotti, E., Zelaya, R. A., Himmelstein, D. S., Zhang, R., Hartmann, B. M., Zaslavsky, E., Sealfon, S. C., Chasman, D. I., FitzGerald, G. A., Dolinski, K., Grosser, T., & Troyanskaya, O. G. (2015). Understanding multicellular function and disease with human tissue-specific networks. *Nature Genetics*, *47*(6), 569–576. https://doi.org/10.1038/ng.3259

Groettrup, M., Kirk, C. J., & Basler, M. (2010). Proteasomes in immune cells: More than peptide producers? *Nature Reviews. Immunology*, *10*(1), 73–78. https://doi.org/10.1038/nri2687

Grondman, I., Arts, R. J. W., Koch, R. M., Leijte, G. P., Gerretsen, J., Bruse, N., Kempkes, R. W. M., Ter Horst, R., Kox, M., Pickkers, P., Netea, M. G., & Gresnigt, M. S. (2019). Frontline Science: Endotoxin-induced immunotolerance is associated with loss of monocyte metabolic plasticity and reduction of oxidative burst. *Journal of Leukocyte Biology*, *106*(1), 11–25. https://doi.org/10.1002/JLB.5HI0119-018R

GTEx Consortium. (2013). The Genotype-Tissue Expression (GTEx) project. *Nature Genetics*, *45*(6), 580–585. https://doi.org/10.1038/ng.2653

Guillemin, A., Kumar, A., Wencker, M., & Ricci, E. P. (2021). Shaping the Innate Immune Response Through Post-Transcriptional Regulation of Gene Expression Mediated by RNA-Binding Proteins. *Frontiers in Immunology*, *12*, 796012. https://doi.org/10.3389/fimmu.2021.796012

Guilliams, M., Mildner, A., & Yona, S. (2018). Developmental and Functional Heterogeneity of Monocytes. *Immunity*, *49*(4), 595–613. https://doi.org/10.1016/j.immuni.2018.10.005

Günther, P., Cirovic, B., Baßler, K., Händler, K., Becker, M., Dutertre, C. A., Bigley, V., Newell, E., Collin, M., Ginhoux, F., Schlitzer, A., & Schultze, J. L. (2019). *A rule-based data-informed cellular consensus map of the human mononuclear phagocyte cell space*. Immunology. https://doi.org/10.1101/658179

Gupta, G., Buonsenso, D., Wood, J., Mohandas, S., & Warburton, D. (2025). Mechanistic Insights Into Long Covid: Viral Persistence, Immune Dysregulation, and Multi-Organ Dysfunction. *Comprehensive Physiology*, *15*(3), e70019. https://doi.org/10.1002/cph4.70019

Hadjadj, J., Yatim, N., Barnabei, L., Corneau, A., Boussier, J., Smith, N., Péré, H., Charbit, B., Bondet, V., Chenevier-Gobeaux, C., Breillat, P., Carlier, N., Gauzit, R., Morbieu, C., Pène, F., Marin, N., Roche, N., Szwebel, T.-A., Merkling, S. H., … Terrier, B. (2020). Impaired type I interferon activity and inflammatory responses in severe COVID-19 patients. *Science (New York, N.Y.)*, *369*(6504), 718–724. https://doi.org/10.1126/science.abc6027

Hall, A. O., Silver, J. S., & Hunter, C. A. (2012). The immunobiology of IL-27. *Advances in Immunology*, *115*, 1–44. https://doi.org/10.1016/B978-0-12-394299-9.00001-1

Hambleton, S., Goodbourn, S., Young, D. F., Dickinson, P., Mohamad, S. M. B., Valappil, M., McGovern, N., Cant, A. J., Hackett, S. J., Ghazal, P., Morgan, N. V., & Randall, R. E. (2013). STAT2 deficiency and susceptibility to viral illness in humans. *Proceedings of the National Academy of Sciences of the United States of America*, *110*(8), 3053–3058. https://doi.org/10.1073/pnas.1220098110

Hansen, K. D., Brenner, S. E., & Dudoit, S. (2010). Biases in Illumina transcriptome sequencing caused by random hexamer priming. *Nucleic Acids Research*, *38*(12), e131. https://doi.org/10.1093/nar/gkq224

Hardcastle, T. J., & Kelly, K. A. (2010). baySeq: Empirical Bayesian methods for identifying differential expression in sequence count data. *BMC Bioinformatics*, *11*, 422. https://doi.org/10.1186/1471-2105-11-422

Harris, M. A., Clark, J., Ireland, A., Lomax, J., Ashburner, M., Foulger, R., Eilbeck, K., Lewis, S., Marshall, B., Mungall, C., Richter, J., Rubin, G. M., Blake, J. A., Bult, C., Dolan, M., Drabkin, H., Eppig, J. T., Hill, D. P., Ni, L., … Gene Ontology Consortium. (2004). The Gene Ontology (GO) database and informatics resource. *Nucleic Acids Research*, *32*(Database issue), D258-261. https://doi.org/10.1093/nar/gkh036

Harrison, P. W., Amode, M. R., Austine-Orimoloye, O., Azov, A. G., Barba, M., Barnes, I., Becker, A., Bennett, R., Berry, A., Bhai, J., Bhurji, S. K., Boddu, S., Branco Lins, P. R., Brooks, L., Ramaraju, S. B., Campbell, L. I., Martinez, M. C., Charkhchi, M., Chougule, K., … Yates, A. D. (2024). Ensembl 2024. *Nucleic Acids Research*, *52*(D1), D891–D899. https://doi.org/10.1093/nar/gkad1049

Hassen, M., Toma, A., Tesfay, M., Degafu, E., Bekele, S., Ayalew, F., Gedefaw, A., & Tadesse, B. T. (2019). Radiologic Diagnosis and Hospitalization among Children with Severe Community Acquired Pneumonia: A Prospective Cohort Study. *BioMed Research International*, *2019*, 6202405. https://doi.org/10.1155/2019/6202405

Hata, A., Lagna, G., Massagué, J., & Hemmati-Brivanlou, A. (1998). Smad6 inhibits BMP/Smad1 signaling by specifically competing with the Smad4 tumor suppressor. *Genes & Development*, *12*(2), 186–197. https://doi.org/10.1101/gad.12.2.186

Hayden, M. S., & Ghosh, S. (2012). NF-κB, the first quarter-century: Remarkable progress and outstanding questions. *Genes & Development*, *26*(3), 203–234. https://doi.org/10.1101/gad.183434.111

He, L., Kang, Q., Chan, K. I., Zhang, Y., Zhong, Z., & Tan, W. (2022). The immunomodulatory role of matrix metalloproteinases in colitis-associated cancer. *Frontiers in Immunology*, *13*, 1093990. https://doi.org/10.3389/fimmu.2022.1093990

Hettinger, J., Richards, D. M., Hansson, J., Barra, M. M., Joschko, A.-C., Krijgsveld, J., & Feuerer, M. (2013). Origin of monocytes and macrophages in a committed progenitor. *Nature Immunology*, *14*(8), 821–830. https://doi.org/10.1038/ni.2638

Hollander, M., Do, T., Will, T., & Helms, V. (2021). Detecting Rewiring Events in Protein-Protein Interaction Networks Based on Transcriptomic Data. *Frontiers in Bioinformatics*, *1*, 724297. https://doi.org/10.3389/fbinf.2021.724297

Hoogerwerf, J. J., de Vos, A. F., van't Veer, C., Bresser, P., de Boer, A., Tanck, M. W. T., Draing, C., van der Zee, J. S., & van der Poll, T. (2010). Priming of alveolar macrophages upon instillation of lipopolysaccharide in the human lung. *American Journal of Respiratory Cell and Molecular Biology*, *42*(3), 349–356. https://doi.org/10.1165/rcmb.2008-0362OC

Hopp, L., Loeffler-Wirth, H., Nersisyan, L., Arakelyan, A., & Binder, H. (2018). Footprints of Sepsis Framed Within Community Acquired Pneumonia in the

Blood Transcriptome. *Frontiers in Immunology*, *9*, 1620. https://doi.org/10.3389/fimmu.2018.01620

Hotamisligil, G. S. (2017). Inflammation, metaflammation and immunometabolic disorders. *Nature*, *542*(7640), 177–185. https://doi.org/10.1038/nature21363

Hotchkiss, R. S., Monneret, G., & Payen, D. (2013a). Immunosuppression in sepsis: A novel understanding of the disorder and a new therapeutic approach. *The Lancet Infectious Diseases*, *13*(3), 260–268. https://doi.org/10.1016/S1473-3099(13)70001-X

Hotchkiss, R. S., Monneret, G., & Payen, D. (2013b). Sepsis-induced immunosuppression: From cellular dysfunctions to immunotherapy. *Nature Reviews Immunology*, *13*(12), 862–874. https://doi.org/10.1038/nri3552

Huang, D. W., Sherman, B. T., & Lempicki, R. A. (2009). Systematic and integrative analysis of large gene lists using DAVID bioinformatics resources. *Nature Protocols*, *4*(1), 44–57. https://doi.org/10.1038/nprot.2008.211

Huang, Q., Sun, M.-A., & Yan, P. (2018). Pathway and Network Analysis of Differentially Expressed Genes in Transcriptomes. *Methods in Molecular Biology (Clifton, N.J.)*, *1751*, 35–55. https://doi.org/10.1007/978-1-4939-7710-9_3

Ibrahim, M., Jassim, S., Cawthorne, M. A., & Langlands, K. (2014). A MATLAB tool for pathway enrichment using a topology-based pathway regulation score. *BMC Bioinformatics*, *15*(1), 358. https://doi.org/10.1186/s12859-014-0358-2

Jaakkola, M. K., & Elo, L. L. (2016). Empirical comparison of structure-based pathway methods. *Briefings in Bioinformatics*, *17*(2), 336–345. https://doi.org/10.1093/bib/bbv049

Jain, S., Self, W. H., Wunderink, R. G., Fakhran, S., Balk, R., Bramley, A. M., Reed, C., Grijalva, C. G., Anderson, E. J., Courtney, D. M., Chappell, J. D., Qi, C., Hart, E. M., Carroll, F., Trabue, C., Donnelly, H. K., Williams, D. J., Zhu, Y., Arnold, S. R., … CDC EPIC Study Team. (2015). Community-Acquired Pneumonia Requiring Hospitalization among U.S. Adults. *The New England Journal of Medicine*, *373*(5), 415–427. https://doi.org/10.1056/NEJMoa1500245

Jakubzick, C. V., Randolph, G. J., & Henson, P. M. (2017). Monocyte differentiation and antigen-presenting functions. *Nature Reviews Immunology*, *17*(6), 349–362. https://doi.org/10.1038/nri.2017.28

Jansen, A., Bruse, N., Waalders, N., Gerretsen, J., Rijbroek, D., Pickkers, P., & Kox, M. (2023). Ex vivo and in vitro Monocyte Responses Do Not Reflect in vivo Immune Responses and Tolerance. *Journal of Innate Immunity*, *15*(1), 174–187. https://doi.org/10.1159/000525572

Javed, S., Marsay, L., Wareham, A., Lewandowski, K. S., Williams, A., Dennis, M. J., Sharpe, S., Vipond, R., Silman, N., Ball, G., & Kempsell, K. E. (2016). Temporal Expression of Peripheral Blood Leukocyte Biomarkers in a Macaca fascicularis Infection Model of Tuberculosis; Comparison with Human Datasets and Analysis with Parametric/Non-parametric Tools for Improved Diagnostic Biomarker Identification. *PloS One*, *11*(5), e0154320. https://doi.org/10.1371/journal.pone.0154320

JGraph Ltd. (n.d.). *Draw.io – diagramming application*. Draw.Io (App.Diagrams.Net). Retrieved October 15, 2024, from https://app.diagrams.net/

Johnson, W. E., Li, C., & Rabinovic, A. (2007). Adjusting batch effects in microarray expression data using empirical Bayes methods. *Biostatistics*, *8*(1), 118–127. https://doi.org/10.1093/biostatistics/kxj037

Kanehisa, M., Furumichi, M., Tanabe, M., Sato, Y., & Morishima, K. (2017). KEGG: New perspectives on genomes, pathways, diseases and drugs. *Nucleic Acids Research*, *45*(D1), D353–D361. https://doi.org/10.1093/nar/gkw1092

Kanehisa, M., Goto, S., Sato, Y., Furumichi, M., & Tanabe, M. (2012). KEGG for integration and interpretation of large-scale molecular data sets. *Nucleic Acids Research*, *40*(Database issue), D109-114. https://doi.org/10.1093/nar/gkr988

Kapellos, T. S., Bonaguro, L., Gemünd, I., Reusch, N., Saglam, A., Hinkley, E. R., & Schultze, J. L. (2019). Human Monocyte Subsets and Phenotypes in Major Chronic Inflammatory Diseases. *Frontiers in Immunology*, *10*, 2035. https://doi.org/10.3389/fimmu.2019.02035

Kaufmann, E., Sanz, J., Dunn, J. L., Khan, N., Mendonça, L. E., Pacis, A., Tzelepis, F., Pernet, E., Dumaine, A., Grenier, J.-C., Mailhot-Léonard, F., Ahmed, E., Belle, J., Besla, R., Mazer, B., King, I. L., Nijnik, A., Robbins, C. S., Barreiro, L. B., & Divangahi, M. (2018). BCG Educates Hematopoietic Stem Cells to Generate Protective Innate Immunity against Tuberculosis. *Cell*, *172*(1–2), 176-190.e19. https://doi.org/10.1016/j.cell.2017.12.031

Kawai, T., & Akira, S. (2007). TLR signaling. *Seminars in Immunology*, *19*(1), 24–32. https://doi.org/10.1016/j.smim.2006.12.004

Kelder, T., van Iersel, M. P., Hanspers, K., Kutmon, M., Conklin, B. R., Evelo, C. T., & Pico, A. R. (2012). WikiPathways: Building research communities on biological pathways. *Nucleic Acids Research*, *40*(Database issue), D1301-1307. https://doi.org/10.1093/nar/gkr1074

Kelly, B., & O'Neill, L. A. J. (2015). Metabolic reprogramming in macrophages and dendritic cells in innate immunity. *Cell Research*, *25*(7), 771–784. https://doi.org/10.1038/cr.2015.68

Khan, M. A., Alanazi, F., Ahmed, H. A., Shamma, T., Kelly, K., Hammad, M. A., Alawad, A. O., Assiri, A. M., & Broering, D. C. (2019). iPSC-derived MSC therapy induces immune tolerance and supports long-term graft survival in mouse orthotopic tracheal transplants. *Stem Cell Research & Therapy*, *10*(1), 290. https://doi.org/10.1186/s13287-019-1397-4

Khoshdel, F., Mottaghi-Dastjerdi, N., Yazdani, F., Salehi, S., Ghorbani, A., Montazeri, H., Soltany-Rezaee-Rad, M., & Goodarzy, B. (2024). CTGF, FN1, IL-6, THBS1, and WISP1 genes and PI3K-Akt signaling pathway as prognostic and therapeutic targets in gastric cancer identified by gene network modeling. *Discover Oncology*, *15*(1), 344. https://doi.org/10.1007/s12672-024-01225-4

Kim, B.-H., Chee, J. D., Bradfield, C. J., Park, E.-S., Kumar, P., & MacMicking, J. D. (2016). Interferon-induced guanylate-binding proteins in inflammasome

activation and host defense. *Nature Immunology*, *17*(5), 481–489. https://doi.org/10.1038/ni.3440

Kim, D., Paggi, J. M., Park, C., Bennett, C., & Salzberg, S. L. (2019). Graph-based genome alignment and genotyping with HISAT2 and HISAT-genotype. *Nature Biotechnology*, *37*(8), 907–915. https://doi.org/10.1038/s41587-019-0201-4

Kim, G.-D., Das, R., Goduni, L., McClellan, S., Hazlett, L. D., & Mahabeleshwar, G. H. (2016). Kruppel-like Factor 6 Promotes Macrophage-mediated Inflammation by Suppressing B Cell Leukemia/Lymphoma 6 Expression. *The Journal of Biological Chemistry*, *291*(40), 21271–21282. https://doi.org/10.1074/jbc.M116.738617

Kim, G.-D., Ng, H. P., Chan, E. R., & Mahabeleshwar, G. H. (2020). Kruppel-like factor 6 promotes macrophage inflammatory and hypoxia response. *FASEB Journal: Official Publication of the Federation of American Societies for Experimental Biology*, *34*(2), 3209–3223. https://doi.org/10.1096/fj.201902221R

Kim, G.-D., Ng, H. P., Patel, N., & Mahabeleshwar, G. H. (2019). Kruppel-like factor 6 and miR-223 signaling axis regulates macrophage-mediated inflammation. *FASEB Journal: Official Publication of the Federation of American Societies for Experimental Biology*, *33*(10), 10902–10915. https://doi.org/10.1096/fj.201900867RR

Klassert, T. E., Bräuer, J., Hölzer, M., Stock, M., Riege, K., Zubiría-Barrera, C., Müller, M. M., Rummler, S., Skerka, C., Marz, M., & Slevogt, H. (2017). Differential

Effects of Vitamins A and D on the Transcriptional Landscape of Human Monocytes during Infection. *Scientific Reports*, *7*, 40599. https://doi.org/10.1038/srep40599

Klein, S. L., & Flanagan, K. L. (2016). Sex differences in immune responses. *Nature Reviews. Immunology*, *16*(10), 626–638. https://doi.org/10.1038/nri.2016.90

Knoll, R., Schultze, J. L., & Schulte-Schrepping, J. (2021). Monocytes and Macrophages in COVID-19. *Frontiers in Immunology*, *12*, 720109. https://doi.org/10.3389/fimmu.2021.720109

Koelwyn, G. J., Corr, E. M., Erbay, E., & Moore, K. J. (2018). Regulation of macrophage immunometabolism in atherosclerosis. *Nature Immunology*, *19*(6), 526–537. https://doi.org/10.1038/s41590-018-0113-3

Kolde, R. (2010). *pheatmap: Pretty Heatmaps* (p. 1.0.13) [Dataset]. https://doi.org/10.32614/CRAN.package.pheatmap

Kovats, S. (2015). Estrogen receptors regulate innate immune cells and signaling pathways. *Cellular Immunology*, *294*(2), 63–69. https://doi.org/10.1016/j.cellimm.2015.01.018

Kox, M., de Kleijn, S., Pompe, J. C., Ramakers, B. P., Netea, M. G., van der Hoeven, J. G., Hoedemaekers, C. W., & Pickkers, P. (2011). Differential ex vivo and in vivo endotoxin tolerance kinetics following human endotoxemia. *Critical Care Medicine*, *39*(8), 1866–1870. https://doi.org/10.1097/CCM.0b013e3182190d5d

Kullberg, R. F. J., Brands, X., Klarenbeek, A. M., Butler, J. M., Otto, N. A., Faber, D. R., Scicluna, B. P., Van Der Poll, T., Wiersinga, W. J., & Haak, B. W. (2022).

Rectal microbiota are coupled with altered cytokine production capacity following community-acquired pneumonia hospitalization. *iScience*, *25*(8), 104740. https://doi.org/10.1016/j.isci.2022.104740

Kumar, V. (2022). Toll-Like Receptors in Adaptive Immunity. *Handbook of Experimental Pharmacology*, *276*, 95–131. https://doi.org/10.1007/164_2021_543

La Mata, S. H.-D., Ramírez-Suástegui, C., Mistry, H., Castañeda-Castro, F. E., Kyyaly, M. A., Simon, H., Liang, S., Lau, L., Barber, C., Mondal, M., Zhang, H., Arshad, S. H., Kurukulaaratchy, R. J., Vijayanand, P., & Seumois, G. (2023). Cytotoxic CD4+ tissue-resident memory T cells are associated with asthma severity. *Med (New York, N.Y.)*, *4*(12), 875-897.e8. https://doi.org/10.1016/j.medj.2023.09.003

Lachmandas, E., Boutens, L., Ratter, J. M., Hijmans, A., Hooiveld, G. J., Joosten, L. A. B., Rodenburg, R. J., Fransen, J. A. M., Houtkooper, R. H., van Crevel, R., Netea, M. G., & Stienstra, R. (2016). Microbial stimulation of different Toll-like receptor signalling pathways induces diverse metabolic programmes in human monocytes. *Nature Microbiology*, *2*, 16246. https://doi.org/10.1038/nmicrobiol.2016.246

Lambrecht, B. N., & Hammad, H. (2009). Biology of lung dendritic cells at the origin of asthma. *Immunity*, *31*(3), 412–424. https://doi.org/10.1016/j.immuni.2009.08.008

Lämmermann, T., & Germain, R. N. (2014). The multiple faces of leukocyte interstitial migration. *Seminars in Immunopathology*, *36*(2), 227–251. https://doi.org/10.1007/s00281-014-0418-8

Landau, W. M., & Liu, P. (2013). Dispersion estimation and its effect on test performance in RNA-seq data analysis: A simulation-based comparison of methods. *PloS One*, *8*(12), e81415. https://doi.org/10.1371/journal.pone.0081415

Langmead, B., & Salzberg, S. L. (2012). Fast gapped-read alignment with Bowtie 2. *Nature Methods*, *9*(4), 357–359. https://doi.org/10.1038/nmeth.1923

Lee, H. S., & Kim, W. J. (2022). The Role of Matrix Metalloproteinase in Inflammation with a Focus on Infectious Diseases. *International Journal of Molecular Sciences*, *23*(18), 10546. https://doi.org/10.3390/ijms231810546

Lee, J., Tam, H., Adler, L., Ilstad-Minnihan, A., Macaubas, C., & Mellins, E. D. (2017). The MHC class II antigen presentation pathway in human monocytes differs by subset and is regulated by cytokines. *PloS One*, *12*(8), e0183594. https://doi.org/10.1371/journal.pone.0183594

Lee, M. N., Ye, C., Villani, A. C., Raj, T., Li, W., Eisenhaure, T. M., Imboywa, S. H., Chipendo, P. I., Ran, F. A., Slowikowski, K., Ward, L. D., Raddassi, K., McCabe, C., Lee, M. H., Frohlich, I. Y., Hafler, D. A., Kellis, M., Raychaudhuri, S., Zhang, F., … Hacohen, N. (2014). Common genetic variants modulate pathogen-sensing responses in human dendritic cells. *Science*, *343*(6175), 1246980. https://doi.org/10.1126/science.1246980

Leek, J. T., & Storey, J. D. (2007). Capturing heterogeneity in gene expression studies by surrogate variable analysis. *PLoS Genetics*, *3*(9), 1724–1735. https://doi.org/10.1371/journal.pgen.0030161

Leentjens, J., Kox, M., Koch, R. M., Preijers, F., Joosten, L. A. B., van der Hoeven, J. G., Netea, M. G., & Pickkers, P. (2012). Reversal of immunoparalysis in humans in vivo: A double-blind, placebo-controlled, randomized pilot study. *American Journal of Respiratory and Critical Care Medicine*, *186*(9), 838–845. https://doi.org/10.1164/rccm.201204-0645OC

Ley, K., Laudanna, C., Cybulsky, M. I., & Nourshargh, S. (2007). Getting to the site of inflammation: The leukocyte adhesion cascade updated. *Nature Reviews. Immunology*, *7*(9), 678–689. https://doi.org/10.1038/nri2156

Li, H., Handsaker, B., Wysoker, A., Fennell, T., Ruan, J., Homer, N., Marth, G., Abecasis, G., Durbin, R., & 1000 Genome Project Data Processing Subgroup. (2009). The Sequence Alignment/Map format and SAMtools. *Bioinformatics (Oxford, England)*, *25*(16), 2078–2079. https://doi.org/10.1093/bioinformatics/btp352

Li, J., & Tibshirani, R. (2013). Finding consistent patterns: A nonparametric approach for identifying differential expression in RNA-Seq data. *Statistical Methods in Medical Research*, *22*(5), 519–536. https://doi.org/10.1177/0962280211428386

Li, L., Weinberg, C. R., Darden, T. A., & Pedersen, L. G. (2001). Gene selection for sample classification based on gene expression data: Study of sensitivity to choice of parameters of the GA/KNN method. *Bioinformatics (Oxford,*

England), *17*(12), 1131–1142. https://doi.org/10.1093/bioinformatics/17.12.1131

Li, Y., Kang, K., Krahn, J. M., Croutwater, N., Lee, K., Umbach, D. M., & Li, L. (2017). A comprehensive genomic pan-cancer classification using The Cancer Genome Atlas gene expression data. *BMC Genomics*, *18*(1), 508. https://doi.org/10.1186/s12864-017-3906-0

Liao, B.-Y., & Zhang, J. (2006). Low rates of expression profile divergence in highly expressed genes and tissue-specific genes during mammalian evolution. *Molecular Biology and Evolution*, *23*(6), 1119–1128. https://doi.org/10.1093/molbev/msj119

Liao, Y., Smyth, G. K., & Shi, W. (2014). featureCounts: An efficient general purpose program for assigning sequence reads to genomic features. *Bioinformatics (Oxford, England)*, *30*(7), 923–930. https://doi.org/10.1093/bioinformatics/btt656

Libert, C., Dejager, L., & Pinheiro, I. (2010). The X chromosome in immune functions: When a chromosome makes the difference. *Nature Reviews. Immunology*, *10*(8), 594–604. https://doi.org/10.1038/nri2815

Liberzon, A., Birger, C., Thorvaldsdóttir, H., Ghandi, M., Mesirov, J. P., & Tamayo, P. (2015). The Molecular Signatures Database (MSigDB) hallmark gene set collection. *Cell Systems*, *1*(6), 417–425. https://doi.org/10.1016/j.cels.2015.12.004

Lim, W. S., van der Eerden, M. M., Laing, R., Boersma, W. G., Karalus, N., Town, G. I., Lewis, S. A., & Macfarlane, J. T. (2003). Defining community acquired

pneumonia severity on presentation to hospital: An international derivation and validation study. *Thorax*, *58*(5), 377–382. https://doi.org/10.1136/thorax.58.5.377

Lin, W., Wang, C., Liu, G., Bi, C., Wang, X., Zhou, Q., & Jin, H. (2020). SLC7A11/xCT in cancer: Biological functions and therapeutic implications. *American Journal of Cancer Research*, *10*(10), 3106–3126.

Lin, X., Liang, Y.-Y., Sun, B., Liang, M., Shi, Y., Brunicardi, F. C., Shi, Y., & Feng, X.-H. (2003a). Smad6 recruits transcription corepressor CtBP to repress bone morphogenetic protein-induced transcription. *Molecular and Cellular Biology*, *23*(24), 9081–9093. https://doi.org/10.1128/MCB.23.24.9081-9093.2003

Lin, X., Liang, Y.-Y., Sun, B., Liang, M., Shi, Y., Brunicardi, F. C., Shi, Y., & Feng, X.-H. (2003b). Smad6 recruits transcription corepressor CtBP to repress bone morphogenetic protein-induced transcription. *Molecular and Cellular Biology*, *23*(24), 9081–9093. https://doi.org/10.1128/MCB.23.24.9081-9093.2003

Lindgreen, S. (2012). AdapterRemoval: Easy cleaning of next-generation sequencing reads. *BMC Research Notes*, *5*, 337. https://doi.org/10.1186/1756-0500-5-337

Liu, B., Yi, H., Fang, J., Han, L., Zhou, M., & Guo, Y. (2019). Antimicrobial resistance and risk factors for mortality of pneumonia caused by Klebsiella pneumoniae among diabetics: A retrospective study conducted in Shanghai, China. *Infection and Drug Resistance*, *12*, 1089–1098. https://doi.org/10.2147/IDR.S199642

Liu, S., Wang, Z., Zhu, R., Wang, F., Cheng, Y., & Liu, Y. (2021). Three Differential Expression Analysis Methods for RNA Sequencing: Limma, EdgeR, DESeq2. *Journal of Visualized Experiments: JoVE*, *175*. https://doi.org/10.3791/62528

Liu, T., Ren, S., Sun, C., Zhao, P., & Wang, H. (2023). Glutaminolysis and peripheral CD4+ T cell differentiation: From mechanism to intervention strategy. *Frontiers in Immunology*, *14*, 1221530. https://doi.org/10.3389/fimmu.2023.1221530

Lönnstedt, I., & Speed, T. (2002). Replicated microarray data. *Statistica Sinica*, 31–46.

Lopes, T. J. S., Schaefer, M., Shoemaker, J., Matsuoka, Y., Fontaine, J.-F., Neumann, G., Andrade-Navarro, M. A., Kawaoka, Y., & Kitano, H. (2011). Tissue-specific subnetworks and characteristics of publicly available human protein interaction databases. *Bioinformatics (Oxford, England)*, *27*(17), 2414–2421. https://doi.org/10.1093/bioinformatics/btr414

López-Collazo, E., & del Fresno, C. (2013). Pathophysiology of endotoxin tolerance: Mechanisms and clinical consequences. *Critical Care (London, England)*, *17*(6), 242. https://doi.org/10.1186/cc13110

Lorente-Sorolla, C., Garcia-Gomez, A., Català-Moll, F., Toledano, V., Ciudad, L., Avendaño-Ortiz, J., Maroun-Eid, C., Martín-Quirós, A., Martínez-Gallo, M., Ruiz-Sanmartín, A., Del Campo, Á. G., Ferrer-Roca, R., Ruiz-Rodriguez, J. C., Álvarez-Errico, D., López-Collazo, E., & Ballestar, E. (2019). Inflammatory cytokines and organ dysfunction associate with the aberrant DNA

methylome of monocytes in sepsis. *Genome Medicine*, *11*(1), 66. https://doi.org/10.1186/s13073-019-0674-2

Love, M. I. (2024). *DESeq2: Differential gene expression analysis based on the negative binomial distribution* (Version 1.44.0) [Computer software]. Bioconductor. https://bioconductor.org/packages/release/bioc/manuals/DESeq2/man/DESeq2.pdf

Love, M. I., Huber, W., & Anders, S. (2014). Moderated estimation of fold change and dispersion for RNA-seq data with DESeq2. *Genome Biology*, *15*(12), 550. https://doi.org/10.1186/s13059-014-0550-8

Lu, H., Zeng, N., Chen, Q., Wu, Y., Cai, S., Li, G., Li, F., & Kong, J. (2019). Clinical prognostic significance of serum high mobility group box-1 protein in patients with community-acquired pneumonia. *The Journal of International Medical Research*, *47*(3), 1232–1240. https://doi.org/10.1177/0300060518819381

Lucas, C., Wong, P., Klein, J., Castro, T. B. R., Silva, J., Sundaram, M., Ellingson, M. K., Mao, T., Oh, J. E., Israelow, B., Takahashi, T., Tokuyama, M., Lu, P., Venkataraman, A., Park, A., Mohanty, S., Wang, H., Wyllie, A. L., Vogels, C. B. F., … Iwasaki, A. (2020). Longitudinal analyses reveal immunological misfiring in severe COVID-19. *Nature*, *584*(7821), 463–469. https://doi.org/10.1038/s41586-020-2588-y

Lyu, B., & Haque, A. (2018). Deep Learning Based Tumor Type Classification Using Gene Expression Data. *Proceedings of the 2018 ACM International Conference*

on Bioinformatics, Computational Biology, and Health Informatics, 89–96. https://doi.org/10.1145/3233547.3233588

Ma, S., Sun, B., Duan, S., Han, J., Barr, T., Zhang, J., Bissonnette, M. B., Kortylewski, M., He, C., Chen, J., Caligiuri, M. A., & Yu, J. (2023). YTHDF2 orchestrates tumor-associated macrophage reprogramming and controls antitumor immunity through CD8+ T cells. *Nature Immunology*, *24*(2), 255–266. https://doi.org/10.1038/s41590-022-01398-6

Ma, W.-T., Gao, F., Gu, K., & Chen, D.-K. (2019). The Role of Monocytes and Macrophages in Autoimmune Diseases: A Comprehensive Review. *Frontiers in Immunology*, *10*, 1140. https://doi.org/10.3389/fimmu.2019.01140

Madej, M. P., Töpfer, E., Boraschi, D., & Italiani, P. (2017). Different Regulation of Interleukin-1 Production and Activity in Monocytes and Macrophages: Innate Memory as an Endogenous Mechanism of IL-1 Inhibition. *Frontiers in Pharmacology*, *8*, 335. https://doi.org/10.3389/fphar.2017.00335

Mages, J., Dietrich, H., & Lang, R. (2007). A genome-wide analysis of LPS tolerance in macrophages. *Immunobiology*, *212*(9–10), 723–737. https://doi.org/10.1016/j.imbio.2007.09.015

Maher, A. K., Burnham, K. L., Jones, E. M., Tan, M. M. H., Saputil, R. C., Baillon, L., Selck, C., Giang, N., Argüello, R., Pillay, C., Thorley, E., Short, C.-E., Quinlan, R., Barclay, W. S., Cooper, N., Taylor, G. P., Davenport, E. E., & Dominguez-Villar, M. (2022). Transcriptional reprogramming from innate immune functions to a pro-thrombotic signature by monocytes in COVID-19. *Nature*

Communications, *13*(1), 7947. https://doi.org/10.1038/s41467-022-35638-y

Majumdar, S. R., Eurich, D. T., Gamble, J.-M., Senthilselvan, A., & Marrie, T. J. (2011). Oxygen saturations less than 92% are associated with major adverse events in outpatients with pneumonia: A population-based cohort study. *Clinical Infectious Diseases: An Official Publication of the Infectious Diseases Society of America*, *52*(3), 325–331. https://doi.org/10.1093/cid/ciq076

Man, S. M., Place, D. E., Kuriakose, T., & Kanneganti, T.-D. (2017). Interferon-inducible guanylate-binding proteins at the interface of cell-autonomous immunity and inflammasome activation. *Journal of Leukocyte Biology*, *101*(1), 143–150. https://doi.org/10.1189/jlb.4MR0516-223R

Mansour, E., Pereira, F. G., Araújo, E. P., Amaral, M. E. C., Morari, J., Ferraroni, N. R., Ferreira, D. S., Lorand-Metze, I., & Velloso, L. A. (2006). Leptin inhibits apoptosis in thymus through a janus kinase-2-independent, insulin receptor substrate-1/phosphatidylinositol-3 kinase-dependent pathway. *Endocrinology*, *147*(11), 5470–5479. https://doi.org/10.1210/en.2006-0223

Marangio, A., Biccari, A., D'Angelo, E., Sensi, F., Spolverato, G., Pucciarelli, S., & Agostini, M. (2022). The Study of the Extracellular Matrix in Chronic Inflammation: A Way to Prevent Cancer Initiation? *Cancers*, *14*(23), 5903. https://doi.org/10.3390/cancers14235903

Márquez, E. J., Chung, C.-H., Marches, R., Rossi, R. J., Nehar-Belaid, D., Eroglu, A., Mellert, D. J., Kuchel, G. A., Banchereau, J., & Ucar, D. (2020). Sexual-

dimorphism in human immune system aging. *Nature Communications*, *11*(1), 751. https://doi.org/10.1038/s41467-020-14396-9

Martin, M. (2011). Cutadapt removes adapter sequences from high-throughput sequencing reads. *EMBnet.Journal*, *17*(1), 10. https://doi.org/10.14806/ej.17.1.200

Martinez, F. O., Gordon, S., Locati, M., & Mantovani, A. (2006). Transcriptional profiling of the human monocyte-to-macrophage differentiation and polarization: New molecules and patterns of gene expression. *Journal of Immunology (Baltimore, Md.: 1950)*, *177*(10), 7303–7311. https://doi.org/10.4049/jimmunol.177.10.7303

Matzinger, P. (2002). The Danger Model: A Renewed Sense of Self. *Science*, *296*(5566), 301–305. https://doi.org/10.1126/science.1071059

McCarthy, D. J., Chen, Y., & Smyth, G. K. (2012). Differential expression analysis of multifactor RNA-Seq experiments with respect to biological variation. *Nucleic Acids Research*, *40*(10), 4288–4297. https://doi.org/10.1093/nar/gks042

McCullagh & Nelder. (1989). *Generalized Linear Models—Second Edition* (Second). Chapman and Hall. https://www.utstat.toronto.edu/brunner/oldclass/2201s11/readings/glmbook.pdf

McCullagh, P. (2019). *Generalized linear models*. Routledge.

McDermaid, A., Monier, B., Zhao, J., Liu, B., & Ma, Q. (2019). Interpretation of differential gene expression results of RNA-seq data: Review and

integration. *Briefings in Bioinformatics*, *20*(6), 2044–2054. https://doi.org/10.1093/bib/bby067

McDonnell Genome Institute – Washington University. (2019). *Genomic visualization and interpretations: Differential expression*. McDonnell Genome Institute. https://genviz.org/module-04-expression/0004/02/01/DifferentialExpression

McGrath, K. E., Frame, J. M., & Palis, J. (2015). Early hematopoiesis and macrophage development. *Seminars in Immunology*, *27*(6), 379–387. https://doi.org/10.1016/j.smim.2016.03.013

Medvedev, A. E., Kopydlowski, K. M., & Vogel, S. N. (2000). Inhibition of lipopolysaccharide-induced signal transduction in endotoxin-tolerized mouse macrophages: Dysregulation of cytokine, chemokine, and toll-like receptor 2 and 4 gene expression. *Journal of Immunology (Baltimore, Md.: 1950)*, *164*(11), 5564–5574. https://doi.org/10.4049/jimmunol.164.11.5564

Medzhitov, R., & Horng, T. (2009). Transcriptional control of the inflammatory response. *Nature Reviews. Immunology*, *9*(10), 692–703. https://doi.org/10.1038/nri2634

Medzhitov, R., & Janeway, C. (2000). Innate immune recognition: Mechanisms and pathways. *Immunological Reviews*, *173*, 89–97. https://doi.org/10.1034/j.1600-065x.2000.917309.x

Mei, J., Liu, Y., Dai, N., Favara, M., Greene, T., Jeyaseelan, S., Poncz, M., Lee, J. S., & Worthen, G. S. (2010). CXCL5 regulates chemokine scavenging and

pulmonary host defense to bacterial infection. *Immunity*, *33*(1), 106–117. https://doi.org/10.1016/j.immuni.2010.07.009

Méndez-Enríquez, E., & Hallgren, J. (2019). Mast Cells and Their Progenitors in Allergic Asthma. *Frontiers in Immunology*, *10*, 821. https://doi.org/10.3389/fimmu.2019.00821

Menéndez, R., Sahuquillo-Arce, J. M., Reyes, S., Martínez, R., Polverino, E., Cillóniz, C., Córdoba, J. G., Montull, B., & Torres, A. (2012). Cytokine activation patterns and biomarkers are influenced by microorganisms in community-acquired pneumonia. *Chest*, *141*(6), 1537–1545. https://doi.org/10.1378/chest.11-1446

Metcalfe, S. M., Strom, T. B., Williams, A., & Fahmy, T. M. (2015). Multiple Sclerosis and the LIF/IL-6 Axis: Use of Nanotechnology to Harness the Tolerogenic and Reparative Properties of LIF. *Nanobiomedicine*, *2*, 5. https://doi.org/10.5772/60622

Mihori, S., Nichols, F., Provatas, A., Matz, A., Zhou, B., Blesso, C. N., Panier, H., Daddi, L., Zhou, Y., & Clark, R. B. (2024). Microbiome-derived bacterial lipids regulate gene expression of proinflammatory pathway inhibitors in systemic monocytes. *Frontiers in Immunology*, *15*, 1415565. https://doi.org/10.3389/fimmu.2024.1415565

Mills, E. L., Kelly, B., Logan, A., Costa, A. S. H., Varma, M., Bryant, C. E., Tourlomousis, P., Däbritz, J. H. M., Gottlieb, E., Latorre, I., Corr, S. C., McManus, G., Ryan, D., Jacobs, H. T., Szibor, M., Xavier, R. J., Braun, T., Frezza, C., Murphy, M. P., & O'Neill, L. A. (2016). Succinate Dehydrogenase

Supports Metabolic Repurposing of Mitochondria to Drive Inflammatory Macrophages. *Cell*, *167*(2), 457-470.e13. https://doi.org/10.1016/j.cell.2016.08.064

Mishra, B., & Ivashkiv, L. B. (2024). Interferons and epigenetic mechanisms in training, priming and tolerance of monocytes and hematopoietic progenitors. *Immunological Reviews*, *323*(1), 257–275. https://doi.org/10.1111/imr.13330

Mohammadnezhad, L., Shekarkar Azgomi, M., La Manna, M. P., Sireci, G., Rizzo, C., Badami, G. D., Tamburini, B., Dieli, F., Guggino, G., & Caccamo, N. (2022). Metabolic Reprogramming of Innate Immune Cells as a Possible Source of New Therapeutic Approaches in Autoimmunity. *Cells*, *11*(10), 1663. https://doi.org/10.3390/cells11101663

Monguió-Tortajada, M., Franquesa, M., Sarrias, M.-R., & Borràs, F. E. (2018). Low doses of LPS exacerbate the inflammatory response and trigger death on TLR3-primed human monocytes. *Cell Death & Disease*, *9*(5), 499. https://doi.org/10.1038/s41419-018-0520-2

Monneret, G., Finck, M.-E., Venet, F., Debard, A.-L., Bohé, J., Bienvenu, J., & Lepape, A. (2004). The anti-inflammatory response dominates after septic shock: Association of low monocyte HLA-DR expression and high interleukin-10 concentration. *Immunology Letters*, *95*(2), 193–198. https://doi.org/10.1016/j.imlet.2004.07.009

Monneret, G., Lepape, A., Voirin, N., Bohé, J., Venet, F., Debard, A.-L., Thizy, H., Bienvenu, J., Gueyffier, F., & Vanhems, P. (2006). Persisting low monocyte

human leukocyte antigen-DR expression predicts mortality in septic shock. *Intensive Care Medicine*, *32*(8), 1175–1183. https://doi.org/10.1007/s00134-006-0204-8

Monroe, K. M., McWhirter, S. M., & Vance, R. E. (2010). Induction of Type I Interferons by Bacteria. *Cellular Microbiology*, *12*(7), 881–890. https://doi.org/10.1111/j.1462-5822.2010.01478.x

Moorman, H. R., Reategui, Y., Poschel, D. B., & Liu, K. (2022). IRF8: Mechanism of Action and Health Implications. *Cells*, *11*(17), 2630. https://doi.org/10.3390/cells11172630

Mootha, V. K., Lindgren, C. M., Eriksson, K.-F., Subramanian, A., Sihag, S., Lehar, J., Puigserver, P., Carlsson, E., Ridderstråle, M., Laurila, E., Houstis, N., Daly, M. J., Patterson, N., Mesirov, J. P., Golub, T. R., Tamayo, P., Spiegelman, B., Lander, E. S., Hirschhorn, J. N., … Groop, L. C. (2003). PGC-1alpha-responsive genes involved in oxidative phosphorylation are coordinately downregulated in human diabetes. *Nature Genetics*, *34*(3), 267–273. https://doi.org/10.1038/ng1180

Morgan, M., & Ramos, M. (2025). *BiocManager: Access the Bioconductor Project Package Repository* (Version 1.30.26) [Computer software]. https://cran.r-project.org/web/packages/BiocManager/index.html

Mostavi, M., Chiu, Y.-C., Huang, Y., & Chen, Y. (2020). Convolutional neural network models for cancer type prediction based on gene expression. *BMC Medical Genomics*, *13*(Suppl 5), 44. https://doi.org/10.1186/s12920-020-0677-2

Murali, T., Pacifico, S., & Finley, R. L. (2014). Integrating the interactome and the transcriptome of Drosophila. *BMC Bioinformatics*, *15*, 177. https://doi.org/10.1186/1471-2105-15-177

Musher, D. M., & Thorner, A. R. (2014). Community-Acquired Pneumonia. *New England Journal of Medicine*, *371*(17), 1619–1628. https://doi.org/10.1056/NEJMra1312885

Nakatsuji, T., Cheng, J. Y., & Gallo, R. L. (2021). Mechanisms for control of skin immune function by the microbiome. *Current Opinion in Immunology*, *72*, 324–330. https://doi.org/10.1016/j.coi.2021.09.001

Nam, D., & Kim, S.-Y. (2008). Gene-set approach for expression pattern analysis. *Briefings in Bioinformatics*, *9*(3), 189–197. https://doi.org/10.1093/bib/bbn001

Napolitani, G., Rinaldi, A., Bertoni, F., Sallusto, F., & Lanzavecchia, A. (2005). Selected Toll-like receptor agonist combinations synergistically trigger a T helper type 1-polarizing program in dendritic cells. *Nature Immunology*, *6*(8), 769–776. https://doi.org/10.1038/ni1223

Nasution, S. A., Dwimartutie, N., Singh, G., R., C. M., Manikam, N. R. M., Kurniawan, J., & Harimurti, K. (2024). Predictors of Hair Zinc Deficiency and Its Association with The Severity of Community-Acquired Pneumonia in Dr. Cipto Mangunkusumo National General Hospital. *Indonesian Journal of CHEST : Critical and Emergency Medicine*, *11*(1), 10–20.

Nathan, C., & Cunningham-Bussel, A. (2013). Beyond oxidative stress: An immunologist's guide to reactive oxygen species. *Nature Reviews. Immunology*, *13*(5), 349–361. https://doi.org/10.1038/nri3423

Negishi, H., Taniguchi, T., & Yanai, H. (2018). The Interferon (IFN) Class of Cytokines and the IFN Regulatory Factor (IRF) Transcription Factor Family. *Cold Spring Harbor Perspectives in Biology*, *10*(11), a028423. https://doi.org/10.1101/cshperspect.a028423

Netea, M. G., Joosten, L. A. B., Latz, E., Mills, K. H. G., Natoli, G., Stunnenberg, H. G., O'Neill, L. A. J., & Xavier, R. J. (2016). Trained immunity: A program of innate immune memory in health and disease. *Science (New York, N.Y.)*, *352*(6284), aaf1098. https://doi.org/10.1126/science.aaf1098

Netea, M. G., Quintin, J., & van der Meer, J. W. M. (2011). Trained immunity: A memory for innate host defense. *Cell Host & Microbe*, *9*(5), 355–361. https://doi.org/10.1016/j.chom.2011.04.006

Ngkelo, A., Meja, K., Yeadon, M., Adcock, I., & Kirkham, P. A. (2012). LPS induced inflammatory responses in human peripheral blood mononuclear cells is mediated through NOX4 and Giα dependent PI-3kinase signalling. *Journal of Inflammation (London, England)*, *9*(1), 1. https://doi.org/10.1186/1476-9255-9-1

Niederman, M. S., & Torres, A. (2022). Severe community-acquired pneumonia. *European Respiratory Review: An Official Journal of the European Respiratory Society*, *31*(166), 220123. https://doi.org/10.1183/16000617.0123-2022

Notarangelo, L. D., Kim, M.-S., Walter, J. E., & Lee, Y. N. (2016). Human RAG mutations: Biochemistry and clinical implications. *Nature Reviews. Immunology*, *16*(4), 234–246. https://doi.org/10.1038/nri.2016.28

Novakovic, B., Habibi, E., Wang, S.-Y., Arts, R. J. W., Davar, R., Megchelenbrink, W., Kim, B., Kuznetsova, T., Kox, M., Zwaag, J., Matarese, F., van Heeringen, S. J., Janssen-Megens, E. M., Sharifi, N., Wang, C., Keramati, F., Schoonenberg, V., Flicek, P., Clarke, L., … Stunnenberg, H. G. (2016). β-Glucan Reverses the Epigenetic State of LPS-Induced Immunological Tolerance. *Cell*, *167*(5), 1354-1368.e14. https://doi.org/10.1016/j.cell.2016.09.034

Núñez, V., Alameda, D., Rico, D., Mota, R., Gonzalo, P., Cedenilla, M., Fischer, T., Boscá, L., Glass, C. K., Arroyo, A. G., & Ricote, M. (2010). Retinoid X receptor alpha controls innate inflammatory responses through the up-regulation of chemokine expression. *Proceedings of the National Academy of Sciences of the United States of America*, *107*(23), 10626–10631. https://doi.org/10.1073/pnas.0913545107

O'Neill, L. A. J., Kishton, R. J., & Rathmell, J. (2016). A guide to immunometabolism for immunologists. *Nature Reviews. Immunology*, *16*(9), 553–565. https://doi.org/10.1038/nri.2016.70

Orchard, S., Ammari, M., Aranda, B., Breuza, L., Briganti, L., Broackes-Carter, F., Campbell, N. H., Chavali, G., Chen, C., del-Toro, N., Duesbury, M., Dumousseau, M., Galeota, E., Hinz, U., Iannuccelli, M., Jagannathan, S., Jimenez, R., Khadake, J., Lagreid, A., … Hermjakob, H. (2014). The MIntAct project—IntAct as a common curation platform for 11 molecular interaction

databases. *Nucleic Acids Research*, *42*(Database issue), D358-363. https://doi.org/10.1093/nar/gkt1115

Oshlack, A., Robinson, M. D., & Young, M. D. (2010). From RNA-seq reads to differential expression results. *Genome Biology*, *11*(12), 220. https://doi.org/10.1186/gb-2010-11-12-220

Otto, N. A., Butler, J. M., Schuurman, A. R., Brands, X., Haak, B. W., Klarenbeek, A. M., Van Weeghel, M., Houtkooper, R. H., Jakobs, M. E., Faber, D. R., De Vos, A. F., Wiersinga, W. J., Scicluna, B. P., & Van Der Poll, T. (2022). Intracellular pyruvate levels positively correlate with cytokine production capacity in tolerant monocytes from patients with pneumonia. *Biochimica et Biophysica Acta (BBA) - Molecular Basis of Disease*, *1868*(11), 166519. https://doi.org/10.1016/j.bbadis.2022.166519

Oughtred, R., Rust, J., Chang, C., Breitkreutz, B.-J., Stark, C., Willems, A., Boucher, L., Leung, G., Kolas, N., Zhang, F., Dolma, S., Coulombe-Huntington, J., Chatr-Aryamontri, A., Dolinski, K., & Tyers, M. (2021). The BioGRID database: A comprehensive biomedical resource of curated protein, genetic, and chemical interactions. *Protein Science: A Publication of the Protein Society*, *30*(1), 187–200. https://doi.org/10.1002/pro.3978

Ozawa, Y., Saito, R., Fujimori, S., Kashima, H., Ishizaka, M., Yanagawa, H., Miyamoto-Sato, E., & Tomita, M. (2010). Protein complex prediction via verifying and reconstructing the topology of domain-domain interactions. *BMC Bioinformatics*, *11*, 350. https://doi.org/10.1186/1471-2105-11-350

Pagès, M. C. H. (2017). *AnnotationDbi* [Computer software]. Bioconductor. https://doi.org/10.18129/B9.BIOC.ANNOTATIONDBI

Palma Medina, L. M., Babačić, H., Dzidic, M., Parke, Å., Garcia, M., Maleki, K. T., Unge, C., Lourda, M., Kvedaraite, E., Chen, P., Muvva, J. R., Cornillet, M., Emgård, J., Moll, K., Karolinska K. I./K. COVID-19 Study Group, Michaëlsson, J., Flodström-Tullberg, M., Brighenti, S., Buggert, M., … Norrby-Teglund, A. (2023). Targeted plasma proteomics reveals signatures discriminating COVID-19 from sepsis with pneumonia. *Respiratory Research*, *24*(1), 62. https://doi.org/10.1186/s12931-023-02364-y

Palmore, T. N., Stock, F., White, M., Bordner, M., Michelin, A., Bennett, J. E., Murray, P. R., & Henderson, D. K. (2009). A cluster of nosocomial Legionnaire's disease linked to a contaminated hospital decorative water fountain. *Infection Control and Hospital Epidemiology : The Official Journal of the Society of Hospital Epidemiologists of America*, *30*(8), 764–768. https://doi.org/10.1086/598855

Pan, Q., Shai, O., Lee, L. J., Frey, B. J., & Blencowe, B. J. (2008). Deep surveying of alternative splicing complexity in the human transcriptome by high-throughput sequencing. *Nature Genetics*, *40*(12), 1413–1415. https://doi.org/10.1038/ng.259

Pang, J., & Koh, T. J. (2023). Proliferation of monocytes and macrophages in homeostasis, infection, injury, and disease. *Journal of Leukocyte Biology*, *114*(6), 532–546. https://doi.org/10.1093/jleuko/qiad093

Parameswaran, N., & Patial, S. (2010). Tumor necrosis factor-α signaling in macrophages. *Critical Reviews in Eukaryotic Gene Expression*, *20*(2), 87–103. https://doi.org/10.1615/critreveukargeneexpr.v20.i2.10

Park, J. E., Park, J. S., Jang, S. Y., Park, S. H., Kim, J.-W., Ki, C.-S., & Kim, D.-K. (2019a). A novel SMAD6 variant in a patient with severely calcified bicuspid aortic valve and thoracic aortic aneurysm. *Molecular Genetics & Genomic Medicine*, *7*(5), e620. https://doi.org/10.1002/mgg3.620

Park, J. E., Park, J. S., Jang, S. Y., Park, S. H., Kim, J.-W., Ki, C.-S., & Kim, D.-K. (2019b). A novel SMAD6 variant in a patient with severely calcified bicuspid aortic valve and thoracic aortic aneurysm. *Molecular Genetics & Genomic Medicine*, *7*(5), e620. https://doi.org/10.1002/mgg3.620

Passlick, B., Flieger, D., & Ziegler-Heitbrock, H. W. (1989). Identification and characterization of a novel monocyte subpopulation in human peripheral blood. *Blood*, *74*(7), 2527–2534.

Pastille, E., Didovic, S., Brauckmann, D., Rani, M., Agrawal, H., Schade, F. U., Zhang, Y., & Flohé, S. B. (2011). Modulation of dendritic cell differentiation in the bone marrow mediates sustained immunosuppression after polymicrobial sepsis. *Journal of Immunology (Baltimore, Md.: 1950)*, *186*(2), 977–986. https://doi.org/10.4049/jimmunol.1001147

Patro, R., Duggal, G., Love, M. I., Irizarry, R. A., & Kingsford, C. (2017). Salmon provides fast and bias-aware quantification of transcript expression. *Nature Methods*, *14*(4), 417–419. https://doi.org/10.1038/nmeth.4197

Pearce, E. L., & Pearce, E. J. (2013). Metabolic pathways in immune cell activation and quiescence. *Immunity*, *38*(4), 633–643. https://doi.org/10.1016/j.immuni.2013.04.005

Pedersen, B. S., & Quinlan, A. R. (2018). Mosdepth: Quick coverage calculation for genomes and exomes. *Bioinformatics (Oxford, England)*, *34*(5), 867–868. https://doi.org/10.1093/bioinformatics/btx699

Pena, O. M., Hancock, D. G., Lyle, N. H., Linder, A., Russell, J. A., Xia, J., Fjell, C. D., Boyd, J. H., & Hancock, R. E. W. (2014). An Endotoxin Tolerance Signature Predicts Sepsis and Organ Dysfunction at Initial Clinical Presentation. *EBioMedicine*, *1*(1), 64–71. https://doi.org/10.1016/j.ebiom.2014.10.003

Pestka, S., Krause, C. D., & Walter, M. R. (2004). Interferons, interferon-like cytokines, and their receptors. *Immunological Reviews*, *202*, 8–32. https://doi.org/10.1111/j.0105-2896.2004.00204.x

Pickart, C. M., & Eddins, M. J. (2004). Ubiquitin: Structures, functions, mechanisms. *Biochimica Et Biophysica Acta*, *1695*(1–3), 55–72. https://doi.org/10.1016/j.bbamcr.2004.09.019

Pinilla-Vera, M., Xiong, Z., Zhao, Y., Zhao, J., Donahoe, M. P., Barge, S., Horne, W. T., Kolls, J. K., McVerry, B. J., Birukova, A., Tighe, R. M., Foster, W. M., Hollingsworth, J., Ray, A., Mallampalli, R., Ray, P., & Lee, J. S. (2016). Full Spectrum of LPS Activation in Alveolar Macrophages of Healthy Volunteers by Whole Transcriptomic Profiling. *PLOS ONE*, *11*(7), e0159329. https://doi.org/10.1371/journal.pone.0159329

Piper, M. M., Radhika Khetani, Mary. (2017, May 12). *Gene-level differential expression analysis with DESeq2*. Introduction to DGE - ARCHIVED. https://hbctraining.github.io/DGE_workshop/lessons/04_DGE_DESeq2_analysis.html

Póvoa, P., Coelho, L., Cidade, J. P., Ceccato, A., Morris, A. C., Salluh, J., Nobre, V., Nseir, S., Martin-Loeches, I., Lisboa, T., Ramirez, P., Rouzé, A., Sweeney, D. A., & Kalil, A. C. (2024). Biomarkers in pulmonary infections: A clinical approach. *Annals of Intensive Care*, *14*(1), 113. https://doi.org/10.1186/s13613-024-01323-0

Pratama, R., Hwang, J. J., Lee, J. H., Song, G., & Park, H. R. (2021). Authentication of differential gene expression in oral squamous cell carcinoma using machine learning applications. *BMC Oral Health*, *21*(1), 281. https://doi.org/10.1186/s12903-021-01642-9

Prina, E., Ranzani, O. T., & Torres, A. (2015). Community-acquired pneumonia. *Lancet (London, England)*, *386*(9998), 1097–1108. https://doi.org/10.1016/S0140-6736(15)60733-4

Prinyakupt, J., & Pluempitiwiriyawej, C. (2015). Segmentation of white blood cells and comparison of cell morphology by linear and naïve Bayes classifiers. *Biomedical Engineering Online*, *14*, 63. https://doi.org/10.1186/s12938-015-0037-1

Prinz, M., & Priller, J. (2014). Microglia and brain macrophages in the molecular age: From origin to neuropsychiatric disease. *Nature Reviews. Neuroscience*, *15*(5), 300–312. https://doi.org/10.1038/nrn3722

Qi, F., Zhang, W., Huang, J., Fu, L., & Zhao, J. (2021). Single-Cell RNA Sequencing Analysis of the Immunometabolic Rewiring and Immunopathogenesis of Coronavirus Disease 2019. *Frontiers in Immunology*, *12*, 651656. https://doi.org/10.3389/fimmu.2021.651656

Quin, C., DeJong, E. N., Cook, E. K., Luo, Y. Z., Vlasschaert, C., Sadh, S., McNaughton, A. J., Buttigieg, M. M., Breznik, J. A., Kennedy, A. E., Zhao, K., Mewburn, J., Dunham-Snary, K. J., Hindmarch, C. C., Bick, A. G., Archer, S. L., Rauh, M. J., & Bowdish, D. M. (2024). Neutrophil-mediated innate immune resistance to bacterial pneumonia is dependent on Tet2 function. *The Journal of Clinical Investigation*, *134*(11), e171002. https://doi.org/10.1172/JCI171002

Quinlan, A. R. (2014). BEDTools: The Swiss-Army Tool for Genome Feature Analysis. *Current Protocols in Bioinformatics*, *47*, 11.12.1-34. https://doi.org/10.1002/0471250953.bi1112s47

Quinlan, A. R., & Hall, I. M. (2010). BEDTools: A flexible suite of utilities for comparing genomic features. *Bioinformatics (Oxford, England)*, *26*(6), 841–842. https://doi.org/10.1093/bioinformatics/btq033

Quinton, L. J., & Mizgerd, J. P. (2015). Dynamics of lung defense in pneumonia: Resistance, resilience, and remodeling. *Annual Review of Physiology*, *77*, 407–430. https://doi.org/10.1146/annurev-physiol-021014-071937

Qureshi, N., Desousa, J., Siddiqui, A. Z., Drees, B. M., Morrison, D. C., & Qureshi, A. A. (2023). Dysregulation of Gene Expression of Key Signaling Mediators in

PBMCs from People with Type 2 Diabetes Mellitus. *International Journal of Molecular Sciences*, *24*(3), 2732. https://doi.org/10.3390/ijms24032732

R Core Team. (2023). *R: A language and environment for statistical computing* [Computer software]. R Foundation for Statistical Computing. https://www.R-project.org/

Ramirez, J. (2017). Burden of Community-Acquired Pneumonia due to PCV-13 Streptococcus pneumoniae Serotypes Among Hospitalized Adults in the United States. *Open Forum Infectious Diseases*, *4*(suppl_1), S573–S573. https://doi.org/10.1093/ofid/ofx163.1499

Ramirez-Carrozzi, V. R., Braas, D., Bhatt, D. M., Cheng, C. S., Hong, C., Doty, K. R., Black, J. C., Hoffmann, A., Carey, M., & Smale, S. T. (2009). A unifying model for the selective regulation of inducible transcription by CpG islands and nucleosome remodeling. *Cell*, *138*(1), 114–128. https://doi.org/10.1016/j.cell.2009.04.020

Ranzani, V., Rossetti, G., Panzeri, I., Arrigoni, A., Bonnal, R. J., Curti, S., Gruarin, P., Provasi, E., Sugliano, E., Marconi, M., De Francesco, R., Geginat, J., Bodega, B., Abrignani, S., & Pagani, M. (2015). The long intergenic noncoding RNA landscape of human lymphocytes highlights the regulation of T cell differentiation by linc-MAF-4. *Nature Immunology*, *16*(3), 318–325. https://doi.org/10.1038/ni.3093

Rapaport, F., Khanin, R., Liang, Y., Pirun, M., Krek, A., Zumbo, P., Mason, C. E., Socci, N. D., & Betel, D. (2013). Comprehensive evaluation of differential gene

expression analysis methods for RNA-seq data. *Genome Biology*, *14*(9), R95. https://doi.org/10.1186/gb-2013-14-9-r95

Rashid, A., Al-Obeidat, F., Kanthimathinathan, H. K., Benakatti, G., Hafez, W., Ramaiah, R., Brierley, J., Hanisch, B., Khilnani, P., Koutentis, C., Brusletto, B. S., Toufiq, M., Hussain, Z., Vyas, H., Malik, Z. A., Schumacher, M., Malik, R. A., Deshpande, S., Quraishi, N., … Hussain, A. (2024). Advancing sepsis clinical research: Harnessing transcriptomics for an omics-based strategy - a comprehensive scoping review. *Informatics in Medicine Unlocked*, *44*, 101419. https://doi.org/10.1016/j.imu.2023.101419

Rayees, S., Rochford, I., Joshi, J. C., Joshi, B., Banerjee, S., & Mehta, D. (2020). Macrophage TLR4 and PAR2 Signaling: Role in Regulating Vascular Inflammatory Injury and Repair. *Frontiers in Immunology*, *11*, 2091. https://doi.org/10.3389/fimmu.2020.02091

Regunath, H., & Oba, Y. (2025). Community-Acquired Pneumonia. In *StatPearls*. StatPearls Publishing. http://www.ncbi.nlm.nih.gov/books/NBK430749/

Reijnders, T. D. Y., Schuurman, A. R., Verhoeff, J., Van Den Braber, M., Douma, R. A., Faber, D. R., Paul, A. G. A., Wiersinga, W. J., Saris, A., Garcia Vallejo, J. J., & Van Der Poll, T. (2023). High-dimensional phenotyping of the peripheral immune response in community-acquired pneumonia. *Frontiers in Immunology*, *14*, 1260283. https://doi.org/10.3389/fimmu.2023.1260283

Reimand, J., Isserlin, R., Voisin, V., Kucera, M., Tannus-Lopes, C., Rostamianfar, A., Wadi, L., Meyer, M., Wong, J., Xu, C., Merico, D., & Bader, G. D. (2019). Pathway enrichment analysis and visualization of omics data using g:Profiler,

GSEA, Cytoscape and EnrichmentMap. *Nature Protocols*, *14*(2), 482–517. https://doi.org/10.1038/s41596-018-0103-9

Ripamonti, C., Spadotto, V., Pozzi, P., Stevenazzi, A., Vergani, B., Marchini, M., Sandrone, G., Bonetti, E., Mazzarella, L., Minucci, S., Steinkühler, C., & Fossati, G. (2022). HDAC Inhibition as Potential Therapeutic Strategy to Restore the Deregulated Immune Response in Severe COVID-19. *Frontiers in Immunology*, *13*, 841716. https://doi.org/10.3389/fimmu.2022.841716

Ritchie, A. I., & Singanayagam, A. (2020). Immunosuppression for hyperinflammation in COVID-19: A double-edged sword? *The Lancet*, *395*(10230), 1111. https://doi.org/10.1016/S0140-6736(20)30691-7

Robinson, M. D., & Smyth, G. K. (2007). Moderated statistical tests for assessing differences in tag abundance. *Bioinformatics (Oxford, England)*, *23*(21), 2881–2887. https://doi.org/10.1093/bioinformatics/btm453

Rock, K. L., York, I. A., Saric, T., & Goldberg, A. L. (2002). Protein degradation and the generation of MHC class I-presented peptides. *Advances in Immunology*, *80*, 1–70. https://doi.org/10.1016/s0065-2776(02)80012-8

Rosati, D., Palmieri, M., Brunelli, G., Morrione, A., Iannelli, F., Frullanti, E., & Giordano, A. (2024). Differential gene expression analysis pipelines and bioinformatic tools for the identification of specific biomarkers: A review. *Computational and Structural Biotechnology Journal*, *23*, 1154–1168. https://doi.org/10.1016/j.csbj.2024.02.018

RStudio Team. (2020). *RStudio: Integrated development environment for R* (Version 2020) [Computer software]. RStudio, PBC. https://www.rstudio.com/

Rudd, K. E., Johnson, S. C., Agesa, K. M., Shackelford, K. A., Tsoi, D., Kievlan, D. R., Colombara, D. V., Ikuta, K. S., Kissoon, N., Finfer, S., Fleischmann-Struzek, C., Machado, F. R., Reinhart, K. K., Rowan, K., Seymour, C. W., Watson, R. S., West, T. E., Marinho, F., Hay, S. I., … Naghavi, M. (2020). Global, regional, and national sepsis incidence and mortality, 1990-2017: Analysis for the Global Burden of Disease Study. *Lancet (London, England)*, *395*(10219), 200–211. https://doi.org/10.1016/S0140-6736(19)32989-7

Rudnik, M., Hukara, A., Kocherova, I., Jordan, S., Schniering, J., Milleret, V., Ehrbar, M., Klingel, K., Feghali-Bostwick, C., Distler, O., Błyszczuk, P., & Kania, G. (2021). Elevated Fibronectin Levels in Profibrotic CD14+ Monocytes and CD14+ Macrophages in Systemic Sclerosis. *Frontiers in Immunology*, *12*, 642891. https://doi.org/10.3389/fimmu.2021.642891

Saeed, S., Quintin, J., Kerstens, H. H. D., Rao, N. A., Aghajanirefah, A., Matarese, F., Cheng, S.-C., Ratter, J., Berentsen, K., van der Ent, M. A., Sharifi, N., Janssen-Megens, E. M., Ter Huurne, M., Mandoli, A., van Schaik, T., Ng, A., Burden, F., Downes, K., Frontini, M., … Stunnenberg, H. G. (2014). Epigenetic programming of monocyte-to-macrophage differentiation and trained innate immunity. *Science (New York, N.Y.)*, *345*(6204), 1251086. https://doi.org/10.1126/science.1251086

Sales, G., Calura, E., Cavalieri, D., & Romualdi, C. (2012). graphite—A Bioconductor package to convert pathway topology to gene network. *BMC Bioinformatics*, *13*, 20. https://doi.org/10.1186/1471-2105-13-20

Salminen, A., Kaarniranta, K., & Kauppinen, A. (2021). Insulin/IGF-1 signaling promotes immunosuppression via the STAT3 pathway: Impact on the aging process and age-related diseases. *Inflammation Research: Official Journal of the European Histamine Research Society ... [et Al.]*, *70*(10–12), 1043–1061. https://doi.org/10.1007/s00011-021-01498-3

Salwinski, L., Miller, C. S., Smith, A. J., Pettit, F. K., Bowie, J. U., & Eisenberg, D. (2004). The Database of Interacting Proteins: 2004 update. *Nucleic Acids Research*, *32*(Database issue), D449-451. https://doi.org/10.1093/nar/gkh086

Sancak, Y., Peterson, T. R., Shaul, Y. D., Lindquist, R. A., Thoreen, C. C., Bar-Peled, L., & Sabatini, D. M. (2008). The Rag GTPases bind raptor and mediate amino acid signaling to mTORC1. *Science (New York, N.Y.)*, *320*(5882), 1496–1501. https://doi.org/10.1126/science.1157535

Santesmasses, D., Castro, J. P., Zenin, A. A., Shindyapina, A. V., Gerashchenko, M. V., Zhang, B., Kerepesi, C., Yim, S. H., Fedichev, P. O., & Gladyshev, V. N. (2020). COVID-19 is an emergent disease of aging. *Aging Cell*, *19*(10), e13230. https://doi.org/10.1111/acel.13230

Sarantopoulou, D., Brooks, T. G., Nayak, S., Mrčela, A., Lahens, N. F., & Grant, G. R. (2021). Comparative evaluation of full-length isoform quantification from RNA-Seq. *BMC Bioinformatics*, *22*(1), 266. https://doi.org/10.1186/s12859-021-04198-1

Savvateeva, E. N., Rubina, A. Y., & Gryadunov, D. A. (2019). Biomarkers of Community-Acquired Pneumonia: A Key to Disease Diagnosis and

Management. *BioMed Research International*, *2019*, 1701276. https://doi.org/10.1155/2019/1701276

Saxton, R. A., & Sabatini, D. M. (2017). mTOR Signaling in Growth, Metabolism, and Disease. *Cell*, *168*(6), 960–976. https://doi.org/10.1016/j.cell.2017.02.004

Schaarschmidt, S., Fischer, A., Zuther, E., & Hincha, D. K. (2020). Evaluation of Seven Different RNA-Seq Alignment Tools Based on Experimental Data from the Model Plant Arabidopsis thaliana. *International Journal of Molecular Sciences*, *21*(5), 1720. https://doi.org/10.3390/ijms21051720

Schefold, J. C., Hasper, D., Volk, H. D., & Reinke, P. (2008). Sepsis: Time has come to focus on the later stages. *Medical Hypotheses*, *71*(2), 203–208. https://doi.org/10.1016/j.mehy.2008.03.022

Schenten, D., & Medzhitov, R. (2011). The control of adaptive immune responses by the innate immune system. *Advances in Immunology*, *109*, 87–124. https://doi.org/10.1016/B978-0-12-387664-5.00003-0

Schmid, S., Mordstein, M., Kochs, G., García-Sastre, A., & Tenoever, B. R. (2010). Transcription factor redundancy ensures induction of the antiviral state. *The Journal of Biological Chemistry*, *285*(53), 42013–42022. https://doi.org/10.1074/jbc.M110.165936

Schmidlin, C. J., Dodson, M. B., Madhavan, L., & Zhang, D. D. (2019). Redox regulation by NRF2 in aging and disease. *Free Radical Biology & Medicine*, *134*, 702–707. https://doi.org/10.1016/j.freeradbiomed.2019.01.016

Schneider, C., Nobs, S. P., Kurrer, M., Rehrauer, H., Thiele, C., & Kopf, M. (2014). Induction of the nuclear receptor PPAR-γ by the cytokine GM-CSF is critical

for the differentiation of fetal monocytes into alveolar macrophages. *Nature Immunology*, *15*(11), 1026–1037. https://doi.org/10.1038/ni.3005

Schreiber, R. D., Old, L. J., & Smyth, M. J. (2011). Cancer immunoediting: Integrating immunity's roles in cancer suppression and promotion. *Science (New York, N.Y.)*, *331*(6024), 1565–1570. https://doi.org/10.1126/science.1203486

Schulte-Schrepping, J., Reusch, N., Paclik, D., Baßler, K., Schlickeiser, S., Zhang, B., Krämer, B., Krammer, T., Brumhard, S., Bonaguro, L., De Domenico, E., Wendisch, D., Grasshoff, M., Kapellos, T. S., Beckstette, M., Pecht, T., Saglam, A., Dietrich, O., Mei, H. E., … Ziebuhr, J. (2020). Severe COVID-19 Is Marked by a Dysregulated Myeloid Cell Compartment. *Cell*, *182*(6), 1419-1440.e23. https://doi.org/10.1016/j.cell.2020.08.001

Schultze, J. L., Schmieder, A., & Goerdt, S. (2015). Macrophage activation in human diseases. *Seminars in Immunology*, *27*(4), 249–256. https://doi.org/10.1016/j.smim.2015.07.003

Schurz, H., Salie, M., Tromp, G., Hoal, E. G., Kinnear, C. J., & Möller, M. (2019). The X chromosome and sex-specific effects in infectious disease susceptibility. *Human Genomics*, *13*(1), 2. https://doi.org/10.1186/s40246-018-0185-z

Schuurman, A. R., Reijnders, T. D., Saris, A., Ramirez Moral, I., Schinkel, M., De Brabander, J., Van Linge, C., Vermeulen, L., Scicluna, B. P., Wiersinga, W. J., Vieira Braga, F. A., & Van Der Poll, T. (2021). Integrated single-cell analysis unveils diverging immune features of COVID-19, influenza, and other

community-acquired pneumonia. *eLife*, *10*, e69661. https://doi.org/10.7554/eLife.69661

Scully, E. P., Haverfield, J., Ursin, R. L., Tannenbaum, C., & Klein, S. L. (2020). Considering how biological sex impacts immune responses and COVID-19 outcomes. *Nature Reviews. Immunology*, *20*(7), 442–447. https://doi.org/10.1038/s41577-020-0348-8

Seibl, R., Birchler, T., Loeliger, S., Hossle, J. P., Gay, R. E., Saurenmann, T., Michel, B. A., Seger, R. A., Gay, S., & Lauener, R. P. (2003). Expression and regulation of Toll-like receptor 2 in rheumatoid arthritis synovium. *The American Journal of Pathology*, *162*(4), 1221–1227. https://doi.org/10.1016/S0002-9440(10)63918-1

Severino, P., Silva, E., Baggio-Zappia, G. L., Brunialti, M. K. C., Nucci, L. A., Rigato Jr., O., Da Silva, I. D. C. G., Machado, F. R., & Salomao, R. (2014). Patterns of Gene Expression in Peripheral Blood Mononuclear Cells and Outcomes from Patients with Sepsis Secondary to Community Acquired Pneumonia. *PLoS ONE*, *9*(3), e91886. https://doi.org/10.1371/journal.pone.0091886

Shalek, A. K., Satija, R., Shuga, J., Trombetta, J. J., Gennert, D., Lu, D., Chen, P., Gertner, R. S., Gaublomme, J. T., Yosef, N., Schwartz, S., Fowler, B., Weaver, S., Wang, J., Wang, X., Ding, R., Raychowdhury, R., Friedman, N., Hacohen, N., … Regev, A. (2014). Single-cell RNA-seq reveals dynamic paracrine control of cellular variation. *Nature*, *510*(7505), 363–369. https://doi.org/10.1038/nature13437

Shalgi, R., Hurt, J. A., Lindquist, S., & Burge, C. B. (2014). Widespread inhibition of posttranscriptional splicing shapes the cellular transcriptome following heat shock. *Cell Reports*, *7*(5), 1362–1370. https://doi.org/10.1016/j.celrep.2014.04.044

Shalova, I. N., Lim, J. Y., Chittezhath, M., Zinkernagel, A. S., Beasley, F., Hernández-Jiménez, E., Toledano, V., Cubillos-Zapata, C., Rapisarda, A., Chen, J., Duan, K., Yang, H., Poidinger, M., Melillo, G., Nizet, V., Arnalich, F., López-Collazo, E., & Biswas, S. K. (2015). Human monocytes undergo functional re-programming during sepsis mediated by hypoxia-inducible factor-1α. *Immunity*, *42*(3), 484–498. https://doi.org/10.1016/j.immuni.2015.02.001

Shaw, A. C., Joshi, S., Greenwood, H., Panda, A., & Lord, J. M. (2010). Aging of the innate immune system. *Current Opinion in Immunology*, *22*(4), 507–513. https://doi.org/10.1016/j.coi.2010.05.003

Shi, C., & Pamer, E. G. (2011). Monocyte recruitment during infection and inflammation. *Nature Reviews Immunology*, *11*(11), 762–774.

Sica, A., & Mantovani, A. (2012). Macrophage plasticity and polarization: In vivo veritas. *The Journal of Clinical Investigation*, *122*(3), 787–795. https://doi.org/10.1172/JCI59643

Siewe, B., Nipper, A. J., Sohn, H., Stapleton, J. T., & Landay, A. (2017). FcRL4 Expression Identifies a Pro-inflammatory B Cell Subset in Viremic HIV-Infected Subjects. *Frontiers in Immunology*, *8*. https://doi.org/10.3389/fimmu.2017.01339

Simonetti, A. F., Garcia-Vidal, C., Viasus, D., García-Somoza, D., Dorca, J., Gudiol, F., & Carratalà, J. (2016). Declining mortality among hospitalized patients with community-acquired pneumonia. *Clinical Microbiology and Infection: The Official Publication of the European Society of Clinical Microbiology and Infectious Diseases*, *22*(6), 567.e1-7. https://doi.org/10.1016/j.cmi.2016.03.015

Sims, D., Sudbery, I., Ilott, N. E., Heger, A., & Ponting, C. P. (2014). Sequencing depth and coverage: Key considerations in genomic analyses. *Nature Reviews. Genetics*, *15*(2), 121–132. https://doi.org/10.1038/nrg3642

Singer, M., Deutschman, C. S., Seymour, C. W., Shankar-Hari, M., Annane, D., Bauer, M., Bellomo, R., Bernard, G. R., Chiche, J.-D., Coopersmith, C. M., Hotchkiss, R. S., Levy, M. M., Marshall, J. C., Martin, G. S., Opal, S. M., Rubenfeld, G. D., van der Poll, T., Vincent, J.-L., & Angus, D. C. (2016). The Third International Consensus Definitions for Sepsis and Septic Shock (Sepsis-3). *JAMA*, *315*(8), 801–810. https://doi.org/10.1001/jama.2016.0287

Singh, A. J., Ramsey, S. A., Filtz, T. M., & Kioussi, C. (2018). Differential gene regulatory networks in development and disease. *Cellular and Molecular Life Sciences: CMLS*, *75*(6), 1013–1025. https://doi.org/10.1007/s00018-017-2679-6

Skevaki, C., Moschopoulos, C. D., Fragkou, P. C., Grote, K., Schieffer, E., & Schieffer, B. (2025). Long COVID: Pathophysiology, current concepts, and future directions. *Journal of Allergy and Clinical Immunology*, *155*(4), 1059–1070. https://doi.org/10.1016/j.jaci.2024.12.1074

Skrzeczyńska-Moncznik, J., Bzowska, M., Loseke, S., Grage-Griebenow, E., Zembala, M., & Pryjma, J. (2008). Peripheral blood CD14high CD16+ monocytes are main producers of IL-10. *Scandinavian Journal of Immunology*, *67*(2), 152–159. https://doi.org/10.1111/j.1365-3083.2007.02051.x

Slowikowski, K. (2016). *ggrepel: Automatically Position Non-Overlapping Text Labels with "ggplot2"* (p. 0.9.6) [Dataset]. https://doi.org/10.32614/CRAN.package.ggrepel

Smyth, G. K. (2004). Linear models and empirical bayes methods for assessing differential expression in microarray experiments. *Statistical Applications in Genetics and Molecular Biology*, *3*, Article3. https://doi.org/10.2202/1544-6115.1027

So, J., Tai, A. K., Lichtenstein, A. H., Wu, D., & Lamon-Fava, S. (2021). Sexual dimorphism of monocyte transcriptome in individuals with chronic low-grade inflammation. *Biology of Sex Differences*, *12*(1), 43. https://doi.org/10.1186/s13293-021-00387-y

Soneson, C., & Delorenzi, M. (2013). A comparison of methods for differential expression analysis of RNA-seq data. *BMC Bioinformatics*, *14*, 91. https://doi.org/10.1186/1471-2105-14-91

Song, R., Gao, Y., Dozmorov, I., Malladi, V., Saha, I., McDaniel, M. M., Parameswaran, S., Liang, C., Arana, C., Zhang, B., Wakeland, B., Zhou, J., Weirauch, M. T., Kottyan, L. C., Wakeland, E. K., & Pasare, C. (2021). IRF1 governs the differential interferon-stimulated gene responses in human

monocytes and macrophages by regulating chromatin accessibility. *Cell Reports*, *34*(12). https://doi.org/10.1016/j.celrep.2021.108891

Souza, C. S., Costa-Silva, G. J., Roxo, F. F., Foresti, F., & Oliveira, C. (2018). Genetic and Morphological Analyses Demonstrate That Schizolecis guntheri (Siluriformes: Loricariidae) Is Likely to Be a Species Complex. *Frontiers in Genetics*, *9*, 69. https://doi.org/10.3389/fgene.2018.00069

Spann, N. J., Garmire, L. X., McDonald, J. G., Myers, D. S., Milne, S. B., Shibata, N., Reichart, D., Fox, J. N., Shaked, I., Heudobler, D., Raetz, C. R. H., Wang, E. W., Kelly, S. L., Sullards, M. C., Murphy, R. C., Merrill, A. H., Brown, H. A., Dennis, E. A., Li, A. C., … Glass, C. K. (2012). Regulated accumulation of desmosterol integrates macrophage lipid metabolism and inflammatory responses. *Cell*, *151*(1), 138–152. https://doi.org/10.1016/j.cell.2012.06.054

Spector, D. L., & Lamond, A. I. (2011). Nuclear speckles. *Cold Spring Harbor Perspectives in Biology*, *3*(2), a000646. https://doi.org/10.1101/cshperspect.a000646

Stankovic-Valentin, N., Deltour, S., Seeler, J., Pinte, S., Vergoten, G., Guérardel, C., Dejean, A., & Leprince, D. (2007). An Acetylation/Deacetylation-SUMOylation Switch through a Phylogenetically Conserved ψKXEP Motif in the Tumor Suppressor HIC1 Regulates Transcriptional Repression Activity. *Molecular and Cellular Biology*, *27*(7), 2661–2675. https://doi.org/10.1128/MCB.01098-06

Stephens, M., Carbonetto, P., Gerard, D., Lu, M., Sun, L., Willwerscheid, J., & Xiao, N. (2016). *ashr: Methods for Adaptive Shrinkage, using Empirical Bayes* (p. 2.2-63) [Dataset]. https://doi.org/10.32614/CRAN.package.ashr

Straub, R. H. (2007). The complex role of estrogens in inflammation. *Endocrine Reviews*, *28*(5), 521–574. https://doi.org/10.1210/er.2007-0001

Subramanian, A., Tamayo, P., Mootha, V. K., Mukherjee, S., Ebert, B. L., Gillette, M. A., Paulovich, A., Pomeroy, S. L., Golub, T. R., Lander, E. S., & Mesirov, J. P. (2005). Gene set enrichment analysis: A knowledge-based approach for interpreting genome-wide expression profiles. *Proceedings of the National Academy of Sciences of the United States of America*, *102*(43), 15545–15550. https://doi.org/10.1073/pnas.0506580102

Sureshchandra, S., Marshall, N. E., Mendoza, N., Jankeel, A., Zulu, M. Z., & Messaoudi, I. (2021). Functional and genomic adaptations of blood monocytes to pregravid obesity during pregnancy. *iScience*, *24*(6), 102690. https://doi.org/10.1016/j.isci.2021.102690

Syafruddin, S. E., Mohtar, M. A., Wan Mohamad Nazarie, W. F., & Low, T. Y. (2020). Two Sides of the Same Coin: The Roles of KLF6 in Physiology and Pathophysiology. *Biomolecules*, *10*(10), 1378. https://doi.org/10.3390/biom10101378

Szaflarska, A., Baj-Krzyworzeka, M., Siedlar, M., Weglarczyk, K., Ruggiero, I., Hajto, B., & Zembala, M. (2004). Antitumor response of CD14+/CD16+ monocyte subpopulation. *Experimental Hematology*, *32*(8), 748–755. https://doi.org/10.1016/j.exphem.2004.05.027

Szklarczyk, D., Kirsch, R., Koutrouli, M., Nastou, K., Mehryary, F., Hachilif, R., Gable, A. L., Fang, T., Doncheva, N. T., Pyysalo, S., Bork, P., Jensen, L. J., & von Mering, C. (2023). The STRING database in 2023: Protein-protein association networks and functional enrichment analyses for any sequenced genome of interest. *Nucleic Acids Research*, *51*(D1), D638–D646. https://doi.org/10.1093/nar/gkac1000

Takahashi, T., Wong, P., Ellingson, M. K., Lucas, C., Klein, J., Israelow, B., Silva, J., Oh, J. E., Mao, T., Tokuyama, M., Lu, P., Venkataraman, A., Park, A., Liu, F., Meir, A., Sun, J., Wang, E. Y., Wyllie, A. L., Vogels, C. B. F., … Yale IMPACT research team. (2020). Sex differences in immune responses to SARS-CoV-2 that underlie disease outcomes. *medRxiv: The Preprint Server for Health Sciences*, 2020.06.06.20123414. https://doi.org/10.1101/2020.06.06.20123414

Takeuchi, O., & Akira, S. (2010). Pattern recognition receptors and inflammation. *Cell*, *140*(6), 805–820. https://doi.org/10.1016/j.cell.2010.01.022

Tanaka, T., Narazaki, M., & Kishimoto, T. (2014). IL-6 in inflammation, immunity, and disease. *Cold Spring Harbor Perspectives in Biology*, *6*(10), a016295. https://doi.org/10.1101/cshperspect.a016295

Taneja, V. (2018). Sex Hormones Determine Immune Response. *Frontiers in Immunology*, *9*, 1931. https://doi.org/10.3389/fimmu.2018.01931

Tang, Y.-C., Chuang, Y.-J., Chang, H.-H., Juang, S.-H., Yen, G.-C., Chang, J.-Y., & Kuo, C.-C. (2023). How to deal with frenemy NRF2: Targeting NRF2 for chemoprevention and cancer therapy. *Journal of Food and Drug Analysis*, *31*(3), 387–407. https://doi.org/10.38212/2224-6614.3463

Tannahill, G. M., Curtis, A. M., Adamik, J., Palsson-McDermott, E. M., McGettrick, A. F., Goel, G., Frezza, C., Bernard, N. J., Kelly, B., Foley, N. H., Zheng, L., Gardet, A., Tong, Z., Jany, S. S., Corr, S. C., Haneklaus, M., Caffrey, B. E., Pierce, K., Walmsley, S., … O'Neill, L. a. J. (2013). Succinate is an inflammatory signal that induces IL-1β through HIF-1α. *Nature*, *496*(7444), 238–242. https://doi.org/10.1038/nature11986

Tarazona, S., Furió-Tarí, P., Turrà, D., Pietro, A. D., Nueda, M. J., Ferrer, A., & Conesa, A. (2015). Data quality aware analysis of differential expression in RNA-seq with NOISeq R/Bioc package. *Nucleic Acids Research*, *43*(21), e140. https://doi.org/10.1093/nar/gkv711

Tarazona, S., García-Alcalde, F., Dopazo, J., Ferrer, A., & Conesa, A. (2011). Differential expression in RNA-seq: A matter of depth. *Genome Research*, *21*(12), 2213–2223. https://doi.org/10.1101/gr.124321.111

Teixeira, P. C., Dorneles, G. P., Santana Filho, P. C., da Silva, I. M., Schipper, L. L., Postiga, I. A. L., Neves, C. A. M., Rodrigues Junior, L. C., Peres, A., Souto, J. T. de, Fonseca, S. G., Eller, S., Oliveira, T. F., Rotta, L. N., Thompson, C. E., & Romão, P. R. T. (2021). Increased LPS levels coexist with systemic inflammation and result in monocyte activation in severe COVID-19 patients. *International Immunopharmacology*, *100*, 108125. https://doi.org/10.1016/j.intimp.2021.108125

Thompson, E. A., Cascino, K., Ordonez, A. A., Zhou, W., Vaghasia, A., Hamacher-Brady, A., Brady, N. R., Sun, I.-H., Wang, R., Rosenberg, A. Z., Delannoy, M., Rothman, R., Fenstermacher, K., Sauer, L., Shaw-Saliba, K., Bloch, E. M.,

Redd, A. D., Tobian, A. A. R., Horton, M., … Powell, J. D. (2021). Metabolic programs define dysfunctional immune responses in severe COVID-19 patients. *Cell Reports*, *34*(11), 108863. https://doi.org/10.1016/j.celrep.2021.108863

Tiemeijer, B. M., Heester, S., Sturtewagen, A. Y. W., Smits, A. I. P. M., & Tel, J. (2023). Single-cell analysis reveals TLR-induced macrophage heterogeneity and quorum sensing dictate population wide anti-inflammatory feedback in response to LPS. *Frontiers in Immunology*, *14*, 1135223. https://doi.org/10.3389/fimmu.2023.1135223

Tizazu, A. M., Mengist, H. M., & Demeke, G. (2022). Aging, inflammaging and immunosenescence as risk factors of severe COVID-19. *Immunity & Ageing: I & A*, *19*(1), 53. https://doi.org/10.1186/s12979-022-00309-5

Torres, A., Blasi, F., Peetermans, W. E., Viegi, G., & Welte, T. (2014). The aetiology and antibiotic management of community-acquired pneumonia in adults in Europe: A literature review. *European Journal of Clinical Microbiology & Infectious Diseases*, *33*(7), 1065–1079. https://doi.org/10.1007/s10096-014-2067-1

Tsoumani, E., Carter, J. A., Salomonsson, S., Stephens, J. M., & Bencina, G. (2023). Clinical, economic, and humanistic burden of community acquired pneumonia in Europe: A systematic literature review. *Expert Review of Vaccines*, *22*(1), 876–884. https://doi.org/10.1080/14760584.2023.2261785

Ucar, D., Márquez, E. J., Chung, C.-H., Marches, R., Rossi, R. J., Uyar, A., Wu, T.-C., George, J., Stitzel, M. L., Palucka, A. K., Kuchel, G. A., & Banchereau, J. (2017). The chromatin accessibility signature of human immune aging stems from CD8+ T cells. *The Journal of Experimental Medicine*, *214*(10), 3123–3144. https://doi.org/10.1084/jem.20170416

Ugel, S., De Sanctis, F., Mandruzzato, S., & Bronte, V. (2015). Tumor-induced myeloid deviation: When myeloid-derived suppressor cells meet tumor-associated macrophages. *The Journal of Clinical Investigation*, *125*(9), 3365–3376. https://doi.org/10.1172/JCI80006

Uhlén, M., Fagerberg, L., Hallström, B. M., Lindskog, C., Oksvold, P., Mardinoglu, A., Sivertsson, Å., Kampf, C., Sjöstedt, E., Asplund, A., Olsson, I., Edlund, K., Lundberg, E., Navani, S., Szigyarto, C. A.-K., Odeberg, J., Djureinovic, D., Takanen, J. O., Hober, S., … Pontén, F. (2015). Proteomics. Tissue-based map of the human proteome. *Science (New York, N.Y.)*, *347*(6220), 1260419. https://doi.org/10.1126/science.1260419

Urbán, P., Italiani, P., Boraschi, D., & Gioria, S. (2022). The SARS-CoV-2 Nucleoprotein Induces Innate Memory in Human Monocytes. *Frontiers in Immunology*, *13*, 963627. https://doi.org/10.3389/fimmu.2022.963627

Van De Wiel, M. A., Leday, G. G. R., Pardo, L., Rue, H., Van Der Vaart, A. W., & Van Wieringen, W. N. (2013). Bayesian analysis of RNA sequencing data by estimating multiple shrinkage priors. *Biostatistics (Oxford, England)*, *14*(1), 113–128. https://doi.org/10.1093/biostatistics/kxs031

van der Poll, T., Coyle, S. M., Moldawer, L. L., & Lowry, S. F. (1996). Changes in endotoxin-induced cytokine production by whole blood after in vivo exposure of normal humans to endotoxin. *The Journal of Infectious Diseases*, *174*(6), 1356–1360. https://doi.org/10.1093/infdis/174.6.1356

van der Poll, T., & Opal, S. M. (2008). Host-pathogen interactions in sepsis. *The Lancet. Infectious Diseases*, *8*(1), 32–43. https://doi.org/10.1016/S1473-3099(07)70265-7

van der Poll, T., van de Veerdonk, F. L., Scicluna, B. P., & Netea, M. G. (2017). The immunopathology of sepsis and potential therapeutic targets. *Nature Reviews. Immunology*, *17*(7), 407–420. https://doi.org/10.1038/nri.2017.36

van Kooten, C., & Banchereau, J. (2000). CD40-CD40 ligand. *Journal of Leukocyte Biology*, *67*(1), 2–17. https://doi.org/10.1002/jlb.67.1.2

Van Rechem, C., Boulay, G., Pinte, S., Stankovic-Valentin, N., Guérardel, C., & Leprince, D. (2010). Differential regulation of HIC1 target genes by CtBP and NuRD, via an acetylation/SUMOylation switch, in quiescent versus proliferating cells. *Molecular and Cellular Biology*, *30*(16), 4045–4059. https://doi.org/10.1128/MCB.00582-09

van ’t Veer, C., van den Pangaart, P. S., van Zoelen, M. A. D., de Kruif, M., Birjmohun, R. S., Stroes, E. S., de Vos, A. F., & van der Poll, T. (2007). Induction of IRAK-M is associated with lipopolysaccharide tolerance in a human endotoxemia model. *Journal of Immunology (Baltimore, Md.: 1950)*, *179*(10), 7110–7120. https://doi.org/10.4049/jimmunol.179.10.7110

Vanhaesebroeck, B., Stephens, L., & Hawkins, P. (2012). PI3K signalling: The path to discovery and understanding. *Nature Reviews. Molecular Cell Biology*, *13*(3), 195–203. https://doi.org/10.1038/nrm3290

Verity, R., Okell, L. C., Dorigatti, I., Winskill, P., Whittaker, C., Imai, N., Cuomo-Dannenburg, G., Thompson, H., Walker, P. G. T., Fu, H., Dighe, A., Griffin, J. T., Baguelin, M., Bhatia, S., Boonyasiri, A., Cori, A., Cucunubá, Z., FitzJohn, R., Gaythorpe, K., … Ferguson, N. M. (2020). Estimates of the severity of coronavirus disease 2019: A model-based analysis. *The Lancet. Infectious Diseases*, *20*(6), 669–677. https://doi.org/10.1016/S1473-3099(20)30243-7

Viasus, D., Nonell, L., Restrepo, C., Figueroa, F., Donado-Mazarrón, C., & Carratalà, J. (2023). A Systematic Review of Gene Expression Studies in Critically Ill Patients with Sepsis and Community-Acquired Pneumonia. *Biomedicines*, *11*(10), 2755. https://doi.org/10.3390/biomedicines11102755

Vigneron, N., & Van den Eynde, B. J. (2014). Proteasome subtypes and regulators in the processing of antigenic peptides presented by class I molecules of the major histocompatibility complex. *Biomolecules*, *4*(4), 994–1025. https://doi.org/10.3390/biom4040994

Visse, R., & Nagase, H. (2003). Matrix Metalloproteinases and Tissue Inhibitors of Metalloproteinases: Structure, Function, and Biochemistry. *Circulation Research*, *92*(8), 827–839. https://doi.org/10.1161/01.RES.0000070112.80711.3D

Vogl, T., Gharibyan, A. L., & Morozova-Roche, L. A. (2012). Pro-inflammatory S100A8 and S100A9 proteins: Self-assembly into multifunctional native and

amyloid complexes. *International Journal of Molecular Sciences*, *13*(3), 2893–2917. https://doi.org/10.3390/ijms13032893

Vogl, T., Tenbrock, K., Ludwig, S., Leukert, N., Ehrhardt, C., van Zoelen, M. A. D., Nacken, W., Foell, D., van der Poll, T., Sorg, C., & Roth, J. (2007). Mrp8 and Mrp14 are endogenous activators of Toll-like receptor 4, promoting lethal, endotoxin-induced shock. *Nature Medicine*, *13*(9), 1042–1049. https://doi.org/10.1038/nm1638

Waldmann, T. A. (2006). The biology of interleukin-2 and interleukin-15: Implications for cancer therapy and vaccine design. *Nature Reviews. Immunology*, *6*(8), 595–601. https://doi.org/10.1038/nri1901

Wang, W., Tang, J., & Wei, F. (2020). Updated understanding of the outbreak of 2019 novel coronavirus (2019-nCoV) in Wuhan, China. *Journal of Medical Virology*, *92*(4), 441–447. https://doi.org/10.1002/jmv.25689

Wang, Z., Gerstein, M., & Snyder, M. (2009). RNA-Seq: A revolutionary tool for transcriptomics. *Nature Reviews. Genetics*, *10*(1), 57–63. https://doi.org/10.1038/nrg2484

Watson, D. W., & Kim, Y. B. (1963). MODIFICATION OF HOST RESPONSES TO BACTERIAL ENDOTOXINS. I. SPECIFICITY OF PYROGENIC TOLERANCE AND THE ROLE OF HYPERSENSITIVITY IN PYROGENICITY, LETHALITY, AND SKIN REACTIVITY. *The Journal of Experimental Medicine*, *118*(3), 425–446. https://doi.org/10.1084/jem.118.3.425

Weber, C., Belge, K. U., von Hundelshausen, P., Draude, G., Steppich, B., Mack, M., Frankenberger, M., Weber, K. S., & Ziegler-Heitbrock, H. W. (2000).

Differential chemokine receptor expression and function in human monocyte subpopulations. *Journal of Leukocyte Biology*, *67*(5), 699–704. https://doi.org/10.1002/jlb.67.5.699

Weijer, S., Lauw, F. N., Branger, J., van den Blink, B., & van der Poll, T. (2002). Diminished interferon-gamma production and responsiveness after endotoxin administration to healthy humans. *The Journal of Infectious Diseases*, *186*(12), 1748–1753. https://doi.org/10.1086/345675

Wickham, H. (2016). Data Analysis. In H. Wickham, *Ggplot2* (pp. 189–201). Springer International Publishing. https://doi.org/10.1007/978-3-319-24277-4_9

Wickham, H., Averick, M., Bryan, J., Chang, W., McGowan, L., François, R., Grolemund, G., Hayes, A., Henry, L., Hester, J., Kuhn, M., Pedersen, T., Miller, E., Bache, S., Müller, K., Ooms, J., Robinson, D., Seidel, D., Spinu, V., … Yutani, H. (2019). Welcome to the Tidyverse. *Journal of Open Source Software*, *4*(43), 1686. https://doi.org/10.21105/joss.01686

Wiersinga, W. J., & van der Poll, T. (2022). Immunopathophysiology of human sepsis. *EBioMedicine*, *86*, 104363. https://doi.org/10.1016/j.ebiom.2022.104363

Wiersinga, W. J., van't Veer, C., van den Pangaart, P. S., Dondorp, A. M., Day, N. P., Peacock, S. J., & van der Poll, T. (2009). Immunosuppression associated with interleukin-1R-associated-kinase-M upregulation predicts mortality in Gram-negative sepsis (melioidosis). *Critical Care Medicine*, *37*(2), 569–576. https://doi.org/10.1097/CCM.0b013e318194b1bf

Wilkinson, N. M., Chen, H.-C., Lechner, M. G., & Su, M. A. (2022). Sex Differences in Immunity. *Annual Review of Immunology*, *40*, 75–94. https://doi.org/10.1146/annurev-immunol-101320-125133

Will, T., & Helms, V. (2016). PPIXpress: Construction of condition-specific protein interaction networks based on transcript expression. *Bioinformatics (Oxford, England)*, *32*(4), 571–578. https://doi.org/10.1093/bioinformatics/btv620

Williams, C. R., Baccarella, A., Parrish, J. Z., & Kim, C. C. (2017). Empirical assessment of analysis workflows for differential expression analysis of human samples using RNA-Seq. *BMC Bioinformatics*, *18*(1), 38. https://doi.org/10.1186/s12859-016-1457-z

Wodrich, M. D., Sawatlon, B., Busch, M., & Corminboeuf, C. (2021). The Genesis of Molecular Volcano Plots. *Accounts of Chemical Research*, *54*(5), 1107–1117. https://doi.org/10.1021/acs.accounts.0c00857

Wong, K. L., Tai, J. J.-Y., Wong, W.-C., Han, H., Sem, X., Yeap, W.-H., Kourilsky, P., & Wong, S.-C. (2011). Gene expression profiling reveals the defining features of the classical, intermediate, and nonclassical human monocyte subsets. *Blood*, *118*(5), e16-31. https://doi.org/10.1182/blood-2010-12-326355

Wong, M.-T., & Chen, S. S.-L. (2016). Emerging roles of interferon-stimulated genes in the innate immune response to hepatitis C virus infection. *Cellular & Molecular Immunology*, *13*(1), 11–35. https://doi.org/10.1038/cmi.2014.127

World Medical Association Declaration of Helsinki: Ethical principles for medical research involving human subjects—PubMed. (2013). https://pubmed.ncbi.nlm.nih.gov/24141714/

Wu, H., Wang, C., & Wu, Z. (2013). A new shrinkage estimator for dispersion improves differential expression detection in RNA-seq data. *Biostatistics (Oxford, England)*, *14*(2), 232–243. https://doi.org/10.1093/biostatistics/kxs033

Wu, Q., Yu, X., Li, J., Sun, S., & Tu, Y. (2021). Metabolic regulation in the immune response to cancer. *Cancer Communications (London, England)*, *41*(8), 661–694. https://doi.org/10.1002/cac2.12182

Wu, T., Hu, E., Xu, S., Chen, M., Guo, P., Dai, Z., Feng, T., Zhou, L., Tang, W., Zhan, L., Fu, X., Liu, S., Bo, X., & Yu, G. (2021). clusterProfiler 4.0: A universal enrichment tool for interpreting omics data. *Innovation (Cambridge (Mass.))*, *2*(3), 100141. https://doi.org/10.1016/j.xinn.2021.100141

Wu, Y., Ma, L., Zhuang, Z., Cai, S., Zhao, Z., Zhou, L., Zhang, J., Wang, P.-H., Zhao, J., & Cui, J. (2020). Main protease of SARS-CoV-2 serves as a bifunctional molecule in restricting type I interferon antiviral signaling. *Signal Transduction and Targeted Therapy*, *5*(1), 221. https://doi.org/10.1038/s41392-020-00332-2

Wu, Z., & McGoogan, J. M. (2020). Characteristics of and Important Lessons From the Coronavirus Disease 2019 (COVID-19) Outbreak in China: Summary of a Report of 72 314 Cases From the Chinese Center for Disease Control and Prevention. *JAMA*, *323*(13), 1239–1242. https://doi.org/10.1001/jama.2020.2648

Wynn, T. A., & Vannella, K. M. (2016). Macrophages in Tissue Repair, Regeneration, and Fibrosis. *Immunity*, *44*(3), 450–462. https://doi.org/10.1016/j.immuni.2016.02.015

Xia, J., Benner, M. J., & Hancock, R. E. W. (2014). NetworkAnalyst—Integrative approaches for protein-protein interaction network analysis and visual exploration. *Nucleic Acids Research*, *42*(Web Server issue), W167-174. https://doi.org/10.1093/nar/gku443

Xu, S., Hu, E., Cai, Y., Xie, Z., Luo, X., Zhan, L., Tang, W., Wang, Q., Liu, B., Wang, R., Xie, W., Wu, T., Xie, L., & Yu, G. (2024). Using clusterProfiler to characterize multiomics data. *Nature Protocols*, *19*(11), 3292–3320. https://doi.org/10.1038/s41596-024-01020-z

Xu, W., Ni, Z., Zhang, M., Chen, J., Zhang, L., Wu, S., & Liang, C. (2019). The Role of Polymorphisms in Genes of PI3K/Akt Signaling Pathway on Prostate. *Journal of Cancer*, *10*(4), 1023–1031. https://doi.org/10.7150/jca.26472

Xue, J., Schmidt, S. V., Sander, J., Draffehn, A., Krebs, W., Quester, I., De Nardo, D., Gohel, T. D., Emde, M., Schmidleithner, L., Ganesan, H., Nino-Castro, A., Mallmann, M. R., Labzin, L., Theis, H., Kraut, M., Beyer, M., Latz, E., Freeman, T. C., … Schultze, J. L. (2014). Transcriptome-based network analysis reveals a spectrum model of human macrophage activation. *Immunity*, *40*(2), 274–288. https://doi.org/10.1016/j.immuni.2014.01.006

Yáñez, A., Coetzee, S. G., Olsson, A., Muench, D. E., Berman, B. P., Hazelett, D. J., Salomonis, N., Grimes, H. L., & Goodridge, H. S. (2017). Granulocyte-Monocyte Progenitors and Monocyte-Dendritic Cell Progenitors

Independently Produce Functionally Distinct Monocytes. *Immunity*, *47*(5), 890-902.e4. https://doi.org/10.1016/j.immuni.2017.10.021

Yang, X., Coulombe-Huntington, J., Kang, S., Sheynkman, G. M., Hao, T., Richardson, A., Sun, S., Yang, F., Shen, Y. A., Murray, R. R., Spirohn, K., Begg, B. E., Duran-Frigola, M., MacWilliams, A., Pevzner, S. J., Zhong, Q., Wanamaker, S. A., Tam, S., Ghamsari, L., … Vidal, M. (2016). Widespread Expansion of Protein Interaction Capabilities by Alternative Splicing. *Cell*, *164*(4), 805–817. https://doi.org/10.1016/j.cell.2016.01.029

Yoshikawa, T. T., & Norman, D. C. (2017). Geriatric Infectious Diseases: Current Concepts on Diagnosis and Management. *Journal of the American Geriatrics Society*, *65*(3), 631–641. https://doi.org/10.1111/jgs.14731

You, M., Dong, G., Li, F., Ma, F., Ren, J., Xu, Y., Yue, H., Tang, R., Ren, D., & Hou, Y. (2017). Ligation of CD180 inhibits IFN-α signaling in a Lyn-PI3K-BTK-dependent manner in B cells. *Cellular & Molecular Immunology*, *14*(2), 192–202. https://doi.org/10.1038/cmi.2015.61

Youness, A., Cenac, C., Faz-López, B., Grunenwald, S., Barrat, F. J., Chaumeil, J., Mejía, J. E., & Guéry, J.-C. (2023). TLR8 escapes X chromosome inactivation in human monocytes and CD4+ T cells. *Biology of Sex Differences*, *14*(1), 60. https://doi.org/10.1186/s13293-023-00544-5

Yu, D., Huber, W., & Vitek, O. (2013). Shrinkage estimation of dispersion in Negative Binomial models for RNA-seq experiments with small sample size. *Bioinformatics (Oxford, England)*, *29*(10), 1275–1282. https://doi.org/10.1093/bioinformatics/btt143

Yu, G. (2018a). *clusterProfiler: An universal enrichment tool for functional and comparative stud*. https://doi.org/10.1101/256784

Yu, G. (2018b). Using meshes for MeSH term enrichment and semantic analyses. *Bioinformatics (Oxford, England)*, *34*(21), 3766–3767. https://doi.org/10.1093/bioinformatics/bty410

Yu, G., Wang, L.-G., Han, Y., & He, Q.-Y. (2012). clusterProfiler: An R package for comparing biological themes among gene clusters. *Omics: A Journal of Integrative Biology*, *16*(5), 284–287. https://doi.org/10.1089/omi.2011.0118

Yu, G., Wang, L.-G., Yan, G.-R., & He, Q.-Y. (2015). DOSE: An R/Bioconductor package for disease ontology semantic and enrichment analysis. *Bioinformatics (Oxford, England)*, *31*(4), 608–609. https://doi.org/10.1093/bioinformatics/btu684

Zang, Y., Liu, S., Rao, Z., Wang, Y., Zhang, B., Li, H., Cao, Y., Zhou, J., Shen, Z., Duan, S., He, D., & Xu, H. (2023). Retinoid X receptor gamma dictates the activation threshold of group 2 innate lymphoid cells and limits type 2 inflammation in the small intestine. *Immunity*, *56*(11), 2542-2554.e7. https://doi.org/10.1016/j.immuni.2023.08.019

Zawada, A. M., Rogacev, K. S., Rotter, B., Winter, P., Marell, R.-R., Fliser, D., & Heine, G. H. (2011). SuperSAGE evidence for CD14++CD16+ monocytes as a third monocyte subset. *Blood*, *118*(12), e50-61. https://doi.org/10.1182/blood-2011-01-326827

Zhang, S., Liu, Y., Zhang, X.-L., Sun, Y., & Lu, Z.-H. (2024). ANKRD22 aggravates sepsis-induced ARDS and promotes pulmonary M1 macrophage

polarization. *Journal of Translational Autoimmunity*, *8*, 100228. https://doi.org/10.1016/j.jtauto.2023.100228

Zhang, S., Xiang, X., Liu, L., Yang, H., Cen, D., & Tang, G. (2021). Bioinformatics Analysis of Hub Genes and Potential Therapeutic Agents Associated with Gastric Cancer. *Cancer Management and Research*, *13*, 8929–8951. https://doi.org/10.2147/CMAR.S341485

Zhang, W., Wang, H., Sun, M., Deng, X., Wu, X., Ma, Y., Li, M., Shuoa, S. M., You, Q., & Miao, L. (2020). CXCL5/CXCR2 axis in tumor microenvironment as potential diagnostic biomarker and therapeutic target. *Cancer Communications (London, England)*, *40*(2–3), 69–80. https://doi.org/10.1002/cac2.12010

Zhao, J., Lin, X., Meng, D., Zeng, L., Zhuang, R., Huang, S., Lv, W., & Hu, J. (2020). Nrf2 Mediates Metabolic Reprogramming in Non-Small Cell Lung Cancer. *Frontiers in Oncology*, *10*, 578315. https://doi.org/10.3389/fonc.2020.578315

Zhao, S., Xi, L., & Zhang, B. (2015). Union Exon Based Approach for RNA-Seq Gene Quantification: To Be or Not to Be? *PloS One*, *10*(11), e0141910. https://doi.org/10.1371/journal.pone.0141910

Zhong, X., Zhang, F., Xiao, H., & Tu, R. (2024). Single-cell transcriptome analysis of macrophage subpopulations contributing to chemotherapy resistance in ovarian cancer. *Immunobiology*, *229*(5), 152811. https://doi.org/10.1016/j.imbio.2024.152811

Zhou, Q., Li, T., & Price, D. H. (2012). RNA polymerase II elongation control. *Annual Review of Biochemistry*, *81*, 119–143. https://doi.org/10.1146/annurev-biochem-052610-095910

Zhou, Y., Tabib, T., Huang, M., Yuan, K., Kim, Y., Morse, C., Sembrat, J., Valenzi, E., & Lafyatis, R. (2024). Molecular Changes Implicate Angiogenesis and Arterial Remodeling in Systemic Sclerosis–Associated and Idiopathic Pulmonary Hypertension. *Arteriosclerosis, Thrombosis, and Vascular Biology*, *44*(8). https://doi.org/10.1161/ATVBAHA.123.320005

Zhou, Z., Xia, G., Xiang, Z., Liu, M., Wei, Z., Yan, J., Chen, W., Zhu, J., Awasthi, N., Sun, X., Fung, K.-M., He, Y., Li, M., & Zhang, C. (2019). A C-X-C Chemokine Receptor Type 2-Dominated Cross-talk between Tumor Cells and Macrophages Drives Gastric Cancer Metastasis. *Clinical Cancer Research: An Official Journal of the American Association for Cancer Research*, *25*(11), 3317–3328. https://doi.org/10.1158/1078-0432.CCR-18-3567

Zhu, A., Ibrahim, J. G., & Love, M. I. (2019). Heavy-tailed prior distributions for sequence count data: Removing the noise and preserving large differences. *Bioinformatics (Oxford, England)*, *35*(12), 2084–2092. https://doi.org/10.1093/bioinformatics/bty895

Zhu, J., Yamane, H., & Paul, W. E. (2010). Differentiation of effector CD4 T cell populations (*). *Annual Review of Immunology*, *28*, 445–489. https://doi.org/10.1146/annurev-immunol-030409-101212

Zhu, Y. P., Thomas, G. D., & Hedrick, C. C. (2016). 2014 Jeffrey M. Hoeg Award Lecture: Transcriptional Control of Monocyte Development. *Arteriosclerosis,*

Thrombosis, and Vascular Biology, *36*(9), 1722–1733. https://doi.org/10.1161/ATVBAHA.116.304054

Ziegler-Heitbrock, L., Ancuta, P., Crowe, S., Dalod, M., Grau, V., Hart, D. N., Leenen, P. J. M., Liu, Y.-J., MacPherson, G., Randolph, G. J., Scherberich, J., Schmitz, J., Shortman, K., Sozzani, S., Strobl, H., Zembala, M., Austyn, J. M., & Lutz, M. B. (2010). Nomenclature of monocytes and dendritic cells in blood. *Blood*, *116*(16), e74-80. https://doi.org/10.1182/blood-2010-02-258558

Zong, D., Huang, B., Li, Y., Lu, Y., Xiang, N., Guo, C., Liu, Q., Sha, Q., Du, P., Yu, Q., Zhang, W., Cai, P., Sun, Y., Tao, J., Li, X., Cai, S., & Qu, K. (2021). Chromatin accessibility landscapes of immune cells in rheumatoid arthritis nominate monocytes in disease pathogenesis. *BMC Biology*, *19*(1), 79. https://doi.org/10.1186/s12915-021-01011-6

Zwack, E. E., Feeley, E. M., Burton, A. R., Hu, B., Yamamoto, M., Kanneganti, T.-D., Bliska, J. B., Coers, J., & Brodsky, I. E. (2017). Guanylate Binding Proteins Regulate Inflammasome Activation in Response to Hyperinjected Yersinia Translocon Components. *Infection and Immunity*, *85*(10), e00778-16. https://doi.org/10.1128/IAI.00778-16

APPENDIX

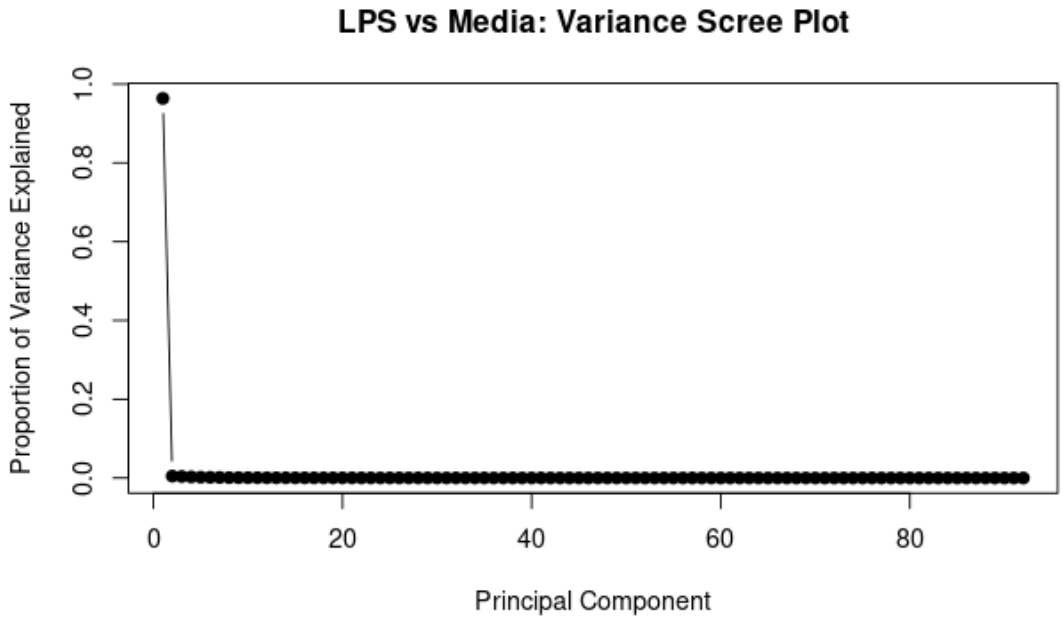

Appendix Figure 1. LPS vs. Media Variance Scree Plot. Scree plot showing the proportion of variance explained by each PC from PCA of VST-transformed gene expression data across 92 samples. *The x-axis represents the PCs, and the y-axis indicates the proportion of total variance explained by each component. PC1 explains the largest share of variance, followed by a sharp decline across subsequent components.*

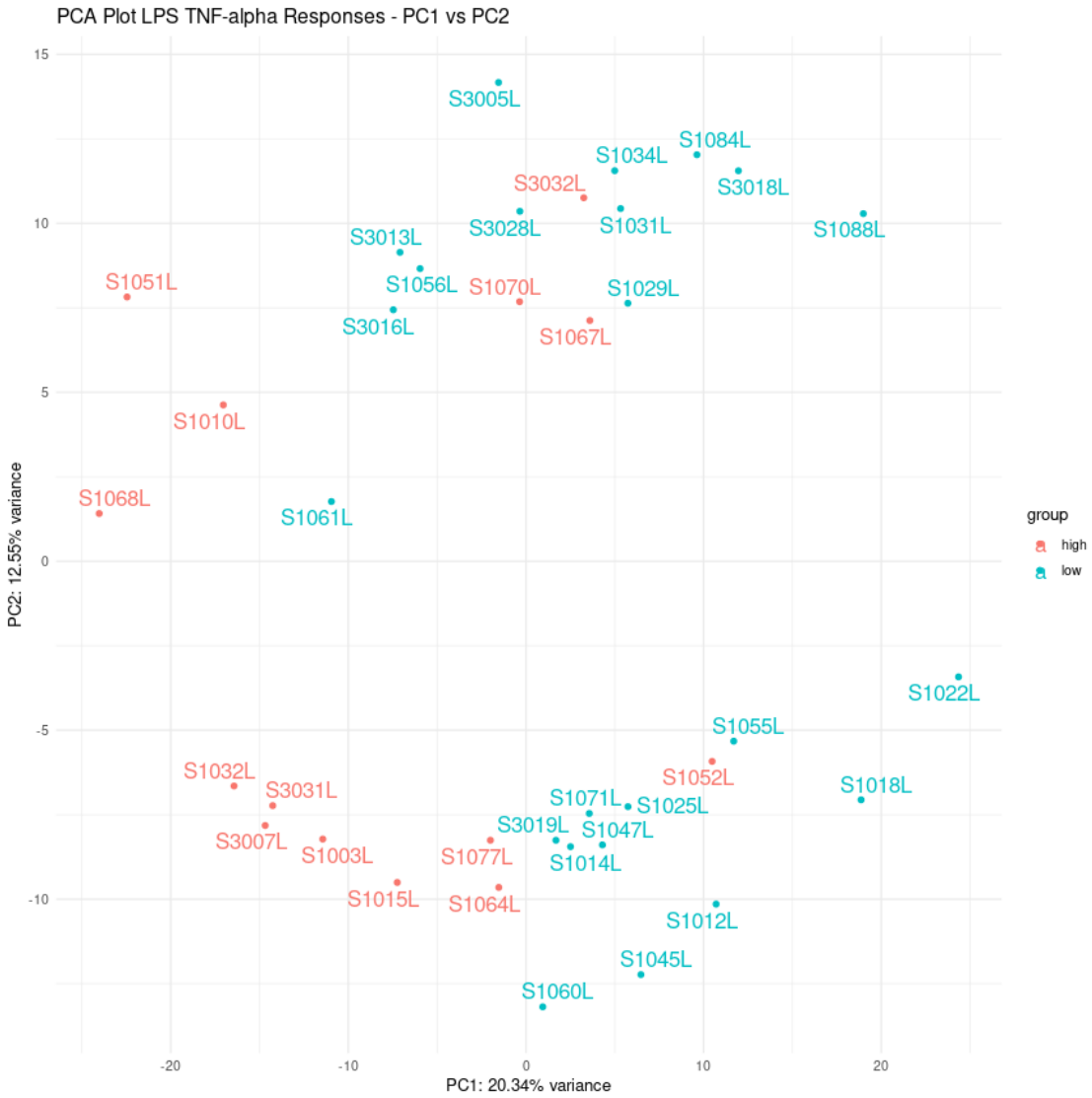

Appendix Figure 2. Preliminary PCA of rlog-transformed gene expression in LPS-stimulated monocytes. *Plot showing the first two PCs derived from rlog-transformed RNA-seq data across monocyte samples. Samples are colour-coded by TNF-α response classification (high vs. low responders). This exploratory analysis revealed separation primarily along PC1 based on TNF-α response and suggested an additional trend along PC2, potentially related to sex. These observations informed the inclusion of sex as a covariate in subsequent multivariate models.*

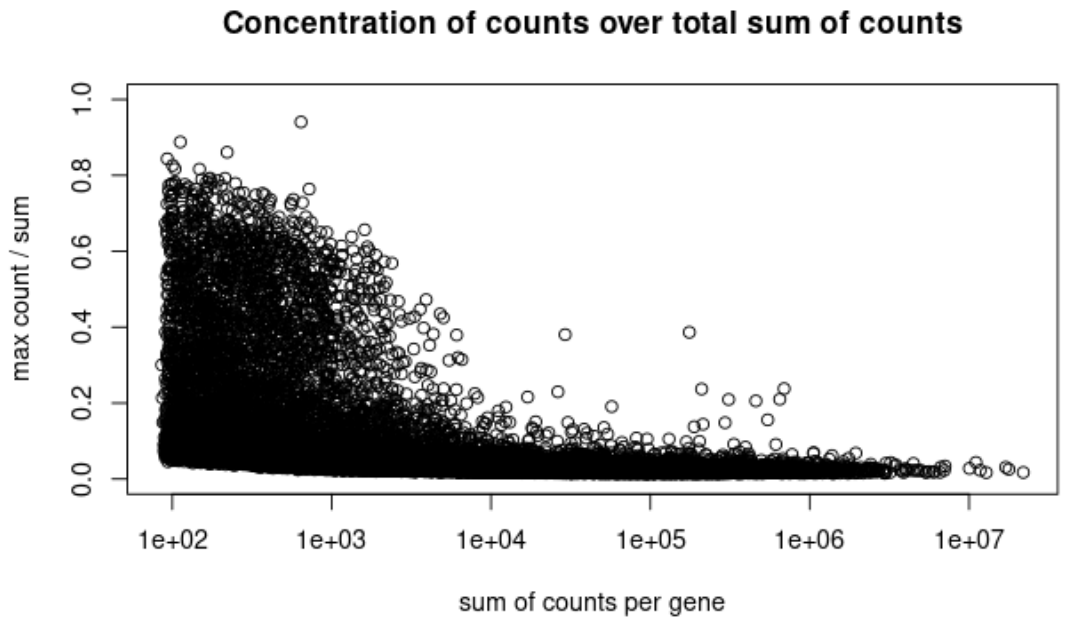

Appendix Figure 3. Gene-level sparsity plot of raw RNA-seq counts. *Scatter plot illustrating count distribution per gene across all samples in the LPS vs. media-treated monocyte dataset. The x-axis shows the total sum of counts per gene (log scale), and the y-axis represents the ratio of the maximum count in a single sample to the total count across all samples for that gene. Genes with high y-values and low overall counts reflect sparsity, where expression is concentrated in a few samples.*

(A)

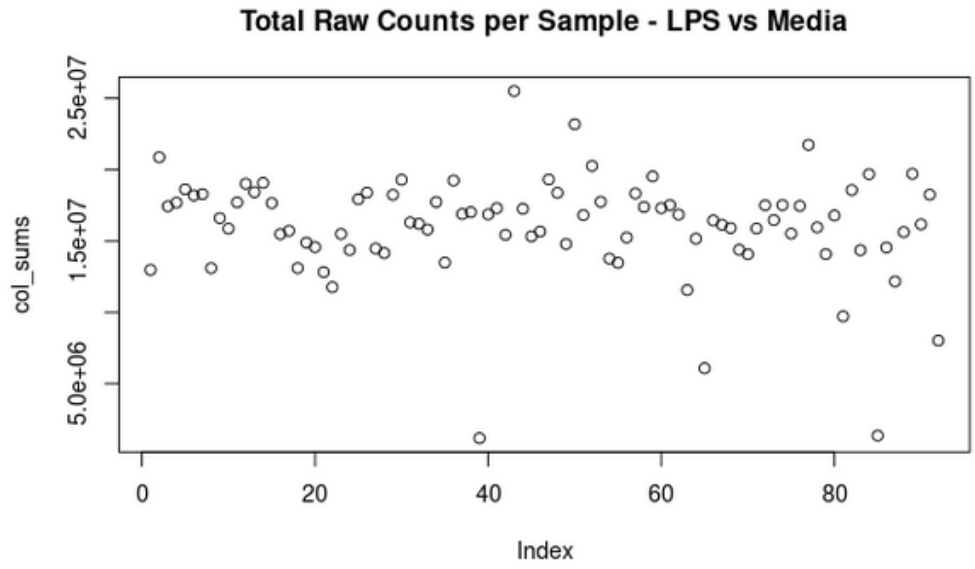

(B)

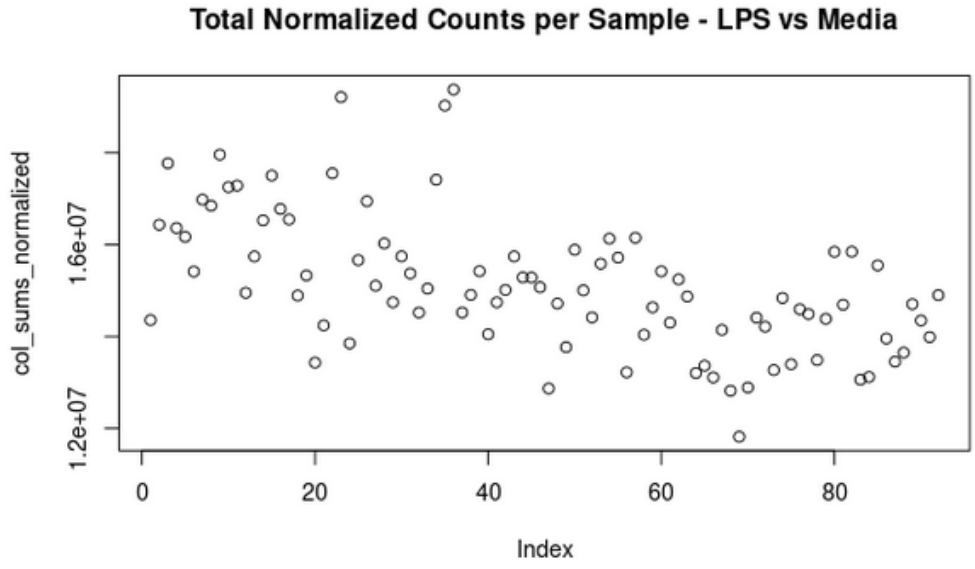

Appendix Figure 4. Total read counts per sample for LPS vs. media-treated monocytes. *(A) Bar plot showing raw total read counts per sample. The x-axis represents individual sample IDs, grouped by treatment condition (LPS or media), and the y-axis shows the total number of sequencing reads per sample (scale: 0 to ~35 million). Samples S3013L and S3013M display notably reduced read depth, each falling below 5 million reads. (B) Bar plot showing total normalised counts per sample following DESeq2 size factor correction. normalisation adjusted for sequencing depth differences with all samples brought into alignment.*

(A)

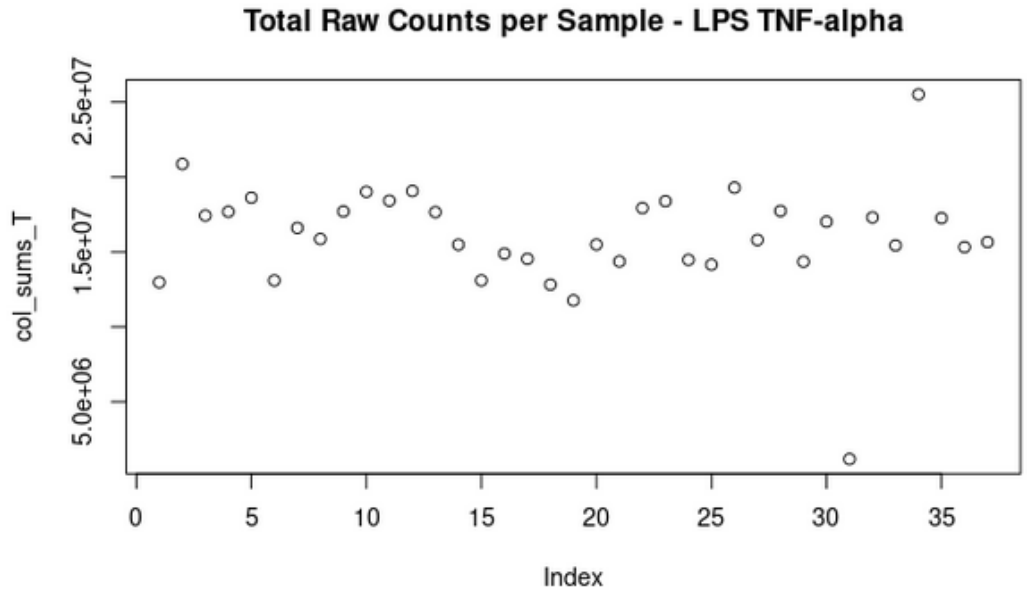

(B)

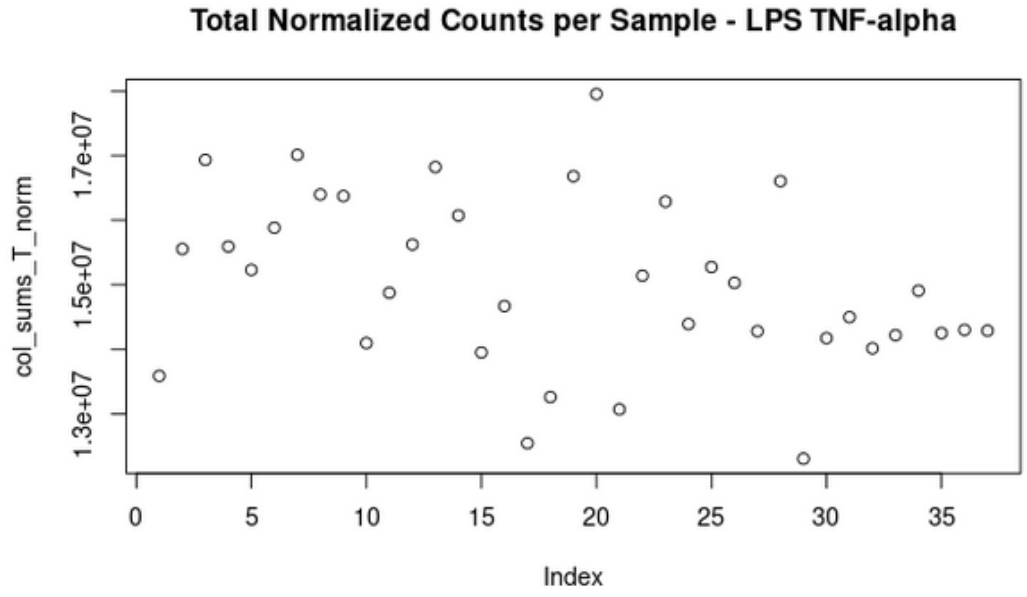

Appendix Figure 5. Scatter plot showing raw total read counts across samples stratified by TNF-α response classification (high vs. low). *The x-axis indicates sample IDs; the y-axis shows total read counts per sample prior to normalisation (range: 0 to ~35 million). S3013L and S3013M appear below the 5 million threshold. (B) Bar plot showing total normalised counts post-normalisation, with all samples exceeding the 5 million read threshold following DESeq2 size factor adjustment.*

(A)

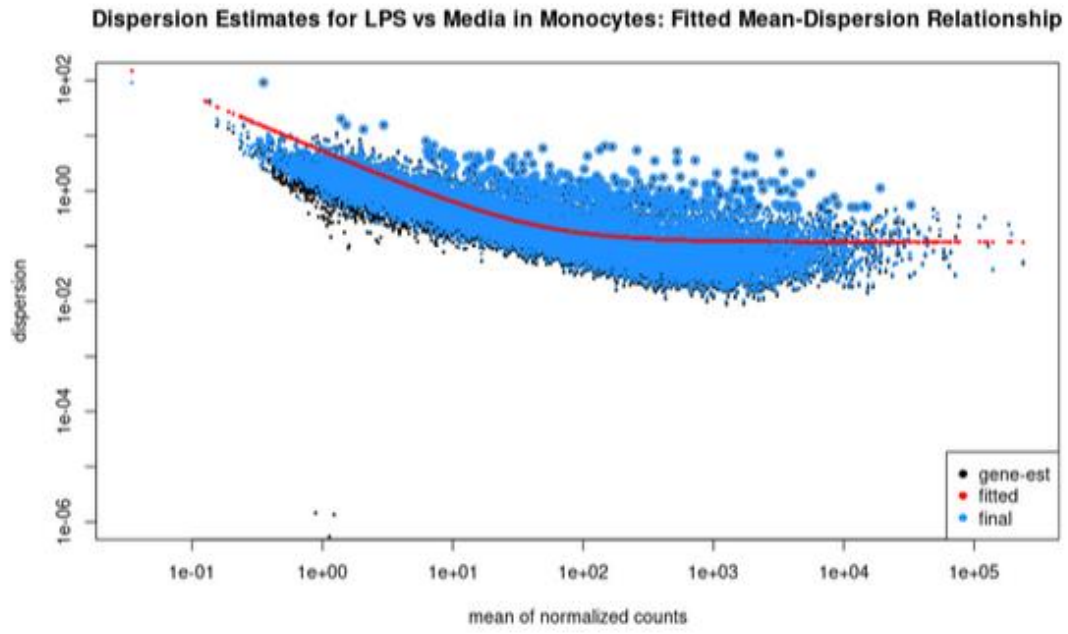

(B)

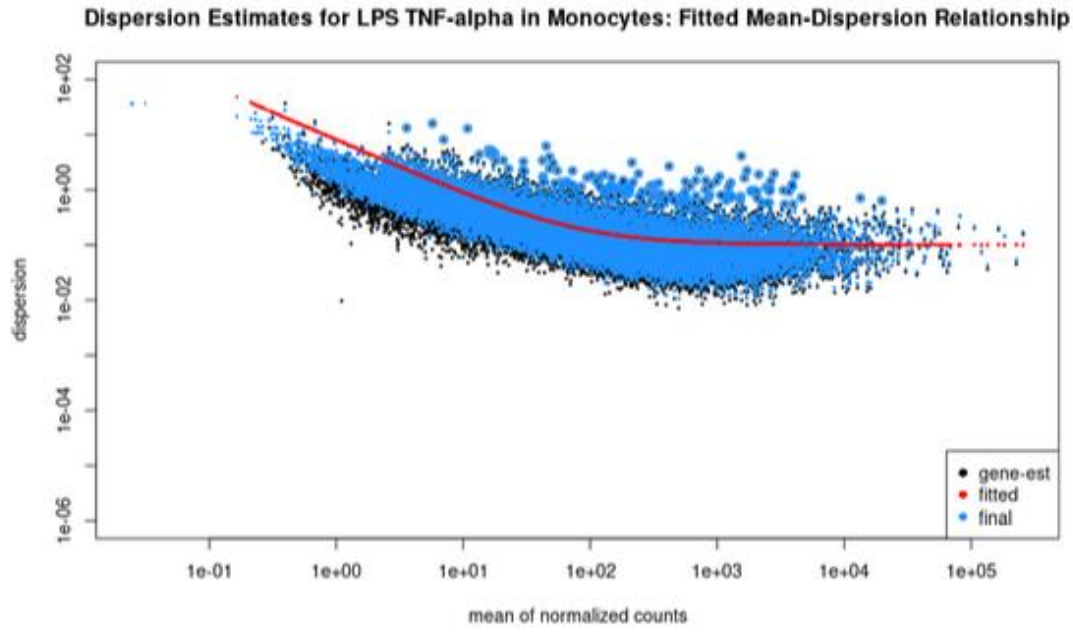

Appendix Figure 6. Dispersion Estimates for Monocyte Gene Expression. *Gene-wise dispersion estimates for monocyte gene expression data calculated using the Cox-Reid APL method in DESeq2. Black dots represented raw dispersion estimates plotted against mean expression levels, while blue points showed the final shrunken dispersion estimates aligned toward the fitted red curve, which depicted the mean-dispersion trend. The logarithmic y-axis displayed dispersion values ranging from 0.000001 to 100, and the x-*

axis represented mean expression levels from 0.1 to 100,000. Genes closely following the red curve were interpreted as having stable dispersion estimates, while those deviating significantly indicated greater biological variability.

(A) LPS-treated vs. Media-treated Monocytes
Dispersion estimates for a dataset of 92 samples. Most genes followed the expected mean-dispersion trend closely, with the red fitted line starting at higher dispersion values around 10 on the y-axis and steadily decreasing towards 0.1, leveling off at higher mean expression levels. A few genes with low mean expression (near 1 on the x-axis) showed extremely low dispersion estimates, around 0.000001.

(B) TNF-α Response in LPS-treated Monocytes with sex covariate
Dispersion estimates for the TNF-α response in LPS-treated monocytes, based on a dataset of 37 samples. Despite the smaller sample size, dispersion values largely followed the fitted mean-dispersion curve, with most genes clustering tightly around the red trendline. No apparent outliers were observed.

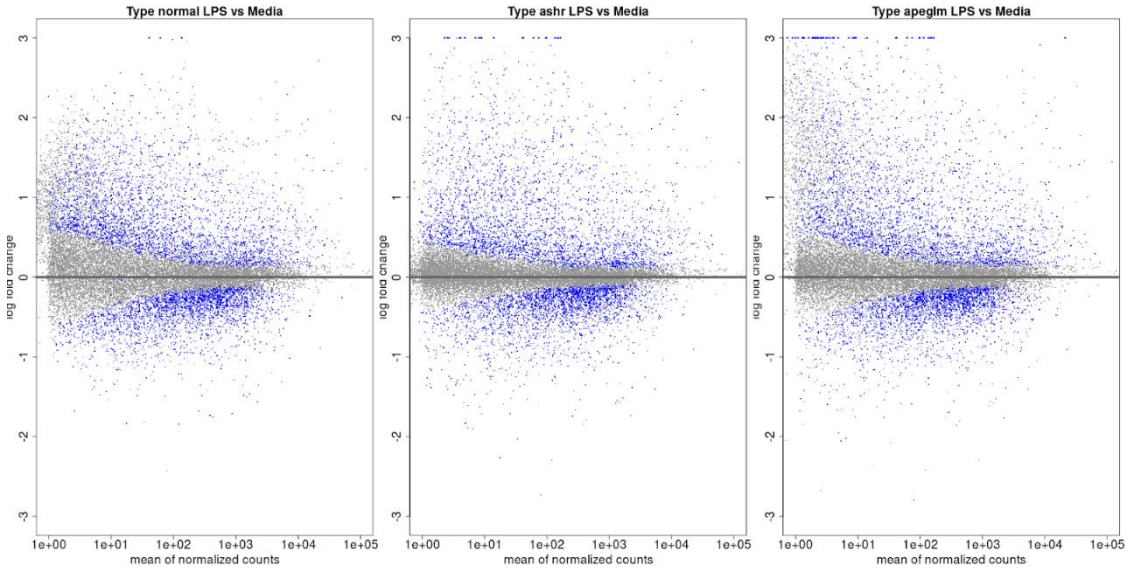

Appendix Figure 7. MA plots comparing log2FC shrinkage estimators in LPS- vs. media-treated monocytes. *MA plots showing shrunken log_2FC values vs. mean normalised counts for 20,576 genes, generated using three DESeq2 shrinkage methods. The x-axis represents the mean of normalised counts per gene (log_{10} scale, range: 1 to 100,000), and the y-axis indicates log_2FC (range: -3 to 3). Each point represents a gene; blue points indicate genes with adjusted p-value < 0.01, and grey points indicate non-significant genes. From left to right: shrinkage was applied using the normal, Ashr, and Apeglm methods. Horizontal grey lines mark the zero log_2FC baseline. Plots were generated using the plotMA() function in DESeq2.*

Metric	LPS vs. Media Dataset (Ashr Shrinkage with contrast)	LPS TNF-α High vs. Low Responders Dataset (Ashr Shrinkage with Contrast)
Total genes with nonzero read count	4,490 From 20,576 (Wald)	555 From 18,195 (Wald)
LFC > 0 (up)	2,463 (55%)	228 (41%)
LFC < 0 (down)	2,027 (45%)	327 (59%)
Outliers ("cooksCutoff")	0 (0%) From 2,133 (10%) (Wald)	0 (0%) From 4,930 (27.1%) (Wald)
Low counts (mean count < 0)	0 (0%)	0 (0%)

Appendix Table 1. Summary Statistics of DEG results for the LPS vs. Media and the LPS TNF-α High vs. Low Responders datasets, using DESeq2 with log2FC shrinkage via the Ashr method and specified contrasts. *Metrics include the number of genes analysed (with nonzero read counts), the number and proportion of significantly upregulated or downregulated genes (adjusted p-value ≤ 0.01, using Wald test results), and the number of genes flagged as outliers (based on Cook's distance) or excluded due to low counts (mean count < 0). Shrinkage was applied for improved FC stability, especially for genes with low counts or high dispersion. Values in parentheses reflect original totals from the unshrunken Wald test, where applicable.*

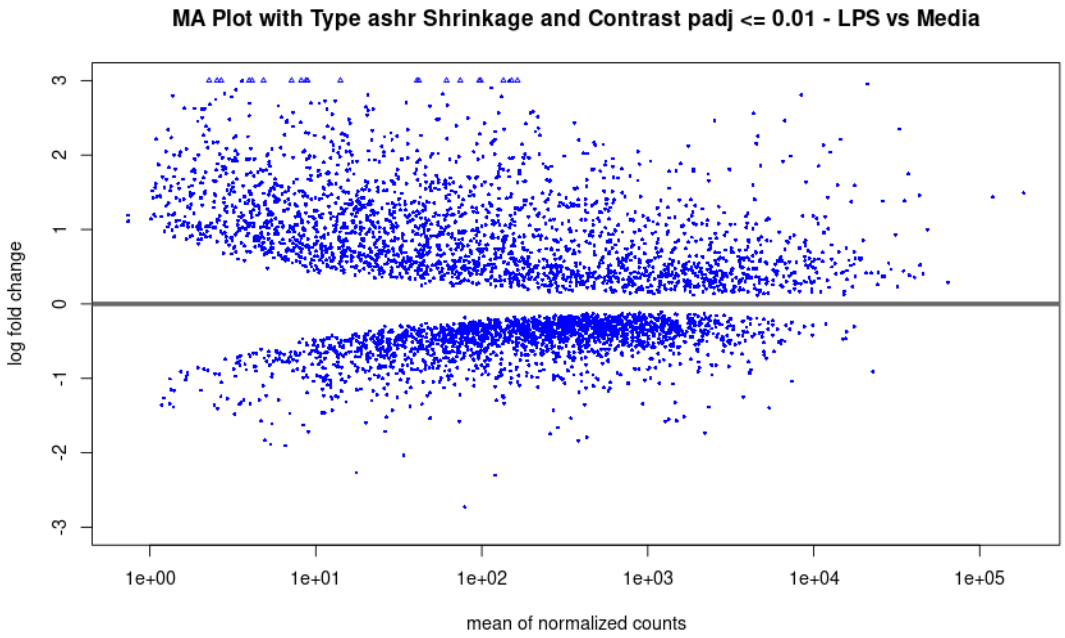

Appendix Figure 8. MA plot of DEG using Ashr shrinkage with stringent contrast filtering (padj ≤ 0.01). *MA plot displaying log_2FCs vs. mean normalised expression levels for 4,490 genes differentially expressed between LPS- and media-treated monocytes. The x-axis shows the mean of normalised counts per gene (log_{10} scale), and the y-axis displays the shrunken log_2FC, limited to a range of -3 to 3 for visualisation. Each point represents a gene with an adjusted p-value ≤ 0.01.*

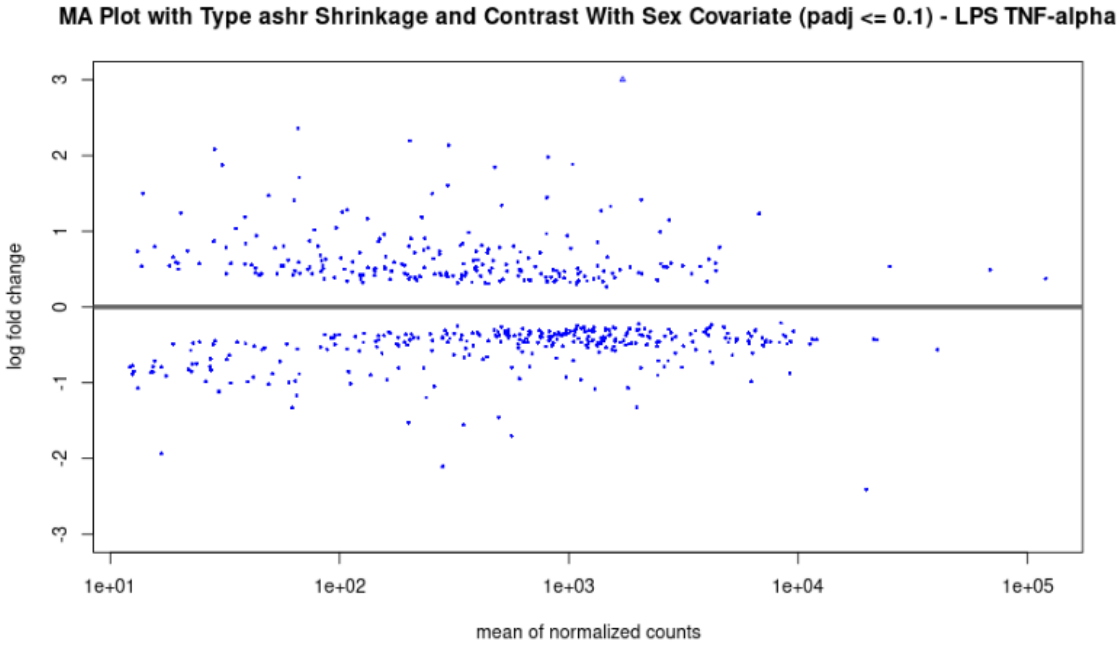

Appendix Figure 9. MA plot of DEGs (padj ≤ 0.01) in LPS-treated monocytes stratified by TNF-α response, adjusted for sex. *MA plot displaying 555 genes with significant differential expression between high and low TNF-α responders. log2FCs were shrunk using the Ashr method to stabilise variance in low-count genes. The x-axis shows the mean of normalised counts (log scale), while the y-axis presents shrunken logFCs, limited to a range of -3 to +3 for visualisation. Each point represents a gene passing the adjusted p-value threshold (padj ≤ 0.01), highlighting transcriptional variation associated with inflammatory responsiveness.*

(A)

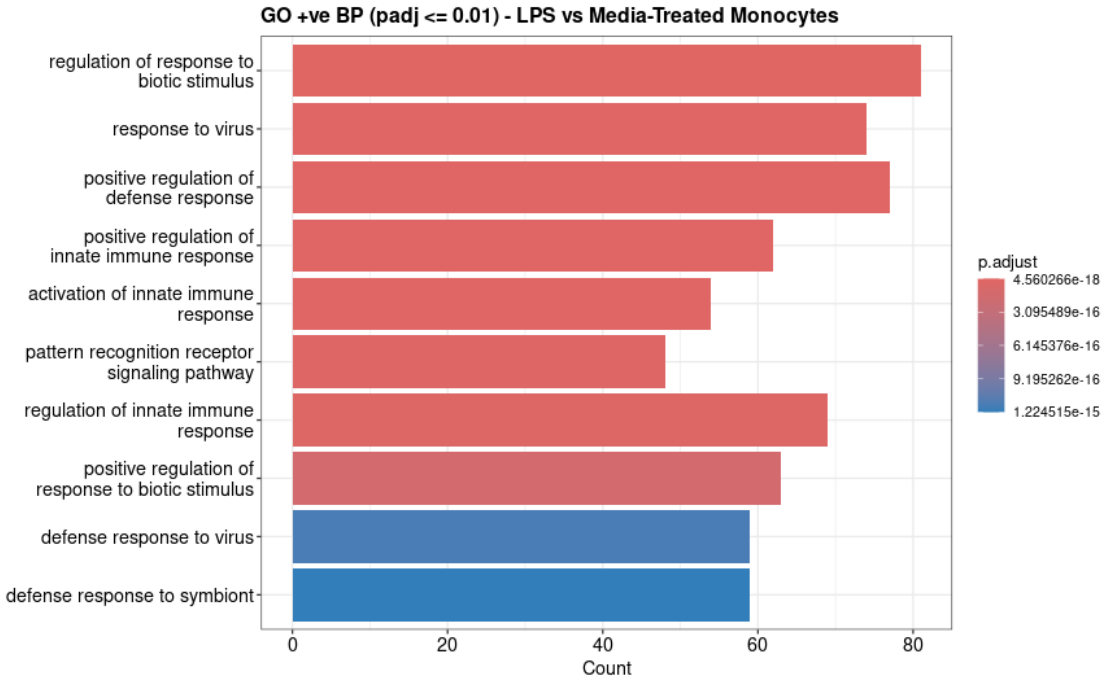
GO +ve BP (padj <= 0.01) - LPS vs Media-Treated Monocytes
regulation of response to biotic stimulus
response to virus
positive regulation of defense response
positive regulation of innate immune response
activation of innate immune response
pattern recognition receptor signaling pathway
regulation of innate immune response
positive regulation of response to biotic stimulus
defense response to virus
defense response to symbiont
0
20
40
60
80
Count
p.adjust
4.560266e-18
3.095489e-16
6.145376e-16
9.195262e-16
1.224515e-15

(B)

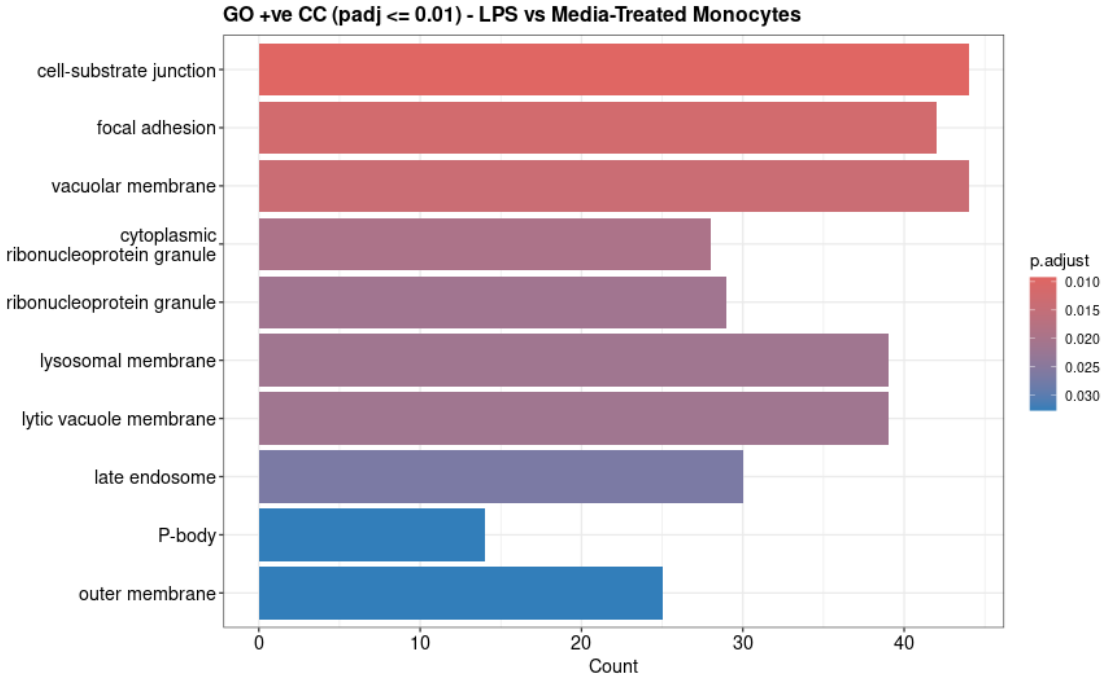
GO +ve CC (padj <= 0.01) - LPS vs Media-Treated Monocytes
cell-substrate junction
focal adhesion
vacuolar membrane
cytoplasmic ribonucleoprotein granule
ribonucleoprotein granule
lysosomal membrane
lytic vacuole membrane
late endosome
P-body
outer membrane
0
10
20
30
40
Count
p.adjust
0.010
0.015
0.020
0.025
0.030

(C)

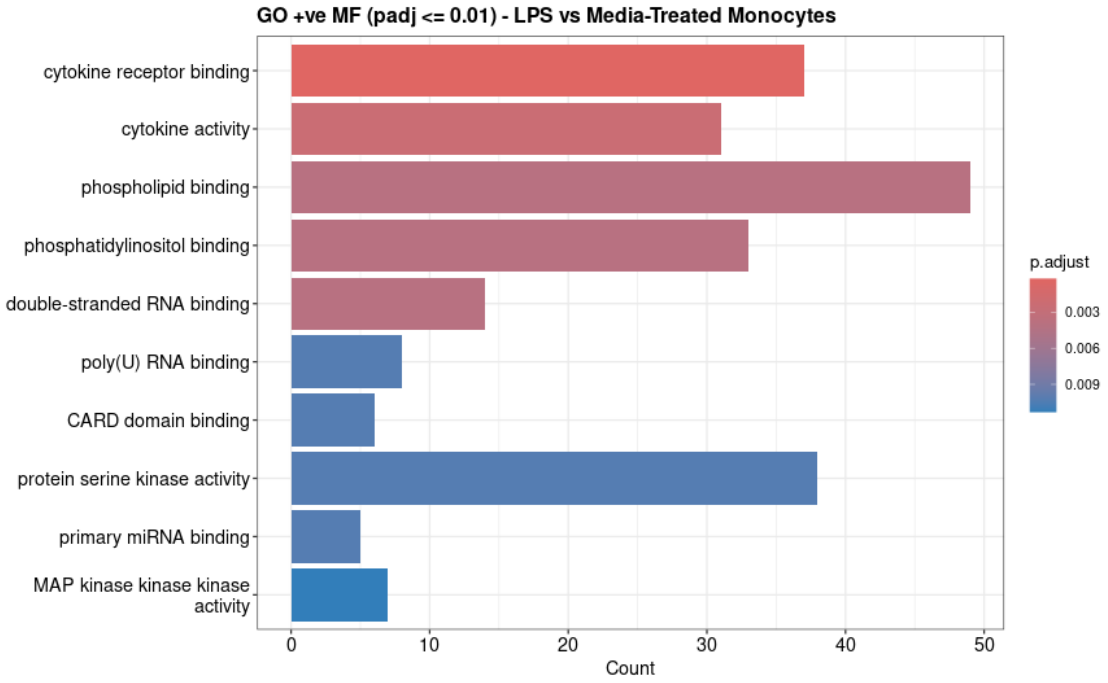

Appendix Figure 10. GO enrichment bar plots for positively enriched terms in LPS-treated vs. media-treated monocytes. *(A) BP, (B) CC, and (C) MF. Each horizontal bar represents a significantly enriched GO term associated with upregulated genes. The x-axis displays the number of genes annotated to each term, while the y-axis lists GO terms ordered by padj. colour gradients reflect enrichment significance, with more intense colours (red) indicating stronger statistical support.*

(A)

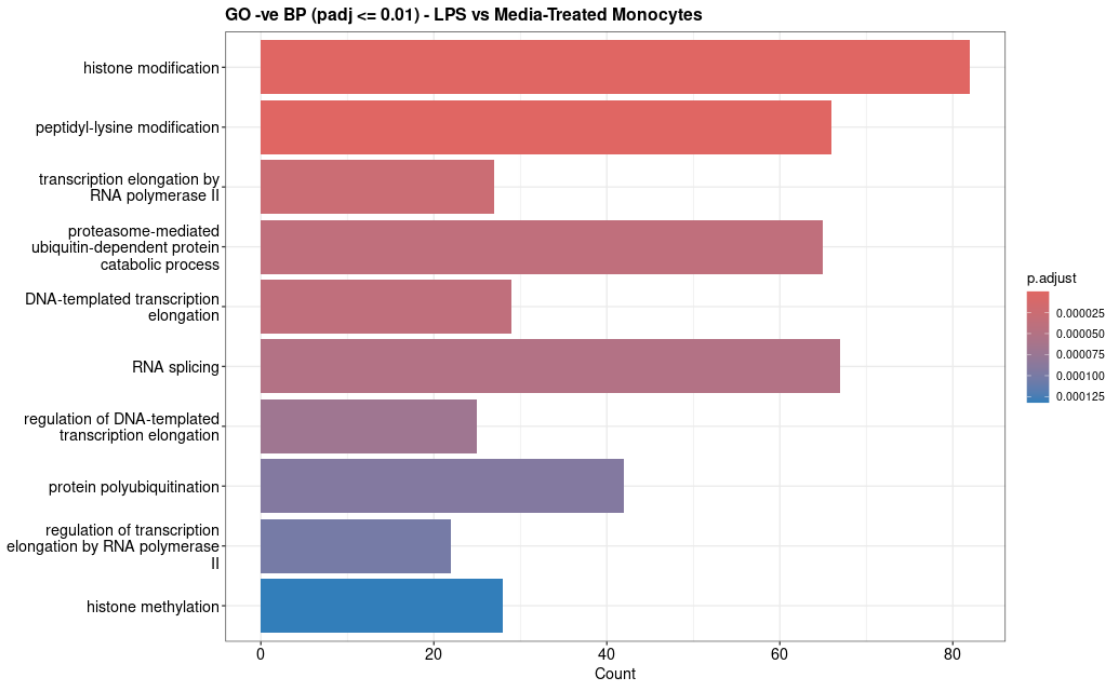
GO -ve BP (padj <= 0.01) - LPS vs Media-Treated Monocytes
histone modification
peptidyl-lysine modification
transcription elongation by RNA polymerase II
proteasome-mediated ubiquitin-dependent protein catabolic process
DNA-templated transcription elongation
RNA splicing
regulation of DNA-templated transcription elongation
protein polyubiquitination
regulation of transcription elongation by RNA polymerase II
histone methylation
0
20
40
60
80
Count
p.adjust
0.000025
0.000050
0.000075
0.000100
0.000125

(B)

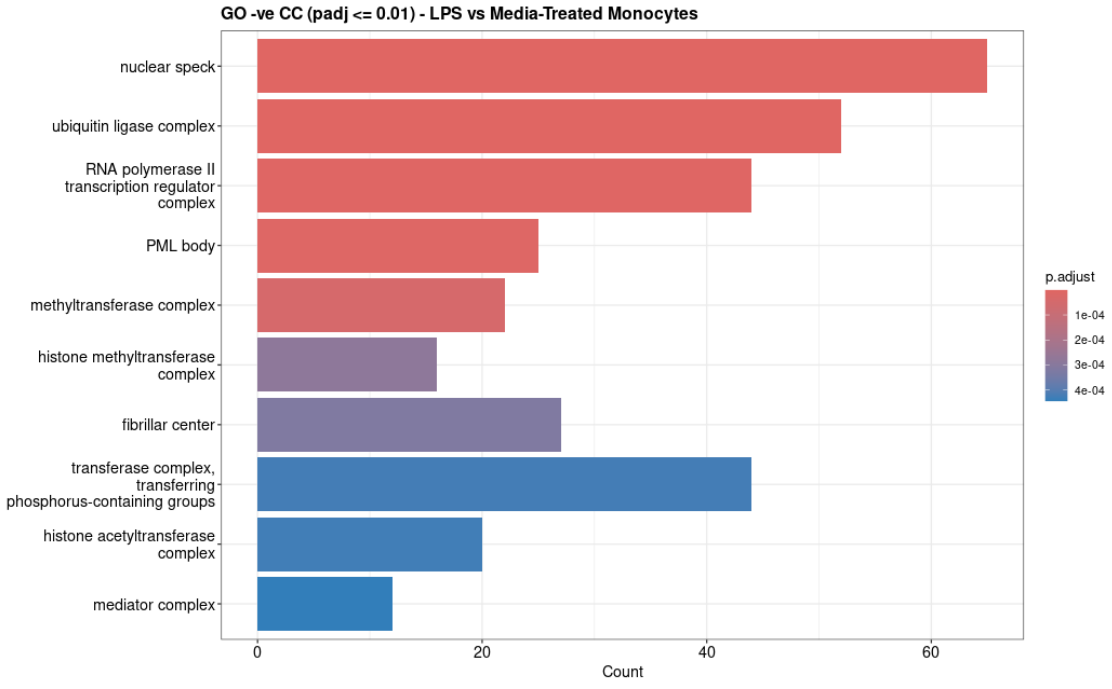
GO -ve CC (padj <= 0.01) - LPS vs Media-Treated Monocytes
nuclear speck
ubiquitin ligase complex
RNA polymerase II transcription regulator complex
PML body
methyltransferase complex
histone methyltransferase complex
fibrillar center
transferase complex, transferring phosphorus-containing groups
histone acetyltransferase complex
mediator complex
0
20
40
60
Count
p.adjust
1e-04
2e-04
3e-04
4e-04

(C)

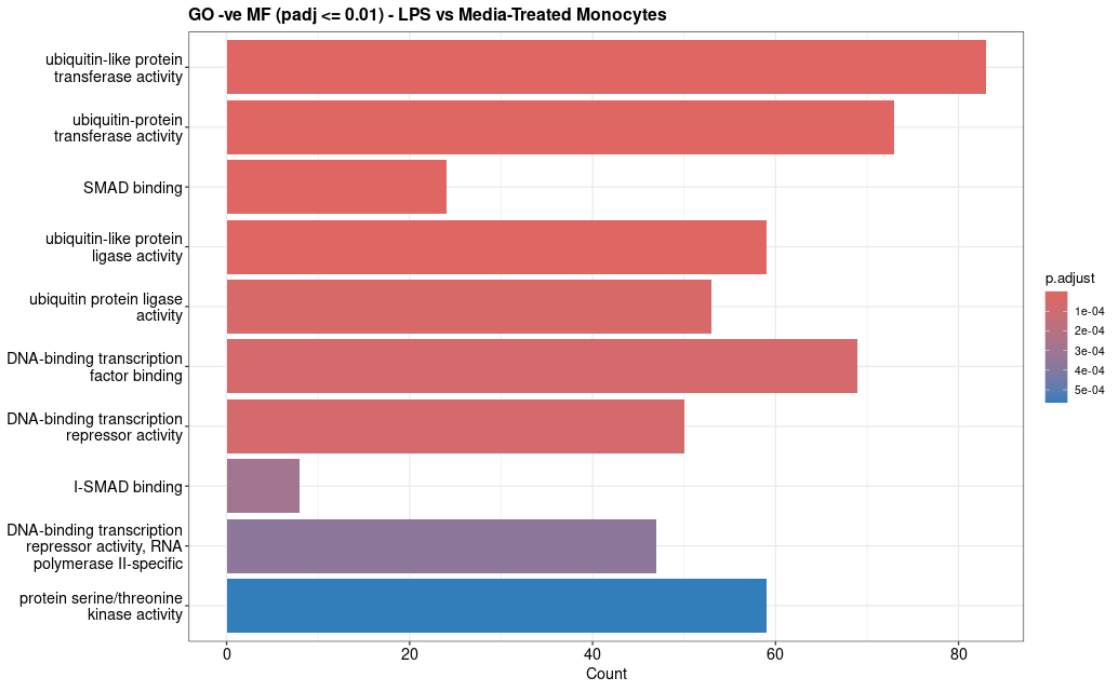

Appendix Figure 11. GO enrichment bar plots for negatively enriched terms in LPS-treated vs. media-treated monocytes. *(A) BP, (B) CC, and (C) MF. Each horizontal bar represents a significantly enriched GO term associated with downregulated genes. The x-axis displays the number of genes annotated to each term, while the y-axis lists GO terms ordered by padj. colour gradients reflect enrichment significance, with more intense colours (red) indicating stronger statistical support.*

(A)

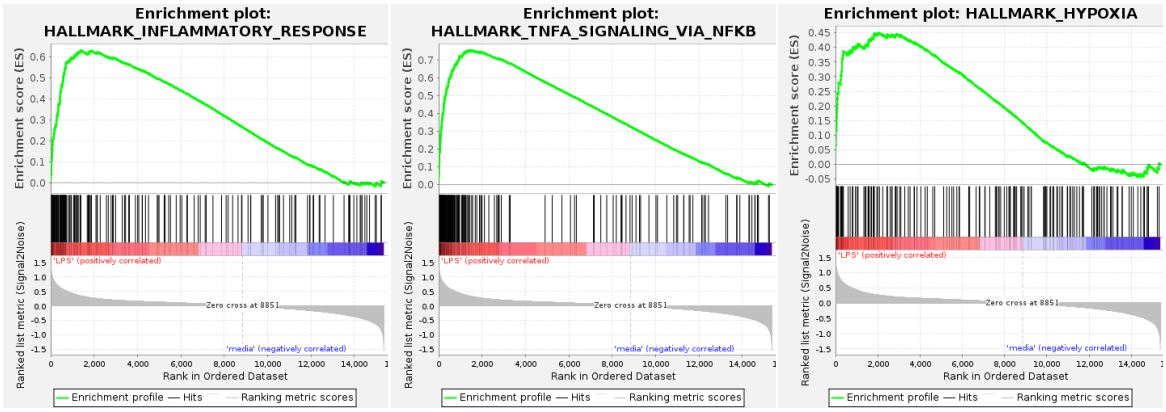

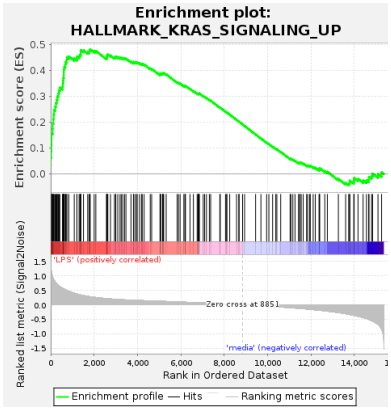
Enrichment plot:
HALLMARK_KRAS_SIGNALING_UP
Enrichment score (ES)
Ranked list metric (Signal2Noise)
'LPS' (positively correlated)
Zero cross at 8851
'media' (negatively correlated)
Rank in Ordered Dataset
Enrichment profile
Hits
Ranking metric scores

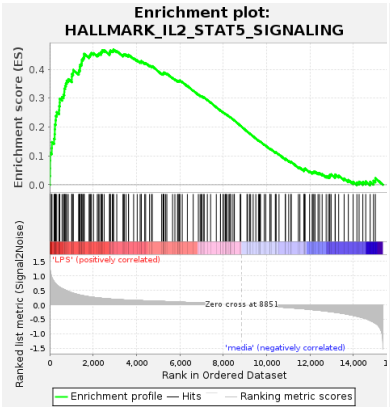
Enrichment plot:
HALLMARK_IL2_STAT5_SIGNALING
Enrichment score (ES)
Ranked list metric (Signal2Noise)
'LPS' (positively correlated)
Zero cross at 8851
'media' (negatively correlated)
Rank in Ordered Dataset
Enrichment profile
Hits
Ranking metric scores

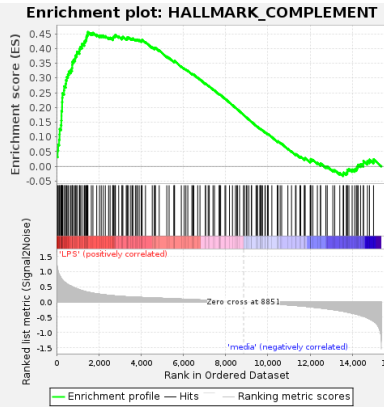
Enrichment plot: HALLMARK_COMPLEMENT
Enrichment score (ES)
Ranked list metric (Signal2Noise)
'LPS' (positively correlated)
Zero cross at 8851
'media' (negatively correlated)
Rank in Ordered Dataset
Enrichment profile
Hits
Ranking metric scores

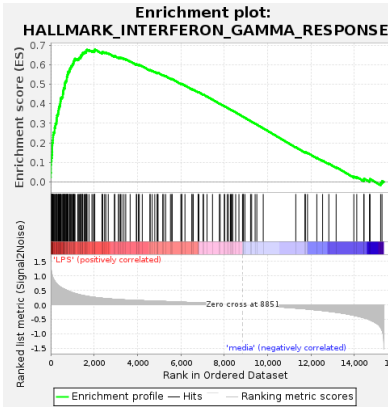
Enrichment plot:
HALLMARK_INTERFERON_GAMMA_RESPONSE
Enrichment score (ES)
Ranked list metric (Signal2Noise)
'LPS' (positively correlated)
Zero cross at 8851
'media' (negatively correlated)
Rank in Ordered Dataset
Enrichment profile
Hits
Ranking metric scores

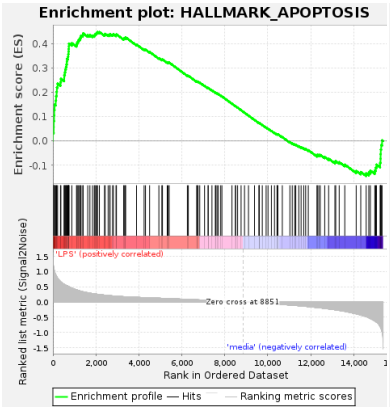
Enrichment plot: HALLMARK_APOPTOSIS
Enrichment score (ES)
Ranked list metric (Signal2Noise)
'LPS' (positively correlated)
Zero cross at 8851
'media' (negatively correlated)
Rank in Ordered Dataset
Enrichment profile
Hits
Ranking metric scores

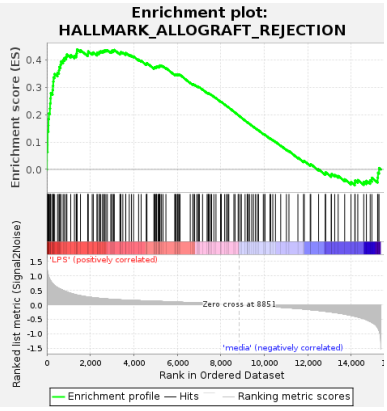
Enrichment plot:
HALLMARK_ALLOGRAFT_REJECTION
Enrichment score (ES)
Ranked list metric (Signal2Noise)
'LPS' (positively correlated)
Zero cross at 8851
'media' (negatively correlated)
Rank in Ordered Dataset
Enrichment profile
Hits
Ranking metric scores

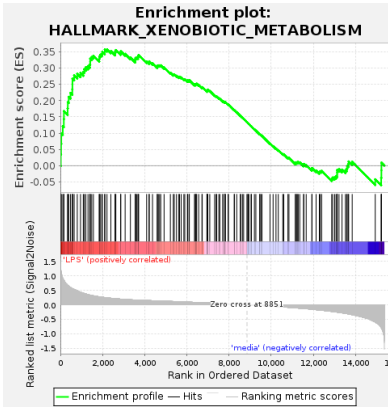
Enrichment plot:
HALLMARK_XENOBIOTIC_METABOLISM
Enrichment score (ES)
Ranked list metric (Signal2Noise)
'LPS' (positively correlated)
Zero cross at 8851
'media' (negatively correlated)
Rank in Ordered Dataset
Enrichment profile
Hits
Ranking metric scores

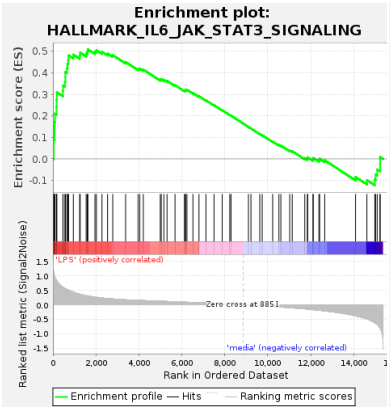
Enrichment plot:
HALLMARK_IL6_JAK_STAT3_SIGNALING
Enrichment score (ES)
Ranked list metric (Signal2Noise)
'LPS' (positively correlated)
Zero cross at 8851
'media' (negatively correlated)
Rank in Ordered Dataset
Enrichment profile
Hits
Ranking metric scores

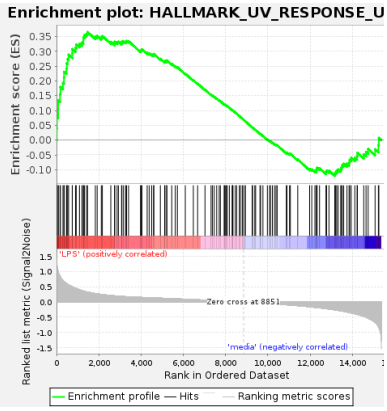
Enrichment plot: HALLMARK_UV_RESPONSE_U
Enrichment score (ES)
Ranked list metric (Signal2Noise)
'LPS' (positively correlated)
Zero cross at 8851
'media' (negatively correlated)
Rank in Ordered Dataset
Enrichment profile
Hits
Ranking metric scores

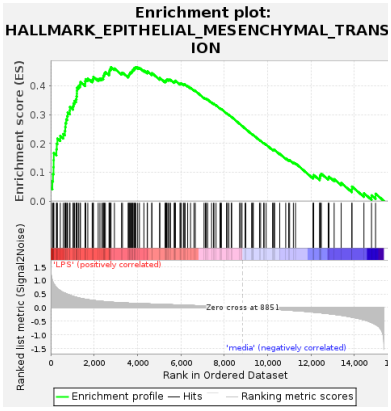
Enrichment plot:
HALLMARK_EPITHELIAL_MESENCHYMAL_TRANSION
Enrichment score (ES)
'LPS' (positively correlated)
Zero cross at 8851
'media' (negatively correlated)
Ranked list metric (Signal2Noise)
Rank in Ordered Dataset
Enrichment profile
Hits
Ranking metric scores

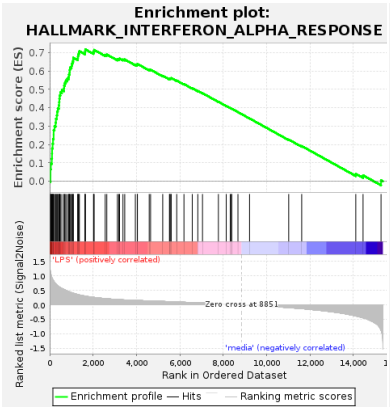
Enrichment plot:
HALLMARK_INTERFERON_ALPHA_RESPONSE
Enrichment score (ES)
'LPS' (positively correlated)
Zero cross at 8851
'media' (negatively correlated)
Ranked list metric (Signal2Noise)
Rank in Ordered Dataset
Enrichment profile
Hits
Ranking metric scores

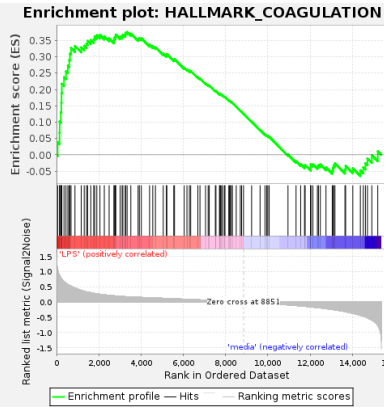
Enrichment plot: HALLMARK_COAGULATION
Enrichment score (ES)
'LPS' (positively correlated)
Zero cross at 8851
'media' (negatively correlated)
Ranked list metric (Signal2Noise)
Rank in Ordered Dataset
Enrichment profile
Hits
Ranking metric scores

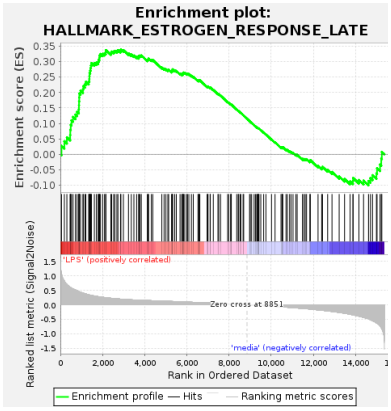
Enrichment plot:
HALLMARK_ESTROGEN_RESPONSE_LATE
Enrichment score (ES)
'LPS' (positively correlated)
Zero cross at 8851
'media' (negatively correlated)
Ranked list metric (Signal2Noise)
Rank in Ordered Dataset
Enrichment profile
Hits
Ranking metric scores

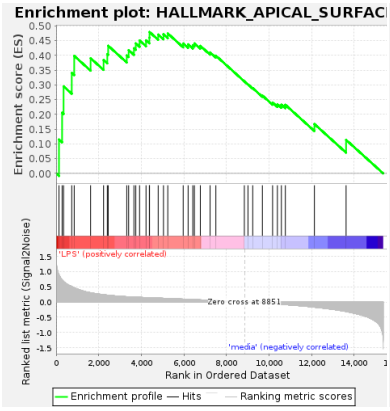
Enrichment plot: HALLMARK_APICAL_SURFAC
Enrichment score (ES)
'LPS' (positively correlated)
Zero cross at 8851
'media' (negatively correlated)
Ranked list metric (Signal2Noise)
Rank in Ordered Dataset
Enrichment profile
Hits
Ranking metric scores

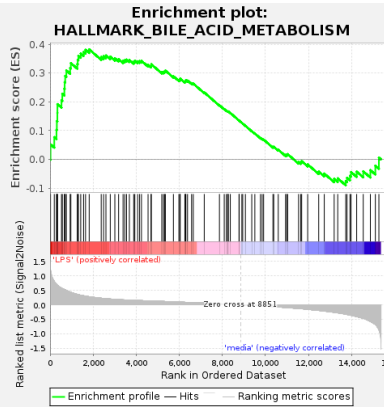
Enrichment plot:
HALLMARK_BILE_ACID_METABOLISM
Enrichment score (ES)
'LPS' (positively correlated)
Zero cross at 8851
'media' (negatively correlated)
Ranked list metric (Signal2Noise)
Rank in Ordered Dataset
Enrichment profile
Hits
Ranking metric scores

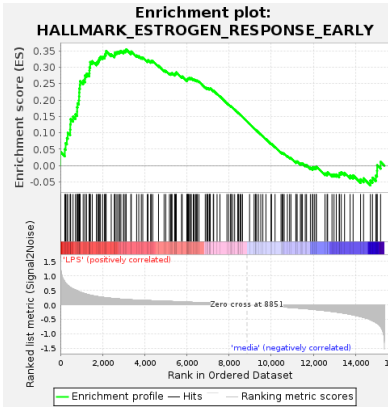
Enrichment plot:
HALLMARK_ESTROGEN_RESPONSE_EARLY
Enrichment score (ES)
'LPS' (positively correlated)
Zero cross at 8851
'media' (negatively correlated)
Ranked list metric (Signal2Noise)
Rank in Ordered Dataset
Enrichment profile
Hits
Ranking metric scores

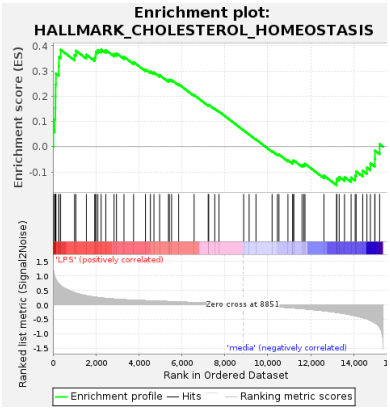
Enrichment plot:
HALLMARK_CHOLESTEROL_HOMEOSTASIS
Enrichment score (ES)
'LPS' (positively correlated)
Zero cross at 8851
'media' (negatively correlated)
Ranked list metric (Signal2Noise)
Rank in Ordered Dataset
Enrichment profile
Hits
Ranking metric scores

(B)

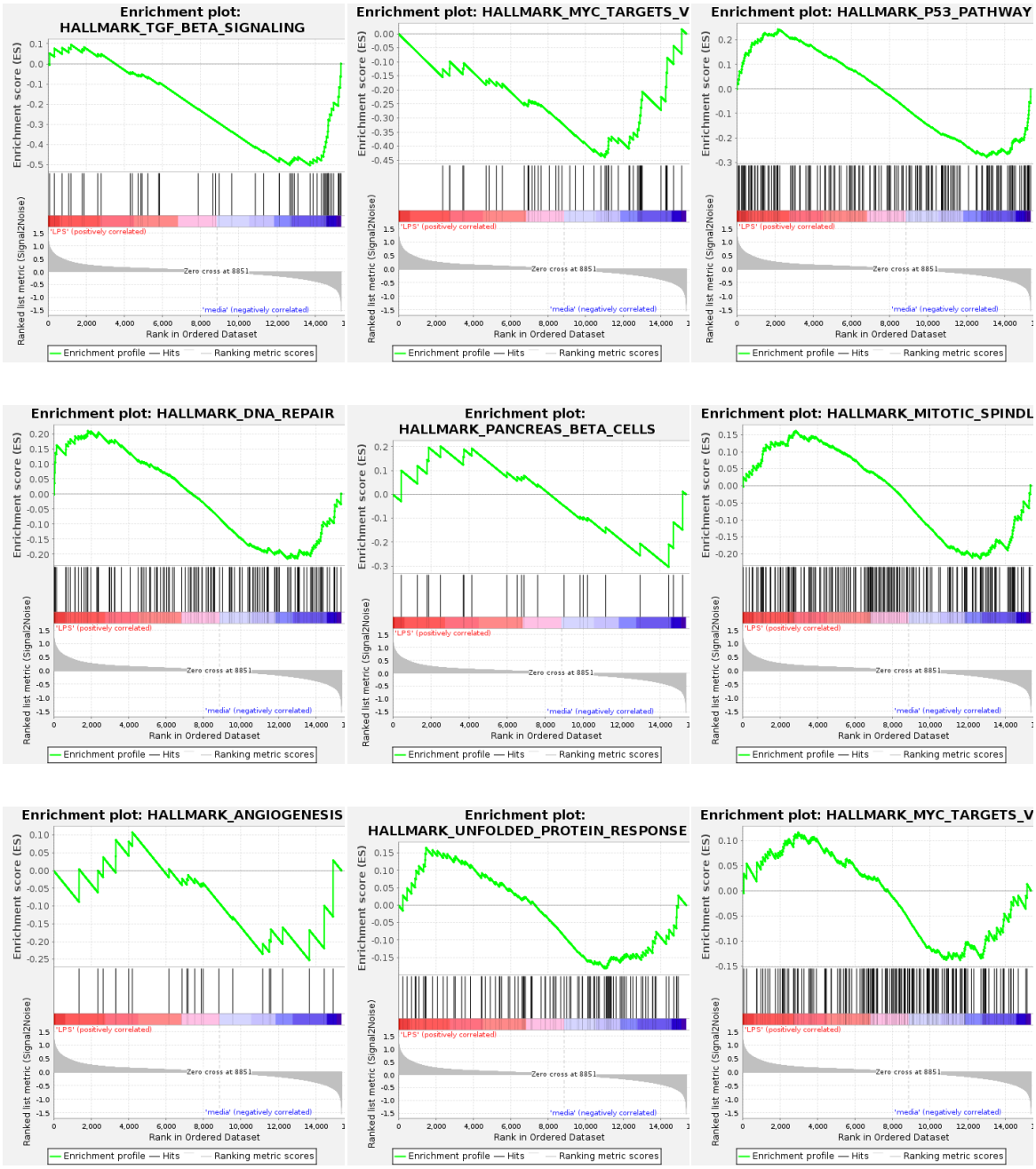

Appendix Figure 12. GSEA HALLMARK Database Snapshots. *GSEA performed using the Hallmark gene set collection from MSigDB to compare LPS-treated monocytes with media-treated controls. Of the 50 Hallmark gene sets, (A) 41 were enriched in the LPS condition, while (B) 9 showed enrichment in the media-treated group.*

(A)

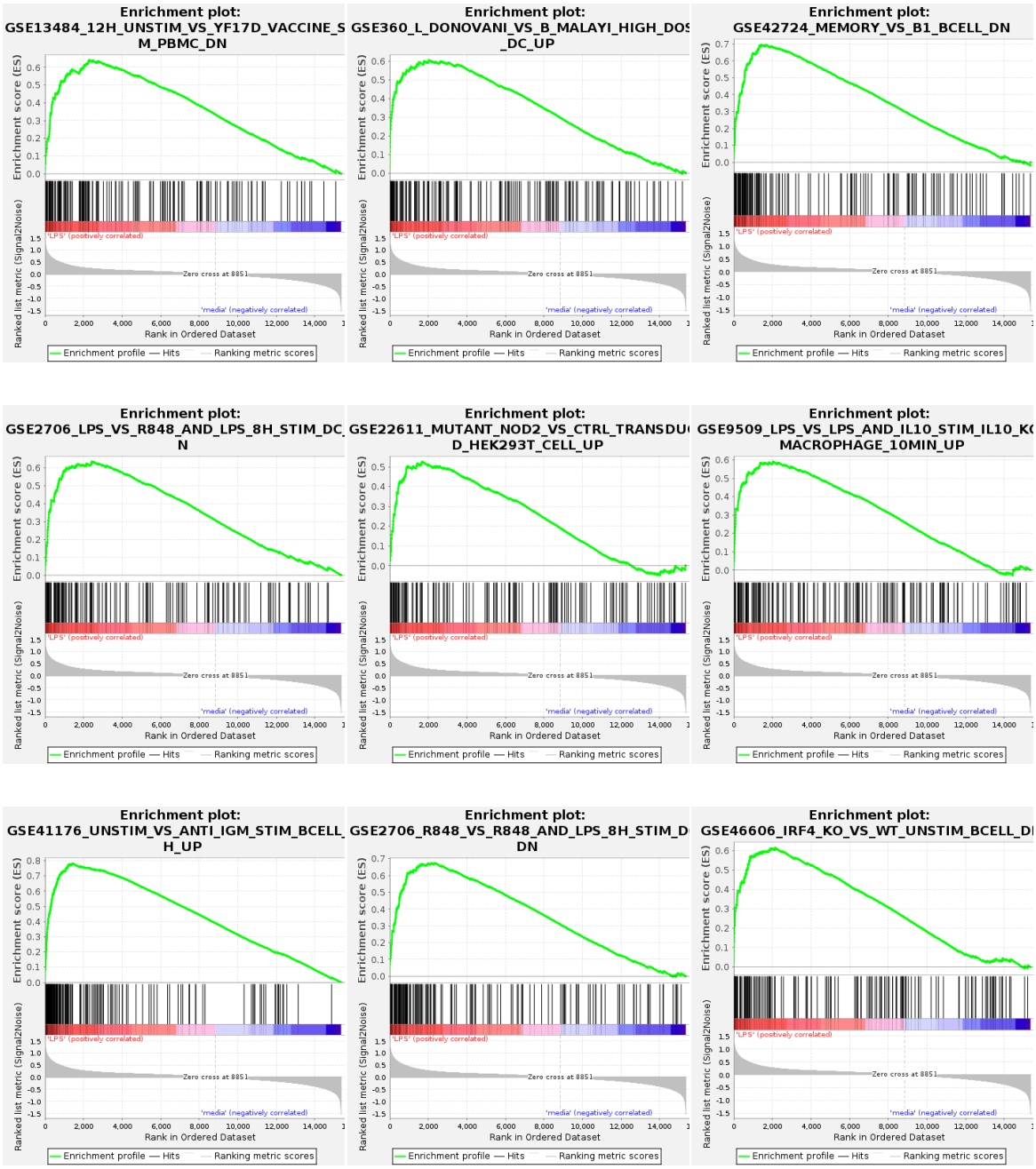
Enrichment plot:
GSE13484_12H_UNSTIM_VS_YF17D_VACCINE_S
M_PBMC_DN
Enrichment plot:
GSE360_L_DONOVANI_VS_B_MALAYI_HIGH_DOS
_DC_UP
Enrichment plot:
GSE42724_MEMORY_VS_B1_BCELL_DN
Enrichment plot:
GSE2706_LPS_VS_R848_AND_LPS_8H_STIM_DC
N
Enrichment plot:
GSE22611_MUTANT_NOD2_VS_CTRL_TRANSDU
D_HEK293T_CELL_UP
Enrichment plot:
GSE9509_LPS_VS_LPS_AND_IL10_STIM_IL10_K
MACROPHAGE_10MIN_UP
Enrichment plot:
GSE41176_UNSTIM_VS_ANTI_IGM_STIM_BCELL_
H_UP
Enrichment plot:
GSE2706_R848_VS_R848_AND_LPS_8H_STIM_D
DN
Enrichment plot:
GSE46606_IRF4_KO_VS_WT_UNSTIM_BCELL_D
Enrichment score (ES)
Ranked list metric (Signal2Noise)
'LPS' (positively correlated)
'media' (negatively correlated)
Zero cross at 8851
Rank in Ordered Dataset
Enrichment profile
Hits
Ranking metric scores

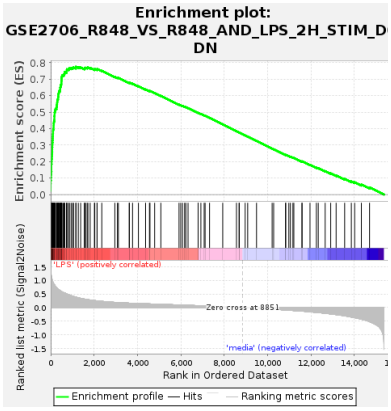
Enrichment plot:
GSE2706_R848_VS_R848_AND_LPS_2H_STIM_D
DN
Enrichment score (ES)
Ranked list metric (Signal2Noise)
'LPS' (positively correlated)
Zero cross at 8851
'media' (negatively correlated)
Rank in Ordered Dataset
Enrichment profile
Hits
Ranking metric scores

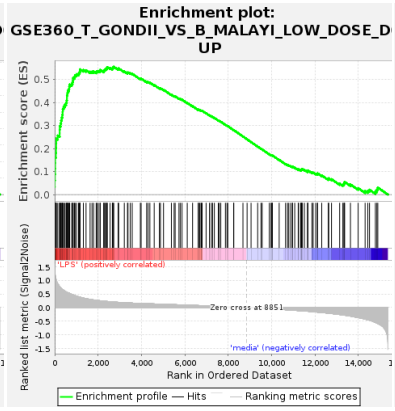
Enrichment plot:
GSE360_T_GONDII_VS_B_MALAYI_LOW_DOSE_D
UP
Enrichment score (ES)
Ranked list metric (Signal2Noise)
'LPS' (positively correlated)
Zero cross at 8851
'media' (negatively correlated)
Rank in Ordered Dataset
Enrichment profile
Hits
Ranking metric scores

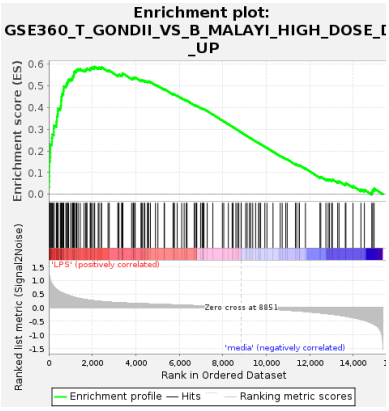
Enrichment plot:
GSE360_T_GONDII_VS_B_MALAYI_HIGH_DOSE_D
_UP
Enrichment score (ES)
Ranked list metric (Signal2Noise)
'LPS' (positively correlated)
Zero cross at 8851
'media' (negatively correlated)
Rank in Ordered Dataset
Enrichment profile
Hits
Ranking metric scores

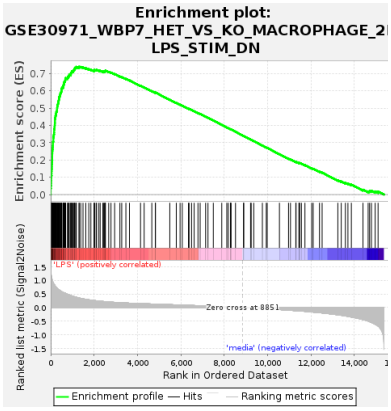
Enrichment plot:
GSE30971_WBP7_HET_VS_KO_MACROPHAGE_2
LPS_STIM_DN
Enrichment score (ES)
Ranked list metric (Signal2Noise)
'LPS' (positively correlated)
Zero cross at 8851
'media' (negatively correlated)
Rank in Ordered Dataset
Enrichment profile
Hits
Ranking metric scores

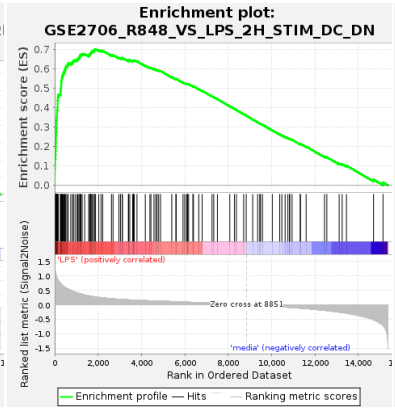
Enrichment plot:
GSE2706_R848_VS_LPS_2H_STIM_DC_DN
Enrichment score (ES)
Ranked list metric (Signal2Noise)
'LPS' (positively correlated)
Zero cross at 8851
'media' (negatively correlated)
Rank in Ordered Dataset
Enrichment profile
Hits
Ranking metric scores

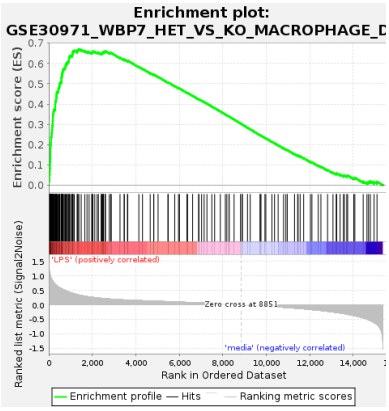
Enrichment plot:
GSE30971_WBP7_HET_VS_KO_MACROPHAGE_D
Enrichment score (ES)
Ranked list metric (Signal2Noise)
'LPS' (positively correlated)
Zero cross at 8851
'media' (negatively correlated)
Rank in Ordered Dataset
Enrichment profile
Hits
Ranking metric scores

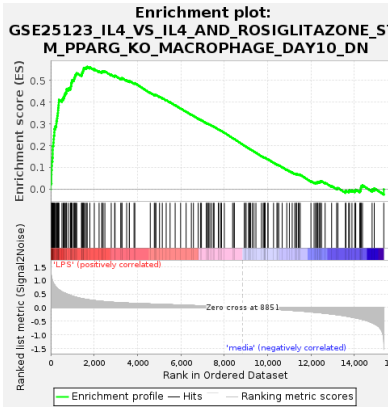
Enrichment plot:
GSE25123_IL4_VS_IL4_AND_ROSIGLITAZONE_S
M_PPARG_KO_MACROPHAGE_DAY10_DN
Enrichment score (ES)
Ranked list metric (Signal2Noise)
'LPS' (positively correlated)
Zero cross at 8851
'media' (negatively correlated)
Rank in Ordered Dataset
Enrichment profile
Hits
Ranking metric scores

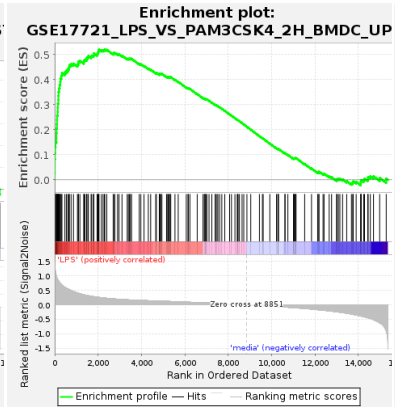
Enrichment plot:
GSE17721_LPS_VS_PAM3CSK4_2H_BMDC_UP
Enrichment score (ES)
Ranked list metric (Signal2Noise)
'LPS' (positively correlated)
Zero cross at 8851
'media' (negatively correlated)
Rank in Ordered Dataset
Enrichment profile
Hits
Ranking metric scores

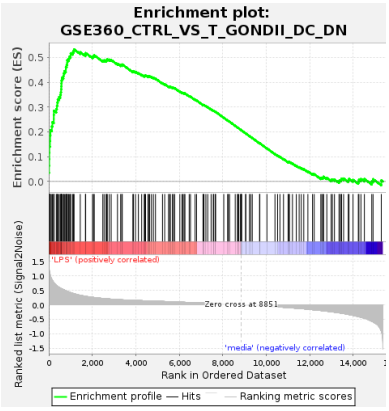
Enrichment plot:
GSE360_CTRL_VS_T_GONDII_DC_DN
Enrichment score (ES)
Ranked list metric (Signal2Noise)
'LPS' (positively correlated)
Zero cross at 8851
'media' (negatively correlated)
Rank in Ordered Dataset
Enrichment profile
Hits
Ranking metric scores

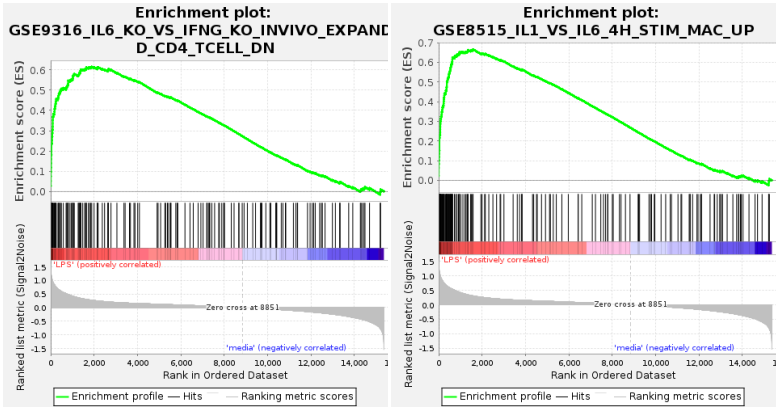
Enrichment plot:
GSE9316_IL6_KO_VS_IFNG_KO_INVIVO_EXPAND_CD4_TCELL_DN
Enrichment plot:
GSE8515_IL1_VS_IL6_4H_STIM_MAC_UP
Enrichment score (ES)
Ranked list metric (Signal2Noise)
'LPS' (positively correlated)
Zero cross at 8851
'media' (negatively correlated)
Rank in Ordered Dataset
Enrichment profile
Hits
Ranking metric scores

(B)

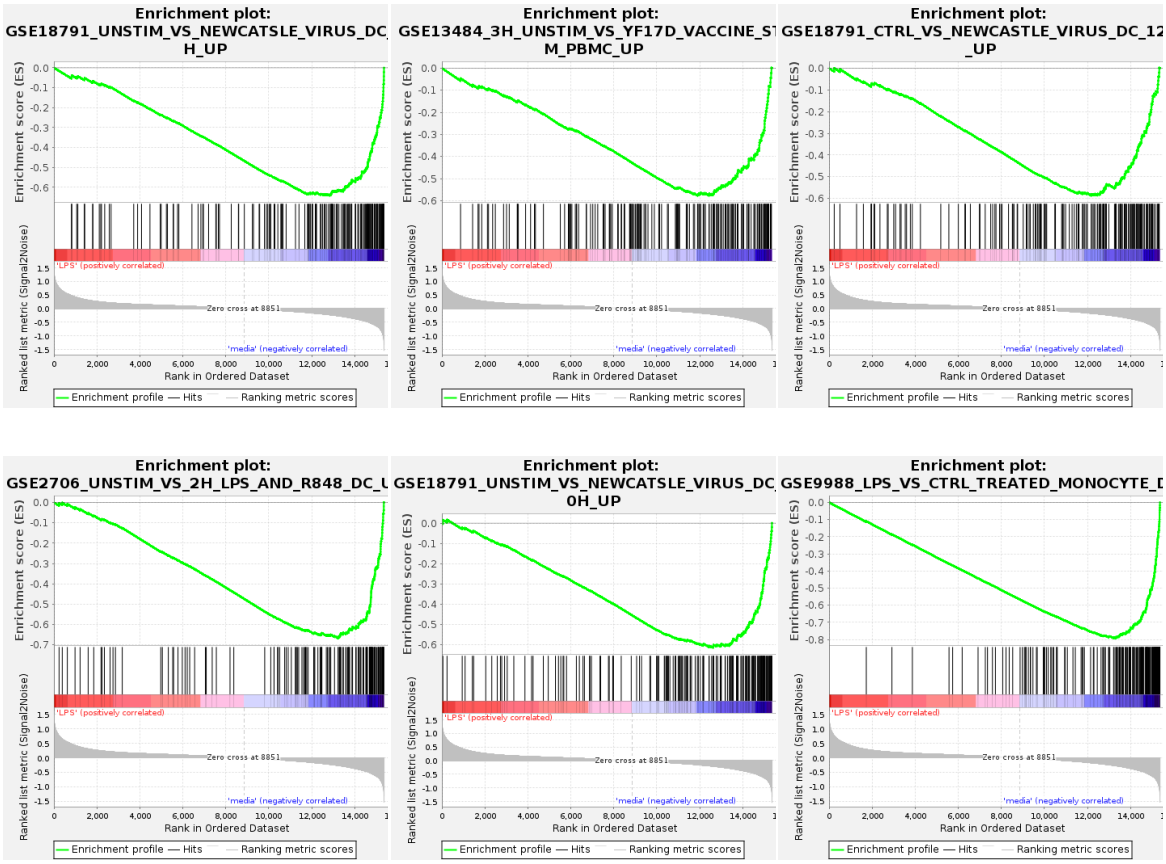
Enrichment plot:
GSE18791_UNSTIM_VS_NEWCATSLE_VIRUS_DC_H_UP
Enrichment plot:
GSE13484_3H_UNSTIM_VS_YF17D_VACCINE_STM_PBMC_UP
Enrichment plot:
GSE18791_CTRL_VS_NEWCASTLE_VIRUS_DC_12_UP
Enrichment plot:
GSE2706_UNSTIM_VS_2H_LPS_AND_R848_DC_U
Enrichment plot:
GSE18791_UNSTIM_VS_NEWCATSLE_VIRUS_DC_0H_UP
Enrichment plot:
GSE9988_LPS_VS_CTRL_TREATED_MONOCYTE_D
Enrichment score (ES)
Ranked list metric (Signal2Noise)
'LPS' (positively correlated)
Zero cross at 8851
'media' (negatively correlated)
Rank in Ordered Dataset
Enrichment profile
Hits
Ranking metric scores

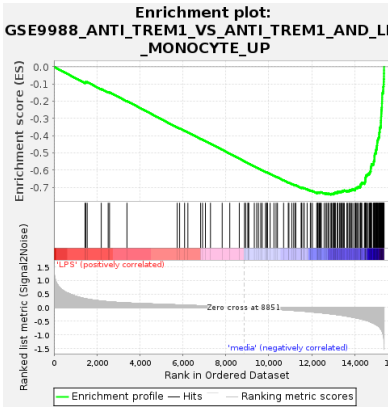
Enrichment plot:
GSE9988_ANTI_TREM1_VS_ANTI_TREM1_AND_LI
_MONOCYTE_UP
Enrichment score (ES)
Ranked list metric (Signal2Noise)
'LPS' (positively correlated)
Zero cross at 8851
'media' (negatively correlated)
Rank in Ordered Dataset
Enrichment profile
Hits
Ranking metric scores

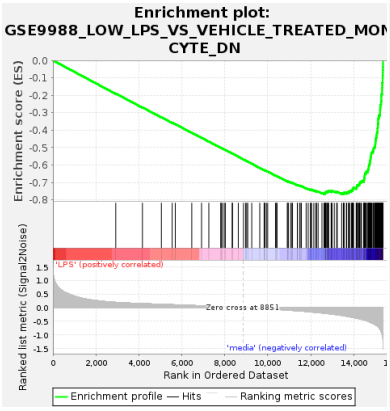
Enrichment plot:
GSE9988_LOW_LPS_VS_VEHICLE_TREATED_MON
CYTE_DN
Enrichment score (ES)
Ranked list metric (Signal2Noise)
'LPS' (positively correlated)
Zero cross at 8851
'media' (negatively correlated)
Rank in Ordered Dataset
Enrichment profile
Hits
Ranking metric scores

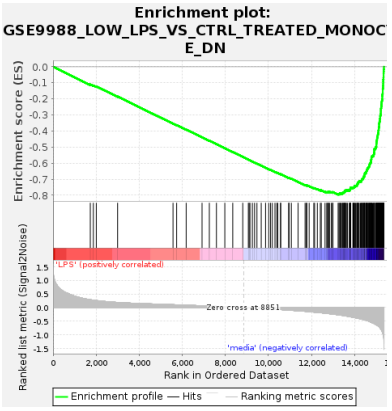
Enrichment plot:
GSE9988_LOW_LPS_VS_CTRL_TREATED_MONOC
E_DN
Enrichment score (ES)
Ranked list metric (Signal2Noise)
'LPS' (positively correlated)
Zero cross at 8851
'media' (negatively correlated)
Rank in Ordered Dataset
Enrichment profile
Hits
Ranking metric scores

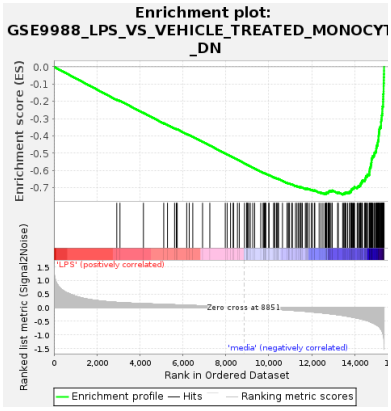
Enrichment plot:
GSE9988_LPS_VS_VEHICLE_TREATED_MONOCYT
_DN
Enrichment score (ES)
Ranked list metric (Signal2Noise)
'LPS' (positively correlated)
Zero cross at 8851
'media' (negatively correlated)
Rank in Ordered Dataset
Enrichment profile
Hits
Ranking metric scores

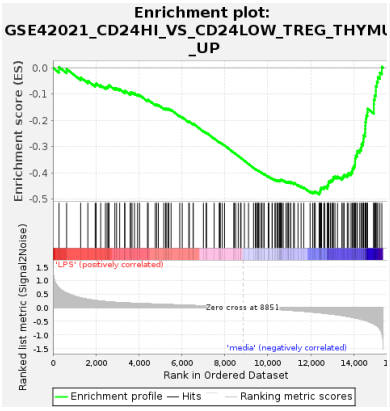
Enrichment plot:
GSE42021_CD24HI_VS_CD24LOW_TREG_THYMU
_UP
Enrichment score (ES)
Ranked list metric (Signal2Noise)
'LPS' (positively correlated)
Zero cross at 8851
'media' (negatively correlated)
Rank in Ordered Dataset
Enrichment profile
Hits
Ranking metric scores

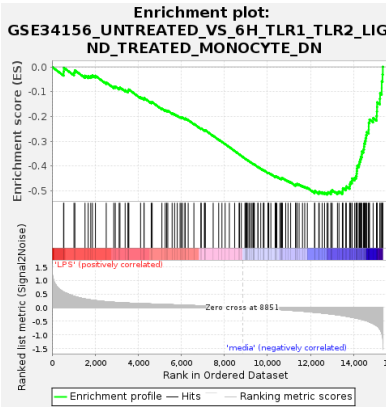
Enrichment plot:
GSE34156_UNTREATED_VS_6H_TLR1_TLR2_LIG
ND_TREATED_MONOCYTE_DN
Enrichment score (ES)
Ranked list metric (Signal2Noise)
'LPS' (positively correlated)
Zero cross at 8851
'media' (negatively correlated)
Rank in Ordered Dataset
Enrichment profile
Hits
Ranking metric scores

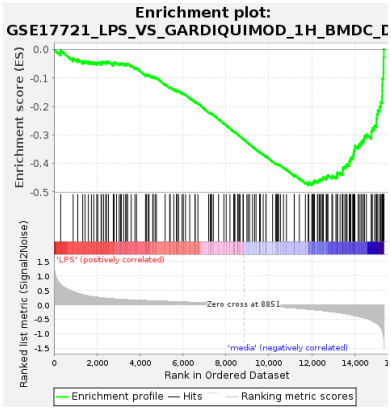
Enrichment plot:
GSE17721_LPS_VS_GARDIQUIMOD_1H_BMDC_D
Enrichment score (ES)
Ranked list metric (Signal2Noise)
'LPS' (positively correlated)
Zero cross at 8851
'media' (negatively correlated)
Rank in Ordered Dataset
Enrichment profile
Hits
Ranking metric scores

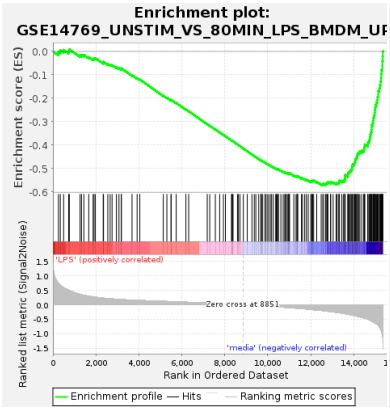
Enrichment plot:
GSE14769_UNSTIM_VS_80MIN_LPS_BMDM_UP
Enrichment score (ES)
Ranked list metric (Signal2Noise)
'LPS' (positively correlated)
Zero cross at 8851
'media' (negatively correlated)
Rank in Ordered Dataset
Enrichment profile
Hits
Ranking metric scores

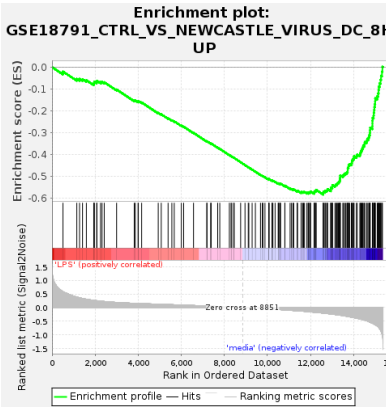
Enrichment plot:
GSE18791_CTRL_VS_NEWCASTLE_VIRUS_DC_8H
UP
Enrichment score (ES)
Ranked list metric (Signal2Noise)
'LPS' (positively correlated)
Zero cross at 8851
'media' (negatively correlated)
Rank in Ordered Dataset
Enrichment profile
Hits
Ranking metric scores

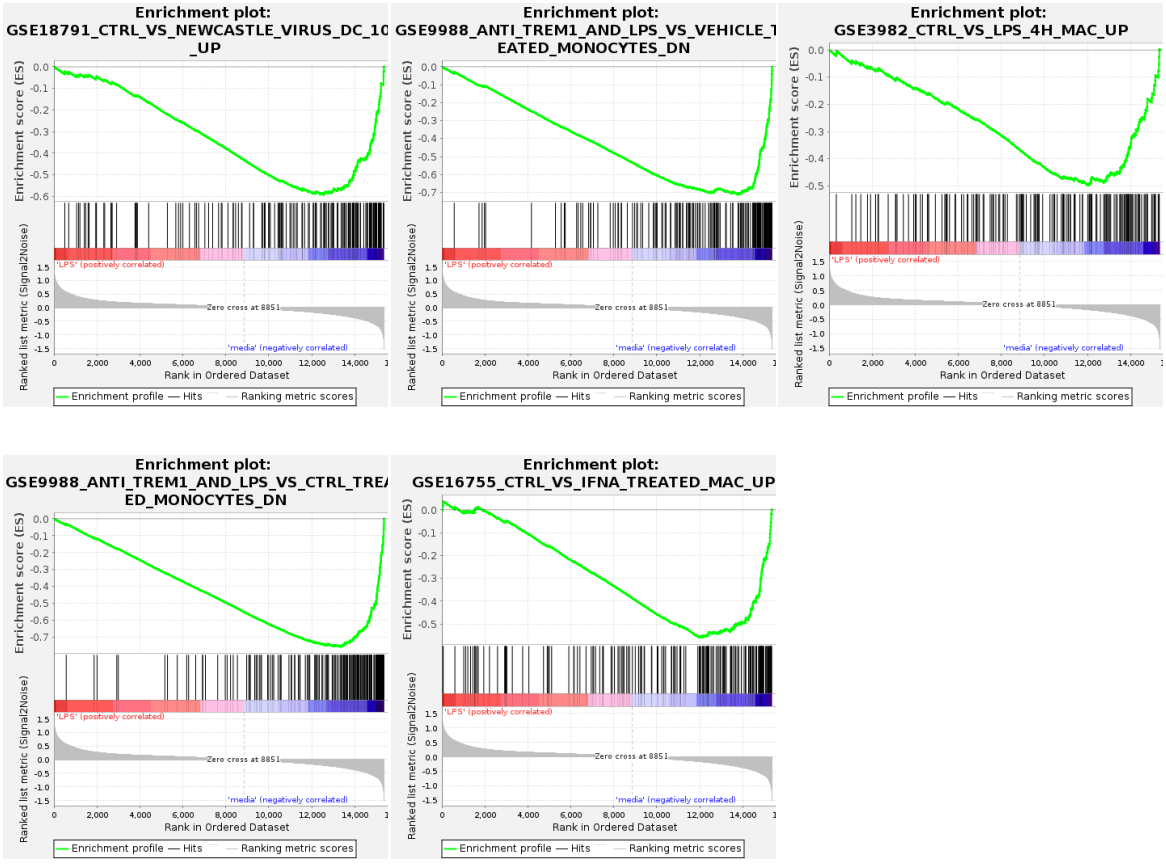

Appendix Figure 13. GSEA ImmuneSigDB (C7) Database Snapshots. *Analysis was performed using the ImmuneSigDB (C7) collection from MSigDB to compare LPS-treated monocytes with media-treated controls. Of the 4,872 curated immune gene sets, (A) 2,890 were enriched in the LPS-treated condition, while (B) 1,982 showed enrichment in the media-treated group.*

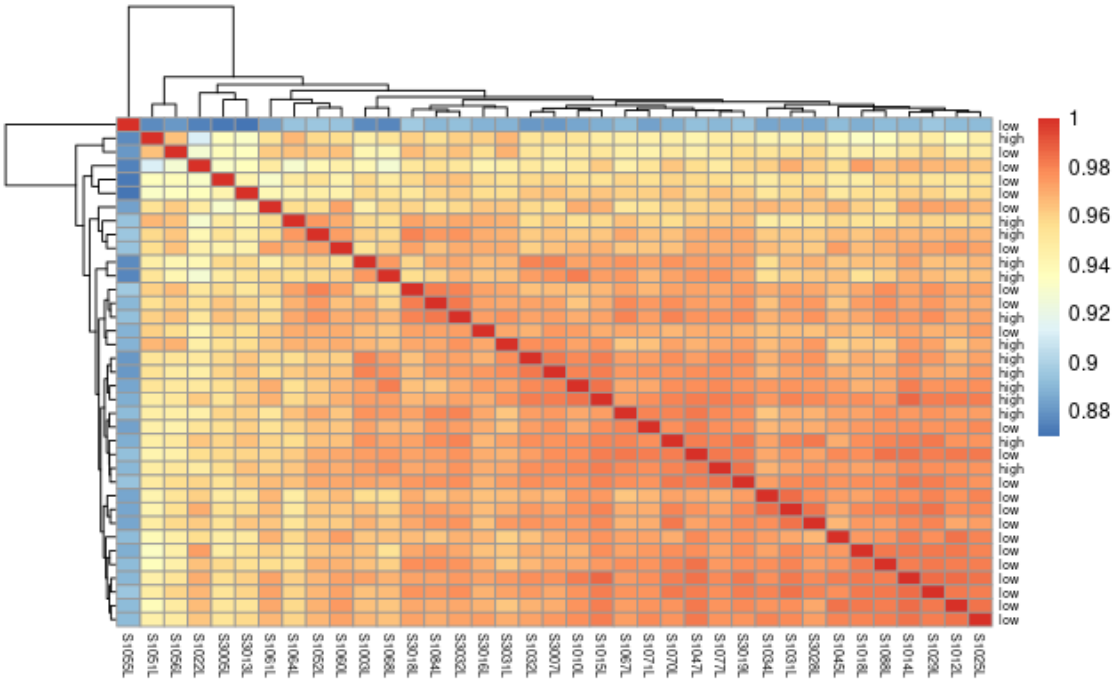

Appendix Figure 14. Sample-to-sample correlation heatmap based on rlog-transformed gene expression. *Pearson correlation heatmap of 46 RNA-Seq samples based on rlog-transformed gene expression values. Each cell represents the correlation between a pair of samples. Columns are labelled by sample ID and rows are annotated by TNF-α response classification (high or low). colour scale ranges from red (high correlation, r ≈ 1.0) to blue (lower correlation, r ≈ 0.88). Hierarchical clustering shows clear grouping by TNF-α response. Heatmap generated using pheatmap (Kolde, 2019).*

Appendix Figure 15. Distribution of mean sequence quality scores across FASTQ files. *Line plot displaying the per-sequence mean Phred quality score distribution for all 184 FASTQ files. The x-axis shows mean Phred scores per read, and the y-axis indicates total read count. Most sequences cluster at Phred scores ≥38, falling well within the high-*

quality "green" zone. Background shading reflects FastQC confidence thresholds: red (<20, low quality), orange (20-30, moderate), and green (>30, high quality). All files passed quality thresholds, though minor deviations were observed in the 3016 sample files.

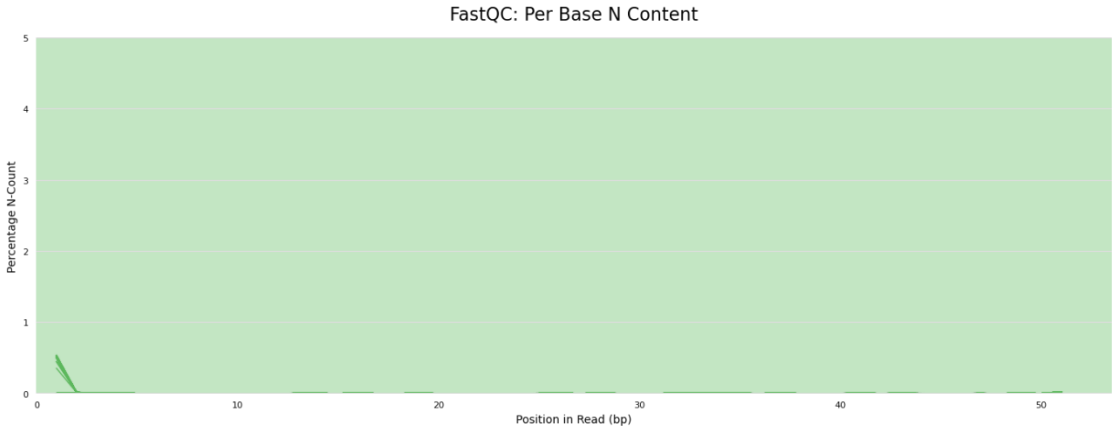

Appendix Figure 16. Per base N content across FASTQ files. *Line plot showing the percentage of N calls at each position in the read across all FASTQ files. The x-axis represents the base position (1-50), and the y-axis shows the percentage of reads containing an N at each position. Each line corresponds to a single FASTQ file.*

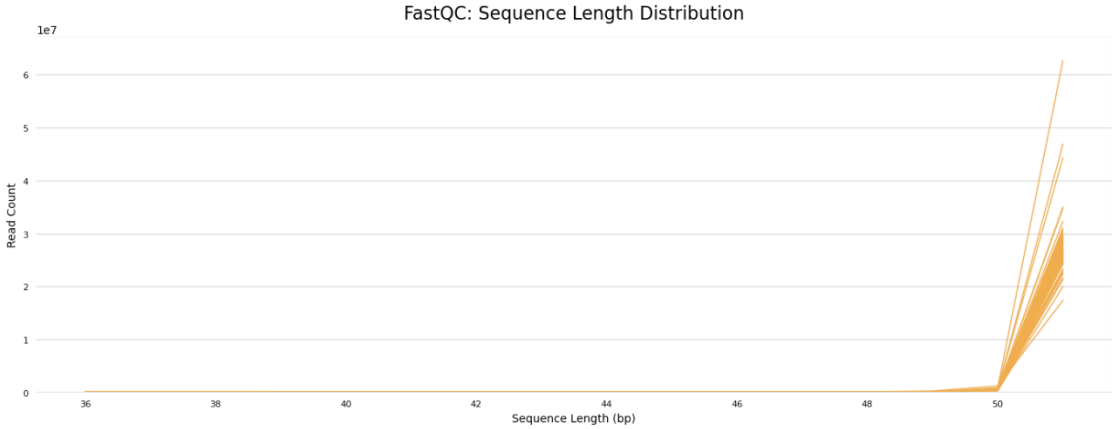

Appendix Figure 17. Sequence length distribution across all FASTQ files. *Line plot showing the distribution of read lengths across 184 FASTQ files. The x-axis represents sequence length in base pairs (bp), and the y-axis indicates read count. Each line corresponds to a single FASTQ file. Most reads cluster at 50-51 bp, with a sharp increase observed at 50 bp.*

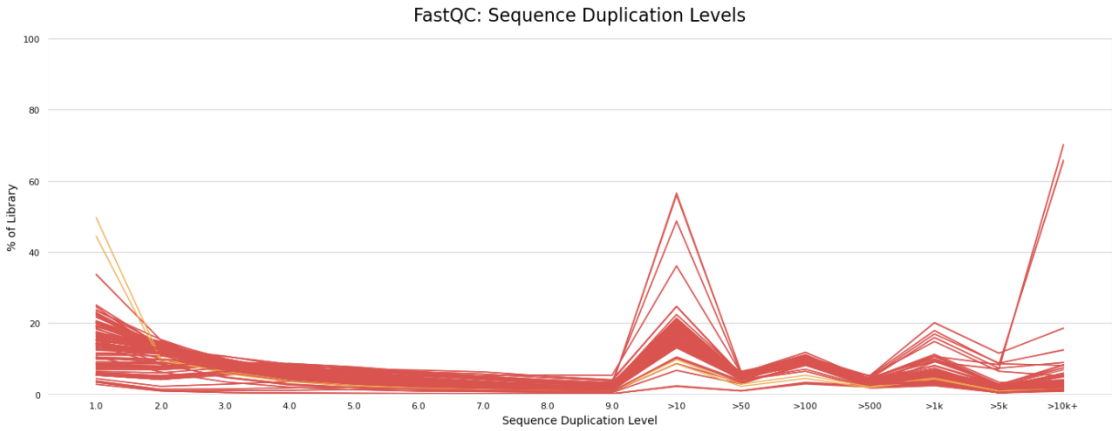

Appendix Figure 18. Sequence duplication levels across all FASTQ files. *Line plot showing the proportion of duplicated sequences across duplication levels in 184 FASTQ files. The x-axis represents duplication levels (1× to >10k×), and the y-axis shows the percentage of the library. Each line represents a FASTQ file and is coloured by FastQC evaluation status: red (fail), orange (warning), and green (pass).*

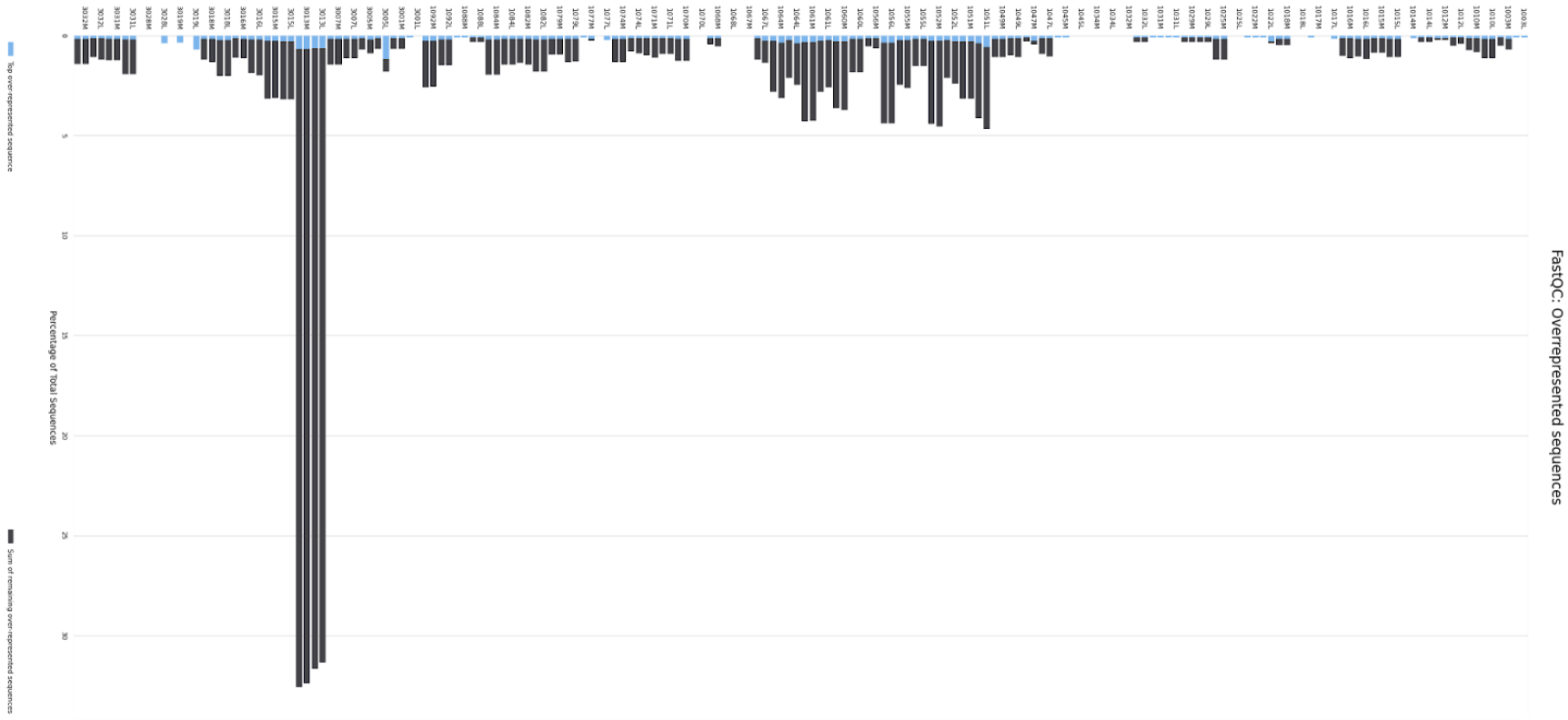

Appendix Figure 19. Overrepresented sequence content across FASTQ files before and after trimming. *Bar plot showing the percentage of total sequences flagged as overrepresented in each of 184 FASTQ files. The y-axis lists samples, ordered by numerical ID, grouped by treatment condition (LPS: L, Media: M), and displayed as raw and trimmed read pairs. Bars are divided into the most abundant overrepresented sequence (blue) and the cumulative percentage of remaining overrepresented sequences (grey). According to FastQC evaluation, 28 files passed, 155 received warnings, and 1 file (3005L_raw) failed this module.*

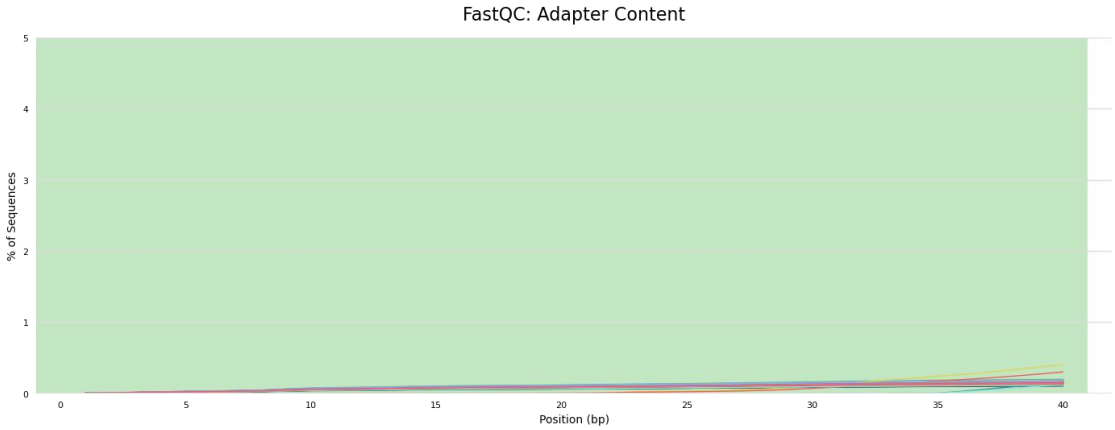

Appendix Figure 20. Adapter content across all FASTQ files. *Line plot showing the percentage of reads containing known adapter sequences at each base position (1-40 bp) across 184 FASTQ files. Each line represents a single file. All files passed the Adapter Content module, with minimal adapter presence detected.*